Universitetet i Stavanger

FACULTY OF SCIENCE AND TECHNOLOGY

MASTER'S THESIS

Study program/specialization: **Petroleum Engineering / Drilling and Wells technology**	Spring semester, 2020 Open
Author: **Henrik Nerhus**	Henrik Nerhus (signature of authors)
Faculty supervisor: **Mesfin Belayneh**	
Title of master's thesis: ***Effect of nanoparticles and elastomers on the mechanical and elastic properties of G-class Portland cement: Experimental and Modelling studies.***	
Credits (ECTS): 30	
Keywords: Portland cement Nanoparticles Elastomers UCS Young's modulus Rheology Leakage Heat of hydration UCS modeling Resilience	Number of pages: 153 + supplemental material/other: 39

Abstract

Properly designed well structure in terms of load carrying capacity and appropriate materials used maintain the sustainability and the long-term structural integrity of the well. An important barrier for oil and gas wells is cement, and on the NCS the NORSOK-D010 has very specific requirements for the barrier material. Some of these properties include the barrier material being ductile, impermeable and resistant to damaging chemicals.[1] However, a study from 2001 shows that approximately 15% of primary cement jobs fail, costing the industry several hundreds of millions of dollars annually.[2] Additional studies show similar results, a study from 2006 shows that around 11% of well integrity issues on the NCS were due to cement related problems[3], around 14500 wells had fluid migration issues due to poor cement quality in Alberta [4] and a study from Pennsylvania showed that a large majority of the wells which experienced some sort of integrity or barrier issue, experienced cementing or casing failures[5]. These studies show that the cement used as barrier material does not always fulfill these requirements.

As nanomaterials continue to grow more useful in various industries, its benefits have also reached the oil and gas sector. Application of nanotechnology contributes to smarter and more efficient solutions to the technical challenges at hand and provides solutions to problems which conventional technology struggles with. In this thesis, several nanoparticles and elastomers have been tested as additives to cement slurries, to examine the benefits which can be achieved. A total of 17 different cement slurry batches were formulated, containing various concentrations of nanoparticles and rubber silicone. It was found that for all tested nanoparticles, the UCS increased with varying degrees given the right concentration added, with the largest increase observed from the addition of 0,26%bwoc of nano-silica which increased UCS by 36,9%. The vast majority of the analyzed slurries containing nanoparticles resulted in a cement with increased resilience. Additionally, it was found that the effects of nanoparticles vary greatly with the water to cement ratio, and that increasing the concentration of nanoparticles beyond a certain % generally resulted in decreased cement strength. The addition of rubber silicone was found to have a negative impact on cement strength in all cases but one, with a decreased resilience in all cases. Additionally, it was found that the addition of nanoparticles could greatly reduce fluid migration through cement. Using the measured data, an empirical UCS-Compressional wave velocity model was developed. Testing the model with data from literature shows a relatively good prediction of UCS based on the wave velocity.

Acknowledgements

First and foremost, I would like to express my sincerest gratitude to my supervisor, professor Mesfin Belayneh Agonafir. The council, mentoring and help he has provided over the course of this thesis has been invaluable. He has been available for discussion from the early mornings to late at night and was always happy to be of assistance. His dedication to his students is unparalleled and greatly appreciated.

Additionally, I would like to thank senior engineer Samdar Kakay for all his help. He instructed me in the use of several of his compressive strength apparatuses located in his laboratory which allowed me to conduct destructive testing on a lot of my cement samples.

Furthermore, I would like to thank the University of Stavanger for allowing me to utilize their equipment and laboratories in order to complete the experimental work performed in this thesis. I would like to especially thank them for their efforts and hard work in making the school as safe as possible during the COVID 19 situation which allowed me and several other students to return to the school and further progress the laboratory work being done.

Lastly, I would like to express my gratitude towards my family and friends, who inspired me and kept me motivated throughout the semester allowing me to finish the thesis on time during this unusual situation.

Table of contents

ABSTRACT ..... **I**

ACKNOWLEDGEMENTS ..... **II**

TABLE OF CONTENTS ..... **II**

LIST OF FIGURES ..... **V**

LIST OF EQUATIONS ..... **VIII**

LIST OF TABLES ..... **VIII**

LIST OF SYMBOLS ..... **IX**

LIST OF ABBREVIATIONS ..... **X**

1. INTRODUCTION **1**

1.1 BACKGROUND 1
1.2 PROBLEM FORMULATION 8
1.3 OBJECTIVE 9
1.4 RESEARCH METHODS 10

2. LITERATURE STUDY **12**

2.1 CEMENT AND CLASSIFICATION 12
2.1.1 Portland Cement *12*
2.1.2 Classification *13*
2.2 HYDRATION PROCESS 15
2.2.1 Effect of temperature on hydration process *17*
2.3 NANOTECHNOLOGY 19
2.3.1 Application of nanotechnology in the oil and gas industry *20*
2.3.2 Carbon nanotubes *21*
2.3.3 Specific applications of nanotechnology in oil-well cementing *22*
2.3.3.1 Effect of nano-silica on compressive cement strength 22
2.3.3.2 Carbon nanotubes effect on mechanical performance on properties of cement composites 23
2.3.3.3 Effect of nano materials on setting time, consistency and compressive strength of cement mortar 25
2.3.3.4 Effect of Iron-oxide on the properties of cement 26
2.3.3.5 Effect of adding graphene oxide nanosheets to cement paste 27
2.3.3.6 Effect of nano aluminum oxide and MWCNT on hardened cement paste 28
2.3.3.7 Effect of nano zinc oxide on cement-based materials 29
2.3.4 Other applications of nano materials in the oil and gas industry *30*
2.3.4.1 Enhanced oil recovery using nanoparticles 30
2.3.4.2 Nano silica on improved EOR 30
2.3.4.3 Scale inhibition using nano silica 31
2.3.4.4 Improving drilling fluids using nano graphene 31
2.3.4.5 Corrosion inhibition using magnetic nanofluid 32
2.3.4.6 Nano-emulsions as cement spacer 32

3. EXPERIMENTAL PROGRAM **34**

3.1 MATERIALS 34
3.1.1 Cement *34*
3.1.2 Water *35*
3.1.3 Nanoparticles *35*
3.1.3.1 Nano SiO_2 35
3.1.3.2 MWCNT/MWCNT-COOH 35
3.1.3.3 Nano TiO_2 36
3.1.3.4 Nano Fe_2O_3 36
3.1.3.5 Nano-Al_2O_3 38
3.1.3.6 Nano-ZnO 38
3.1.4 Rubber *38*
3.1.5 Cement molds *39*
3.2 TEST BATCHES 40
3.2.1 Introduction *40*

3.2.1.1 Test batch 1 42
3.2.1.2 Test batch 2 43
3.2.1.3 Test batch 3 44
3.2.1.4 Test batch 4 45
3.2.1.5 Test batch 5 46
3.2.1.6 Test batch 6 46
3.2.1.7 Test batch 7 47
3.2.1.8 Test batch 8 48
3.2.1.9 Test batch 9 49
3.2.1.10 Test batch 10 50
3.2.1.11 Test batch 11 50
3.2.1.12 Test batch 12 51
3.2.1.13 Test batch 13 52
3.2.1.14 Test batch 14 53
3.2.1.15 Test batch 15 53
3.2.1.16 Test batch 16 54
3.2.1.17 Test batch 17 55
3.3 THEORY, TEST SET-UP AND PROCEDURE 56
3.3.1 Non-destructive testing 56
3.3.2 Ultrasonic velocity measurements 56
3.3.2.1 Theory 56
3.3.2.2 Test set-up 57
3.3.2.3 Procedure 57
3.3.3 Water absorption 58
3.3.3.1 Theory 58
3.3.4 Modeling of UCS 58
3.3.4.1 Theory 58
3.3.4.2 Procedure 59
3.3.5 Modulus of elasticity 59
3.3.5.1 Theory 59
3.3.5.2 Procedure 59
3.3.6 Destructive testing 61
3.3.7 UCS 61
3.3.7.1 Theory 61
3.3.7.2 Test set-up 62
3.3.7.3 Procedure 63
3.3.8 Young's modulus and Resilience 63
3.3.9 Heat development 65
3.3.9.1 Theory 65
3.3.9.2 Procedure 65
3.3.10 Leakage test 66
3.3.10.1 Theory 66
3.3.10.2 Procedure 67
3.3.11 Rheology 68
3.3.11.1 Theory 68
3.3.11.2 Procedure 69

4. RESULTS AND DISCUSSION 71

4.1 EFFECT OF NANOPARTICLES ON 0,52 AND 0,44 WCR G CLASS CEMENT 71
4.1.1 Change of mass with nanoparticles on 0,52 and 0,44 WCR G class cement 72
4.1.2 Destructive results of 0,52 and 0,44 WCR G class cement with nanoparticle additives 74
4.1.2.1 Uniaxial compressive strength of 0,52 and 0,44 WCR G class cement with nanoparticle additives ... 74
4.1.2.2 Young´s modulus of 0,52 and 0,44 WCR G class cement with nanoparticle additives 77
4.1.2.3 Resilience of 0,52 and 0,44 WCR G class cement with nanoparticle additives 79
4.1.3 Modulus of elasticity of 0,52 and 0,44 WCR G class cement with nanoparticle additives 80
4.1.4 Effect of SiO_2 83
4.1.5 Effect of MWCNT-COOH 86
4.1.6 Effect of Fe_2O_3 91
4.1.7 Effect of TiO_2 94
4.1.8 Effect of hybrid mixture 97
4.1.9 Results from test matrices 10-12 100
4.1.9.1 Effect of nano-silica on 0,44 WCR G class cement 100
4.1.9.2 Effect of MWCNT 102
4.1.9.3 Effect of Al_2O_3 104

4.1.10 Results from test batch 13-16 ..... *105*
4.1.10.1 Effect of ZnO 105
4.1.10.2 Effect of MWCNT and Al_2O_3 hybrid 107
4.1.10.3 Effect of SiO_2 and Fe_2O_3 hybrid 108
4.1.10.4 Effect of MWCNT-COOH and TiO_2 hybrid 109
4.2 EFFECT OF SILICONE RUBBER ON 0,44 WCR G CLASS CEMENT 110
4.2.1 Change of mass with plastic additives on 0,44 WCR G class cement *111*
4.2.2 Destructive results of rubber additives on 0,44 WCR G class cement *113*
4.2.2.1 Uniaxial compressive strength of rubber on 0,44 WCR G class cement 113
4.2.2.2 Effect of rubber ash on 0,44 WCR G class cement 115
4.2.2.3 Young´s modulus of rubber additives on 0,44 WCR G class cement 116
4.2.2.4 Resilience of rubber additives on 0,44 WCR G class cement 117
4.2.3 M-modulus of rubber on 0,44 WCR G class cement *119*
4.3 FURTHER INVESTIGATION OF BEST SYSTEM 122
4.3.1 Compressive strength of heat-treated cement *122*
4.3.2 Leakage testing of best system *123*
4.3.3 Rheology of cement slurry *125*
4.3.4 Heat development *128*
4.4 UNCERTAINTY 129
5. EMPIRICAL UCS VS VP MODELING 131
5.1 ANALYSIS OF HORSRUD MODEL 131
5.2 NEW MODEL DEVELOPMENT AND TESTING 132
6. SUMMARY AND CONCLUSION 135
7. FUTURE WORK 138
REFERENCES 140
APPENDIX A – FORCE VS DEFORMATION FOR ALL CEMENT SAMPLES 143
APPENDIX B – NON-DESTRUCTIVE MEASUREMENTS FOR ALL BATCHES 171
APPENDIX C – MISCELLANEOUS PICTURES 178

LIST OF FIGURES

Figure 1.1 Conventional well construction[7] 2
Figure 1.2 Leak paths due to cement integrity failure[8] 3
Figure 1.3 P&A of a well [9] 4
Figure 1.4 SCP vs age of well GOM[2] 6
Figure 1.5 Well integrity issues NCS[3] 7
Figure 1.6 Contents of theoretical work 10
Figure 1.7 Contents of experimental work 11
Figure 2.1 Evolution of heat vs time of hydration[2] 16
Figure 2.2 Temperature effect on hydration [2] 18
Figure 2.3 Top-down and Bottom-up strategies for producing nanoparticles[14] 20
Figure 2.4 Application of nanotechnology to different stages of oil production [18] 21
Figure 2.5 Categories of carbon nanotubes based on their physical structure[18] 22
Figure 2.6 Effect of nano-SiO2 on compressive strength[11] 23
Figure 2.7 Strength of samples containing MWCNT [19] 24
Figure 2.8 Final setting time of cement with varying concentration of nanomaterials[20] 25
Figure 2.9 Compressive stress-strain model parameters for nano-Fe2O3 modified smart cement[21] 26

Figure 2.10 Change in flexural and compressive strength with varying concentration of GO nanosheets[22] 27
Figure 2.11 Increase in UCS per added nanoparticle [23] 28
Figure 2.12 Compressive strength of Portland cement mortars with 0-5 wt% ZnO[24] 29
Figure 3.1 Chemical composition of the utilized G class cement 34
Figure 3.2 Aqueous dispersion of SiO2 35
Figure 3.3 Aqueous dispersion of TiO2 36
Figure 3.4 Iron oxide powder (left) mixture after mixing (middle) mixture after 48 hours (right) 37
Figure 3.5 Machine used for sonication of iron oxide solution 37
Figure 3.6 Silicone rubber coarsely cut (left) and finely cut (right) 39
Figure 3.7 Cement mold coated in oil (left) and oil for lubrication (right) 40
Figure 3.8 Scope of experimental work 56
Figure 3.9 CNS Farnell Pundit 7 ultrasonic measurement device 57
Figure 3.10 Zwick Z020 with cement plug in place for destructive testing 62
Figure 3.11 Stress-strain curve from a UCS test 64
Figure 3.12 Temperature logger from ESK-EL 65
Figure 3.13 Styrofoam box used for temperature logging with cement in one compartment 66
Figure 3.14 Oven used to store samples during heat cycles of approximately 105 degrees Celsius 66
Figure 3.15 Heat vs duration for testing of leakage 67
Figure 3.16 Set-up for measuring leakage rate of cement 68
Figure 3.17 Fann 35 viscometer used for measuring rheology 70
Figure 4.1 Percent change in mass of the 0,52 WCR samples after 24 and 72 hours of being submerged in water 72
Figure 4.2 Percent change in mass of the 0,44 WCR samples after 24 and 48 hours of being submerged in water 73
Figure 4.3 UCS of the various nanoparticles on 0,52 WCR G class cement 75
Figure 4.4 UCS of the various nanoparticles on 0,44 WCR G class cement 76
Figure 4.5 Young´s modulus of various nanoparticles on 0,52 WCR G class cement 77
Figure 4.6 Young´s modulus of various nanoparticles on 0,44 WCR G class cement 78
Figure 4.7 Resilience of various nanoparticles on 0,52 WCR G class cement 79
Figure 4.8 Resilience of various nanoparticles on 0,44 WCR G class cement 80
Figure 4.9 M-modulus for test batch 1-4 81
Figure 4.10 Modulus of elasticity for 0,44 WCR batches with added nanoparticles 82
Figure 4.11 UCS for different concentrations of nano-silica 83
Figure 4.12 Young´s modulus for various concentrations of SiO2 on 0,52 WCR G class cement 85
Figure 4.13 Resilience for various concentrations of SiO2 on 0,52 WCR G class cement 85
Figure 4.14 UCS for different concentrations of MWCNT-COOH on 0,52 WCR cement 86
Figure 4.15 Young´s modulus for various concentrations of MWCNT-COOH on 0,52 WCR G class cement 87
Figure 4.16 Resilience for various concentrations of MWCNT-COOH on 0,52 WCR G class cement 88

Figure 4.17 UCS for different concentrations of MWCNT-COOH on 0,44 WCR cement 89
Figure 4.18 Young´s modulus for various concentrations of MWCNT-COOH on 0,44 WCR G class cement 90
Figure 4.19 Resilience for various concentrations of MWCNT-COOH on 0,44 WCR G class cement 91
Figure 4.20 UCS for different concentrations of Fe2O3 92
Figure 4.21 Young´s modulus for various concentrations of Fe2O3 on 0,52 WCR G class cement 93
Figure 4.22 Resilience for various concentrations of Fe2O3 on 0,52 WCR G class cement 94
Figure 4.23 UCS for different concentrations of TiO2 95
Figure 4.24 Young´s modulus for various concentrations of TiO2 on 0,52 WCR G class cement 96
Figure 4.25 Resilience for various concentrations of TiO2 on 0,52 WCR G class cement 97
Figure 4.26 UCS for different combinations of hybrid mixture 98
Figure 4.27 Young´s modulus of hybrid mixture on 0,44 WCR G class cement 99
Figure 4.28 Resilience for various concentrations of hybrid mixture on 0,44 WCR G class cement 100
Figure 4.29 UCS for various concentrations of SiO2 on 0,44 WCR G class cement 101
Figure 4.30 UCS for various concentrations of MWCNT on 0,44 WCR G class cement 103
Figure 4.31 UCS for various concentrations of Al2O3 on 0,44 WCR G class cement 104
Figure 4.32 UCS for various concentrations of ZnO on 0,44 WCR G class cement 106
Figure 4.33 UCS for various combinations of MWCNT and Al2O3 on 0,44 WCR G class cement 107
Figure 4.34 UCS for various combinations of SiO2 and Fe2O3 on 0,44 WCR G class cement 108
Figure 4.35 UCS for various combinations of MWCNT-COOH and TiO2 on 0,44 WCR G class cement 109
Figure 4.36 Change of mass with samples containing untreated rubber 111
Figure 4.37 Change of mass with samples containing acid treated rubber 112
Figure 4.38 UCS for different concentrations of untreated rubber 113
Figure 4.39 UCS for different dosages of treated rubber 114
Figure 4.40 UCS for different dosages of rubber ash 115
Figure 4.41 Young´s modulus for untreated rubber on 0,44 WCR G class cement 116
Figure 4.42 Youngs Modulus for different dosages of acid treated rubber 117
Figure 4.43 Resilience of samples containing untreated rubber 118
Figure 4.44 Resilience of samples containing acid treated rubber 119
Figure 4.45 M-modulus of untreated rubber on 0,44 WCR cement 120
Figure 4.46 M-modulus of acid treated rubber on 0,44 WCR cement 121
Figure 4.47 UCS of best system on 0,44 WCR G class cement after heat treatment 122
Figure 4.48 Shear stress of cement slurries 125
Figure 4.49 Casson yield stress of the two tested systems 126
Figure 4.50 Casson plastic viscosity of the two tested systems 127
Figure 4.51 Heat development as a result of cement hydration 128
Figure 5.1 Horsrud vs actual UCS for test batch no. 3 131

Figure 5.2 Horsrud vs actual UCS for test batch no. 2 132
Figure 5.3 UCS vs Vp plot using measured data 133
Figure 5.4 Actual UCS vs model predictions 133

LIST OF EQUATIONS

Equation 3-1 58
Equation 3-2 59
Equation 3-3 60
Equation 3-4 60
Equation 3-5 60
Equation 3-6 60
Equation 3-7 61
Equation 3-8 63
Equation 3-9 64
Equation 3-10 64
Equation 3-11 69
Equation 3-12 69
Equation 5-1 133

LIST OF TABLES

Table 2.1 Mineralogical composition of classic Portland cement clinker 13
Table 2.2 API&ASTM Classification of cement 14
Table 2.3 Usage and availability of different API classifications of cement 14
Table 3.1 Elemental analysis (EDS) of silicone rubber[35] 38
Table 3.2 Test batch no. 1 43
Table 3.3 Test batch no. 2 44
Table 3.4 Test batch no. 3 44
Table 3.5 Test batch no. 4 45
Table 3.6 Test batch no. 5 46
Table 3.7 Test batch no. 6 47
Table 3.8 Test batch no. 7 48
Table 3.9 Test batch no. 8 49
Table 3.10 Test batch no. 9 49
Table 3.11 Test batch no. 10 50
Table 3.12 Test batch no. 11 51
Table 3.13 Test batch no. 12 52
Table 3.14 Test batch no. 13 52
Table 3.15 Test batch no. 14 53
Table 3.16 Test batch no. 15 54
Table 3.17 Test batch no. 16 54
Table 4.1 Leakage of zero-additive cement sample 123
Table 4.2 Leakage of nano-additive cement sample 124
Table 6.1 Best results from destructive tests 137

LIST OF SYMBOLS

A = Cros-sectional area, mm^2

E = Young's modulus, MPa

F = Load applied, N

G = Shear modulus, GPa

K = Bulk modulus, GPa

M = P-wave modulus, GPa

Mt = Mass after a given time t, g

$M0$ = Mass before immersion in water, g

ΔM = Change in mass, %

R = Modulus of resilience, J/m^3

V_p = Compressional wave velocity, m/s

ρ = Density of the given cement plug, kg/m^3

$\Delta\sigma$ = Change in stress in the linear area of the curve, MPa

$\Delta\varepsilon$ = change in strain in the linear area of the curve, m/m

σ_{UCS} = Uniaxial compressive strength at yield point, Pa

ε_{max} = Strain at the time of failure, m/m

τ = Shear stress, $lb_f/100ft^2$

τ_c = Casson yield stress, $lb_f/100ft^2$

μ_c = Casson plastic viscosity, $lb_fs/100ft^2$

γ = Shear rate, Sec^{-1}

σ = Compressive strength, MPa

LIST OF ABBREVIATIONS

API = The American Petroleum Institute

APS = Average Particle Size

ASTM = American Society for Testing and Materials

BHA = Bottomhole Assembly

DEP = Department of Environmental Protection

EOR = Enhanced Oil Recovery

EUB = Energy and Utilities Board

GOM = Gulf of Mexico

HPHT = High Pressure High Temperature

ID = Inner Diameter

MNF = Ferromagnetic nanofluids

MWCNT = Multiwalled Carbon Nanotubes

NCS = Norwegian Continental Shelf

OBM = Oil-Based Mud

OD = Outer Diameter

OPC = Ordinary Portland Cement

PSA = Petroleum Safety Authority

PV = Plastic Viscosity

P&A = Plug and Abandonment

ROP = Rate Of Penetration

SCP = Sustained Casing Pressure

SCVF = Surface Casing Vent Flow

UCS = Uniaxial Compressive Strength

WAG = Water Alternating Gas

WBM = Water-Based Mud

WCR = Water to Cement Ratio

WOC = Wait On Cement

Wt% = Weight percent

%bwoc = Percent by weight of cement

1. Introduction

This MSc thesis presents the experimental and empirical modelling studies regarding the effect of nanoparticles and elastomers on conventional G-class cement as well as a literature review. There are several factors which determine the mechanical, rheological and petro-physical properties of cement such as; the type and concentration of the chemical added, the curing temperature and the curing pressure. In this thesis, the effect of several nanoparticle solutions and elastomers were examined relative to zero-additive cement slurries which endured the same conditions. The measured data was used to generate an empirical model used to predict the UCS of the samples. The literature review's function is to inform the reader and author of the basic background knowledge of Portland cement as well as nanotechnology and its applications in the oil and gas industry.

1.1 Background

Well construction is a large cost factor for the oil industry. Properly designed well structure in terms of load carrying capacity and appropriate materials used maintain the sustainability and the long-term structural integrity of the well. For this, cement is one of the vital parts which constitutes the longevity of the well. Cement is primarily used during construction of the well and figure 1.1 illustrates how this cement is applied during well construction. Additionally, it may also be utilized for abandonment and in some cases, intervention activities. During well construction, the main function of cement is to seal the annular spacing between the casing and the wellbore, supporting the casing and restricting fluid movement between formations to provide zonal isolation. Moreover, cement also assists other aspects such as protecting the casing from corrosion, preventing blowouts, protecting casing from shock loads in deeper drilling and sealing off thief zones or lost circulation zones. For an unsuccessful or poor primary cement job, a remedial cement job may be needed.[2], [6]

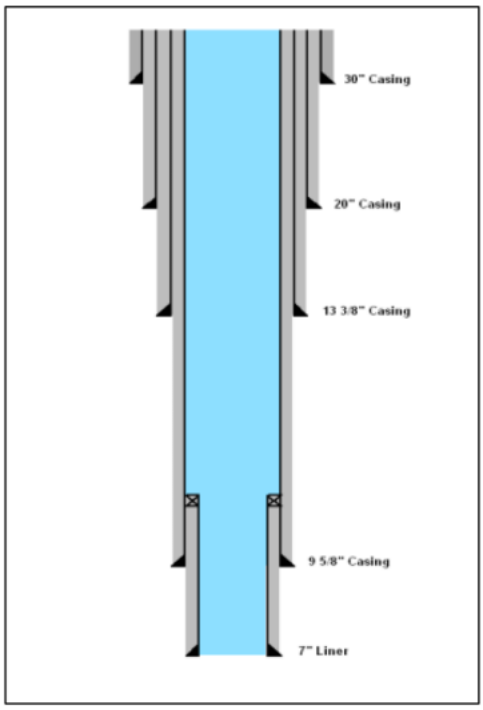

Figure 1.1 Conventional well construction[7]

From figure 1.1 one can observe how the primary cement is placed during construction in a traditional well layout. The quality of this primary cement job plays a major role in the economical longevity of the well. If cement is allowed to set uninterrupted, the matrix permeability is predominantly extremely low, however, during the lifetime of the well, the cement is bound to experience various different loads which can affect its integrity and properties.

During the drilling phase of the well, the temperatures are generally low as the drilling fluid works as a cooling agent to keep the temperatures down, however, when production starts up, the hot reservoir fluid will fill up the well and cause both thermal and pressure changes. The heating will instigate casing expansion, but the casing is locked in place by the surrounding cement which will be put under strain. Large pressure changes may also occur in gas wells experiencing large drawdown pressure. Effects like these make the casing and cement expand and contract in different ways which may lead to cracking of the cement which causes loss of cement integrity.[2]

The term debonding means that the bond in the cement to pipe interface, or the bond in the cement to rock interface, fails. There are several parameters which can cause debonding of the cement; [2]

- Gradual pressure decrease as reservoir pressure is depleted
- Casing movement due to formation subsidence
- Cement shrinkage with time
- Temperature and pressure fluctuations
- Stimulation practices

The main issue stemming from debonding is the loss of cement integrity. During reservoir pressure depletion with no pressure support, formation subsidence may occur. This is especially common in the carbonate reservoirs. The subsidence may be so severe that it completely deforms the pipe and the surrounding cement, or it may be significantly smaller which may cause leak paths in the cement. The natural cement shrinkage with time may cause the cement to contract from the pipe interfaces generating a micro-annulus for the fluids to migrate through. Figure 1.2 shows different possible leak paths through the cement due to cement integrity failure. (a) and (b) are leak paths in the micro-annulus between cement and casing, (c) is leak path through the cement, (d) is through the casing, (e) is through fractures and (f) is through the micro-annulus between the cement and the formation.

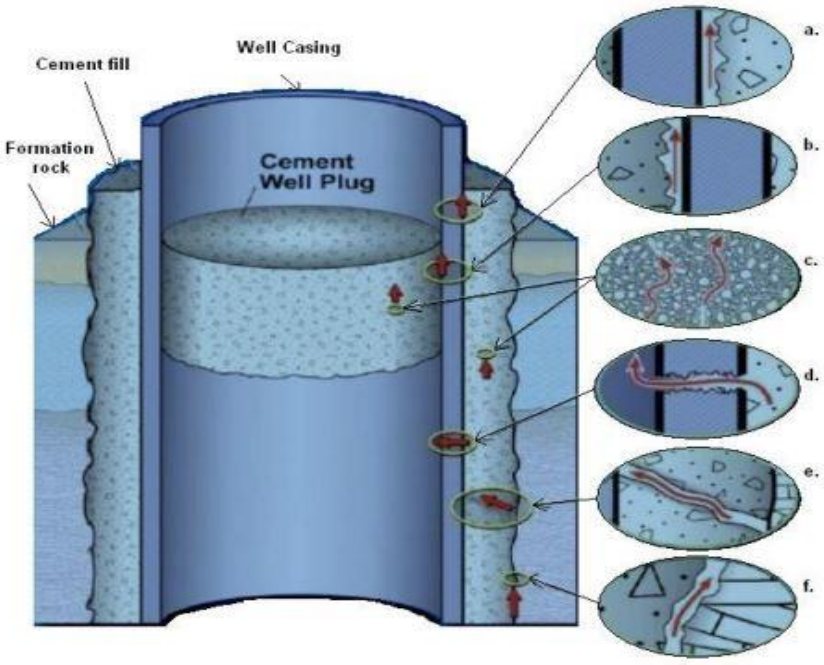

Figure 1.2 Leak paths due to cement integrity failure[8]

For a well which has been producing for an extended period, such that the water cut is too high or other parameters dictates that the well is no longer economically attractive, the well will be permanently plugged and abandoned. The decision to P&A a well may also come from problems caused by a poor cement job as this may cause corrosion of casing or cause other major issues which reduces the integrity of the well to a level which is unacceptable. During the Plug and Abandonment operation, cement is the most commonly used plugging material since it is readily available, cheap and has been proven to work.

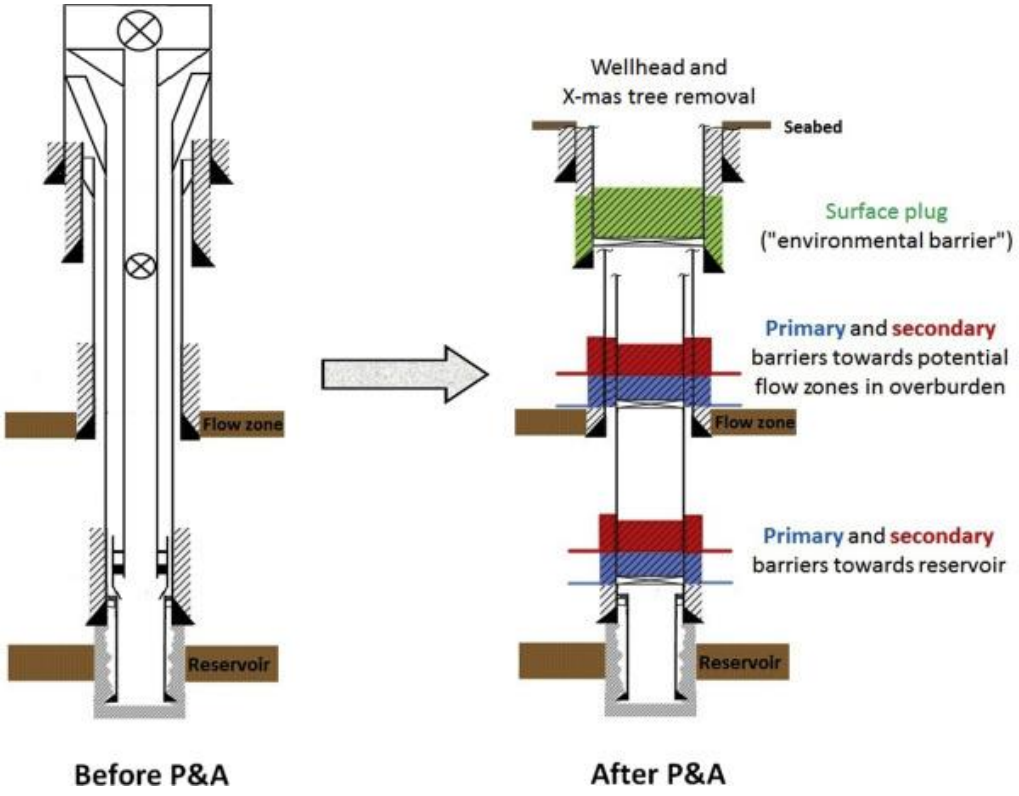

Figure 1.3 P&A of a well [9]

Figure 1.3 showcases the required barriers for a permanent plug and abandonment operation, where the primary barriers are colored in blue and the secondary barriers are colored in red. There are no specifications as to what the plugging material shall be, but there are requirements for the characteristics it should have. As can be observed in figure 1.3, the primary cement which lays outside the casing string may be used as a barrier element in the permanent barrier if it is qualified through logging or other means. This cement will over the course of the well-life experience a multitude of external forces which may impact the integrity or strength of the cement, which may ultimately lead to it being unsuitable to seal the well in the eternal

perspective. The new cement used during P&A will also experience similar disturbances and thus may fail in the same way.

According to NORSOK D-010 well integrity is defined as "*application of technical, operational and organizational solutions to reduce risk of uncontrolled release of formation fluids throughout the life cycle of a well*". Additionally, it states some characteristics which cement should exhibit: [1]

- Provide long term integrity
- Impermeable (or sufficiently low permeability)
- Non-shrinking
- Able to withstand mechanical loads/impact
- Resistant to chemicals/substances (H_2S, CO_2 and hydrocarbons)
- Ensure bonding to steel
- Not harmful to the steel tubulars integrity

These characteristics are required to ensure solid well integrity and to minimize the problems occurring from a well. Despite this, several surveys from different countries around the world show that cement failure not only occurs but is one of the major reasons for well integrity failure. The main purpose of maintaining well integrity is to prevent accidents from happening. Loss off well integrity could in the worst-case lead to loss of lives or major damage to environment, and very often it leads to high costs in remedial work. A study performed in the Gulf of Mexico (GOM) states that about 15% of primary cement jobs fail, which leads to remedial work at an estimated cost of $450 million annually. [2]

One of the major failure modes which can occur due to a poor primary cement job is the presence of Sustained casing pressure (SCP). SCP disregards pressure buildup due to temperature fluctuations and induced pressures and is defined as the measurable pressure in the casing that rebuilds after pressure has been bled down. It originates from gas leakage which often occurs due to a poor primary cement job. This is highly problematic as it makes intervention activities harder and can significantly shorten the life of the well. [10] Figure 1.4 shows the number of wells experiencing SCP vs age of wells from a sample size of roughly

22000 wells. From the figure one can observe that approximately 45%, or 8000-11000 of the surveyed wells have issues with SCP and that the trend increases with the age of the well.

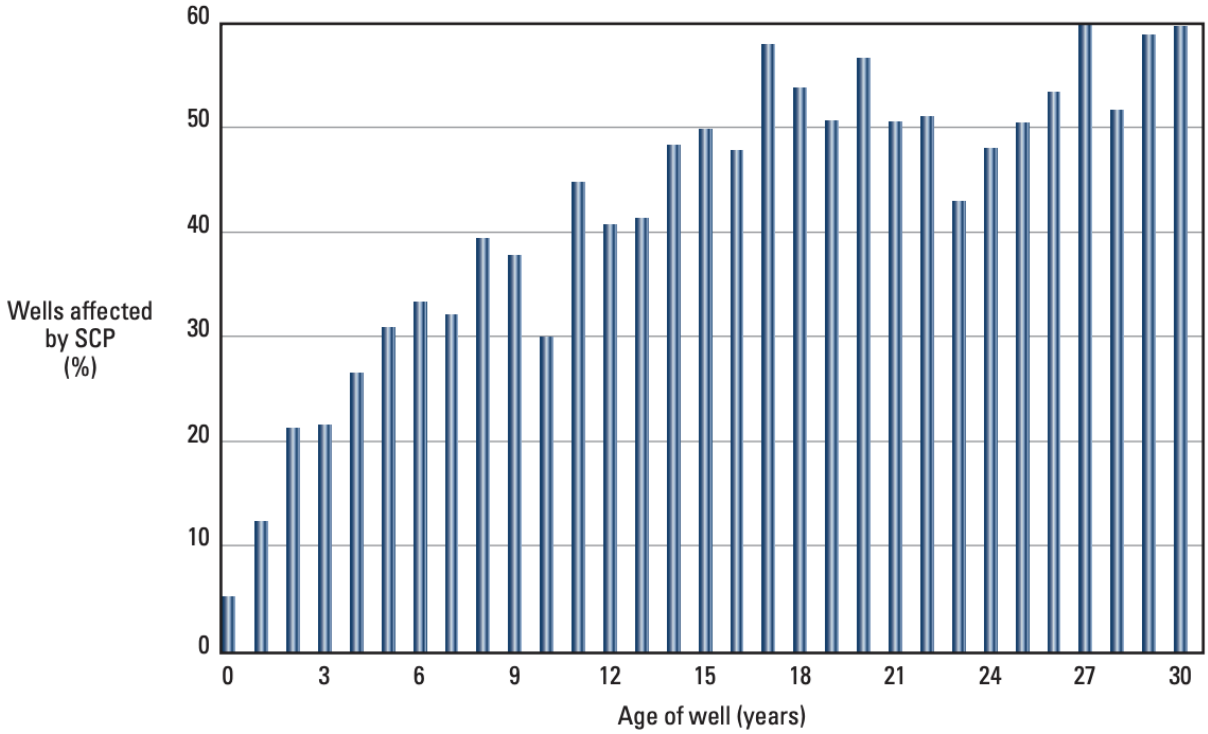

Figure 1.4 SCP vs age of well GOM[2]

In a similar study the Petroleum Safety Authority (PSA) performed a survey on the Norwegian Continental Shelf (NCS) of 406 wells with a representation of both production and injection wells which varied in age. It is worth noting that P&A wells were not included in the survey. The study found that 75 of the wells had integrity failure, issue or an uncertainty of some kind. Figure 1.5 illustrates the number of wells with integrity issues and the element of which causes the well integrity problem. From the figure one observes that the majority of integrity issues stem from the elements: Tubing (39%), Annular safety valve (ASV) (12%), Cement (11%) and Casing (11%). Amongst the casing issues reported, casing collapse was one of them. A failed or poor cement bond may cause a gas leakage leading to SCP which can attribute to this happening, but it is also possible to collapse casing due to tubing leak. Leaks likely along cement bond or through micro annulus were also reported, showcasing poor primary cement jobs.[3]

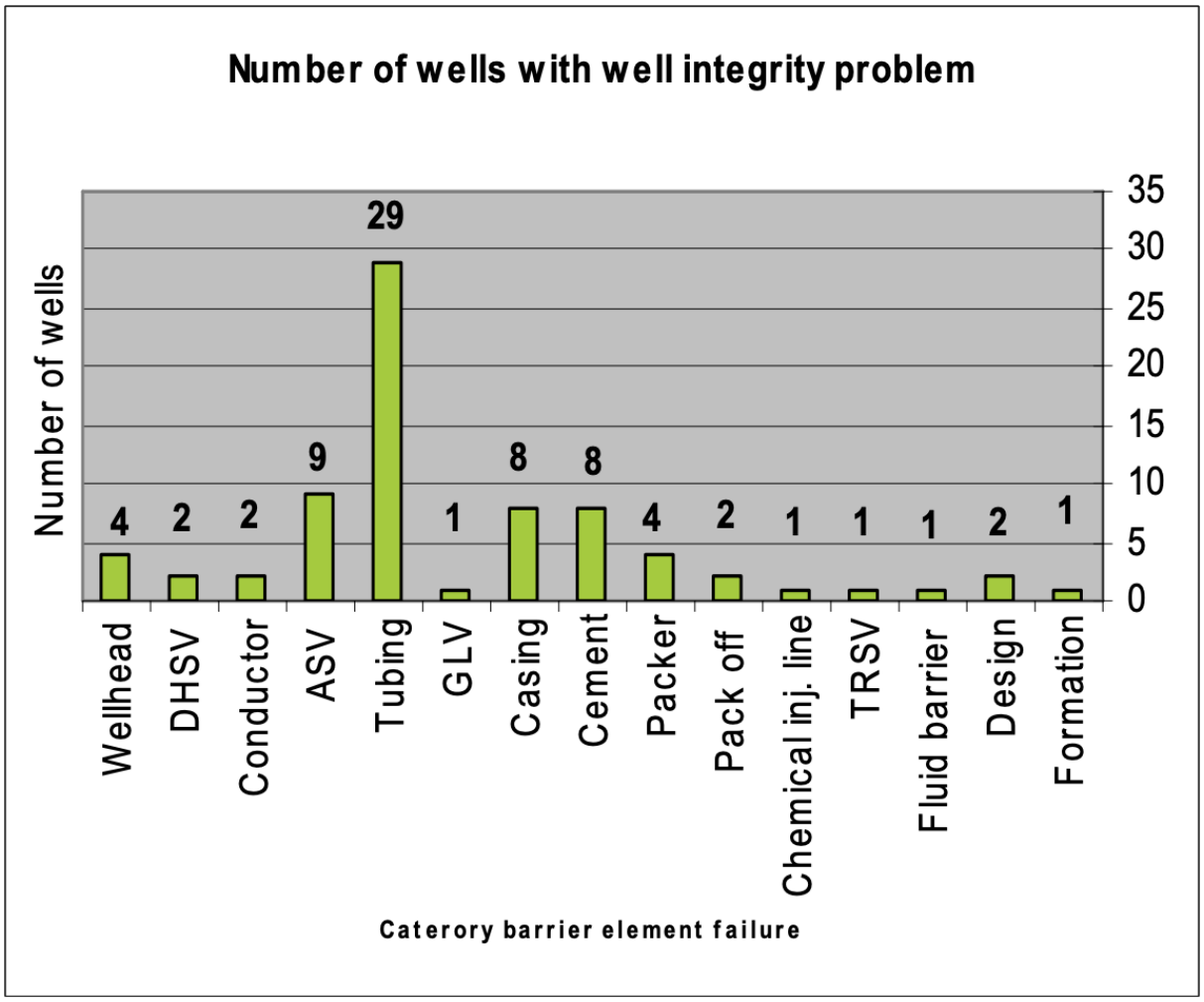

Figure 1.5 Well integrity issues NCS[3]

Another study was performed with data from Energy and Utilities Board (EUB) in Alberta, Canada. The study was performed to assess potential for CO_2 leakage through wells and it was discovered that around 4,6% of the approximate 315000 wells examined have either surface casing vent flow (SCVF) or gas migration. The study established that the vast majority of the incidents where this occurred were in shallow depths, and it concluded that one of the main causes was the poor cement quality at the upper part of the well.[4]

In another study regarding well integrity with data gathered from around the world, information was gathered from an online database collated by Department of Environmental Protection (DEP) which contains data from oil and gas wells in Pennsylvania. The study states that of 3533 individual wells examined, 85 out of the 91 wells which experienced some sort of integrity or barrier issue, experienced cementing or casing failures.[5]

As these surveys strongly indicate, the current cement slurry composition and the way the environmental factors affect the cement is prone to failure, which is associated with high remedial costs and well integrity issues. From the studies, there are various random effects which affects the cement, but one can deduce that the underlying issue lies with the current cement slurry composition. Improving on the current cement slurry would be beneficial if the improvements made are great enough to substantially lower the risk associated with cement failure.

1.2 Problem formulation

With the current cement slurry formula being sub-optimal for the purposes of which it is being used, improving it may be beneficial. In the recent years, the documented nanotechnology research results in the oil and gas sector have shown improved performances in drilling fluid, cement and enhanced oil recovery. To solve conventional engineering problems which the readily available technology of the day struggles with, the application of nanotechnology might prove to be an efficient and cost-effective solution to these problems. However, the researches in the petroleum industry is ongoing and is not fully developed for the application yet. Therefore, this thesis is designed to look at the effect of nanoparticles and other additives on G-class cement and will address issues such as:

- How will various nanoparticles affect the uniaxial compressive strength, modulus of elasticity, Young's modulus, resilience and water absorption of the cement?
- How does the effect of nanoparticles vary with varying water to cement ratio?
- How does different concentrations of the same nanoparticle change the cement properties?
- How will different types of elastomers affect the UCS, modulus of elasticity, Young's modulus and resilience of cement?
- How will nanoparticles affect the cement when it is combined in a hybrid mixture compared to each nanoparticle's own effect?
- What are the effects of MWCNT with a COOH group compared to MWCNT without a COOH group?
- How will the addition of a certain nano-system affect the leakage through the cement?

- How will the addition of a certain nano-system affect the cement properties in a high temperature environment?
- How will the addition of a certain nano-system affect the rheological properties of the cement slurry?
- How will the addition of a certain nano-system affect the heat development of the cement?

1.3 Objective

The primary objective of this thesis is to investigate the questions raised in chapter 1.2, which will be done through experimental work. In a more detailed overview, this thesis also aims to go through;

Literature review:

- Portland cement
- Hydration process of Portland cement
- Nanotechnology
- Application of nanoparticles in the petroleum industry

Examine the effects of the following nanoparticles:

- nano-SiO_2
- MWCNT-COOH
- nano-TiO_2
- nano-Fe_2O_3
- MWCNT
- nano-Al_2O_3
- nano-ZnO

With respect to varying properties such as

- Uniaxial compressive strength
- Modulus of elasticity (M)
- Young's Modulus
- Resilience
- Water absorption

Investigate the effects of elastomers:

- Untreated silicone rubber
- Acid treated silicone rubber
- Silicone rubber debris

Define a suitable system and further investigate:

- Effects of a high temperature environment
- Leakage
- Heat development
- Rheology

Modeling

- Empirical UCS vs compressional wave velocity modeling

1.4 Research methods

Figure 1.6 presents an overview of the theoretical work performed in this thesis, while figure 1.7 provides an overview of the experimental work.

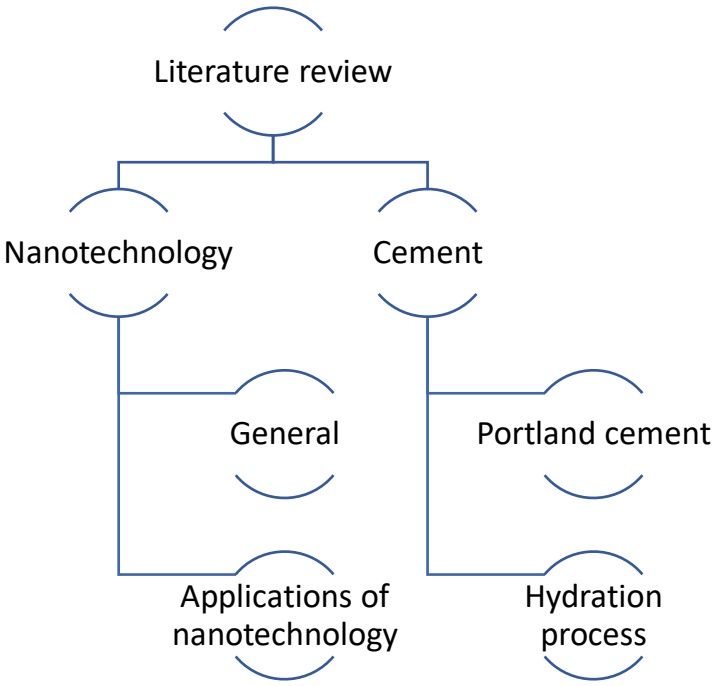

Figure 1.6 Contents of theoretical work

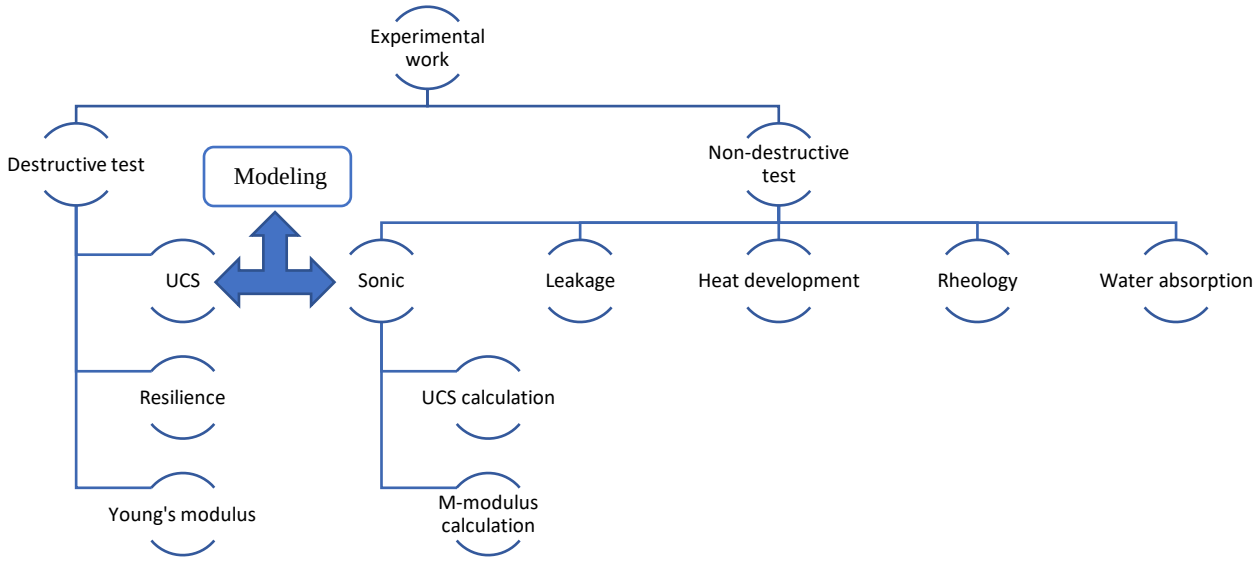

Figure 1.7 Contents of experimental work

2. Literature study

The following chapter is a literature review of cement, the properties of cement and some applications in the life cycle of oil and gas wells. Chapter 2.3 is a literature review of nanotechnology and some applications of nanoparticles in cement.

2.1 Cement and classification

2.1.1 Portland Cement

In terms of quantity produced, Ordinary Portland Cement (OPC) is possibly the most abundant material manufactured. OPC has several uses in the construction industry as it is used in the production of concrete and in terms of quantity produced, it is also the most paramount oil-well binding material and it is used in nearly all wells. [2]

The reason for its widespread usage is its availability, strength development, cost and flexibility of use. It sets relatively fast and quickly gains strength, combine this with its good bonding properties and it makes for an excellent building material. It also has the ability to set in wet conditions, which makes it usable for well cementing applications. It does, however, also have its drawbacks such as poor mechanical properties (ductility and flexural strength) and limited resistance to chemical components.

Production of Ordinary Portland cement is done by pulverizing the clinker, which is the burned (calcined) material that exits the rotary kiln in the cement plant. It primarily consists of hydraulic calcium silicates, calcium aluminoferrites or calcium aluminates. The clinker must contain appropriate amounts of silica, calcium, alumina and iron. Therefore, frequent chemical analysis of the material is performed during manufacturing to ensure high quality and uniformity. The term “Ordinary” in OPC specifies that the clinker comes from a rotary kiln and that the ingredients are correctly proportioned. [2]

2.1.2 Classification

To produce the mixture for Portland cement clinker, two types of raw materials are required; argillaceous and calcareous materials. Argillaceous materials contain silica, iron oxide and alumina whilst calcareous materials contain lime. Natural calcareous materials include limestones, shell deposits, coral and "Cement rock" which are the ones of highest importance. Artificial materials can also be used such as precipitated calcium carbonate or other waste products from industrial processes. Natural argillaceous materials include shales, clays, mudstone, volcanic ashes, schist and alluvial silt with the most important artificial ones being fly ash from coal fired power works or slag from steelworks blast furnaces. The properties which the finished Portland cement exhibits are determined by the mineralogical composition of the clinker, in which the main oxides make up about 95% of the composition. Table 2.1 displays the concentration of various oxides in a classic Portland cement clinker.[2]

Table 2.1 Mineralogical composition of classic Portland cement clinker

Oxide Composition	Cement Notation	Common Name	Concentration (wt%)
$3CaO \cdot SiO_2$	C_3S	Alite	55–65
$2CaO \cdot SiO_2$	C_2S	Belite	15–25
$3CaO \cdot Al_2O_3$	C_3A	Aluminate	8–14
$4CaO \cdot Al_2O_3 \cdot Fe_2O_3$	C_4AF	Ferrite phase	8–12

When OPC is used for building or other construction purposes, it is only exposed to atmospheric conditions which is relatively unproblematic for the cement. In a well however, the conditions are wildly different and thus special Portland cements are manufactured for the purpose of well cementing. To differentiate between the types of cement and to provide consistency in cement properties among different cement manufacturers, several institutions have established various classification systems and specifications. The American Society for Testing and Materials (ASTM) created the C 150 classification system which is the "Standard Specification for Portland Cement". The American Institute of Petroleum (API) created the API Spec 10A which is the "Specification for Cements and Materials for Well Cementing". These two systems are the best-known systems, and the latter has been adopted by ISO into Standard 10426-1. Shown in table 2.2 below is the different classifications from API and ASTM.[2]

Table 2.2 API&ASTM Classification of cement

API Class	ASTM Type	Typical Potential Phase Composition (wt%)				Typical Blaine Fineness (cm^2/g)
		C_3S	β-C_2S	C_3A	C_4AF	
A	I	45	27	11	8	1,600
B	II	44	31	5	13	1,600
C	III	53	19	11	9	2,200
D	–‡	28	49	4	12	1,500
E	–	38	43	4	9	1,500
G	Nominal II	50	30	5	12	1,800
H	Nominal II	50	30	5	12	1,600

The requirements for the quality and predictability of the cement used in wells are harsher compared to the ones used for construction. This partly because for well applications the conditions the cement is going to be exposed to varies greatly with respect to both temperature and pressure, and because the cement requires more consistent and predictable performance from batch to batch with regards to the potential supplements that are later added to the cement. The API classification system deals mainly with the classification and specification of cement used in wells. It is divided into eight categories, A through H, arranged after the temperature and pressures of which they are exposed to.[2]

Table 2.3 Usage and availability of different API classifications of cement

API Class	Requirements and Availability
A	No special properties required. Available in grade O.
B	Moderate or high sulfate resistance required. Available in grades MSR and HSR
C	High early strength required. Available in grades O, MSR and HSR
D, E and F	Used for moderately high pressure and temperature. Available in grades MSR and HSR
G and H	Basic well cement. Available in grades MSR and HSR

MSR = Moderate Sulfate Resistance
HSR = High Sulfate Resistance
O = Ordinary

Usage of classes D, E and F are severely limited as during the production of said cements, additives for processing purposes may be used. The additives used in the production of these classes are currently outdated, making newer additives more efficient and more stable. During

production of classes G and H, no additives are allowed. This is to ensure no interference of substances when at a later stage adding cement additives, such as retarders or accelerators, to obtain desired cement properties.

2.2 Hydration process

Portland cement is what is called a hydraulic cement, and these types of cement set and develop strength as a result of hydration. The hydration process consists of chemical reactions between the cement mixture and water. This happens because the compounds present in the cement mixture are anhydrous, meaning that they are decomposed when in contact with water and will as a result form hydrated compounds. The solubility of the hydrated compound is lower than that of the original anhydrous compound, and thus, complete hydration saturation will eventually occur. For Portland cement, it is shown that a volumetric shrinkage will occur during the hydration process. [2]

There are four main components of Portland cement; C_3S, C_2S, C_3A and C_4AF. These structure different hydration products and demonstrate different hydration kinetics. Due to this fact, the research regarding cement hydration has mainly focused on the hydration of each individual clinker phase in water. A table displaying the approximate weight percent of each of the components are seen in table 2.1.

The most abundant phase, constituting 70-90 wt% of the Portland cement, is the silica phase. The main component consisting of 55-65wt% is C_3S whereas 15-25wt% is comprised of C_2S. Hydration of these silica phases therefore plays an important role in the properties of the cement. The resultant hydrated compound from the hydration process of both these phases are calcium silicate hydrate and calcium hydroxide. Shown below are the idealized chemical equations; [2]

$$2C_3S \rightarrow C_3S_2H_3 + 3CH$$
$$2C_2S + 4H \rightarrow C_3S_2H_3 + CH$$

Even though the resultant hydrated compound from the chemical reaction of both these components are the same, the function of the hydration for both of these are different. The resultant compound is often referred to as C-S-H gel. The principal reason for setting and early

strength development is the hydration of the C_3S present, whilst the hydration of the C_2S mainly contributes to the final strength of the hardened cement. As the mechanism of the hydration of these phases are very similar, the Portland cement hydration behavior is often analog to C_3S hydration. [2]

The hydration rate of C_3S can be measured by heat release as it is an exothermic process and it is defined in five different stages:

- Preinduction period
- Induction period
- Acceleration period
- Deceleration period
- Diffusion period

From figure 2.1 one can observe the evolution of heat in the different stages of the cement hydration.[2]

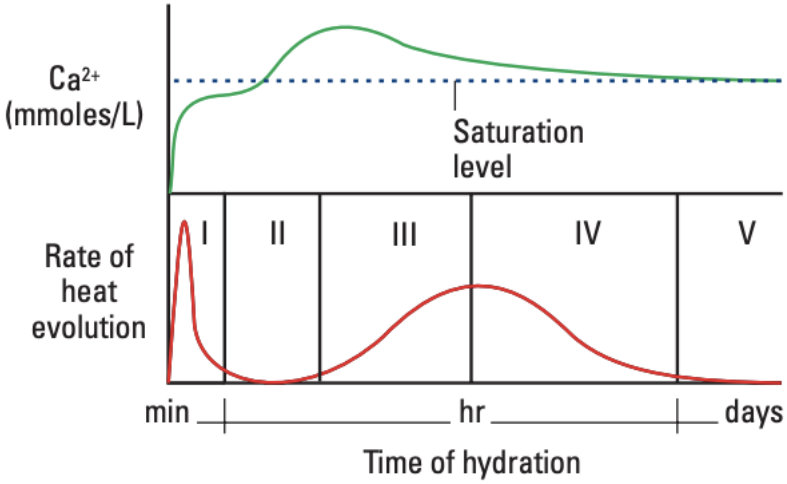

Figure 2.1 Evolution of heat vs time of hydration[2]

Stage I: The Preinduction period:

Immediately after the water is added to the cement mix the pre-induction period starts. The period is active during mixing and only a few minutes after mixing is complete. Addition of water to the cement powder starts a fast hydration reaction between the C_3S and the water. During this phase, the first layer of C-S-H will precipitate on the surface. It can be observed as a large exothermic reaction on figure 2.1.[2]

Stage II: The induction period:

During the induction period, relatively little hydration can be observed. The release of heat is nearly non-existent which translates to very little hydration and slow precipitation of additional C-S-H. When the mixture is critically supersaturated, precipitation of calcium hydroxide takes place, thereby resuming the hydration at a higher rate and marking the end of the induction period. The length of the period varies with temperature, but at atmospheric conditions it lasts a few hours.[2]

Stage III: The acceleration period:

During the acceleration stage the initial setting occurs. This period contains the interval with the most rapid hydration as can be seen in the heat signature in figure 2.1. During stage III calcium hydroxide crystalizes from the solution whilst the C-S-H phase deposits into the remaining water filled phase leading to a network to be formed which causes the mix to start developing strength.[2]

Stage IV: The deceleration period:

As this network continues to grow, the porosity of the system decreases. The end result of this is a network where water transportation to the C-S-H phase is no longer possible, and the hydration rate decelerates which can be observed in the heat signature in figure 2.1. The combined duration of stage III and IV at atmospheric conditions can be several days. [2]

Stage V: The diffusion period:

During the diffusion period, hydration continues but at a very relaxed pace. This can be observed on figure 2.1. The hydrated products become denser, and as a result the strength increases. The duration of stage V at atmospheric conditions are indefinite, but no major structural changes takes place during this period. [2]

2.2.1 Effect of temperature on hydration process

While there are various aspects affecting the hydration of Portland cement, one of the major factors is the effect of temperature. This parameter strongly affects the rate of hydration, the morphology-, nature and stability of the hydration products. When the temperature in the area of which the hydration occurs is elevated, the hydration of the cement is accelerated. This

shortens the duration of the induction and setting period and increases the rate of hydration of the setting period substantially, but often reduces ultimate strength and degree of hydration upon extended curing as can be observed in figure 2.2.

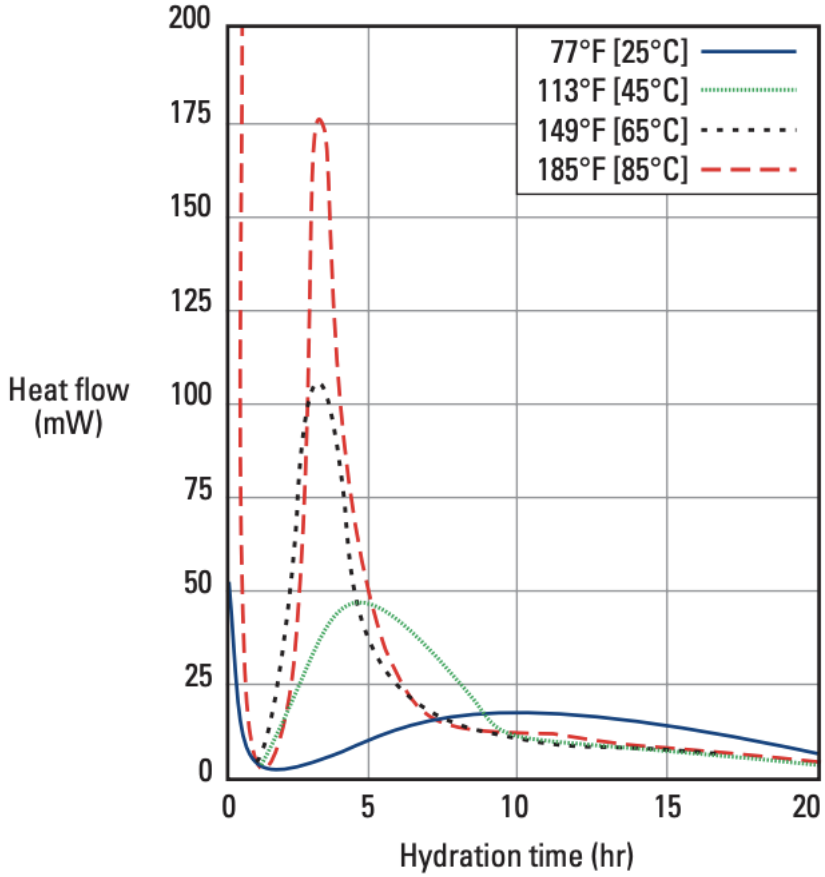

Figure 2.2 Temperature effect on hydration [2]

For degrees below 40°C the resultant products created by hydration will be the same as those created at atmospheric conditions, whereas at higher temperatures (T>40°C) the morphology and microstructure of the CSH phase will change. As a result of these changes, the material becomes more fibrous, and polymerization of silicate is observed at a higher degree. For temperatures exceeding 110°C which cannot be observed on figure 2.2, the formation of crystalline calcium silicate hydrates will occur due to the fact that the CSH phase is no longer stable. As a result of this, the matrix may shrink which results in decreased compressive strength and increased permeability of the set cement.[2]

2.3 Nanotechnology

A material can be categorized as a nanomaterial if one of its dimensions is less than 100nm (nano = one billionth = $*10^{-9}$). Due to its versatility, it continues to gain traction in areas of academics as well as applied research. With the given microscopic dimensions, nanomaterials display a large surface area to volume ratio compared to its larger counterparts, which gives it different chemical and physical properties.

The term "nanotechnology" refers to the practice of manipulating these small structures to create viable solutions to technical challenges in variable industries ranging from biomedicine to construction to the Oil and gas industry. Whilst the use and variation of materials from the different industries varies greatly, the prevalent concept is that a more functional and superior organization of matter is achieved through an intelligent design by the use of nanomaterials. The increased surface area creates more ways for other materials to bond and makes for a more lightweight and stronger material.[11]–[13]

The majority of the synthetically produced nanomaterials are nanoparticles. To meet the required design specifications, various production processes have been developed. To achieve the desired size dependent particle features, production and reaction conditions are critical. There are two main methods for producing synthetic nanoparticles; "top down" and "bottom-up". The strategy of "top-down" is based on reducing larger source material through mechanical crushing. The crushing involves several different milling techniques, and is a staged process where the basic material is coarsely ground and consequently finely ground. The top-down strategy is applied for production of nanomaterials of ceramics and metals. The "bottom-up" strategy works the opposite way and is based on building the nanoparticle from smaller particles using chemical processes. More accurately, it is based on physicochemical principles of atomic or molecular self-organization. The bottom-up strategy allows for more complex nanomaterials with more control over the dimensions and specifications of the resultant material. From figure 2.3 one can observe the principles of both the aforementioned methods.[14]

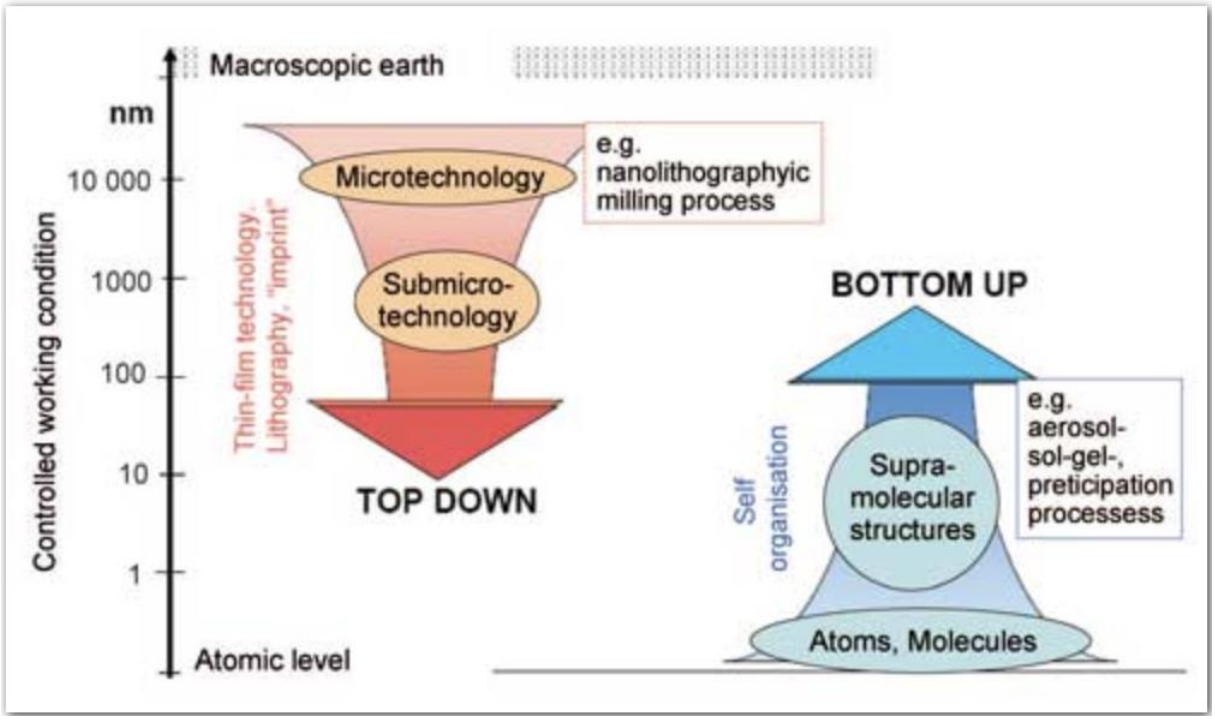

Figure 2.3 Top-down and Bottom-up strategies for producing nanoparticles[14]

2.3.1 Application of nanotechnology in the oil and gas industry

As nanomaterials continues to grow more useful in various industries, its benefits have also reached the oil and gas sector. Application of nanotechnology contributes to smarter and more efficient solutions to the technical challenges at hand and provides solutions to problems which conventional technology currently struggles to solve. Use of nanomaterials in the drilling fluid can improve filtration and rheological properties of the fluid whilst ensuring a thin mud cake to prevent differential sticking. According to a study performed, the mud cake thickness produced by the nano-fluids were less than 1mm thick and tightly packed, which prevents differential sticking and fluid loss to the formation.[15] Addition of nanomaterial to the fracturing fluid could also prove to be beneficial in ensuring a successful fracturing operation. Furthermore, during displacement of one fluid to another, cement-spacers which were formed of nano-emulsions were found to efficiently clean the bore walls of oil based mud (OBM) whilst reversing the wettability of the cleaned surface to ensure good cement bonding.[16] Additionally, the application of nanotechnology proved to be helpful in the areas of corrosion inhibition, logging operations, control over formation fines during production, enhanced oil recovery, viscosity reduction of heavy oil and hydrocarbon detection.[17] From figure 2.4 one can observe the various applications of nanotechnology to different stages of the oil production process.

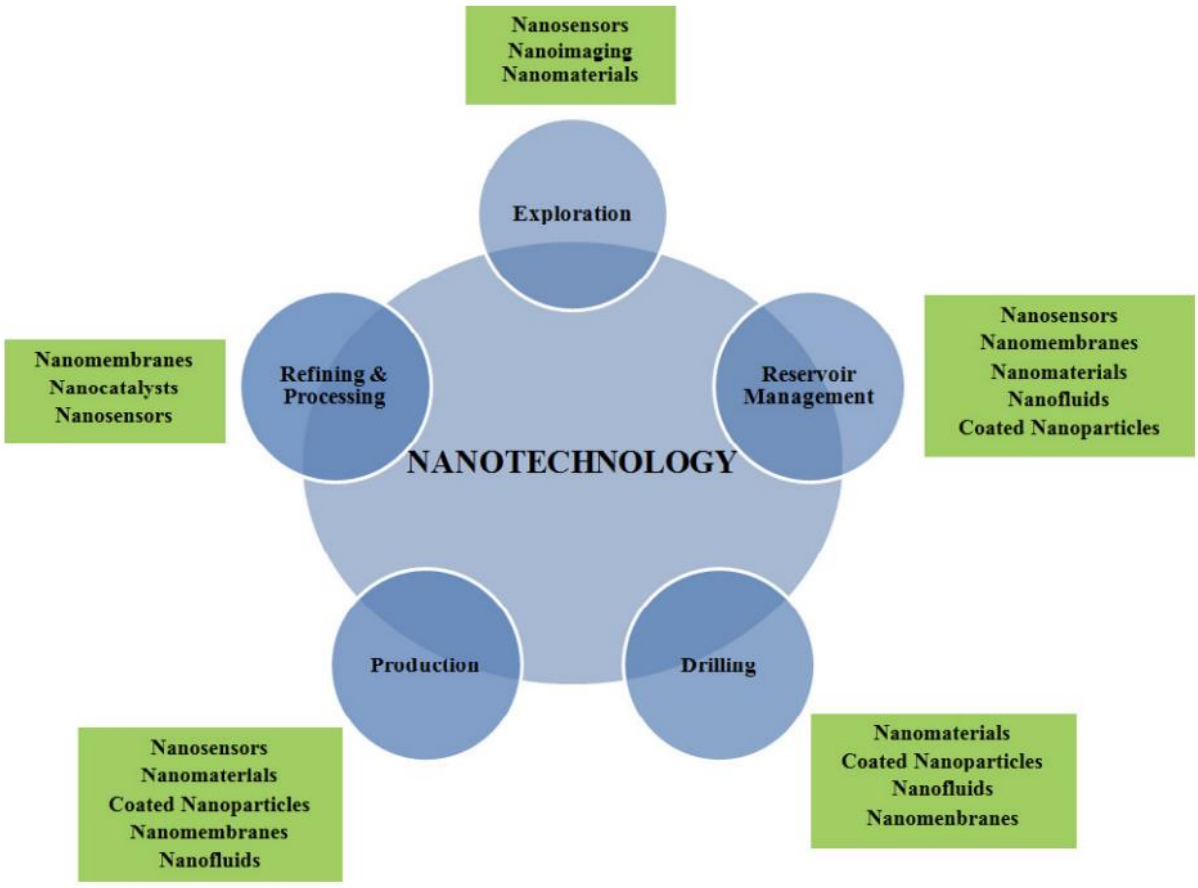

Figure 2.4 Application of nanotechnology to different stages of oil production [18]

2.3.2 Carbon nanotubes

Carbon nanotubes (CNTs), which were discovered in 1952, have since attracted much interest in terms of research due to its unique chemical and physical properties. As can be deduced from its name, CNTs are a structurally built tube-like shape made out of carbon-material with a diameter ranging from a few nanometers to approximately 50 nanometers while the length of the tubes can be up to several centimeters long. There has over the years been developed several systematic methods for synthesizing CNTs. One of its distinct physical properties is its mechanical flexibility and strength, and its potential application in the oil and gas industry has therefore been widely studied. Carbon nanotubes can be divided into three categories, based on their physical structures; Single-Walled carbon nanotubes (SWNT), Double-Walled carbon nanotubes (DWNT) and Multi-Walled carbon nanotubes (MWCNT).[18] These structures are depicted below in figure 2.5.

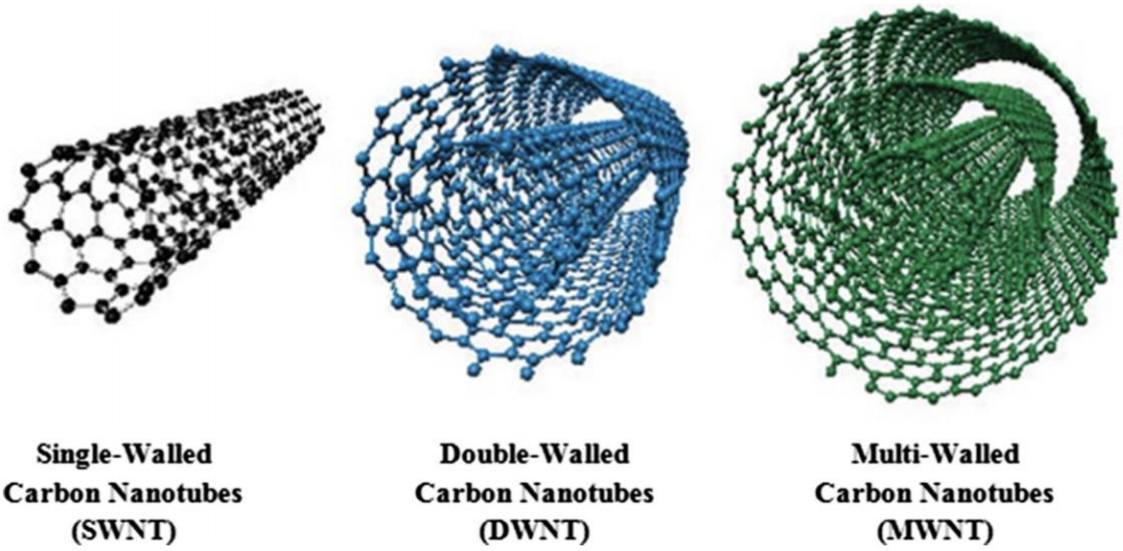

Figure 2.5 Categories of carbon nanotubes based on their physical structure[18]

For the purpose of this thesis, the effects of added muti-walled carbon nanotubes to different cement slurries will be analyzed with respect to changes in cement properties.

2.3.3 Specific applications of nanotechnology in oil-well cementing

As previously mentioned, the application of nanotechnology in the oil and gas industry has proved highly beneficial. The next sub-chapters will be covering specific studies regarding the application of nanotechnology to ascertain various specific desirable properties in oil-well cementing. The aforementioned properties may be an increase compressive or flexural strength of the cement, improved setting time or a more expeditious strength development.

2.3.3.1 Effect of nano-silica on compressive cement strength

Patil et al. (2012) [11] Studied the effect of adding nanomaterials to improve properties of cement. To prevent common cement issues like fluid loss to formation or gas migration through the cement, smaller sized elastomer particles, like latex, may be added to the cement. The addition of these particles even further imposes the importance of achieving early strength development to reduce the wait time on cement (WOC) and be able to continue drilling as soon as possible. Addition of the aforementioned particles tend to reduce the early strength development, which was counteracted by the addition of nano-silica particles to the cement system.

Using API procedures and standards, several cement slurries of API H-class cement with varying concentration of nano-silica were tested with respect to different properties. The study found that addition of nano-SiO_2 improves mechanical properties of the cement, and especially increases compressive strength. It increases early strength development to reduce WOC time and to some extent it also helps with fluid loss. It was found to be applicable in a range of temperatures, which allows for use in various different scenarios. The silica was also found to be synergetic in the cement, meaning it easily can be combined with other additives to achieve required cement properties. Below is a figure showcasing the effect the nano-silica had on the compressive strength development. [11]

TABLE 1—EFFECT OF NANOSILICA ON COMPRESSIVE STRENGTH[a]

Latex (gal/sk)	Silica	Retarder (gal/sk)	Time to 500 psi (hr:min)	UCA Strength Rate of Strength Development (psi/hr)	24-hr Strength (psi)
1.5	0	0.05	23:05	172	690
1.5	Micron sized silica	0.05	21:45	160	610
1.5	Nanosilica	0.05	13:29	460	2203

[a]Premium Class H cement, defoamer 0.05 gal/sk, stabilizer 0.2 gal/sk, dispersant 0.143 gal/sk, density 16.4 lbm/gal, Yield 1.1 ft^3/sk.

Figure 2.6 Effect of nano-SiO2 on compressive strength[11]

From figure 2.6 one can clearly observe the massive impact the addition of nano-SiO_2 has on the compressive strength of the cement. Inclusion of the nanoparticle increases the 24 hr compressive strength by roughly 3 times compared to the control group, from 690 psi to 2203 psi, which corresponds to an increase in strength development from 172 psi/hr to 460 psi/hr. This improved strength development is highly beneficial, and it is found in the study that this effect persists even when the temperature is changed drastically. The study also found that the addition of the nano-silica reduced the fluid loss from 52 ml/30min to 34 ml/30min. [11]

2.3.3.2 *Carbon nanotubes effect on mechanical performance on properties of cement composites*

Gillani et al. (2017) [19] studied the effect of adding various concentrations of multi-walled carbon nanotubes to a concrete mixture. A huge amount of concrete is manufactured and used every year, and this number can be greatly reduced by improving the mechanical and durability properties of the concrete. One way of achieving these enhanced properties is the addition of dispersed MWCNTs to the composite matrix.

The study includes three different samples, one control sample with no addition of MWCNT, one containing 0,05wt.% MWCNT and additionally one containing 0,1wt.% of MWCNT. The samples used ordinary Portland cement of type A (API) which corresponds to ASTM type I. The dispersion of MWCNT was achieved using bath sonification in the presence of modified acrylic based surfactant. Firstly, the ingredients were mixed in dry conditions before being poured into cylinders, where they stayed for 24hr. Afterwards, the samples were cured in water up until the day the samples were being tested. [19]

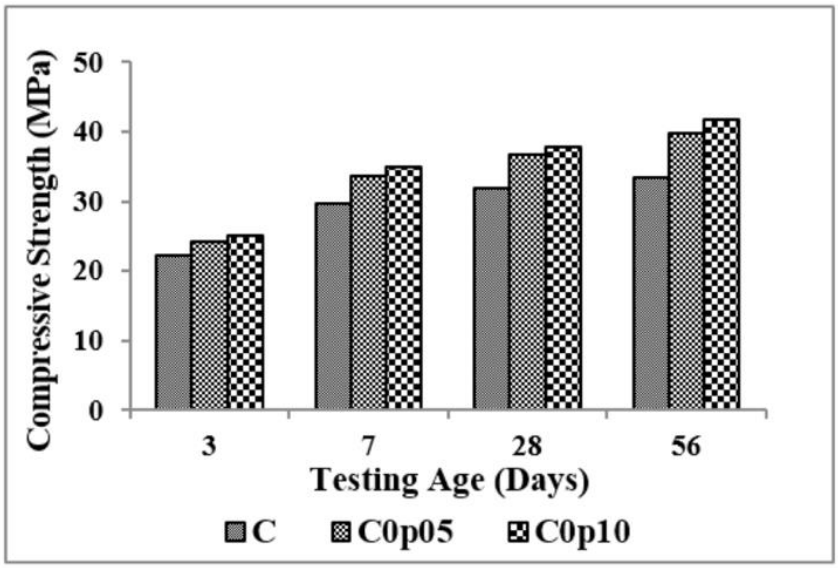

Figure 2.7 Strength of samples containing MWCNT [19]

Figure 2.7 displays some of the results found in the study where C means no addition of MWCNT, C0p05 means 0,05wt.% and C0p10 means 0,1wt.% of MWCNT added. The samples were tested after 3, 7, 28 and 56 days and the tests conducted were to inspect the splitting tensile strength, modulus of rapture and compressive strength. The greatest increase in splitting tensile strength is observed at 56 days with 0,05wt.% of MWCNT added. The enhancement is around 26% compared to control sample whereas the 0,1wt.% had an increase of 18%. For the modulus of rupture (flexural strength) the same results are established. The greatest increase in flexural strength was observed from the addition of 0,05wt.% MWCNT whilst the higher concentration MWCNT showed a smaller increase compared to the control sample. For compressive strength however, the results change. While addition of MWCNT of any concentration increases compressive strength, the greatest increase is observed by the addition of 0,1wt.% MWCNT at roughly 25% higher compressive strength compared to the control mix. The addition of

0,05wt.% of MWCNT causes the compressive strength to increase by approximately 19% compared to control sample.[19]

The study found that inclusion of a small amount of MWCNT in the concrete matrix leads to major improvements in the mechanical properties of the resultant concrete. The addition of MWCNT proved to be beneficial with regards to all measured mechanical properties, however the fraction added varied the results. For splitting tensile strength and flexural strength the addition of a smaller amount of MWCNT is favorable while for increase of compressive strength adding a larger fraction proved to be more beneficial.[19]

2.3.3.3 Effect of nano materials on setting time, consistency and compressive strength of cement mortar

Carmichael et al. (2012)[20] conducted a study to investigate the effects nano-materials would have on the setting time, consistency and compressive strength of cement mortar. Reducing the setting time whilst retaining the consistency of the cement slurry may prove beneficial, and thus this study was performed to investigate this further.

A total of 18 mixes were made by replacing 0, 10, 20, 30, 40 and 50% of the cement with nanomaterials. The nanomaterials used in this study were nano-cement, nano-silica fume and nano-fly ash. Preparation of nano-cement was done by using Ordinary Portland cement ground down to nano-size (less than 100nm). The same procedure was applied in the making of nano-fly ash and nano-silica fume.

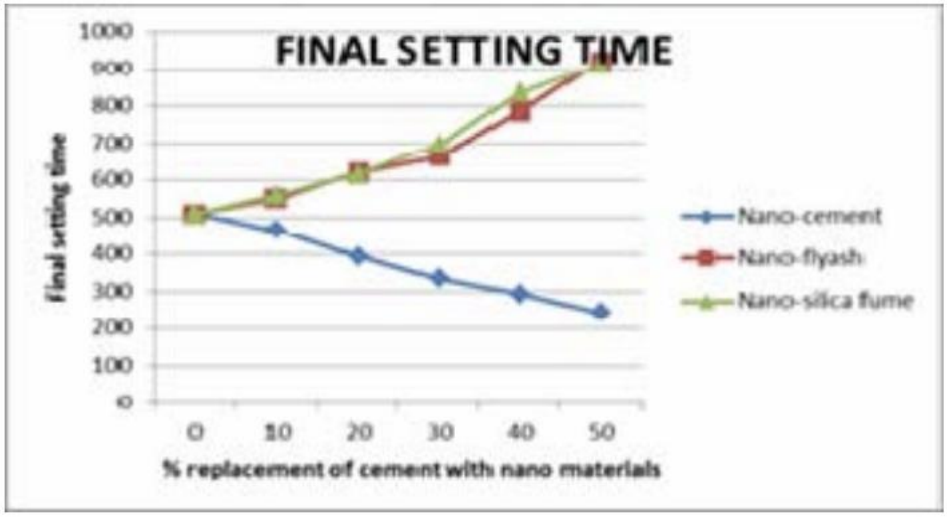

Figure 2.8 Final setting time of cement with varying concentration of nanomaterials[20]

As can be observed from figure 2.8, the final setting time is drastically reduced with increasing concentration of nano cement, but it increases with addition of nano-fly ash and nano-silica fume. By addition of nano-cement the final setting time is more than halved, from 510 minutes with no nano replacement to 245 minutes at 50% replaced with nano-cement. The study also found that there were no/insignificant changes in the consistency of the cement paste.

2.3.3.4 Effect of Iron-oxide on the properties of cement

Vipulanandan et al. (2015) [21] conducted a study to investigate the effects of adding iron oxide nanomaterial to cement. This study was performed as a result of the findings from several studies on the Macondo incident which found that cement failures were the major cause for blowouts. A strong cement sheath and a cementing process which can be properly monitored and tracked is an important factor in ensuring cement integrity during the life of the well.

Whilst conducting this study, class H cement was used to investigate the impact nano-Fe_2O_3 would have on the compressive strength, piezoresistive behavior, density and electrical resistivity. The samples were tested after 1 and 28 days of curing. The study uses resistivity and change in resistivity to quantify sensing properties of the cement, which was used for its many benefits such as accuracy, easy test procedure, non-destructive testing and the ability to monitor long term behavior of cement in practice.

NanoFe_2O_3 (%)	Curing time (days)	σ_f (MPa)	ε_f (%)	Ei (MPa)	p_o	q_o	R^2
0	1	10.9 ± 2	0.28 ± 0.01	967 ± 21	0.034 ± 0.01	0.36 ± 0.02	0.99
	28	19.3 ± 3.5	0.21 ± 0.02	1936 ± 20	0.160 ± 0.03	0.87 ± 0.04	0.99
1	1	13.7 ± 2.6	0.20 ± 0.01	1239 ± 28	0.095 ± 0.001	0.54 ± 0.03	0.99
	28	27.0 ± 3.2	0.20 ± 0.01	2479 ± 38	0.097 ± 0.002	0.57 ± 0.03	0.99

Figure 2.9 Compressive stress-strain model parameters for nano-Fe2O3 modified smart cement[21]

The addition of nano-Fe_2O_3 increased the average compressive strength of the cement regardless of concentration added and curing time compared to the control sample containing no nanomaterial. After 1-day curing, the addition of 0,5% NanoFe_2O_3 increased the average compressive strength by 7%, whereas the addition of 1% NanoFe_2O_3 increased the strength by 26%. These effects grow larger with additional curing time, where after 28 days of curing the same amounts increased the average compressive strength by 32% and 40% respectively.

Furthermore, the study found that the modulus of elasticity was increased by the addition of 1% NanoFe_2O_3 by 29% for 1 day curing and 28% for 28 days of curing. Additionally, it found that the initial resistivity was sensitive to the amount of nano-Fe_2O_3 added, which means the amount of nano-Fe_2O_3 can be detected in the change of initial resistivity and can be a good indicator for quality control.

2.3.3.5 Effect of adding graphene oxide nanosheets to cement paste

LV et al. (2014) [22] conducted a study to work out the effects nanosheets made of graphene oxide would have on the properties of hardened cement paste with special emphasis on changes in compressive and flexural strength. Cement paste is the mixture of several hydration products which during hardening undergoes the conversion from soft paste to a hard solid. The resultant concrete exhibits high compressive strength but shows low flexural strength. The most common way to improve these properties is the addition of reinforcing materials or the reduction of water to cement ratio. The main issue with both of these methods is the fact that the resultant flexural strength increase is small. Previous research of graphene oxide nanosheets have shown that it is possible to significantly increase mechanical strength, especially flexural strength, by including these materials (in the paste) which is the reasoning behind this study.

For the purposes of this study, a Portland cement (spec Shengwei 42,5R) was used. The graphene oxide nanosheets were prepared as an aqueous dispersion which were later added to the cement paste mixture. Test were performed after 28 days according to GB/T 17671-1999, the Chinese national standard.

GO dosage (%)	Flexural strength (MPa)/increase (%)	Compressive strength (MPa)/increase (%)
0 (control sample)	8.84/100	59.31/100
0.01	10.86/122.9	66.51/112.1
0.02	11.52/130.3	72.48/122.2
0.03	12.66/143.2	76.31/128.6
0.04	12.57/142.1	79.72/134.5
0.05	12.56/142.1	79.06/133.3
0.06	11.43/139.3	79.86/134.7

Figure 2.10 Change in flexural and compressive strength with varying concentration of GO nanosheets[22]

As is clearly shown in figure 2.10, the flexural and compressive strength of the hardened cement paste is greatly increased by addition of graphene oxide nanosheets in the soft cement paste mixture. These results indicate that the maximum increase in flexural strength comes from a dosage of 0,03% GO nanosheets added with an increase of 143,2% whereas the highest increase of compressive strength is achieved at a GO dosage of 0,06% with an increase of 134,7%.

2.3.3.6 Effect of nano aluminum oxide and MWCNT on hardened cement paste

Gurumurthy et al (2014) [23] conducted a study to further investigate the effect of nanoparticles incorporated in hardened cement paste. As some nanomaterials can create bonding to the CSH and further increase the strength of the cement paste, this study aimed to investigate the effects MWCNT and nano-Al_2O_3 would have on the compressive and flexural strength of the hardened cement paste.

The study utilized ACC grade 43 OPC and the testing method is a slight variation of ASTM general standards. The nanomaterials were applied to the cement as an aqueous solution, where the MWCNTs were dispersed with the use of sonication and ethanol as a dispersant and the aluminum oxide was pre-dispersed using the sonication method in water only. The amount of added nano was fixed at 0,75 wt% of MWCNT and 1,0 wt% of Al_2O_3, with three separate samples being made; MWCNT only, aluminum oxide only and a mixture of both. The samples were left to cure in water for 28 days before testing commenced.

Addition:	Percentage increase in UCS:
MWCNT	36,13
Nano-Al_2O_3	24,11
Mixture	58,31

Figure 2.11 Increase in UCS per added nanoparticle [23]

As can be observed from figure 2.11, the addition of any of the chosen nanoparticles proved to be beneficial towards the desired strength increase of the cement. The addition of MWCNT and nano-Al_2O_3 enhanced the UCS by 36% and 24% respectively, but more interestingly the combination of the two had the greatest increase of 58%. It was also found that the addition of the nanoparticles had a remarkable increase on other parameters such as flexural strength, toughness and ultimate load. [23]

2.3.3.7 *Effect of nano zinc oxide on cement-based materials*

Nochaiya et al (2014) [24] investigated the effect of nano ZnO on the setting time, compressive strength and porosity of cement pastes. Previous research has determined that there are benefits with the addition of nanoparticles on cement, however the studies regarding the effect of zinc oxide nanoparticles are limited. This study aims to further investigate the effect nano-ZnO has on Portland cement paste.

For this study, Portland cement type I (API class A equivalent) was used for creation of the test specimen. Three different concentrations of zinc oxide nanoparticles were added to the cement mixture to examine the effect the varying concentrations would have. The samples were subjected to compressive tests at 3, 7, 28 and 90 days. Depicted below are some of the results obtained when studying the samples strength; 1Z contains 1 wt% ZnO, 2Z contains 2 wt% ZnO, 5Z contains 5 wt% ZnO and PC is the control sample with no nanoparticles added.

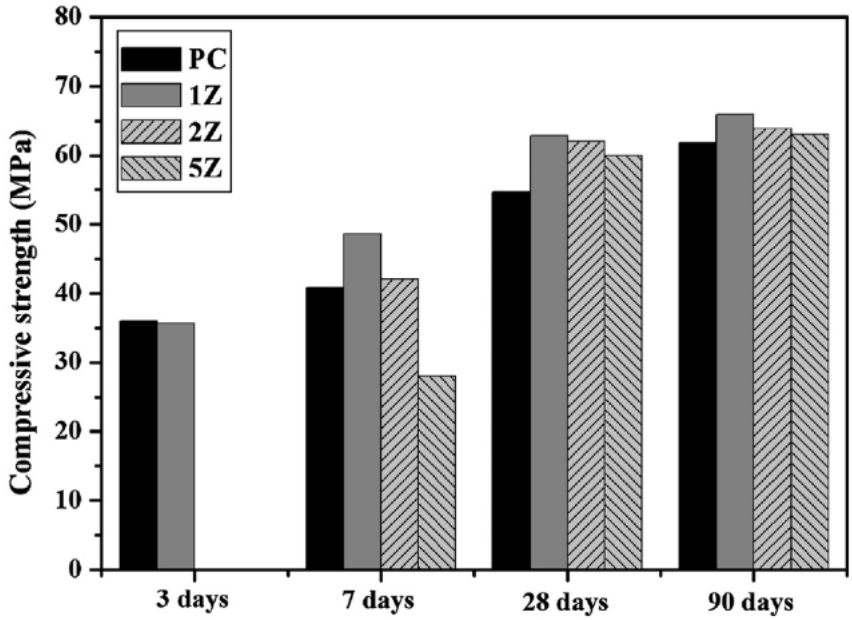

Figure 2.12 Compressive strength of Portland cement mortars with 0-5 wt% ZnO[24]

As can be observed from figure 2.12 the strength of the cement mortar increases with the addition of nano-ZnO, especially after an extended period of time. The study found that after three days, the strength of the ZnO mix was lower than that of the pure cement mixture, but at seven days and later, the strength of the ZnO mix was higher than the PC mix. It also found that

with the addition of ZnO, the volume of the permeable pore space in the Portland cement mortars decreased. [24]

2.3.4 Other applications of nano materials in the oil and gas industry

The potential for using nanotechnology is enormous, which is why there has been conducted research of the applications in many areas, and the application is not limited to areas concerning cementing. The next sub-chapters will be covering the application of nanotechnology within various areas of the oil recovery process and the benefits it may provide. The following topics will be discussed more in-depth; applications of nanotechnology for EOR purposes, in drilling fluid, for corrosion inhibition and for scale prevention.

2.3.4.1 Enhanced oil recovery using nanoparticles

Ogolo et al. (2012) [25] conducted a study which was focused on enhanced oil recovery using nanomaterials. From previous research it is known that the wettability of a formation can be changed with the use of nanoparticles, and that a water wet formation will produce better than an oil wet formation. This study examined the effects of nine different metal oxides and silica on the recovery factor. The study concludes that not all of the metal oxides are beneficial to oil recovery, some even worsen the EOR, and that the type of fluid used for dispersion of nanoparticles is important as it plays a vital part in the process. The study suggests that aluminum oxides dispersed in brine and distilled water improves oil recovery through reduction of oil viscosity and that silica dispersed in ethanol improves oil recovery through changing the rock wettability. [25]

2.3.4.2 Nano silica on improved EOR

Moradi et al. (2015) [26] performed a study on the effects of SiO_2 on performance of water alternate gas injection with respect to enhanced oil recovery. The study was conducted using core samples from a carbonate reservoir in which several different core flooding methods were used to compare recovery factor of various EOR methods. The study used SiO_2 to spread on the surfaces of the reservoir rock and alter its wettability from oil-wet to strongly water-wet to increase oil recovery. The results from the study found that the implementation of the nano-

WAG process lead to a 20% increase in recovery factor compared to the conventional WAG process. [26]

2.3.4.3 Scale inhibition using nano silica

Kumar et al. (2012) [27] conducted a study examining the use of nano-silica to reduce the everlasting problem of scale precipitation of pipelines. Buildup of scale in pipelines is highly problematic as it increases roughness of the pipe wall and reduces inner diameter and thereby increases pressure drop which leads to decreased production rate and a loss of profit. In the worst-case scenario, the precipitation can be so severe that it leads to total blockage of the pipe. The problematic agent is mainly found in the water associated with the crude oil.

The study aims to decrease the contact angle of water with the surface of the pipe by making the pipe wall superhydrophobic. This can be achieved in several ways, but in this study the focus was to apply nano-silica following a well-known procedure. The study concludes that by creating a superhydrophobic surface area using nano-silica the chance of scale precipitation can be greatly reduced and that this concept is applicable in other areas where scaling is common.[27]

2.3.4.4 Improving drilling fluids using nano graphene

Taha et al. (2015) [28] conducted a study regarding nano graphene engineered drilling fluids. The study was conducted to enhance properties of water-based mud (WBM) especially lubrication and thermal stability. The concept is rather simple, because of the small size of the graphene it can enter the tubular metal through microscopic pores and crystallize under the high pressure. Because of this crystallization combined with the properties of the graphene, it will form a protective film which improves lubricity, BHA lifespan and ROP whilst preventing bit balling and improving thermal stability.

For laboratory measurements the product proved exceptionally useful, decreasing torque by 50-80% depending on mud weight and improving mud properties while never causing any shale inhibition issues. The study also found that the application of nano graphene drilling fluids in a high-pressure high temperature (HPHT) well with hard formation in a field trial was found

effective. ROP was improved to 125% by addition of 2-3% of the product, reaming torque was reduced by 20% and the bit lifespan was increased by over 75%. [28]

2.3.4.5 Corrosion inhibition using magnetic nanofluid

Parekh et al. (2016) [29] investigated the effect of nanomagnetic fluids for the purpose of acid corrosion inhibition. Carbon steel is a material widely used in several industries for various applications, including petrochemical or chemical processes. The problem occurs when the steel is in contact with acid or is located in an acidic environment as in these situations the carbon steel is highly prone to corrosion. Various strategies are used to prevent corrosion of the pipe such as; surface coating of the steel, controlling PH, using inhibitors or using cathodic/anodic protection. This study focuses on using ferromagnetic nanoparticles to prevent corrosion.

The study found that the use of ferromagnetic nanofluids (MNF) could be used to protect carbon steel from an acid attack by adsorption of nanoparticles to the attacked surface which in turn forms a barrier between the metal and the aggressive media. The study found that the inhibition efficiency will increase up until the point where the MNF concentration is optimal.[29]

2.3.4.6 Nano-emulsions as cement spacer

Maserati et al. (2010) [16] understood the importance of a thorough mud displacement before a cementing operation commenced and decided to study the effect of using nano-emulsions as a cement spacer rather than using conventional spacers. Spacers are the term for the fluid which lies between the cement slurry and the mud which is used for cleaning out the old mud in the system in order for the cement to properly bond to the steel. Its job is to wash away old mud, and in case of oil-based mud (OBM) it should reverse the wettability of the walls so that the cement can create a proper bond. Several types of spacers have been developed over the years with varying degrees of success, and this study focused on using nano-emulsions as cement spacer.

The study found that due to the small size of the nano-emulsion droplets (20-500nm) they were found the increase the performance of cleaning during displacement of old OBM. Furthermore, the wettability was also able to be changed by the nano-spacers using only a minor volume

quantity and the nano-spacers were found to be compatible with the fluid systems. As a result of these benefits, increased cement sheath bonding was confirmed through shear bond tests.[16]

3. Experimental program

This chapter contains information about the materials used, the contents and reasoning behind the various test batches as well as some theory and explanation behind the different experiments performed.

3.1 Materials

All the materials used in this thesis was provided by the University of Stavanger, either by itself or through its collaborating companies.

3.1.1 Cement

The cement used was provided by NORCEM and is a high sulfate resistant (HSR) API class G type cement. Prior to usage the cement was tested, by another entity, in accordance to API SPEC 10A/NS-EN ISO 10426-1. The chemical composition of the cement is shown below

CHEMICAL COMPOSITION			
Water soluble Chromium	Cr(VI)	0.00	mg/kg
Sulfur Trioxide-IR	SO3	1.73	%
Loss On Ignition	LOI	0.79	%
Insoluble Residue	I.R	0.10	%
Magnesium Oxide	MgO	1.43	%
Sodium Oxide Equivalent	Na2O Eq.	0.48	%
Tricalcium Silicate	C3S	56.5	%
Tricalcium Aluminate	C3A	1.7	%
C4AF+2C3A	C4AF+2C3A	15.2	%

Figure 3.1 Chemical composition of the utilized G class cement

3.1.2 Water

The water used to prepare cement slurries was freshwater available from the faucet in the laboratory. It was used with the assumption that is was pure and free from significant contamination of any sort.

3.1.3 Nanoparticles

3.1.3.1 Nano SiO_2

The nano silica was purchased from Sigma-Aldrich Norway AS. It is a colloidal mixture with a concentration of 50 wt.% suspension in H_2O. The mixture has a density of 1,4 g/mL at 25 °C with a pH ranging from 9,0 to 10,5. [30]

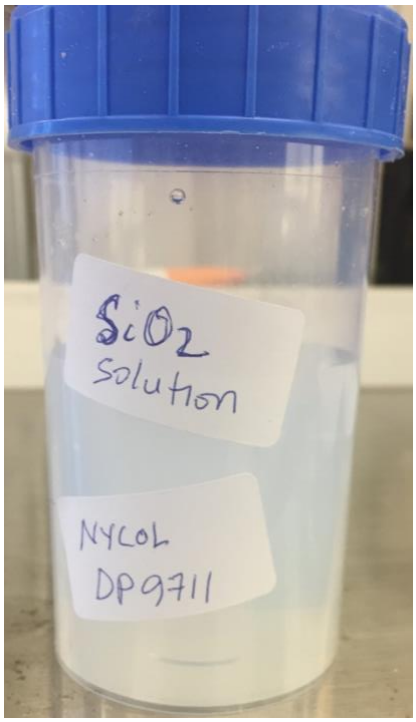

Figure 3.2 Aqueous dispersion of SiO2

3.1.3.2 MWCNT/MWCNT-COOH

A description of multiwalled carbon nanotubes are given in chapter 2. These MWCNTs were purchased from US-Nano. These multiwalled carbon nanotubes are dispersed in water with a purity >95 wt% for the carbon nanotubes and purity >97 wt% for the carbon content. The tubes

have an OD between 20-30 nanometer and an ID of 5-10 nanometer with a length between 10-30 micrometers. The density is 2,1 g/cm3. [31]

3.1.3.3 Nano TiO_2

The nano titanium oxide was purchased from US-nano. It is TiO2 nanoparticles with a size in the range from 5-15 nanometer in an anatase aqueous dispersion. The solution has a concentration of approximately 15,3 wt% TiO2 and ~85 wt% water. Depicted below is the aqueous solution which was added to the water before being mixed with the cement powder. [32]

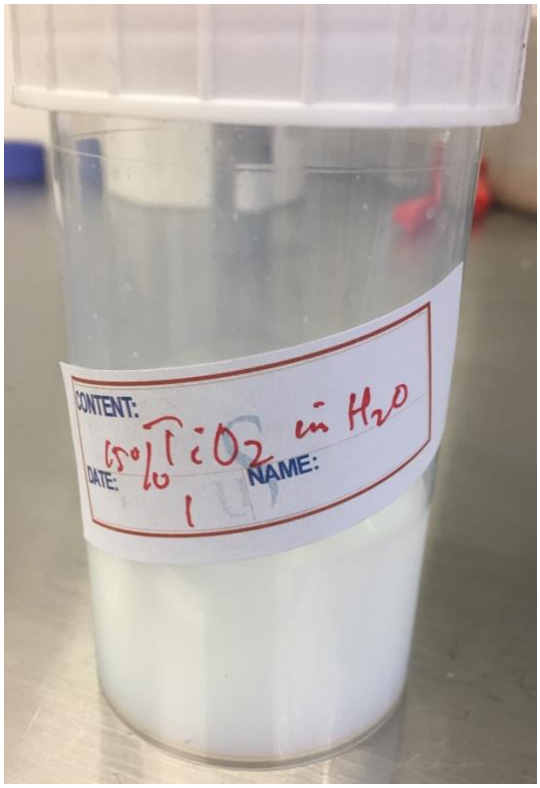

Figure 3.3 Aqueous dispersion of TiO2

3.1.3.4 Nano Fe_2O_3

The iron(III) oxide was purchased from Thermofisher in powder form with a purity of 99,999%. The powder is brown to brown-red and was dispersed in a water solution using a sonicator before the mixture was utilized for testing. The solution used has a concentration of 50wt%. The mixture was combined by the use of sonication due to the benefits it provides, such as a

more even distribution of particles and rarer precipitation of particles. Depiction of powder, solution and sonicator is found below.

Figure 3.4 Iron oxide powder (left) mixture after mixing (middle) mixture after 48 hours (right)

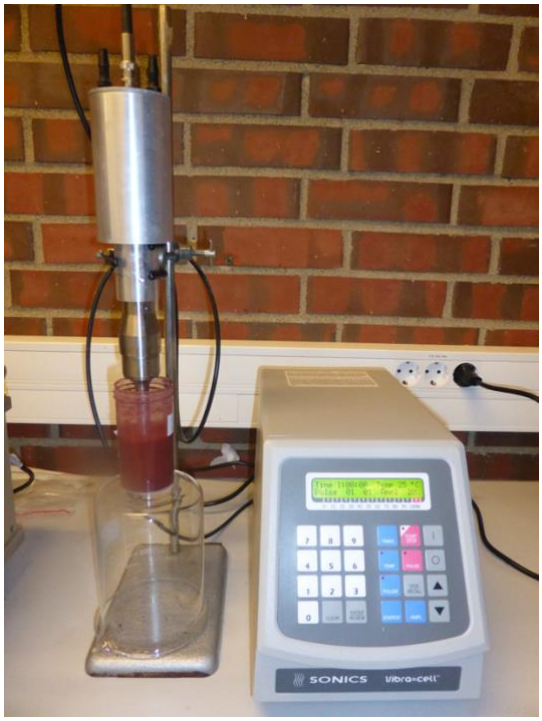

Figure 3.5 Machine used for sonication of iron oxide solution

3.1.3.5 Nano-Al_2O_3

The nano aluminum oxide was purchased from US research nanomaterials incorporated. The particles are 100% alpha and have average particle size (APS) of 80nm with a purity of 99+%. The nanoparticles are white and is fully dispersed in water with a concentration of 20wt% in which the nanoparticles have a density of 3,97 g/cm3. [33]

3.1.3.6 Nano-ZnO

The zinc oxide nanoparticles were purchased from US research nanomaterials incorporated. They are fully dispersed in water and made using the High-Temperature combustion method. The particles have an APS of 18nm with a purity of 99,95%. The concentration of the mixture is 20wt% where the true density is 5,606 g/cm3. [34]

3.1.4 Rubber

The rubber utilized for testing in this thesis was rubber cut from a silicone cup. According to previous elemental analysis performed on this rubber, the composition of the silicone rubber is listed below; [35]

Table 3.1 Elemental analysis (EDS) of silicone rubber[35]

Element	Wt%
C	50,51
O	23,02
Si	30,48

The silicone cup was cut using a grater and it was cut into two separate sizes which were mixed together before it was added to the cement mixture. The procedure for acid treating the rubber is covered in below.

Figure 3.6 Silicone rubber coarsely cut (left) and finely cut (right)

The procedure for acid treating the rubber was executed in order with instructions from Colom et al. [36] in which the following steps are taken;

1) Immerse the specimen in a 95-97% sulphuric acid (H_2SO_4) for one minute
2) Retrieve specimen from the acid and leave them to air dry for two minutes to allow for further reaction
3) Use hot distilled water (approximately 50ºC) to wash the specimen and ammonium hydroxide (NH_4OH) (15% ammonia) to neutralize the remaining acid
4) Wash the specimen with room temperature distilled water (approx. 23ºC) an additional time

3.1.5 Cement molds

The cement molds used for creating the plugs are standard plastic cylinders with a measured diameter of 34,50mm and a length of 69,25mm. To ensure that the plug could be safely retrieved from the mold without sustaining structural damage of any sort, the mold was coated in a thin layer of oil to act as lubrication for retrieval of the plug.

Figure 3.7 Cement mold coated in oil (left) and oil for lubrication (right)

3.2 Test batches

3.2.1 Introduction

Various collections of test specimens with different components and recipes, named test batches, were created for testing purposes. Each sub chapter explains the purpose and the components found in each of the test batches.

In brief;

Test batch 1 investigated the effect of nano-SiO_2 on 0,52 WCR G class cement.

Test batch 2 studied the effect of MWCNT-COOH on 0,52 WCR G class cement.

Test batch 3 examined the effect of nano-TiO_2 on 0,52 WCR G class cement

Test batch 4 analyzed the effect of nano-Fe_2O_3 on 0,52 WCR G class cement

Test batch 5 aimed to increase certainty in strength measurements of the zero-additive cement plugs

Test batch 6 studied the effect of MWCNT-COOH on 0,44 WCR G class cement

Test batch 7 identified the effect of acid treated and non-treated rubber on 0,44 WCR G class cement

Test batch 8 observed the effect of a combined mixture of nano-SiO_2 and MWCNT-COOH on 0,44 WCR G class cement.

Test batch 9 investigated the effect of rubber-ash on 0,44 WCR G class cement.

Test batch 10 examined the effect of nano-silica on 0,44 WCR G class cement.

Test batch 11 studied the effect of MWCNT on 0,44 WCR G class cement.

Test batch 12 observed the effect of nano-Al_2O_3 on 0,44 WCR G class cement.

Test batch 13 investigated the effect of nano-ZnO on 0,44 WCR G class cement.

Test batch 14 observed the effect of a combined mixture of nano-Al_2O_3 and MWCNT on 0,44 WCR G class cement.

Test batch 15 studied the effect of a combined mixture of MWCNT-COOH and nano-TiO_2 on 0,44 WCR G class cement

Test batch 16 analyzed the effect of a combined mixture of nano-SiO_2 and nano-Fe_2O_3 on 0,44 WCR G class cement

Test batch 17 further investigated the effects of a certain concentration of the nano-SiO_2 and MWCNT-COOH mixture on 0,44 WCR G class cement.

In the making of the various test batches, the procedure between slurry formulation and destructive testing varied slightly. For **test batch 1-4** the slurry was created and then poured into the cement molds where it was left to cure for 48 hours. After 48 hours the cement samples were polished and the molds, still containing the cement, were placed in a 62°C oven for 60 minutes. Subsequently, the molds were retrieved from the oven and the cement plugs were retrieved from the molds. The OD and the length of the plugs were then measured using a digital caliper. The specimens were then marked with the appropriate contents. All specimens were then subjected to non-destructive testing such as weight measurements and ultrasonic velocity measurements whilst remaining dry. Afterwards, the specimens were placed in a water tank and these measurements were repeated every 24 hours for three consecutive days. The samples were then left in the water tank until the day they were being subjected to destructive testing. Before being destructed, all samples underwent a final round of non-destructive testing. Test batch 1-4 used a 7-day timeframe from slurry formulation to destructive testing.

Test batch 5-8: the procedure was nearly identical. The difference being that after 72hrs in water, the plugs were then left in air until the destructive test was performed. As the first four plugs in test batch 5 were used in conjunction with test batch 1-4, they followed the same procedure. Test batch 5-8 also used a 7-day timeframe from creation to destruction.

Test batch 9-12: The procedure for these batches deviated significantly from the others. Test batch no. 12 was poured into cement molds on the 12th of march, which was the day the Norwegian government announced a temporary shutdown of all the schools in the country. This made it impossible to conduct the necessary tests on the samples for the duration of the shutdown. Even though the procedure deviated from the other batches, it was decided that test batch 9-12 would be tested as soon as it was possible, and due to the differences in procedure and curing time the samples would only be compared to its own control samples.

Test batch 13-16: The procedure which was used was the same as for test batch 5-8. The only slight variation is that all the samples were made on the same day. Additionally, the samples were crushed using a different apparatus than the previous samples.

3.2.1.1 Test batch 1

The primary objective of test batch 1 was to investigate the effect of adding aqueous nano-silica on the final compressive strength and modulus of elasticity of the cement, and to find the optimal amount of added silica which would yield the greatest strength increase. The slurry utilized the cement described in chapter 3.1.1 with a water/cement ratio of 100/191 ≈ 0,524. Test batch 1 consists of 12 plugs, where the first two plugs are reference plugs with no added nanoparticles. Thereafter, a gradually increasing amount of nano-silica was added to the water whilst the total amount of liquid always equaled 100 grams. The mixture of the different components and the concentration of nanoparticles in the solution is shown in table 3.2 below. To increase the accuracy of the strength measurements of an added amount of silica, each concentration has two separate, but in theory identical, plugs which would be measured. This was also the case for the pure cement plugs.

To create the plugs, the first step was to measure the cement to 191 ± 0,05 grams in a container. Afterwards, the water was measured to 100 ± 0,05 grams, or in the case for added silica the water was measured to 100grams – number of grams of silica. The accuracy of added nano-silica is amount ± 0,005 grams. These two parts were then added together in a container and mixed using a stirring pin until the solution was homogenous and smooth. Following the mixing, the mixture was poured into the cement molds whilst repeatedly tapping the cement

mold against a flat surface. This was performed to prevent the forming of large unwanted air bubbles in the plug which could have led to large inconsistencies in the final measurements.

Table 3.2 Test batch no. 1

Plug (#)	Freshwater (g)	Cement (g)	SiO_2 (g) (aq) (50% sol)
1	100	191	0,00
2	100	191	0,00
3	99,75	191	0,25
4	99,75	191	0,25
5	99,50	191	0,50
6	99,50	191	0,50
7	99,25	191	0,75
8	99,25	191	0,75
9	99,00	191	1,00
10	99,00	191	1,00
11	98,5	191	1,50
12	98,5	191	1,50

3.2.1.2 Test batch 2

The main objective of test batch 2 was to investigate the effect of adding aqueous MWCNT-COOH on the final compressive strength and modulus of elasticity of the cement, and to find the optimal amount of added MWCNT-COOH which would yield the greatest strength increase. The slurry utilized the cement described in chapter 3.1.1 with a water/cement ratio of 100/191 ≈ 0,524. Test batch 2 consists of 10 plugs which were made in the same way as described for test batch 1. The first two plugs are pure cement plugs with no addition of nanoparticles used as reference plugs, then, an increasing amount of MWCNT-COOH were added for the consecutive plugs. Table 3.3 displays the grams of each component as well as the concentration of the nanoparticle solution.

Table 3.3 Test batch no. 2

Plug (#)	Freshwater (g)	Cement (g)	MWCNT-COOH (g) (aq) (3% sol)
1	100	191	0,00
2	100	191	0,00
3	99,9	191	0,10
4	99,9	191	0,10
5	99,8	191	0,20
6	99,8	191	0,20
7	99,7	191	0,30
8	99,7	191	0,30
9	99,6	191	0,40
10	99,6	191	0,40

3.2.1.3 Test batch 3

The main purpose of test batch 3 was to investigate the effect of adding aqueous nano-TiO_2 on the final compressive strength and modulus of elasticity of the cement, and to find the optimal amount of added TiO_2 which would yield the greatest strength increase. The slurry utilized the cement described in chapter 3.1.1 with a water/cement ratio of 100/191 ≈ 0,524. Test batch 3 consists of 12 plugs which were made in the same way as described for test batch 1. The first two plugs are pure cement plugs with no addition of nanoparticles used as reference plugs, then, an increasing amount of TiO_2 were added for the consecutive plugs. Table 3.4 displays the contents of the plugs as well as the concentration of the nanoparticle solution.

Table 3.4 Test batch no. 3

Plug (#)	Freshwater (g)	Cement (g)	TiO_2 (g) (aq) (15% sol)
1	100	191	0,00
2	100	191	0,00
3	99,9	191	0,10
4	99,9	191	0,10
5	99,8	191	0,20

6	99,8	191	0,20
7	99,7	191	0,30
8	99,7	191	0,30
9	99,6	191	0,40
10	99,6	191	0,40
11	99,0	191	1,00
12	99,0	191	1,00

3.2.1.4 Test batch 4

The reason for making test batch 4 was to investigate the effect of adding aqueous nano-Fe_2O_3 on the final compressive strength and modulus of elasticity of the cement, and to find the optimal amount of added Fe_2O_3 which would yield the greatest strength increase. The slurry utilized the cement described in chapter 3.1.1 using a water/cement ratio of 100/191 ≈ 0,524. This was the final test batch which utilized the 0,52 WCR cement and the newer batches used 0,44 WCR as per API standards.[37] The nano-Fe_2O_3 was available as a powder, and an aqueous dispersion with 50% concentration was made in the lab by use of a sonicator as mentioned in chapter 3.1.3.4. Test batch 4 consists of 12 plugs which were made in the same way as described for test batch 1. The first two plugs are pure cement plugs with no addition of nanoparticles used as reference plugs, then, an increasing amount of Fe_2O_3 were added for the consecutive plugs. Table 3.5 displays the contents of the plugs as well as the concentration of the nanoparticle solution.

Table 3.5 Test batch no. 4

Plug (#)	Freshwater (g)	Cement (g)	Fe2O3 (g) (aq) (50% sol)
1	100	191	0,00
2	100	191	0,00
3	99,9	191	0,10
4	99,9	191	0,10
5	99,8	191	0,20
6	99,8	191	0,20
7	99,7	191	0,30

8	99,7	191	0,30
9	99,6	191	0,40
10	99,6	191	0,40
11	99,0	191	1,00
12	99,0	191	1,00

3.2.1.5 Test batch 5

Test batch 5 was created to further strengthen the accuracy of the UCS measurements. When comparing the plugs with added nanoparticles to the reference plugs, an average value emanating from all the reference plugs were used. Due to some inconsistencies in the measurements of the reference plugs which occurred due to certain deviations in the surface flatness of the plug, an additional batch consisting of only reference plugs (zero additives) was made. Test batch 5 consists of 8 plugs, where the first four plugs were made with a WCR of 0,524 to be compared to test batch 1-4, and the last four were made with a WCR of 0,441 for further test batches.

Table 3.6 Test batch no. 5

Plug (#)	Freshwater (g)	Cement (g)	Nanoparticles (g)
1	100	191	0,00
2	100	191	0,00
3	100	191	0,00
4	100	191	0,00
5	100	227	0,00
6	100	227	0,00
7	100	227	0,00
8	100	227	0,00

3.2.1.6 Test batch 6

The objective of test batch 6 was to investigate the effect of adding aqueous MWCNT-COOH on the final compressive strength and modulus of elasticity of G class cement with a water to

cement ratio of 0,44. It is similar to test batch 2, but differentiates in the WCR of the cement slurry and test batch 6 aims to confirm the findings of test batch 2 whilst testing in accordance to API standards for G class cement. The same cement described in chapter 3.1.1 was utilized for this batch. Test batch 6 consists of 12 plugs which were made in the same way as described in chapter 3.2.1. The first two plugs are pure cement plugs with no addition of nanoparticles used as reference plugs, then, an increasing amount of MWCNT-COOH were added for the consecutive plugs. Table 3.7 displays the contents of the plugs as well as the concentration of the nanoparticle solution.

Table 3.7 Test batch no. 6

Plug (#)	Freshwater (g)	Cement (g)	MWCNT-COOH (g) (aq) (3% sol)
1	100	227	0,00
2	100	227	0,00
3	99,9	227	0,10
4	99,9	227	0,10
5	99,8	227	0,20
6	99,8	227	0,20
7	99,7	227	0,30
8	99,7	227	0,30
9	99,6	227	0,40
10	99,6	227	0,40
11	99,0	227	1,00
12	99,0	227	1,00

3.2.1.7 Test batch 7

The main purpose of test batch 7 was to investigate the effect of adding acid treated and non-treated silicone rubber on the final compressive strength and modulus of elasticity of the cement, and to find the optimal amount of added rubber which would yield the greatest strength increase. The slurry utilized the cement described in chapter 3.1.1 with a water/cement ratio of 100/227 ≈ 0,441 as a baseline. Test batch 7 consists of 14 plugs where all samples were made with 100 grams of water, and the total weight of solids equaled 227 grams, where any silicone

rubber added was substituted in for cement in the total weight. The first two plugs are pure cement plugs with no addition of rubber used as reference plugs, then, an increasing amount of rubber were added for the consecutive plugs. Table 3.8 showcases the composition of the plugs and whether the rubber added was treated with acid.

Table 3.8 Test batch no. 7

Plug (#)	Freshwater (g)	Cement (g)	Rubber (g) (treated)	Rubber (g) (untreated)
1	100	227	0,00	0,00
2	100	227	0,00	0,00
3	100	226	0,00	1,00
4	100	226	0,00	1,00
5	100	226	1,00	0,00
6	100	226	1,00	0,00
7	100	225	0,00	2,00
8	100	225	0,00	2,00
9	100	225	2,00	0,00
10	100	225	2,00	0,00
11	100	224	0,00	3,00
12	100	224	0,00	3,00
13	100	224	3,00	0,00
14	100	224	3,00	0,00

3.2.1.8 Test batch 8

The primary objective of test batch 8 was to investigate the effect of adding a mixture of aqueous nano- MWCNT-COOH & SiO_2 on the final compressive strength and modulus of elasticity of the cement, and to find the optimal amount and ratio of added MWCNT-COOH & SiO_2 which would yield the greatest strength increase. The slurry utilized the cement described in chapter 3.1.1 with a water/cement ratio of 100/227 ≈ 0,441. Test batch 8 consists of 8 plugs which were made in the same way as described for test batch 6. The first two plugs are pure cement plugs with no addition of nanoparticles used as reference plugs, then, an increasing amount of MWCNT-COOH & SiO_2 were added for the consecutive plugs. Table 3.9 displays the contents of the plugs as well as the concentration of the nanoparticle solutions.

Table 3.9 Test batch no. 8

Plug (#)	Freshwater (g)	Cement (g)	SiO_2 (g) (50% sol)	MWCNT-COOH (g) (3%sol)
1	100	227	0,00	0,00
2	100	227	0,00	0,00
3	99,3	227	0,50	0,20
4	99,3	227	0,50	0,20
5	99,5	227	0,40	0,10
6	99,5	227	0,40	0,10
7	99,65	227	0,30	0,05
8	99,65	227	0,30	0,05

3.2.1.9 Test batch 9

When creating the acid treated rubber for test batch 7, the rubber surface was shed when it came into contact with the acid. These pieces of rubber were air dried and named "rubber-ash". The objective of test batch 9 was to investigate the effect of adding rubber-ash on the final compressive strength of G class cement with a water to cement ratio of 0,44. The same cement described in chapter 3.1.1 was utilized for this batch. Test batch 9 consists of 6 plugs which were made in the same way as described for test batch 7. The first two plugs are pure cement plugs with no addition of rubber-ash used as reference plugs, then, an increasing amount of rubber-ash were added for the consecutive plugs. Table 3.10 displays the contents of the plugs.

Table 3.10 Test batch no. 9

Plug (#)	Freshwater (g)	Cement (g)	Rubber-ash (g)
1	100	227	0,00
2	100	227	0,00
3	100	226,5	0,50
4	100	226,5	0,50
5	100	225,5	1,50
6	100	225,5	1,50

3.2.1.10 Test batch 10

The objective of test batch 10 was to investigate the effect of adding aqueous nano-SiO_2 on the final compressive strength of G class cement with a water to cement ratio of 0,44. It is similar to test batch 1, but differentiates in the WCR of the cement slurry and test batch 10 aims to confirm the findings of test batch 1 whilst testing in accordance to API standards for G class cement, such that further investigations into other properties of the slurry could be undergone at a later time if the results were as good as for 0,52 WCR. The same cement described in chapter 3.1.1 was utilized for this batch. Test batch 10 consists of 8 plugs which were made following the procedure from test batch 1, with the difference being the amount of silica and cement added. The first two plugs are pure cement plugs with no addition of nanoparticles used as reference plugs, then, an increasing amount of nano-silica were added for the consecutive plugs. Table 3.11 displays the contents of the plugs as well as the concentration of the nanoparticle solution.

Table 3.11 Test batch no. 10

Plug (#)	Freshwater (g)	Cement (g)	SiO_2 (g) (aq) (50% sol)
1	100	227	0,00
2	100	227	0,00
3	99,60	227	0,40
4	99,60	227	0,40
5	99,50	227	0,50
6	99,50	227	0,50
7	99,40	227	0,60
8	99,40	227	0,60

3.2.1.11 Test batch 11

The main objective of test batch 11 was to investigate the effect of adding aqueous MWCNT on the final compressive strength of the cement, and to find the optimal amount of added MWCNT which would yield the greatest strength increase. The slurry utilized the cement

described in chapter 3.1.1 with a water/cement ratio of 100/227 ≈ 0,441. Test batch 11 consists of 8 plugs which were made in the same manner as test batch 10. The first two plugs are pure cement plugs with no addition of nanoparticles used as reference plugs, then, an increasing amount of MWCNT were added for the consecutive plugs. Table 3.12 displays the grams of each component as well as the concentration of the nanoparticle solution.

Table 3.12 Test batch no. 11

Plug (#)	Freshwater (g)	Cement (g)	MWCNT (g) (aq) (3% sol)
1	100	227	0,00
2	100	227	0,00
3	99,90	227	0,10
4	99,90	227	0,10
5	99,80	227	0,20
6	99,80	227	0,20
7	99,70	227	0,30
8	99,70	227	0,30

3.2.1.12 Test batch 12

The primary objective of test batch 12 was to investigate the effect of adding aqueous nano-Al_2O_3 on the final compressive strength of the cement, and to find the optimal amount of added Al_2O_3 which would yield the greatest strength increase. The slurry utilized the cement described in chapter 3.1.1 with a water/cement ratio of 100/227 ≈ 0,441. Test batch 12 consists of 8 plugs which were made in the same way as described for test batch 10. The first two plugs are pure cement plugs with no addition of nanoparticles used as reference plugs, then, an increasing amount of nano aluminum oxide were added for the consecutive plugs. Table 3.13 displays the contents of the plugs as well as the concentration of the nanoparticle solutions.

Table 3.13 Test batch no. 12

Plug (#)	Freshwater (g)	Cement (g)	Al_2O_3 (g) (aq) (20% sol)
1	100	227	0,00
2	100	227	0,00
3	99,90	227	0,10
4	99,90	227	0,10
5	99,80	227	0,20
6	99,80	227	0,20
7	99,70	227	0,30
8	99,70	227	0,30

3.2.1.13 Test batch 13

The main objective of test batch 13 was to investigate the effect of adding aqueous nano-ZnO on the final compressive strength of the cement, and to find the optimal amount of added ZnO which would yield the greatest strength increase. The slurry utilized the cement described in chapter 3.1.1 with a water/cement ratio of 100/227 ≈ 0,441. Test batch 12 consists of 8 plugs which were made in the same way as described for test batch 10. The first two plugs are pure cement plugs with no addition of nanoparticles used as reference plugs, then, an increasing amount of nano zinc oxide was added for the consecutive plugs. Table 3.14 displays the contents of the plugs as well as the concentration of the nanoparticle solutions.

Table 3.14 Test batch no. 13

Plug (#)	Freshwater (g)	Cement (g)	ZnO (g) (aq) (20% sol)
1	100	227	0,00
2	100	227	0,00
3	99,80	227	0,20
4	99,80	227	0,20
5	99,70	227	0,30
6	99,70	227	0,30

7	97,73	227	2,27
8	97,73	227	2,27

3.2.1.14 Test batch 14

Test batch 14 was made to investigate the effect of adding a combination of aqueous nano-MWCNT and nano-Al_2O_3 on the final compressive strength of the cement, while preparing different combinations of the nanoparticles to screen out the mixture of the two which would yield the greatest strength increase. The slurry utilized the cement described in chapter 3.1.1 with a water/cement ratio of 100/227 ≈ 0,441. Test batch 14 consists of 8 plugs which were made in the same way as described for test batch 10. The first two plugs are pure cement plugs with no addition of nanoparticles used as reference plugs, then, an increasing amount of nano-mixture was added for the consecutive plugs. Table 3.15 displays the contents of the plugs as well as the concentration of the nanoparticle solutions.

Table 3.15 Test batch no. 14

Plug (#)	Freshwater (g)	Cement (g)	MWCNT(g) (3% sol)	Al2O3 (g) (20%sol)
1	100	227	0,00	0,00
2	100	227	0,00	0,00
3	99,8	227	0,10	0,10
4	99,8	227	0,10	0,10
5	99,4	227	0,30	0,30
6	99,4	227	0,30	0,30
7	96,03	227	1,70	2,27
8	96,03	227	1,70	2,27

3.2.1.15 Test batch 15

The primary objective of test batch 15 was to investigate the effect of adding a mixture of aqueous nano-TiO_2 and MWCNT-COOH on the final compressive strength of the cement, and to find the optimal amount of added mixture which would yield the greatest strength increase. The slurry utilized the cement described in chapter 3.1.1 with a water/cement ratio of 100/227 ≈ 0,441. Test batch 12 consists of 8 plugs which were made in the same way as described for

test batch 10. The first two plugs are pure cement plugs with no addition of nanoparticles used as reference plugs, then, an increasing amount of nanoparticle was added for the consecutive plugs. Table 3.16 displays the contents of the plugs as well as the concentration of the nanoparticle solutions.

Table 3.16 Test batch no. 15

Plug (#)	Freshwater (g)	Cement (g)	MWCNT-COOH(g) (3% sol)	TiO2 (g) (15%sol)
1	100	227	0,00	0,00
2	100	227	0,00	0,00
3	99,8	227	0,10	0,10
4	99,8	227	0,10	0,10
5	99,6	227	0,20	0,20
6	99,6	227	0,20	0,20
7	99,4	227	0,30	0,30
8	99,4	227	0,30	0,30

3.2.1.16 Test batch 16

The main goal of test batch 16 was to investigate the effect of adding a mixture of aqueous nano-SiO_2 and nano-Fe_2O_3 on the final compressive strength and modulus of elasticity of the cement, and to find the optimal amount of added mixture which would yield the greatest strength increase. The slurry utilized the cement described in chapter 3.1.1 with a water/cement ratio of 100/227 ≈ 0,441. Test batch 12 consists of 8 plugs which were made in the same way as described for test batch 10. The first two plugs are pure cement plugs with no addition of nanoparticles used as reference plugs, then, an increasing amount of nanoparticle was added for the consecutive plugs. Table 3.17 displays the contents of the plugs as well as the concentration of the nanoparticle solutions.

Table 3.17 Test batch no. 16

Plug (#)	Freshwater (g)	Cement (g)	SiO2(g) (50% sol)	Fe2O3 (g) (50%sol)
1	100	227	0,00	0,00
2	100	227	0,00	0,00

3	99,7	227	0,20	0,10
4	99,7	227	0,20	0,10
5	99,5	227	0,30	0,20
6	99,5	227	0,30	0,20
7	99,1	227	0,50	0,40
8	99,1	227	0,50	0,40

3.2.1.17 Test batch 17

Based off previous results from testing on 0,44 WCR cement samples containing nanoparticles, test batch 17 was made to further investigate the effects of the best performing system in terms of strength increase. The system that was chosen contained a mixture of nano-SiO_2 and MWCNT-COOH with a dosage of 0,3grams silica + 0,05 grams of MWCNT-COOH. The slurry utilized the cement described in chapter 3.1.1 with a water/cement ratio of 100/227 ≈ 0,441.

Test batch 17 consists of 7 plugs which were made with a different procedure than the other batches. The batch contains five regular cylindrical cement samples, where two of them contain no nanoparticles and three of them contain the aforementioned mixture. These plugs were mixed and poured according to regular procedure before being left in air for 24 hours. They were then placed in an oven with a temperature of 105°C for six days before being removed. The samples were then polished, measured and subjected to non-destructive testing before eventually being crushed.

The remaining two samples were poured into a pipe, such that water leakage rates could be observed. One sample contained zero additives whilst the other contained the mixture of nanoparticles. The cement slurries were poured into the pipe which contained a cap at the end to allow the cement to set for 24 hours. Afterwards, the cap was removed and the pipes containing the cement were placed in an oven of 105°C for various time periods, as described in chapter 3.3.10.2. The batch aimed to study the effect of heat treatment on the final compressive strength of the samples, as well as leakage rates of heat-treated cement.

3.3 Theory, test set-up and procedure

The figure below shows how the various tests which are going to be described in this chapter fits within the experimental program in this thesis.

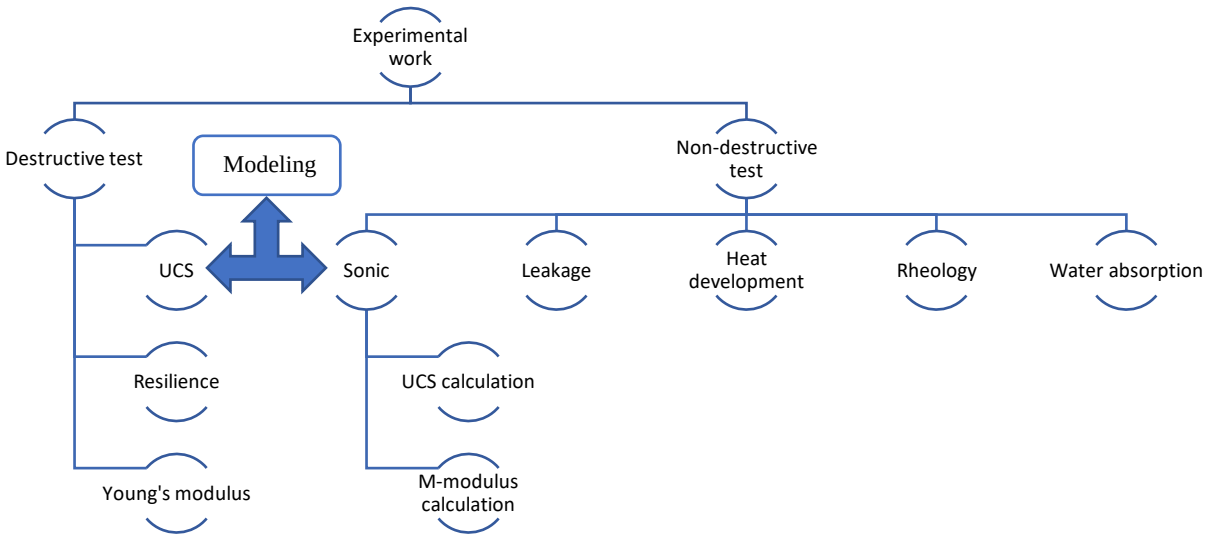

Figure 3.8 Scope of experimental work

3.3.1 Non-destructive testing

3.3.2 Ultrasonic velocity measurements

3.3.2.1 Theory

Ultrasonic velocity tests are applicable to assess the mechanical properties of a material. The theory behind the test is to emit an ultrasonic pulse through a specimen and record the time it takes to go from the sender to the receiver, which is placed at opposite ends of the bulk material. This information can be used to indicate the presence of cracks or trapped air and determine the durability, strength and density of the material.

3.3.2.2 Test set-up

For the ultrasonic measurements, a Pundit 7 made by CNS Farnell was used. The device measures the travel time through the test sample and displays the value on screen in the unit µs (microseconds). The Pundit 7 has a range from 0,1µs to 6553µs which is more than sufficient for the purposes of this thesis. Figure 3.9 below shows the test set-up used for the ultrasonic measurements.

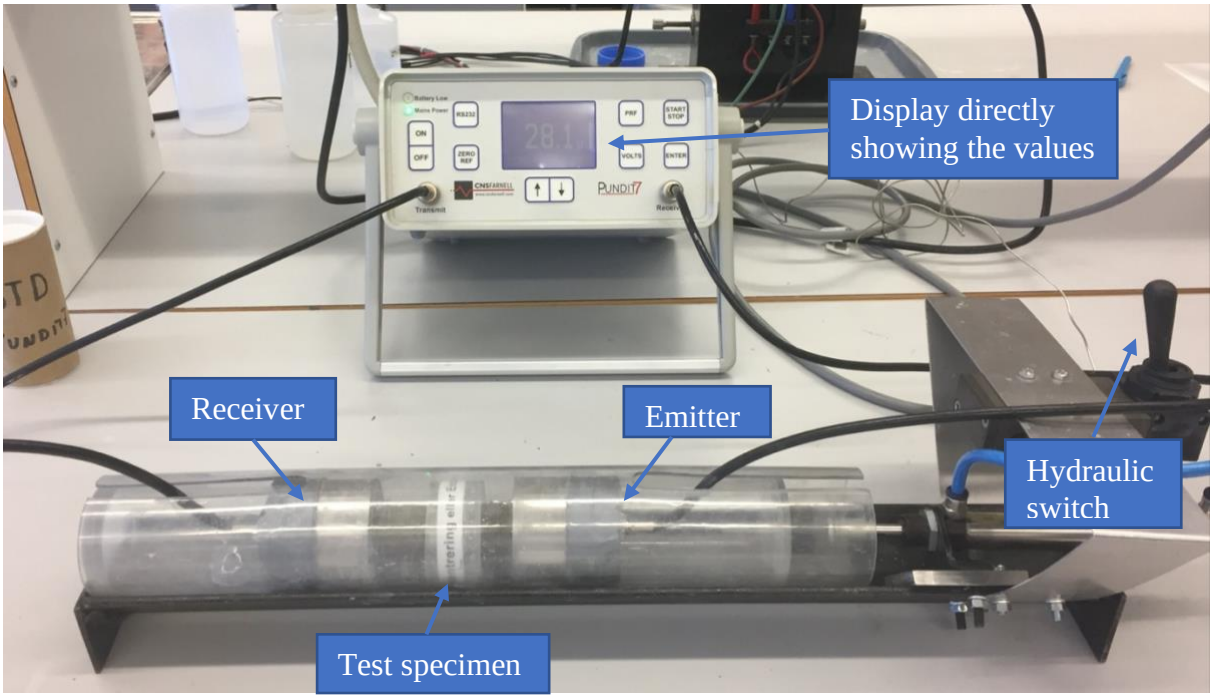

Figure 3.9 CNS Farnell Pundit 7 ultrasonic measurement device

To ensure accurate measurements, the machine must be calibrated before each use. This is done by placing a plastic cylinder with known properties between the emitting unit and the receiver and manually resetting the clock display to 25,2 µs.

3.3.2.3 Procedure

After calibration of the machine is complete, the measurement of the test samples can be done. As the diameter of the cement plugs are smaller than that of the diameter of the test tube, the samples are placed inside a plastic ring with OD equal to the ID of the test tube. This is done to ensure full contact area between the plug surface and the emitter/receiver. Furthermore, the switch from figure 3.9 is applied to activate a small hydraulic press to ensure that the emitter is

properly pressed against the sample for a more reliable measurement. The receiver is also pressed against the wall by this hydraulic press so that the sample sits tight in-between the two units.

3.3.3 Water absorption

3.3.3.1 Theory

To gain information about the microstructure and the pore volume of the cement plugs, one can study the water absorption of the plug. As the pore volume increases, the water absorption will also increase which is correlated to a higher likelihood of fluid migration through the cement. Increased water absorption can also be an indication of a faulty microstructure or cracks which can affect the cement integrity at a later stage. The addition of nanoparticles usually reduces water absorption as the particles are sufficiently small and will fill some or all of the pore space.

To calculate the mass-change the following equation is used:

Equation 3-1

$$\Delta M = \frac{Mt - M0}{M0} * 100$$

Where;

ΔM = Change in mass (%)

Mt = mass after a given time t

$M0$ = mass before immersion in water

3.3.4 Modeling of UCS

3.3.4.1 Theory

During compression of a right cylindrical sample, the maximum axial compression the sample can withstand before failing is termed the uniaxial compressive strength or the ultimate compressive strength (UCS). The uniaxial compressive strength is also sometimes known as the unconfined compressive strength as during loading of the cylindrical sample only the top and bottom surface areas are in contact with the compressing device and there will be no forces working in other directions which means that the confining stresses will be zero. The axial load

is one of the most common loads concrete will be exposed to in industrial appliance which is why the UCS is such a prevalent and important measurement of the strength of concrete.

3.3.4.2 Procedure

A method to obtain the uniaxial compressive strength of the cement through other means than destructive testing is needed for convenience sake. This can be achieved by the use of a model developed through non-destructive testing such as ultrasonic measurements. Per Horsrud developed such a model using sonic and the uniaxial compressive strength measurement of shale obtained from the North Sea and arrived at the following relationship:[38]

Equation 3-2

$$UCS = 0{,}77 * V_P^{2{,}93}$$

Where;
UCS = uniaxial compressive strength [MPa]
V_p = P-wave velocity through the material [km/s]

As this model was developed from shale measurements exclusively, it may be limited in its use. However, its application will be tested on cement data later in chapter 5.

3.3.5 Modulus of elasticity

3.3.5.1 Theory

To describe isotropic homogenous materials the P-wave modulus (modulus of elasticity), M, is one of the elastic moduli that can be used. The P-wave modulus is defined as the ratio of axial stress to axial strain in a uniaxial strain state. [39] This is not to be confused with the conventional modulus of elasticity, which is a quantity that measures a material or substance´s resistance to elastically deform when a stress is applied to the material.[40]

3.3.5.2 Procedure

When describing the P-wave modulus through the bulk modulus (K) and shear modulus (G) the following relation is used; [39]

Equation 3-3

$$M = K + \frac{4G}{3}$$

As the M modulus is defined as stress v strain the following relationship between the density and the velocity of a pressure wave propagating through the material has been developed: [39]

Equation 3-4

$$V_p = \sqrt{\frac{K + \frac{4G}{3}}{\rho}}$$

Which gives;

Equation 3-5

$$V_p^2 * \rho = K + \frac{4G}{3}$$

When substituting in eq 3-3 we get the following formula to calculate the modulus of elasticity (M);

Equation 3-6

$$M = \frac{V_p^2 * \rho}{10^9}$$

Where:

M = P-wave modulus, [GPa] (after dividing by 10^9)

K = Bulk modulus, [GPa]

G = Shear modulus, [GPa]

ρ = Density of the given cement plug [kg/m^3]

V_p = Compressional wave velocity [m/s], which is calculated from the ultrasonic travel time (Δt) through the length of the plug, L.

And:

Bulk-modulus describes how resistant a substance is to uniform compression (i.e physical changes to its bulk as a result of external forces)[41]

Shear-modulus describes a substances ability to withstand forces parallel to its surface (i.e torsion or shear resistance) [42]

3.3.6 Destructive testing

To gain more accurate and detailed information about the specimen after non-destructive testing is complete, destructive testing can commence. As implied by its name, destructive testing is when the material's strength is tested up until its point of failure by imposing heavy mechanical loads on said material. When obtaining information about a material's strength through testing, the destructive tests give more direct information, and are easier to carry out in comparison to the non-destructive tests.

3.3.7 UCS

3.3.7.1 Theory

Mentioned in chapter 3.3.4.1

After performing the destructive test and obtaining the required force to break the cement plug specimen the following formula is used to calculate the uniaxial stress which is also the compressive strength;

Equation 3-7

$$\sigma = \frac{F}{A}$$

Where;

σ = Compressive strength, [MPa]

F = Maximum load applied at fracture point, [N]

A = Cross-sectional area of cement plug specimen, [mm^2]

3.3.7.2 Test set-up

For the destructive compressive tests run in this thesis, three different apparatuses were used; Zwick Z020 and Z050 were used for test batch 1-8. The Zwick Z020 consists of two detachable surfaces which can be configured to fit a wide array of tests. For UCS measurements, two flat surfaces were used with the cement plug placed between them. The machine is configured such that it could deliver a force of 20000N. Depicted below is the Zwick Z020 configured for a compressive test of a cement plug. For samples which were expected to exceed the 20000N force limit, the Zwick Z050 was utilized, which is essentially the same machine with a higher force threshold.

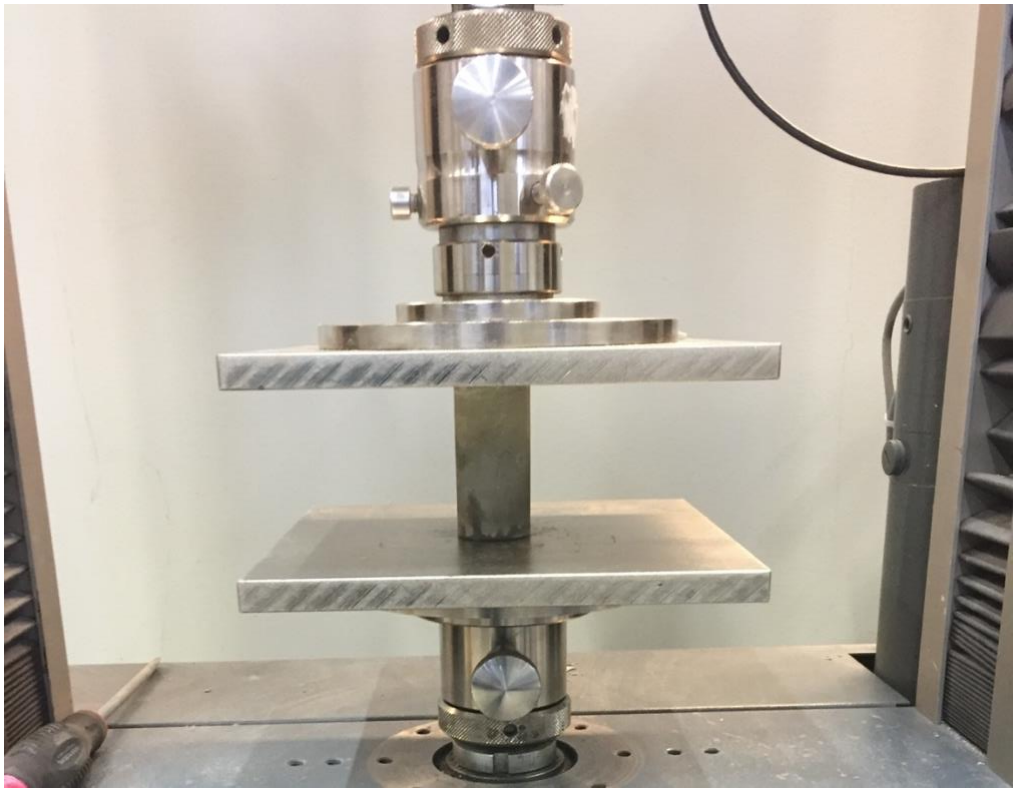

Figure 3.10 Zwick Z020 with cement plug in place for destructive testing

For test batch 9-17, a separate apparatus had to be used due to safety and access regulations as a result of the partial reopening of the laboratories. This machine is a hydraulic hand operated press installed with a state-of-the-art load cell to ensure accuracy in the measurements. The deformation measurements which the machine provided is prone to a large range of inaccuracies and thus this measurement is not in focus for these batches. The machine operates on the same principles and in the same way as the Zwick machines.

3.3.7.3 Procedure

The Zwick Z020 is capable of running a series of different tests measuring different properties. Firstly, a compressive test program is formulated through the software testXpert II where all the desired parameters are chosen. The program for UCS-testing uses a load speed of 50 N/s, a pre-load of 5 N (required force before the program starts recording the force-strain profile) and a start position which can be varied depending on the specimen length. The cement plug specimen is then placed between the two plates and centralized, and a protective plastic plate is placed in front of the machine to prevent splinters of cement from potentially harming other people in the room or other equipment before the program is started. As the end result of the test is unknown before it has been run, the test has to be stopped manually when it is observed that the sample has been fractured.

3.3.8 Young's modulus and Resilience

Through measurement of UCS, a stress-strain curve will be generated which can be used to calculate Young´s modulus and resilience for the given sample. Young´s modulus is used to describe the stiffness of a solid material, and is defined as the normal stress divided by the linear strain. [43] In the stress-strain curve, it is calculated from the slope of the linear area with the following equation;

Equation 3-8

$$E = \frac{\Delta\sigma}{\Delta\varepsilon}$$

Where,
E is the Young´s modulus (MPa)
$\Delta\sigma$ is the change in stress in the linear area of the curve (MPa)
$\Delta\varepsilon$ is the change in strain in the linear area of the curve (m/m)

Resilience is the total amount of energy a material can absorb while being deformed within the elastic region and is able to release upon unloading. The modulus of resilience is defined as the maximum amount of energy a material can absorb without sustaining permanent deformation,

i.e area under the stress-strain curve from zero to the elastic limit.[44] To estimate the modulus of resilience, the following formula can be used;

Equation 3-9

$$R = \frac{\sigma_{UCS}^2}{2E} = \frac{\sigma_{UCS}\varepsilon_{max}}{2}$$

Where,

R is the modulus of resilience (J/m3)

σ_{UCS} is the uniaxial compressive strength at yield point (Pa)

ε_{max} is the strain at the time of failure (m/m)

E is the Young´s modulus (Pa)

Additionally, one can use the trapezoidal method for calculation of resilience to obtain a more accurate value when equation 3-9 does not yield a representative result.

Equation 3-10

$$R = \sum \frac{\big(Strain(i+1) - Strain(i)\big) * \big(Stress(i+1) + Stress(i)\big)}{2}$$

Depicted below is a stress-strain curve which highlights the resilience, R, as the area under the curve, and Young´s modulus, E, as the slope of the curve in the linear area.

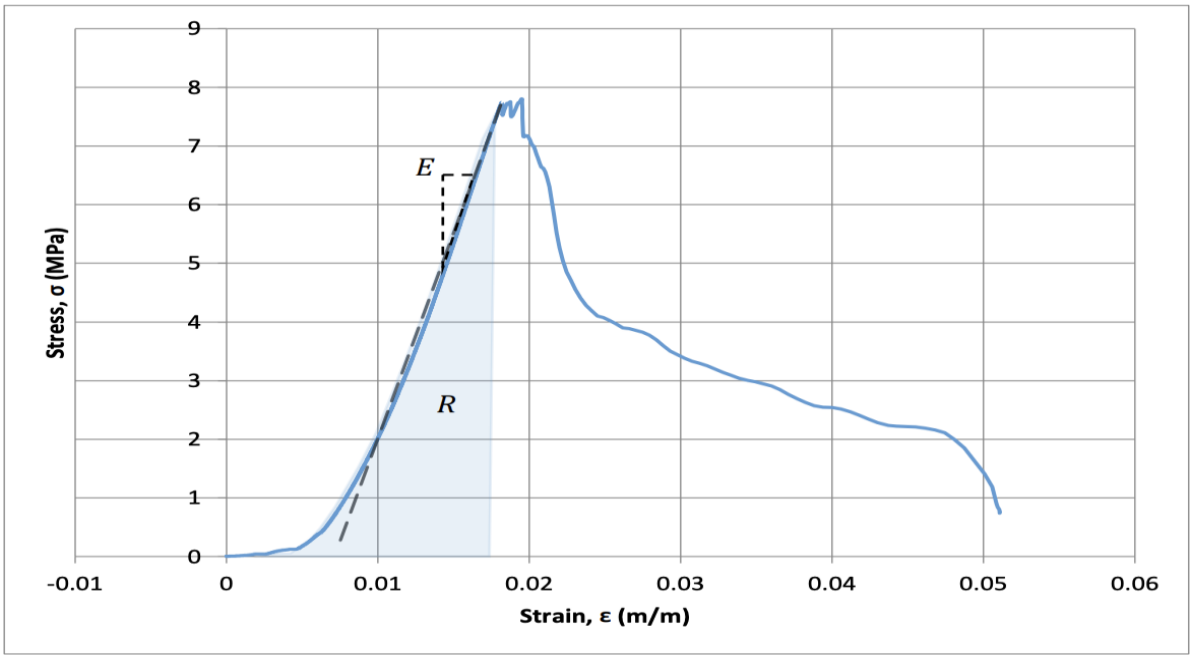

Figure 3.11 Stress-strain curve from a UCS test

3.3.9 Heat development

3.3.9.1 Theory

When cement is mixed with water, an exothermic reaction occurs which liberates heat. The heat development of Portland cement has several stages which was covered in chapter 2.2. When this reaction occurs in common applications of cement such as in construction works or similar, it poses little to no challenges as the heat simply dissipates into the air or ground leaving the quality of the work intact. When cement is used in well cementing however, this heat can cause massive problems if it is freely released as it could cause thermal expansion of the casing and cement. Furthermore, if the exothermic reaction is sufficiently large causing the temperature to reach a certain level, the rapid or nonuniform cooling could cause major stresses due to thermal contraction which in turn could cause cracks in the cement. [45] As a result of this, it is highly interesting to investigate what effects the additives will have on the cements heat development in terms of heat liberated and at what speed this heat will develop.

For this experiment, two temperature loggers from Eskeland electronics (ESK-EL) was connected to sensors which was placed inside the cement slurry, and these were used to measure the temperature of the cement. The loggers were programmed using the program Easy Log, and the data from the loggers was also retrieved by use of the same program.

Figure 3.12 Temperature logger from ESK-EL

3.3.9.2 Procedure

In order to isolate cement from the room temperature, an insulated box made out of Styrofoam was used to store the cement specimen when measuring the heat development. These boxes consist of two compartments, each of dimensions 10x10x10 cm, where only one of these compartments were used for each box. The cement was made according to the usual procedure with the only difference being that twice the normal amount of cement was made. The cement slurry underwent rheologic testing before being poured into plastic bags in the insulated boxes.

The sensor was placed inside the cement slurry before the lids were put on the boxes and they were stored in a locker for three days before being retrieved.

Figure 3.13 Styrofoam box used for temperature logging with cement in one compartment

3.3.10 Leakage test

3.3.10.1 Theory

The theory behind cracked cement or other ways of leakage has been discussed in chapter 1.1

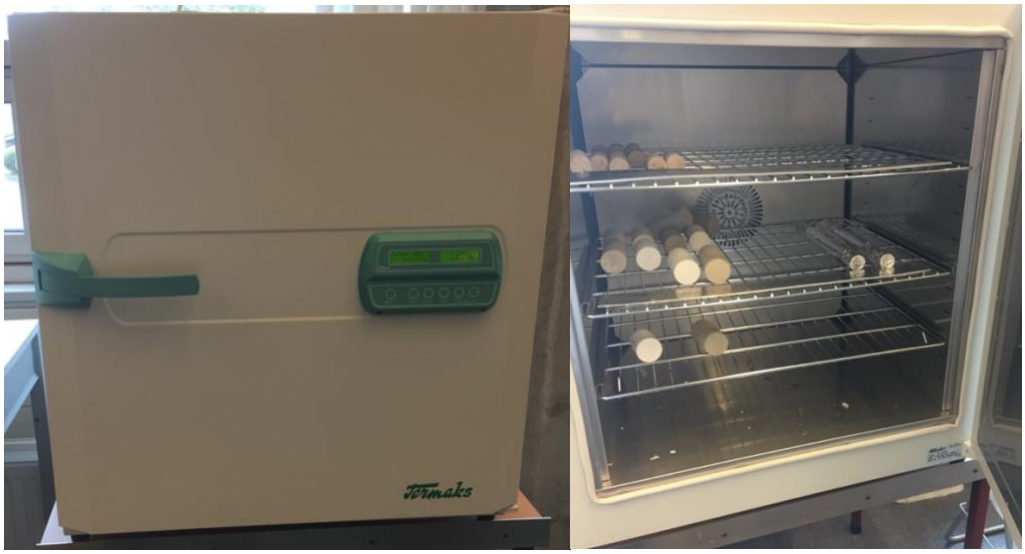

Figure 3.14 Oven used to store samples during heat cycles of approximately 105 degrees Celsius

3.3.10.2 Procedure

A regular batch of cement was made with the desired additives according to standard procedure. This cement was then poured into a steel pipe with a plug in one end and left to set for 24 hours before being placed into a 105°C oven. Afterwards, the sample was exposed to the worst-case scenario where it was rapidly cooled under running water, before being filled with water in order to measure leakage rates. A number of measurements were taken in order to calculate the leakage, mass absorption and water evaporation. The heating cycle is displayed in the figure below:

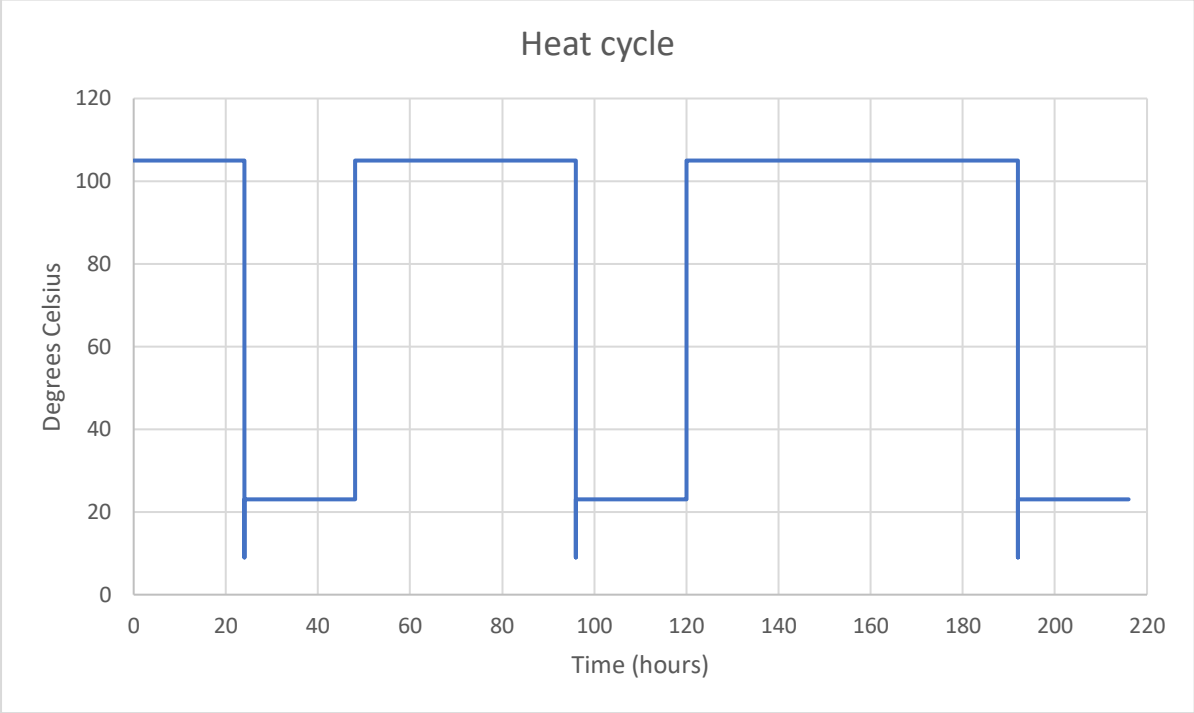

Figure 3.15 Heat vs duration for testing of leakage

From figure 3.15 one can see that the cycles goes as follows; (1) 24 hours in the oven at 105°C, (2) Pipe is removed from oven and cooled under 9°C running water for a short period of time, (3) Pipe is filled with water and left at room temperature (approximately 23°C) for 24 hours to measure amount of water leakage, (4) 48 hours in the oven, (5) repeat 2&3, (6) 72 hours in the oven, (7) repeat 2&3. During the testing interval, both the top of the pipe and the area where the pipe enters the cup where the leaked water accumulates is covered in aluminum foil to minimize water evaporation.

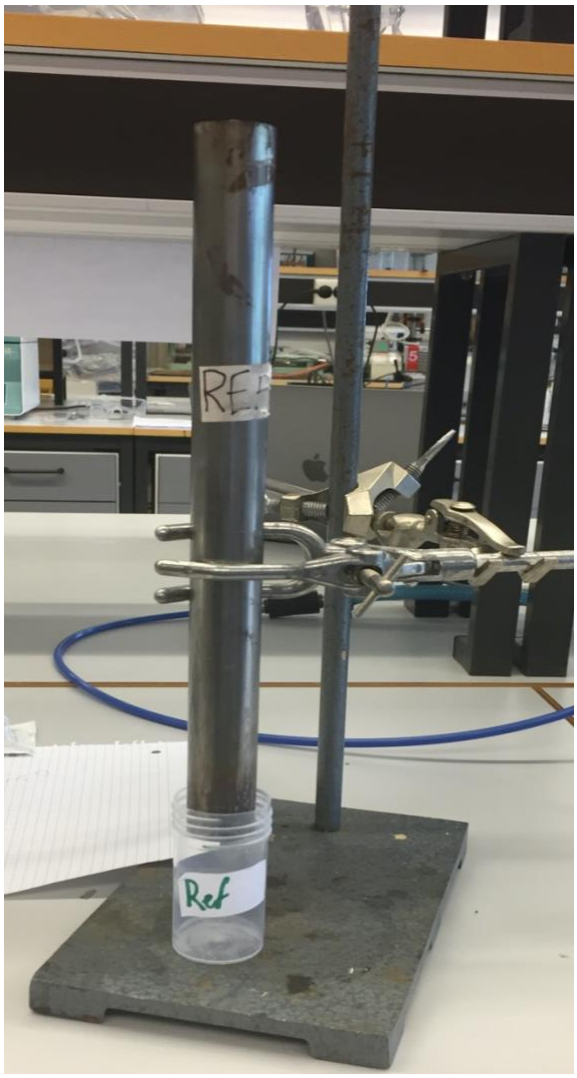

Figure 3.16 Set-up for measuring leakage rate of cement

3.3.11 Rheology

3.3.11.1 Theory

Rheology is a term that means: “The study of the deformation and flow of matter” [46]. Matter is a broad term which includes fluids, gels, pastes and other types of soft solids. The rheology of fluids is an extremely important factor in the petroleum industry due to the amount of fluid transport happening (mud/cement pumping, crude oil producing, wet gas producing etc). When circulating e.g cement it is of utmost importance to know its rheological properties as the ECD (equivalent circulating density) might be too high due to the friction created by the cement, or that the cement is too high viscosity because it is shear thickening and therefore the cement pumps are not able to properly displace it or other scenarios which can occur. There are many

developed rheology models, but this thesis will apply the Casson model described in the PhD thesis of Marylin Ochoa [47] because it is the model of choice for describing cement properties in the petroleum industry.

Equation 3-11

$$\tau^{0.5} = \tau_c^{0.5} + \mu_c^{0.5}\gamma^{0.5} \quad For\ \tau < \tau_c$$

Equation 3-12

$$\gamma = 0 \quad For\ \tau \geq \tau_c$$

Where;

τ = Shear stress [$lb_f/100ft_2$]

τ_c = Casson yield stress [$lb_f/100ft_2$]

μ_c = Casson plastic viscosity [$lb_fs/100ft_2$]

γ = Shear rate [Sec^{-1}]

The term yield stress describes the amount of applied stress which is necessary to make a "soft solid" (e.g ketchup, mayonnaise etc) flow. This is an important factor for processes such as pumping or spreading. [48] Plastic viscosity describes the resistance to flow of a fluid, and it is an important parameter for any fluid that is being pumped. A low plastic viscosity would mean that a drilling fluid would exit the bit with low viscosity and thus the fluid could be used to drill rapidly.

3.3.11.2 Procedure

A Fann 35 viscometer was used for measuring the rheological properties of the cement slurries. The cement was prepared as per standard procedure and placed in the measuring cup which was set in position. Then the readings for 300,200,100,6 and 3 RPM (revolutions per minute) were taken.

Figure 3.17 Fann 35 viscometer used for measuring rheology

4. Results and discussion

Chapter 4 presents all the results obtained throughout the testing period, both destructive (UCS & resilience) and non-destructive (modulus of elasticity, change of mass, leakage rates, rheology and heat development) results as well as relevant discussion and comparisons with other available data. All raw data for destructive tests can be found in Appendix A and data for non-destructive tests can be found in Appendix B.

4.1 Effect of nanoparticles on 0,52 and 0,44 WCR G class cement

The first four batches of testing utilized a 7-day timeframe and a water to cement ratio of 0,52, and further details has been described in chapter 3.2.1. When comparing the results obtained from testing various nanoparticles from these batches, the reference point is a single value comprised of several measurements.

The reference point was obtained by measuring all zero-additive plugs with a WCR of 0,52 and subsequently taking the average value of the measurements after removing the highest and lowest value. This includes the 0,52 WCR plugs created in test batch 5, which had the purpose of strengthening the certainty of the measured properties of the reference plugs. The large quantity of zero-additive cement plugs ensures that the average value is representative of the cement properties of this WCR.

The same was done for obtaining the average value of the zero-additive 0,44 water to cement ratio plugs, where samples from test batch 6-8 with the addition of half of test batch 5 all were used. Out of the available 8 test results, the highest and lowest UCS plugs were removed and the average of the remaining 6 are used as a reference point.

As mentioned earlier, two plugs were created for each concentration of the different nanoparticles. When presenting the data for change of mass, UCS and modulus of elasticity, the concentration of nanoparticle presented is chosen based off the largest strength increase for each nanoparticle according to the destructive testing. For 0,52 WCR measurements, this value is obtained by taking the average of the two plugs which contain the same amount of the relevant nanoparticle. This is not always the case for 0,44 WCR cement samples from test batch

6-8, as there were some difficulties regarding uncertainty (which will be covered later in chapter 4), the value is based off of one single measurement per sample.

4.1.1 Change of mass with nanoparticles on 0,52 and 0,44 WCR G class cement

After the samples had completed curing, they were weighed every 24 hours to record the change in mass observed when submerged in water. This is detailed in chapter 3.3.3.1, and to calculate the change in mass equation 3-1 is used. The change in mass is calculated based on the plugs own dry weight, measured after curing. Depicted below is the mass change of the selected concentrations from the various 0,52 WCR test batches;

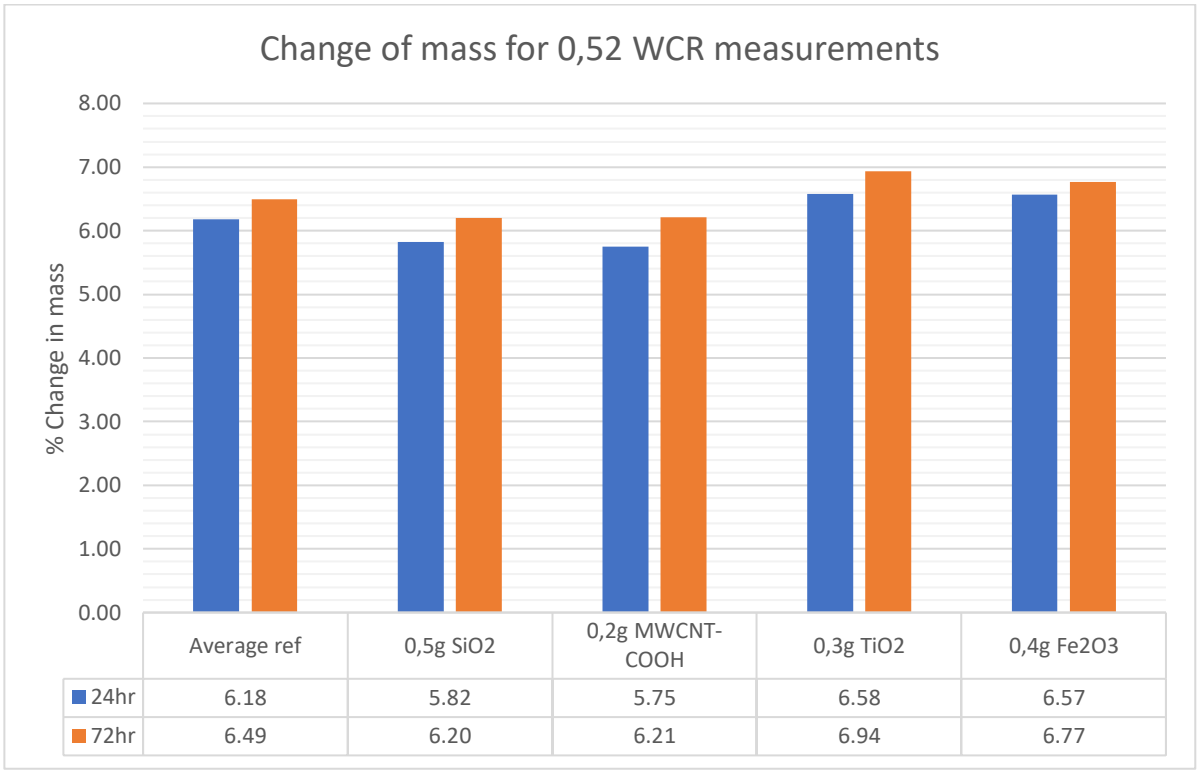

	Average ref	0,5g SiO2	0,2g MWCNT-COOH	0,3g TiO2	0,4g Fe2O3
24hr	6.18	5.82	5.75	6.58	6.57
72hr	6.49	6.20	6.21	6.94	6.77

Figure 4.1 Percent change in mass of the 0,52 WCR samples after 24 and 72 hours of being submerged in water

From figure 4.1 one can observe that the zero-additive reference plug increases approximately 6,2% and 6,5% in weight after 24 and 72 hours respectively. It was found that after 72 hours the fluid absorption had stabilized to the point where the following measurements only showed minor changes, and that this was the case for all specimen.

From figure 4.1 one observes that the lowest mass increase after 72 hours is found in the sample with added nano-SiO_2, displaying an increase of 6,2% relative to its own dry weight. The

sample containing MWCNT-COOH displays similar values to that of the nano-silica, where both of them are below the given reference at both measuring points. This could indicate that the nanoparticles have contributed to binding the cement in such a way that it helps partly or fully block some of the pore space. This is also an indication that these samples will be less prone to fluid migration through the cement.

For both nano titanium dioxide and nano-Fe_2O_3 it is observed that the mass change is larger than that of the reference point at both measured times. This might indicate that the pores have not been filled or sealed off by nano bindings, but it might also indicate that the addition of these nanoparticles have decreased the regular amount shrinkage of the cement experiences during hydration and as a result the sample has a larger bulk volume for water absorption.

In terms of procedure for the measurement and calculation of change in mass, the 0,44 and 0,52 WCR plugs are the same. It was also found that for the 0,44 WCR plugs, the sample was fully water saturated at 48 hours, and it was therefore decided to use change of mass at 24 and 48 hours instead. Depicted below are the results from the change of mass for 0,44 WCR plugs with added nanoparticle, as well as the average zero-additive reference.

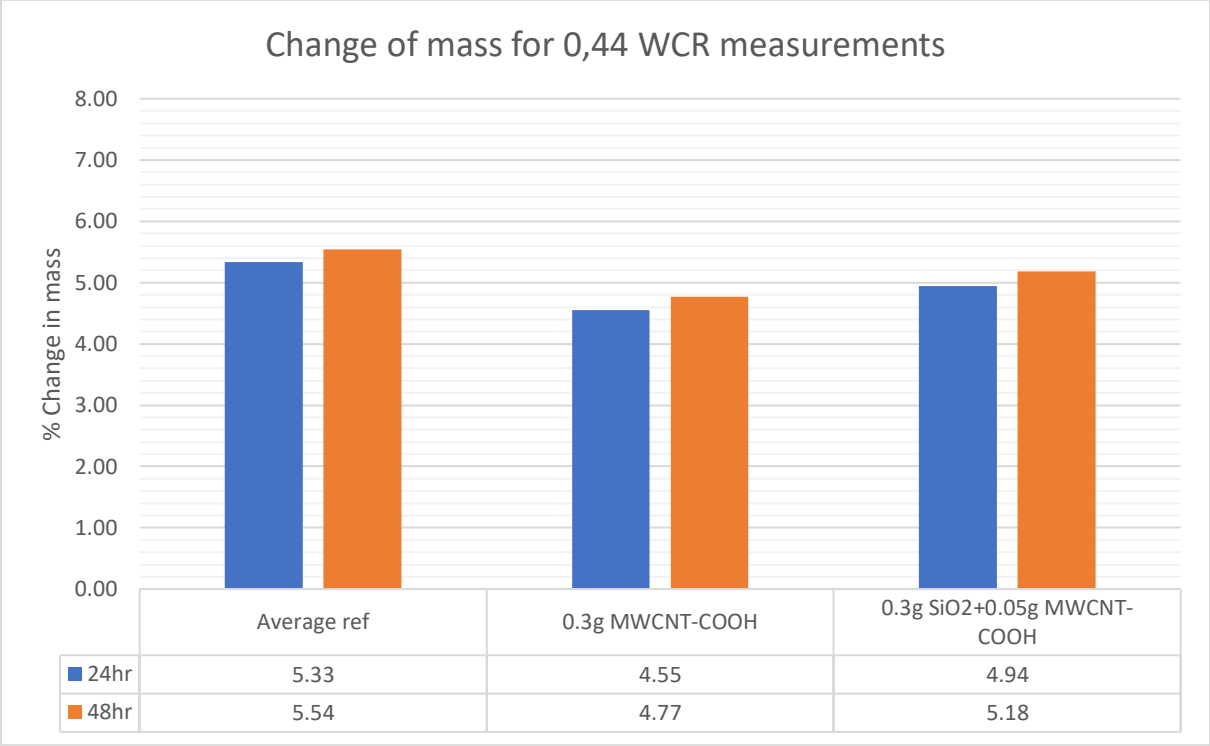

Figure 4.2 Percent change in mass of the 0,44 WCR samples after 24 and 48 hours of being submerged in water

From figure 4.2 one can observe that the zero-additive reference plug increases approximately 5,3% and 5,5% in weight after 24 and 48 hours respectively. The lowest increase in mass is observed from the addition of 0,3 grams of MWCNT-COOH with an increase of 4,6% and 4,8% after 24 and 48 hours respectively. It is also observed that for both nano-samples, the increased mass is lower than that of the control sample.

From 0,52 WCR measurements it was observed that both SiO_2 and MWCNT-COOH reduced the increase in mass, and from figure 4.2 one can observe that the mixture of the two nanoparticles also contributes to a reduction in mass change, which is to be expected. Interestingly, it seems that the mixture of both performs worse than either of the two nanoparticles by themselves, this could however easily be due to the vastly different dosages added. From figure 4.2 one can observe that the pure MWCNT-COOH performs exceptionally well and contributes to a large reduction in mass change compared to the control. This indicates that the nano has contributed to binding the cement in such a way that the nanoparticle helps partly or fully block some of the pore space as mentioned earlier, however it is observed that this effect appears to be greater when the dosage of MWCNT-COOH is increased from 0,2 grams to 0,3 grams. It is also possible that this is due to the fact that it performs the bindings in a more efficient or different manner in the 0,44 WCR cement rather than the 0,52 WCR cement.

4.1.2 Destructive results of 0,52 and 0,44 WCR G class cement with nanoparticle additives

4.1.2.1 Uniaxial compressive strength of 0,52 and 0,44 WCR G class cement with nanoparticle additives

The procedure for obtaining the destructive test results are explained in chapter 3.3.7.1 and is calculated using equation 3-7. In figure 4.3 the straight line is the UCS value of the reference point, and it is included to easier visualize where the different additives place in terms of strength increase. The destructive results from test batch 1 through 4 and part of test batch 5 is depicted below;

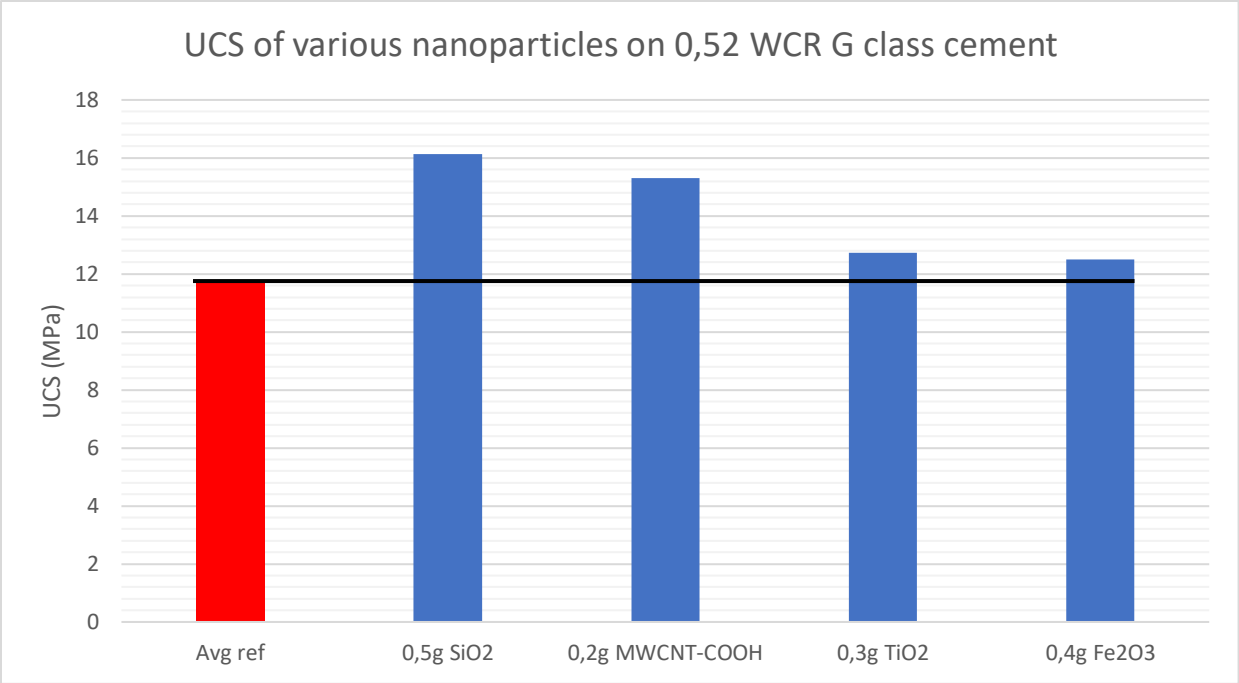

Figure 4.3 UCS of the various nanoparticles on 0,52 WCR G class cement

From figure 4.3 one can observe that the average UCS of the zero-additive samples is approximately 11,8 MPa, and that all of the samples with nanoparticle additives lies above this value. The highest UCS is achieved through the addition of nano-silica, and it is at 16,1 MPa which is a 36,9% increase compared to the zero-additive cement. Furthermore, one observes that also MWCNT-COOH results in a substantial increase in UCS with a 29,6% increase at a value of 15,3 MPa. The increase in strength is also present for both TiO_2 and Fe_2O_3, with an 8,0% and a 6,3% increase respectively. This figure shows that at the correct concentration, all of the tested nanoparticles proved to be beneficial with regards to uniaxial strength development.

The UCS value for the zero-additive 0,44 WCR cement plugs is marked in dark red and a straight line is drawn from it to easier compare the results of the added nanoparticles relative to the control. The destructive test results which yielded the highest UCS from 0,44 WCR cement plugs with added nanoparticles is shown below.

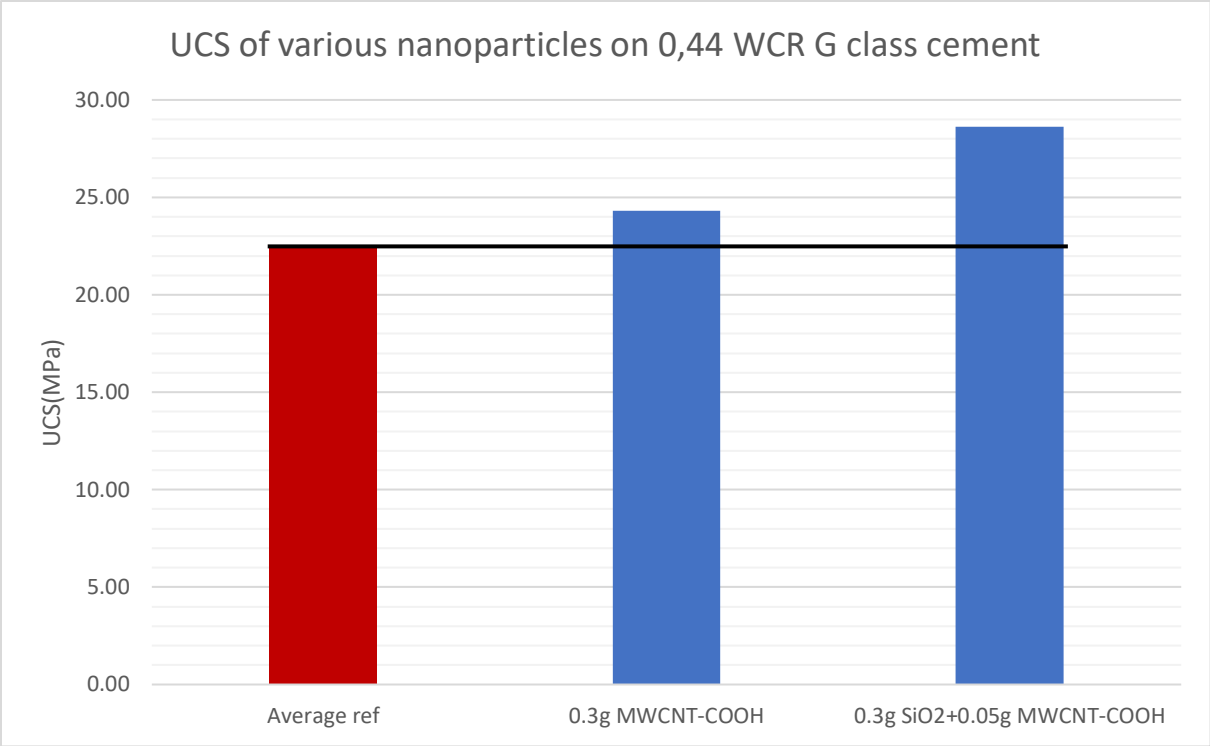

Figure 4.4 UCS of the various nanoparticles on 0,44 WCR G class cement

From figure 4.4 it shows that the UCS of the reference plug is approximately 22,5 MPa, which is nearly twice as high as the 0,52 WCR reference point. Furthermore, the addition of 0,3 grams of MWCNT-COOH increased the UCS to 24,3 MPa, which is a 7,9% increase. On 0,44 WCR cement, the highest UCS increase was obtained through the addition of 0,3grams SiO_2 + 0,05grams of MWCNT-COOH, which resulted in an increase of 27,1%.

An interesting difference between figure 4.3 and 4.4 is the massive difference between the performance of MWCNT-COOH. Going from a 29,6% to a 7,9% increase is an unexpected disparity in the results. This is a good example showcasing the different effects of the same nanoparticle on two different ratios of cement and water, meaning the results obtained may be closely related to several factors within the cement slurry, and not exclusively dependent on dosage and type of nanoparticle added. Other factors may also influence the results, especially uncertainties in the experiments.

From other conducted studies, it has been found that nano-silica synergizes well with additional additives in the cement slurry, and that it does not impede their function. [11] This was found to be valid for regular cement additives, such as retarder, but can also be applied to better describe the positive effect with the hybrid. It is anticipated that the hybrid mixture would result

in an increase in the uniaxial compressive strength due to the benefits showcased by each individual nanoparticle in their own respective measurements, but there were large uncertainties in the matter of how effective it would be.

4.1.2.2 Young´s modulus of 0,52 and 0,44 WCR G class cement with nanoparticle additives

To give a description of a materials brittleness or ductility, Young's modulus (E) can be applied. A high Young's modulus corresponds to a material with high elasticity which translates into a material that is brittle, and a low E will then correspond to a material which is more ductile. Young's modulus was calculated using equation 3-8. Shown in the figure below is the Young's modulus of the best performing plugs with 0,52 WCR from various nanoparticles with respect to UCS measurements.

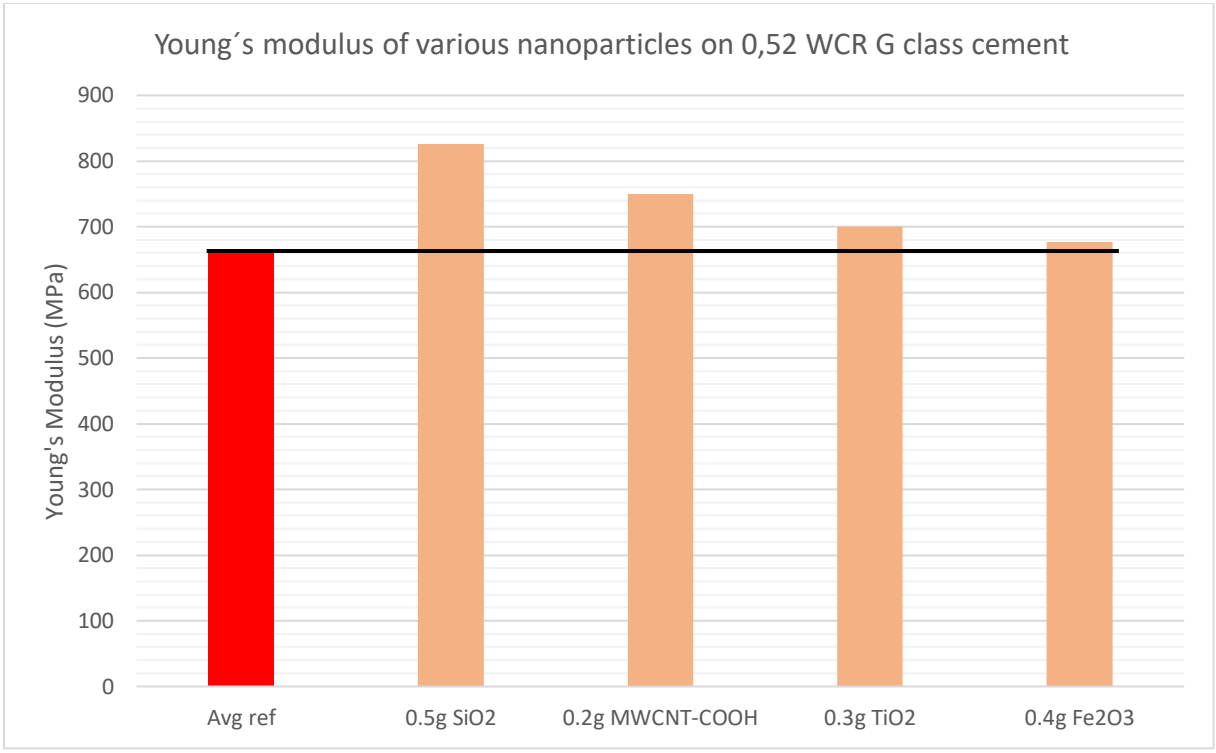

Figure 4.5 Young´s modulus of various nanoparticles on 0,52 WCR G class cement

From figure 4.5 one can observe that the average Young's modulus of the zero-additive plugs is marked in red, and a straight line is drawn from it to easier compare the other results to the control. Furthermore, one can observe that all of the displayed values which contain added nanoparticles, lie above the control sample. The trend displayed from figure 4.5 matches the trend observed in figure 4.3 with the plug which had the highest UCS also displaying the highest

Young's modulus. The largest increase in E is 24,9% and stems from the addition of 0,5grams of nano-silica. The lowest increase is observed from the addition of nano-Fe_2O_3 which yields an increase of 2,4%. These results could indicate that for the measured plugs, an increase in UCS corresponds to a cement which is more brittle than the cement with no additives, as E increases in a similar manner to UCS.

The same calculations were done for 0,44 WCR, and shown below is the Young's modulus for the best performing plugs from test batch 5-7 with respect to their UCS measurements.

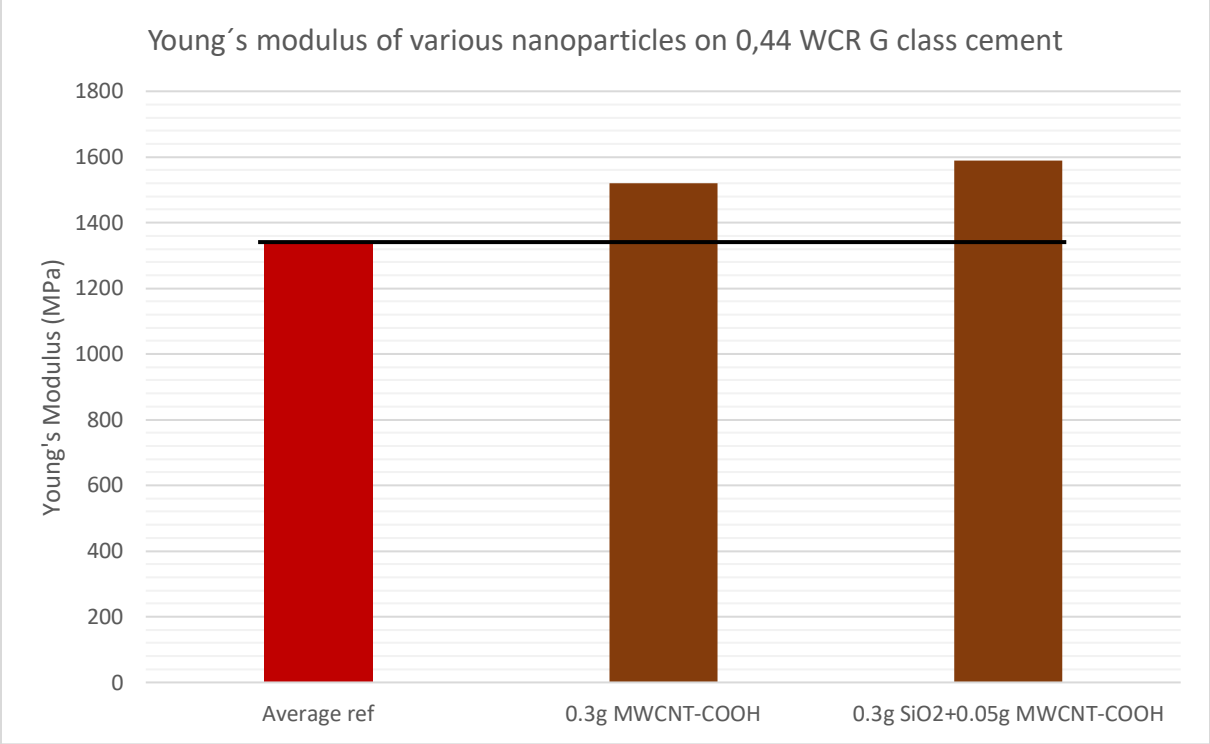

Figure 4.6 Young´s modulus of various nanoparticles on 0,44 WCR G class cement

From figure 4.6 it shows that both of the tested nanoparticles resulted in an increase of Young´s modulus. The largest increase is observed from the hybrid mixture, and the trend shown in figure 4.6 matches the trend from figure 4.4 closely. The sample with added MWCNT-COOH has an increase in E of 13,0% whilst the hybrid increases by 18,2%. The results observed from figure 4.6 correspond well with the results observed from the 0,52 WCR cement samples, as from the observed results it appears that for any of the tested additives, a major increase in UCS leads to an increase in Young´s modulus, and that these additives do not make the material more ductile.

4.1.2.3 Resilience of 0,52 and 0,44 WCR G class cement with nanoparticle additives

As mentioned in chapter 3.3.8, resilience measures the total amount of energy the sample can absorb until reaching maximum stress, known as UCS. This parameter takes both the UCS and the Young's modulus into account and can be used to better describe the property of the cement sample. One of the primary objectives of the additives is to increase the UCS, as it is highly desirable to obtain a high UCS, but combining this with a low value of E will cause the plug to be able to deform without sustaining permanent damage whilst still being able to withstand high pressures. Calculation of resilience was done using equation 3-10. Shown in the figure below is the resilience of the best performing concentrations with respect to UCS.

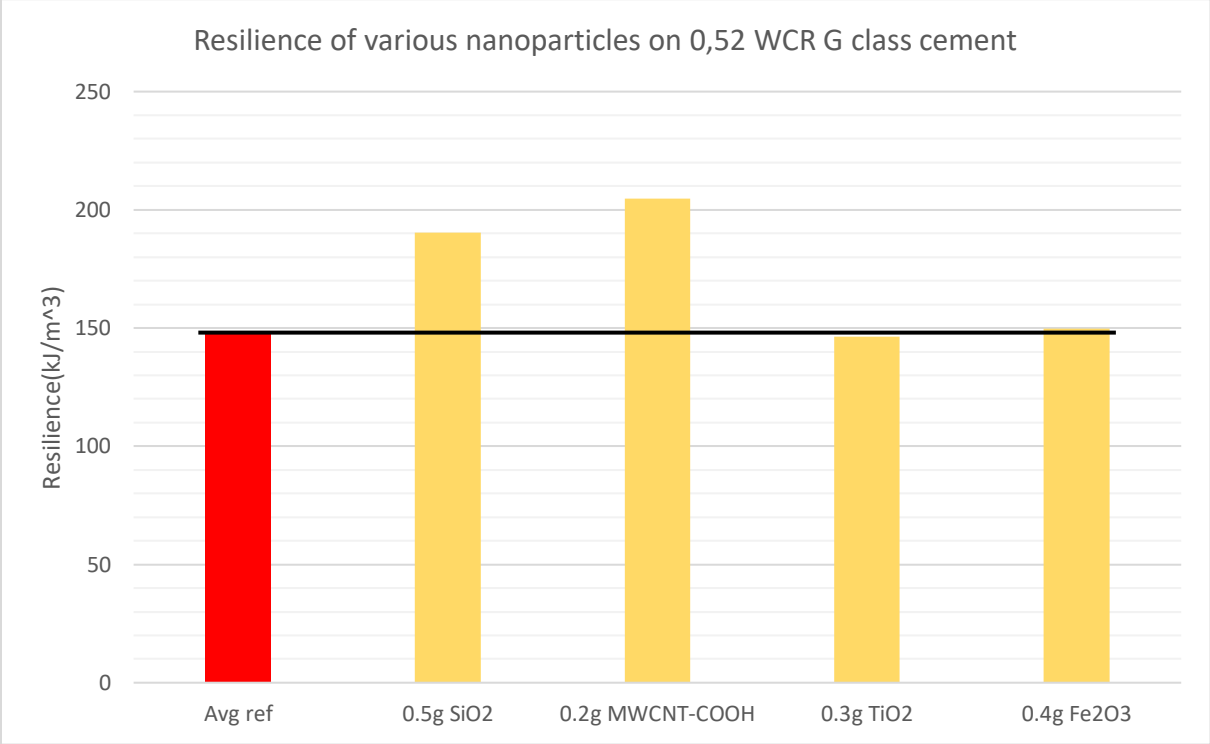

Figure 4.7 Resilience of various nanoparticles on 0,52 WCR G class cement

From figure 4.7 one can observe the average zero-additive plug marked in red with a straight line drawn from it to easier compare the other results to the control. From figure 4.7 it shows that the largest increase in resilience was obtained by adding MWCNT-COOH to the cement slurry, which yielded an increase of 38,7% compared to the control. One can also observe that for all but one of the tested nanoparticles, the resilience is improved compared to the control. For the addition of nano-TiO_2, the resilience decreased by 0,9%.

From previous results it is known that the largest increase in UCS and E comes from the addition of nano-silica, but that does not yield the largest increase in resilience. This shows that because the Young´s modulus of the MWCNT-COOH additive is smaller, while the UCS is still high, the result is a material which is able to absorb more energy before it reaches the maximum stress.

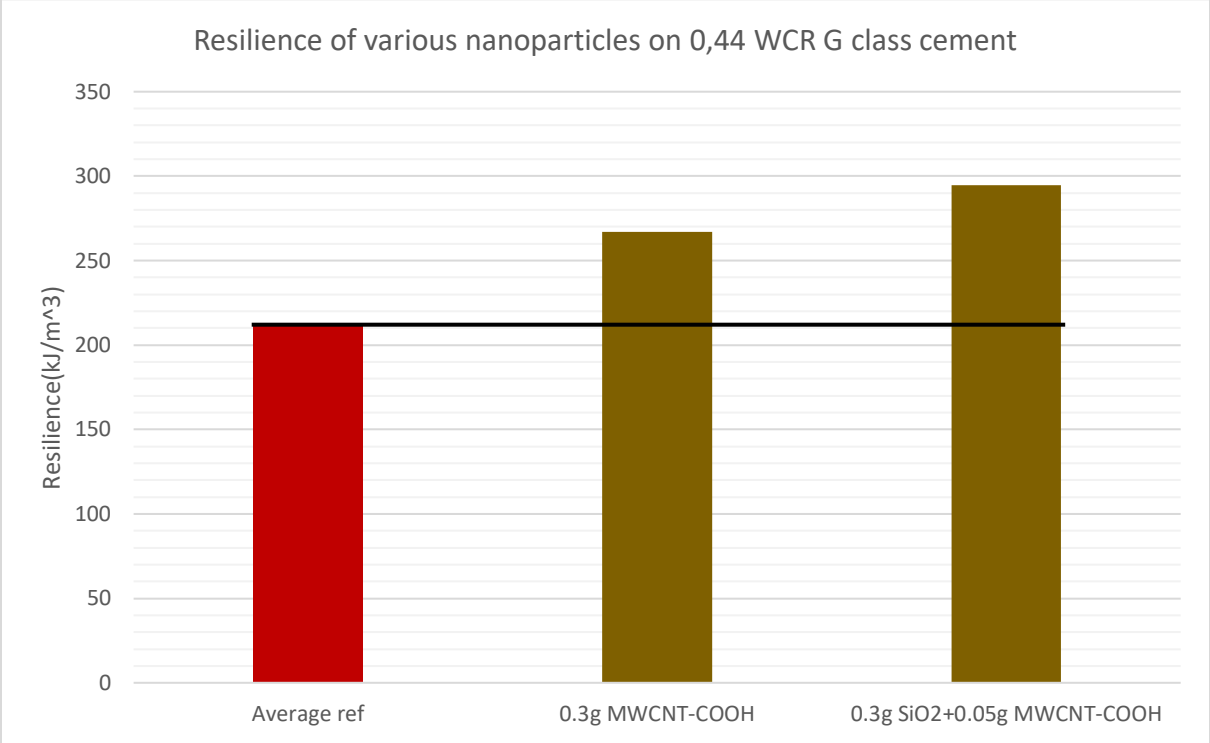

Figure 4.8 Resilience of various nanoparticles on 0,44 WCR G class cement

From figure 4.8 one can observe that both of the tested samples yield a relatively large increase in resilience compared to the reference point. The highest increase of 38,4% comes from the hybrid sample, while the MWCNT-COOH increases by 25,4%. These resilience results show that both the UCS and Young´s modulus increase at the same rate for the two tested samples, and thus the resilience of the hybrid is the highest.

4.1.3 Modulus of elasticity of 0,52 and 0,44 WCR G class cement with nanoparticle additives

The procedure for obtaining the non-destructive test results are explained in chapter 3.3.5.2 and is calculated using equation 3-6 with data measured at 7 days, right before the samples were subjected to destructive testing. In figure 4.9 the straight line is the M-modulus value of the reference point, and it is included to easier visualize where the different additives place in terms

of change of M-modulus relative to the reference point. The non-destructive results from test batch 1 through 4, where part of test batch 5 is included in creating the reference point, is depicted below;

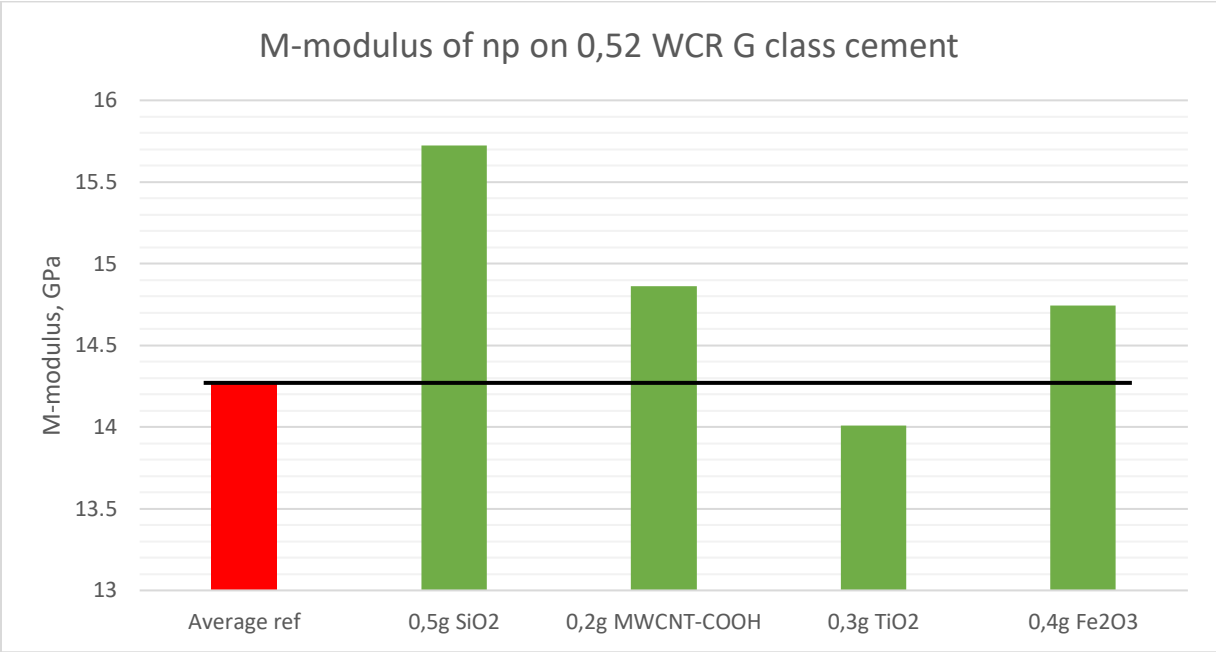

Figure 4.9 M-modulus for test batch 1-4

From figure 4.9 it shows that the average modulus of elasticity of the zero-additive plugs is approximately 14,3 GPa, and that all but one of the nano-plugs lie above that value. One can observe that the trend from figure 4.9 is similar to that of figure 4.3, with the highest M-modulus being the nano-silica plug with a 10,2% increase compared to the zero-additive plug. Furthermore, the second highest M-modulus is observed to be the MWCNT-COOH plug, which also had the second highest UCS value.

A correlation between figure 4.9 and 4.3 was expected due to the fact of what the M-modulus represents. It is calculated and based on the sonic travel time through the test sample, which is heavily impacted on the inner structure of said sample. High M-modulus values (corresponding to low sonic values) are associated with an inner structure which is intact and contains little to no cracks or big pore spaces. A high modulus of elasticity directly corresponds to a dense material, making it reasonable to assume that this would result in a higher compressive strength which appears to be the case for most of the samples.

Figure 4.9 shows that even though the nano-silica, MWCNT-COOH and nano-Fe_2O_3 matches well with respect to UCS values, the titanium dioxide appears to be an anomaly. Here one can observe that the M-modulus decreases whilst the UCS value increases.

The same method was used to obtain the M-modulus for 0,44 WCR samples which contained nanoparticles, and the results are shown below.

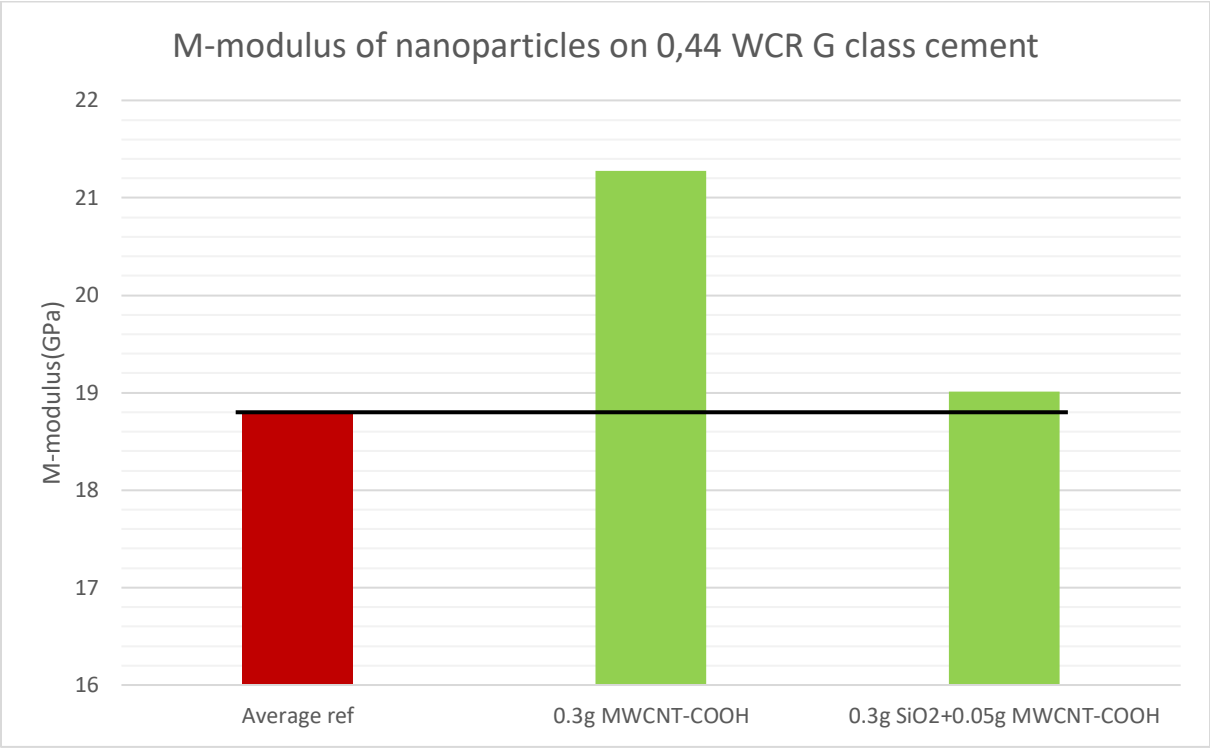

Figure 4.10 Modulus of elasticity for 0,44 WCR batches with added nanoparticles

From figure 4.10 it shows that the average M-modulus for the zero-additive plugs of 0,44 WCR is 18,8 GPa, and a straight line was drawn from it to easier visualize where the other measurements lay compared to control. One can observe that the results found in figure 4.4 does not correspond well with the results shown here, even though that could be reasonably expected. It does, however, show an increase in M-modulus for both samples which is expected, as the UCS was also increased for both samples.

From the graph above one can observe that the greatest increase in M-modulus is observed for the addition of pure MWCNT-COOH, which resulted in a M-modulus of 21,3 GPa which corresponds to an increase of 13,2%. The addition of the nanoparticle hybrid mixture also results in an increased M-modulus; however, this increase is significantly smaller, at 1,1%.

One can expect a strong correlation between figure 4.4 and 4.10, as they are closely related through the properties of the sample. The interesting part is that contrary to the 0,52 WCR results, this graph does not show a good correlation. The sample with the smallest UCS increase shows a significant increase in M-modulus, whereas the sample which significantly increased UCS shows a very small increase in M-modulus. This could be explained by geometric uncertainties in the sample affecting the destructive measurements.

4.1.4 Effect of SiO_2

From other conducted experiments we know that the addition of nano-silica provides a positive effect on the cement paste. [35], [49][11] These results are however, under other procedures and conditions which differs from the ones used in this thesis. When making the test batch using a colloidal mixture of nano-SiO_2 it was unsure what to expect in terms of degree of success and optimal concentration. Therefore, a wide range of concentrations were used to screen out the approximate concentration which yielded the largest strength increase. Depicted below are the destructive results from the various concentrations of nano-SiO_2;

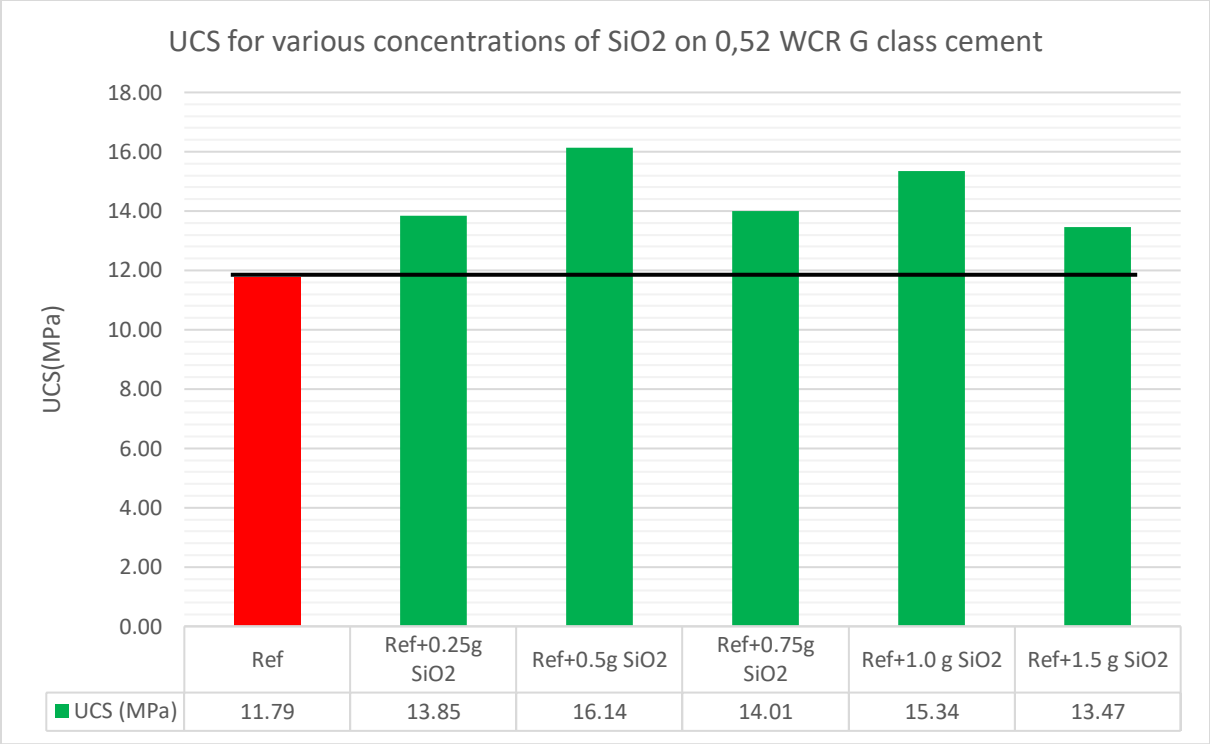

Figure 4.11 UCS for different concentrations of nano-silica

The value for the zero-additive plugs, named “ref”, is an average value calculated based on 9 different destructive measurements. The value is marked red on the graph and a straight line is drawn from it to easier visualize the values of the other measurements relative to the reference point. From figure 4.11 one can observe that for all concentrations of SiO_2 added, an increase in uniaxial compressive strength is observed.

One observes from the graph that the different concentrations display a varying degree of success in terms of increased strength, and that the largest increase is observed from the addition of 0,5 grams of nano-silica. The general trend observed is that the strength increase peaks at this concentration and that the increase is smaller for both lower and higher concentrations of added nano. The exception to the trend is observed for 1,0 grams added, as it displays a second smaller peak. It is reasonable to assume that this is an abnormality and that the general trend still applies, as too much nano might impair the quality of the cement as seen from the addition of 1,5 grams of nano silica. It is therefore reasonable to assume that the optimal concentration of SiO_2 for 0,52 WCR lies in the proximity of 0,5 grams added.

During the hydration phase of the cement, the added nano-silica may accelerate the formation of C-S-H gel and therefore improve cement strength. Additionally, the size of the silica particles may allow it to fill the gaps between the larger cement particles, resulting in a denser matrix, which could explain the results obtained through the destructive testing.[11]

Based on the stress-strain curve generated for the UCS measurements, the Young´s modulus of the plugs were calculated, and the results are shown below:

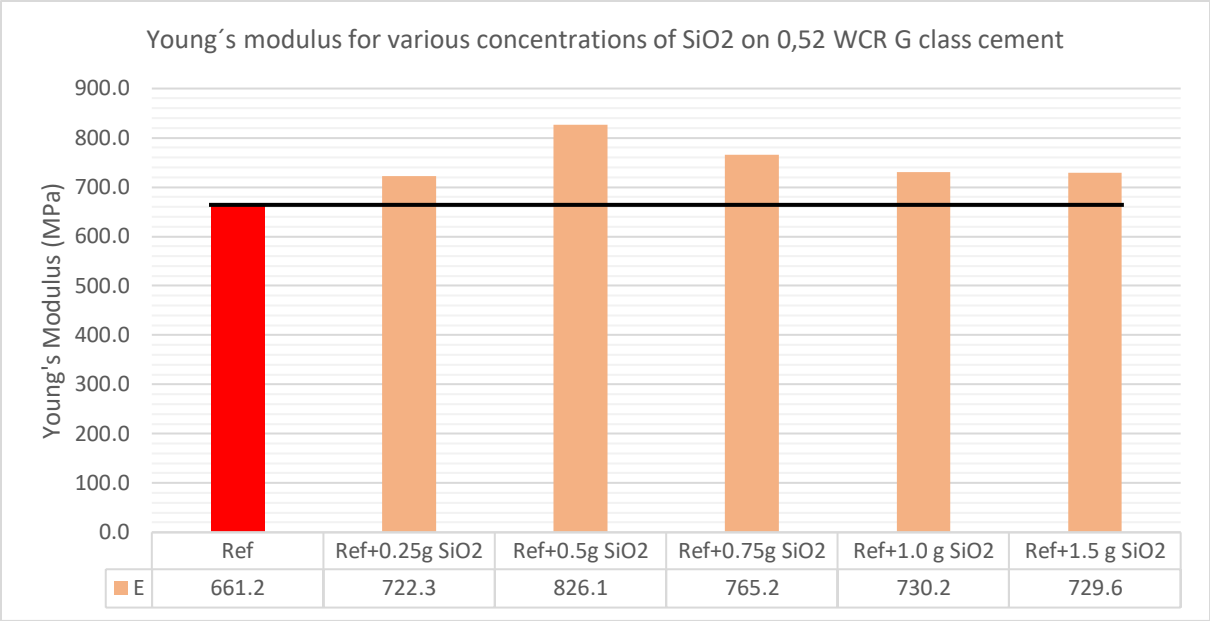

Figure 4.12 Young´s modulus for various concentrations of SiO2 on 0,52 WCR G class cement

From figure 4.12 it shows that for all the tested concentrations of nano-silica, the Young´s modulus increases. The increase is most prominent at the intermediate concentrations, with the highest E being achieved from the addition of 0,5g SiO_2. Furthermore, it indicates that even though the UCS increased, the amount of deformation the plugs were able to withstand did not increase substantially and hence an increase in Young´s modulus is observed.

From the stress-strain curve generated by UCS measurements, the resilience was calculated by finding the area under the curve, and the results are shown below;

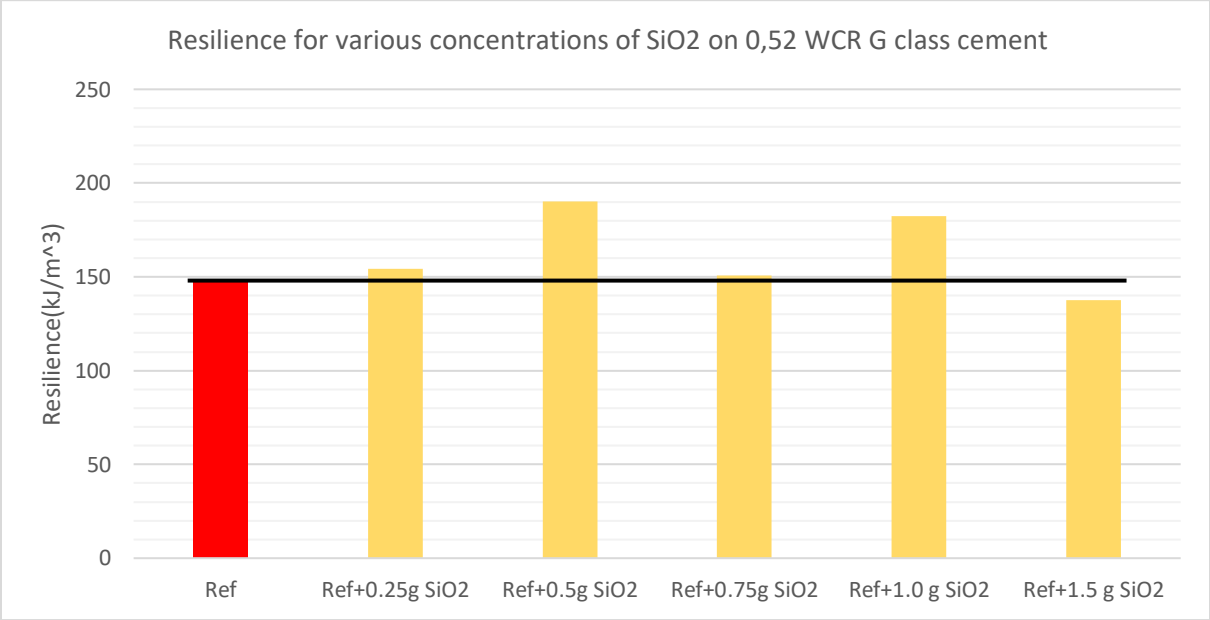

Figure 4.13 Resilience for various concentrations of SiO2 on 0,52 WCR G class cement

From figure 4.13 it is observed that all but one of the tested concentrations gives a resilience which is higher than the control. Through the addition of 1,5 grams of nano-silica, the resilience decreases by 6,8% which indicates that the concentration is suboptimal compared to the other concentrations. Additionally, the results show that the resilience varies greatly between concentrations, and that there are no apparent trends visible. The highest resilience is achieved through the concentration which yields both the highest UCS and the highest Young´s modulus, which is the addition of 0,5 grams of nano-silica.

4.1.5 Effect of MWCNT-COOH

The effect of MWCNTs on cement paste has been studied, and proved to be beneficial. [49][19]. These results were obtained through testing procedures differing from this thesis, so the effect of an aqueous dispersion of MWCNT-COOH were relatively unknown, and a wide range of concentrations were tested to screen out the optimal dosage which would yield the largest strength increase. Presented below are the destructive test results obtained from all the MWCNT-COOH concentrations.

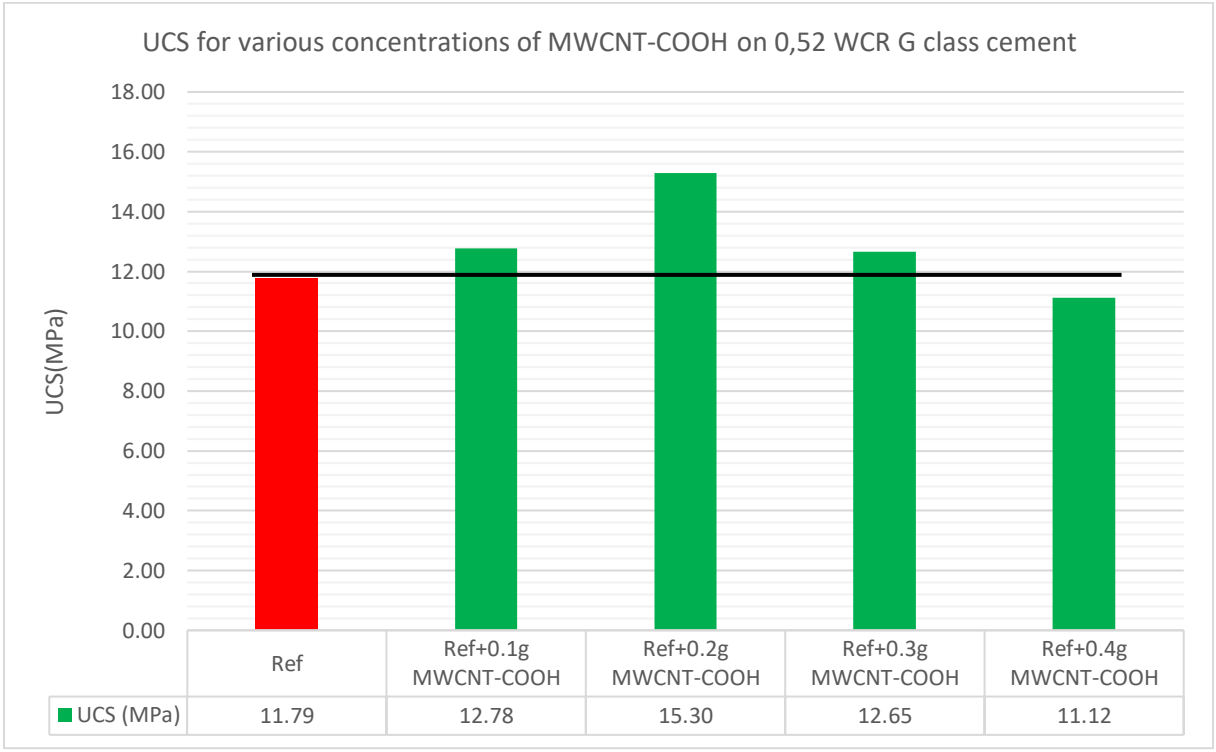

Figure 4.14 UCS for different concentrations of MWCNT-COOH on 0,52 WCR cement

The average zero-additive plug value is again marked in red, and a straight line is drawn from it to easier compare the results to the control plug. From figure 4.14 one can observe that the strength increase peaks at an added dosage of 0,2 grams of MWCNT-COOH. Additionally, a clear trend is observed; the strength increase grows until it reaches its peak at 0,2 grams added, and decreases nearly linearly with concentrations above the peak value. An interesting note is that for the addition of 0,4 grams, the highest tested dosage, the destructive test results yielded a UCS lower than that of the control.

Carbon nanotubes have a tendency to agglomerate due to the high van der Waals forces of their surfaces. When adding too much MWCNT to the cement mixture, it is possible that the MWCNTs would remain agglomerated after the cement has hardened causing impaired strength due to induced local stresses, which could be what is observed for ref+0.4g MWCNT-COOH on the destructive test results for 0,52 WCR. [50]

Based on the stress-strain curve generated for the UCS measurements, the Young´s modulus of the plugs were calculated, and the results are shown below:

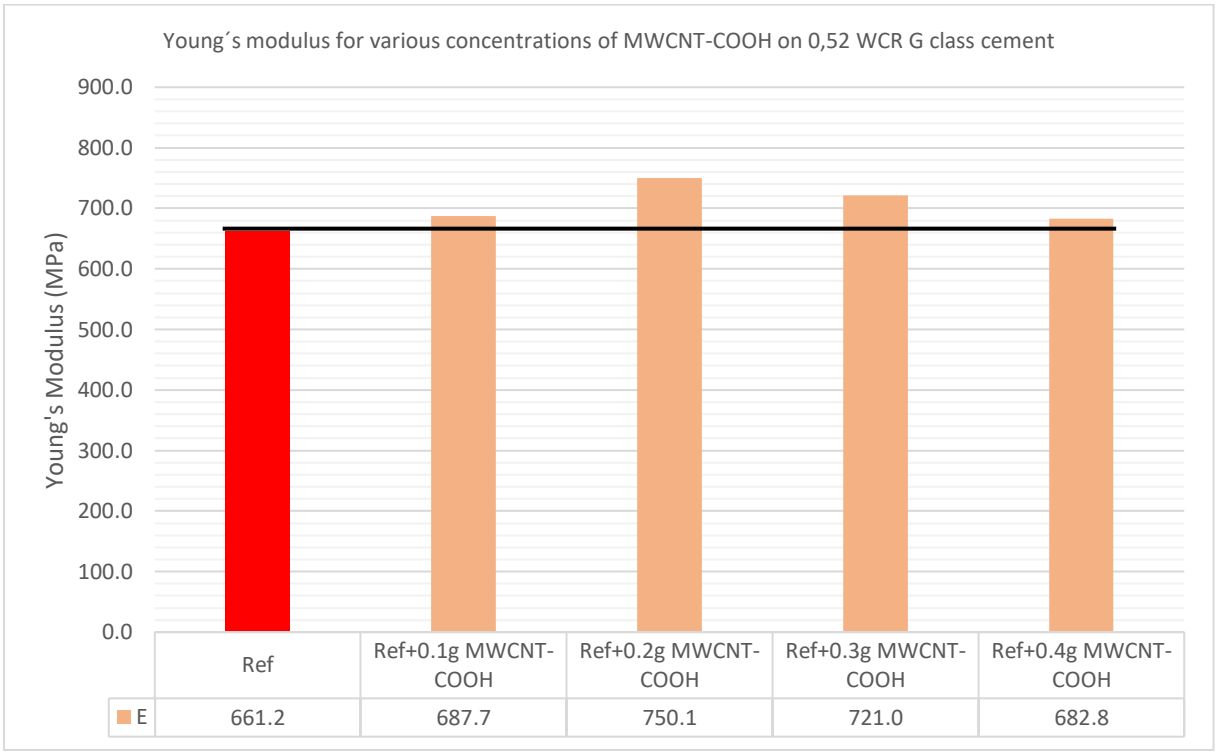

Figure 4.15 Young´s modulus for various concentrations of MWCNT-COOH on 0,52 WCR G class cement

From figure 4.15 it shows that for all the tested concentrations of MWCNT-COOH, the Young´s modulus increases. This effect is best observed from the addition of 0,2 grams MWCNT-COOH where the increase is 13,4%. The lowest increase is observed from the highest concentration tested, and is at 3,3%. When excluding the highest concentration, these results indicates that the total amount of deformation the plugs were able to withstand before breaking did not increase, even though the UCS did increase and thus, made the slope in the stress-strain curve steeper which corresponds to an increase in Young´s modulus.

From the stress-strain curve generated by UCS measurements, the resilience was calculated by finding the area under the curve, and the results are shown below;

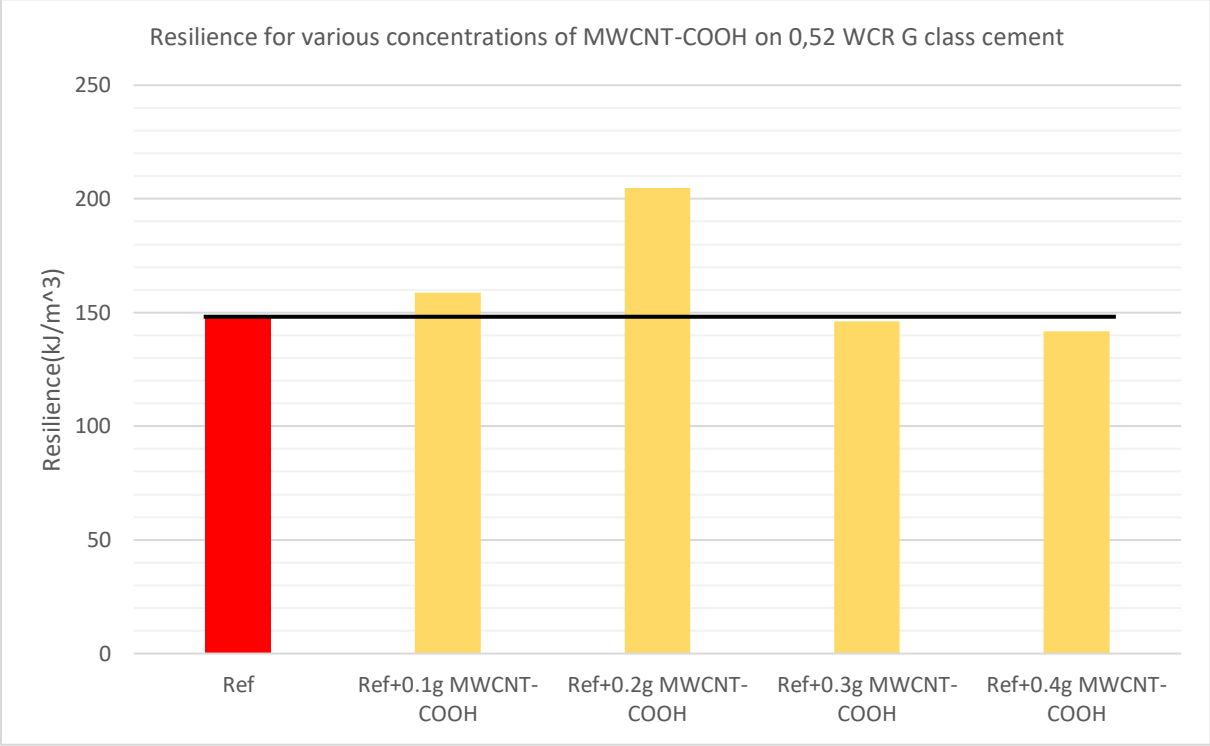

Figure 4.16 Resilience for various concentrations of MWCNT-COOH on 0,52 WCR G class cement

From figure 4.16 one can observe that the greatest increase in resilience comes from the addition of 0,2 grams of MWCNT-COOH and is at an increase of 38,7%. Furthermore, the addition of 0,1 grams increases resilience whilst both 0,3 and 0,4 grams decreases resilience. The trend observed from figure 4.16 matches the trend of the UCS plot closely even though 0,3 grams added lies below the control in figure 4.16. These results demonstrate that by adding too much of the nanoparticles to the cement slurry, the resultant cement will be able to absorb less energy before reaching its maximum stress.

As described in chapter 3.2.1.6 the purpose of test batch no. 6 was to confirm the findings of the 0,52 WCR measurements whilst testing in accordance to API standards for G class cement. The dosages chosen were therefore the same, with an additional higher concentration added to further investigate the effect of high concentration of nanoparticle. The 0,44 WCR results are shown below in figure 4.17

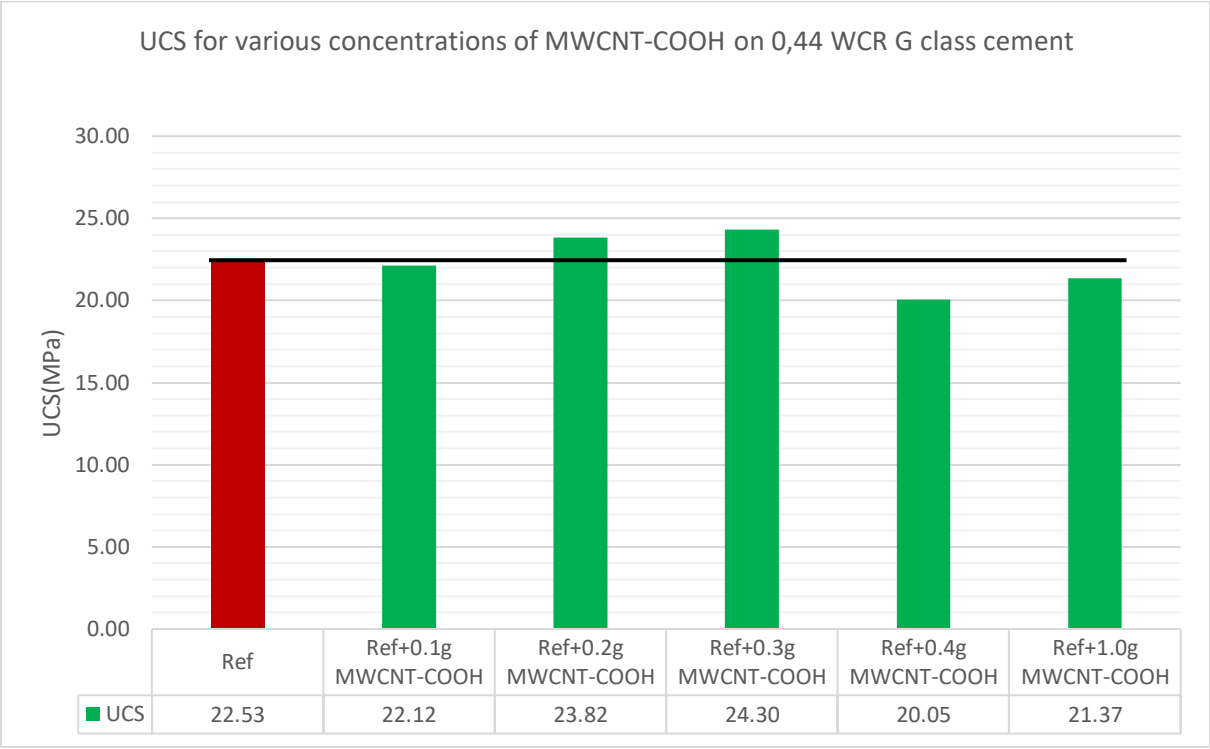

Figure 4.17 UCS for different concentrations of MWCNT-COOH on 0,44 WCR cement

From figure 4.17 it shows that the percentage increases obtained from 0,52 WCR testing are not replicated when utilizing 0,44 WCR cement. Naturally, the UCS of any given sample is higher for 0,44 WCR cement, but the effect of added MWCNT-COOH is not as noticeable when comparing it to the relevant control value. For 0,1-0,4 grams added, a similar trend observed from 0,52 WCR testing is recognized. The peak concentration is 0,3 grams of added MWCNT-COOH which yields a strength increase of 7,87% which is substantially lower than the peak strength increase for 0,52 WCR testing. Tested concentrations below 0,3 grams show a lower UCS, with the added dosage of 0,1 grams lying below the control. Dosages 0,4 grams and 1,0 grams both lie below the control, where 0,4 grams appears to be the weakest plug of all concentrations tested, which is consistent with what was observed for testing with 0,52 WCR cement. Overall, the same type of trend appears for both WCRs, but the relative change in

strength is vastly different, additionally, several dosages in these results lie below the control value, which was not observed from the 0,52 WCR results.

Based on the stress-strain curve generated for the 0,44 WCR UCS measurements, the Young's modulus of the plugs was calculated, and the results are shown below:

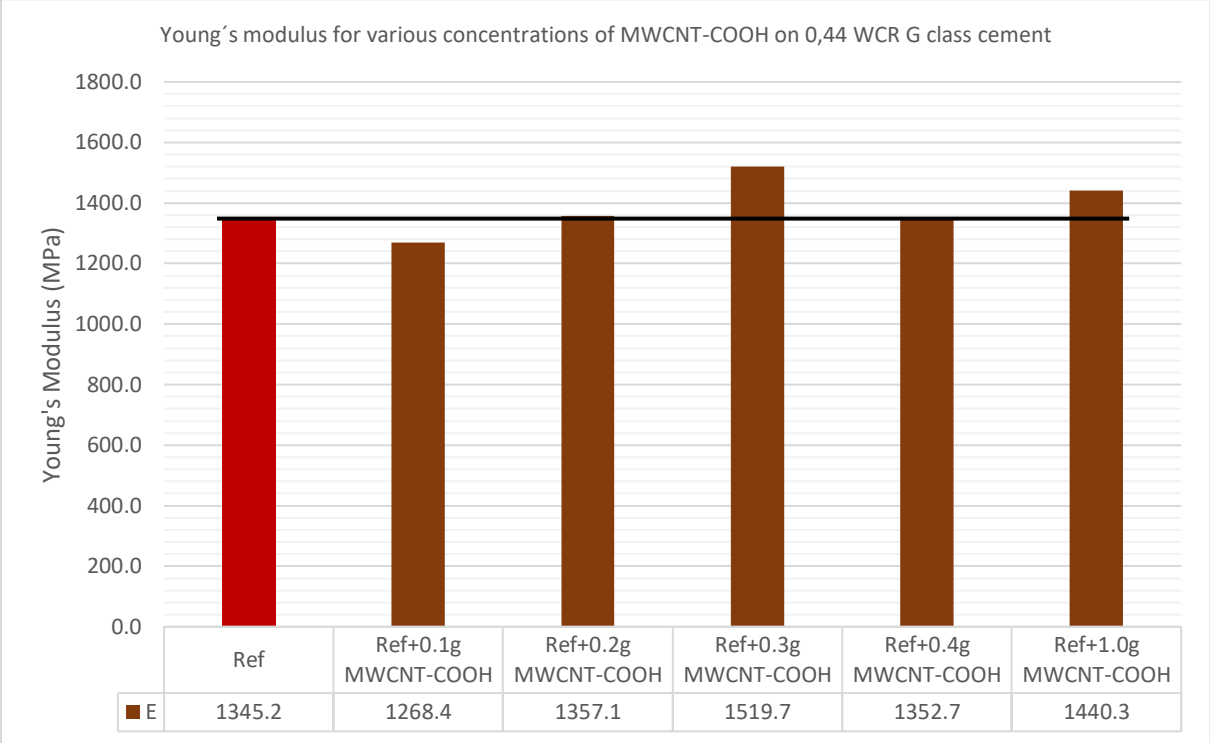

Figure 4.18 Young´s modulus for various concentrations of MWCNT-COOH on 0,44 WCR G class cement

The result shown in figure 4.18 show different results from the Young´s modulus of the same nanoparticle on 0,52 WCR cement. When changing from 0,52 WCR to 0,44 WCR, the %bwoc of the nanoparticle changes when applying the same dosage. This explains the change in the peak to 0,3 grams instead of 0,2 grams added. This new peak at 0,3 grams of MWCNT-COOH added causes an increase of 13%. Furthermore, the trend from figure 4.18 is similar to the one observed from Young´s modulus of 0,52 WCR cement. The addition of 1,0 grams of MWCNT-COOH appears to increase the Young´s modulus quite substantially, creating an anomaly in the trendline.

From the stress-strain curve generated by 0,44 WCR UCS measurements, the resilience was calculated by finding the area under the curve, and the results are shown below;

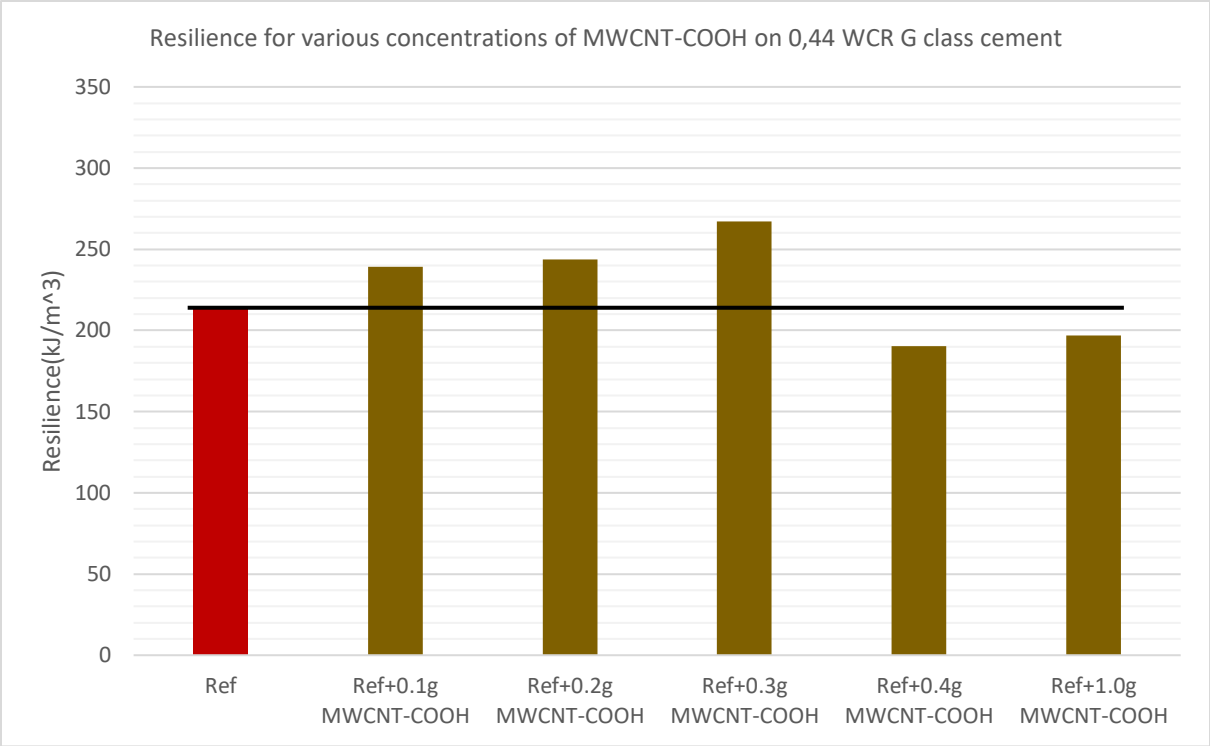

Figure 4.19 Resilience for various concentrations of MWCNT-COOH on 0,44 WCR G class cement

When taking into account the change in %bwoc, the results shown in figure 4.19 appears to match those of the 0,52 WCR quite closely. It shows that from the addition of too much nano, the plugs overall ability to absorb energy decreases. The largest increase in resilience is observed from the addition of 0,3 grams MWCNT-COOH and is at a 25,4% increase. The results show that for lower concentrations of added MWCNT-COOH the values of UCS and E change in such a way that the resultant cement plugs have higher energy storage than the zero-additive control plug.

4.1.6 Effect of Fe_2O_3

From previous studies, various benefits of nano-Fe_2O_3 on oil-well cement has been found. [21] This study deals with a different grade of cement (H class) and a different WCR (0,38) as well as iron oxide in powder form, so the expected results from this test were largely unknown. Therefore, a wide range of concentrations were tested to screen out the optimal amount of iron oxide which would most improve the strength of the hardened cement. Below is a graph displaying the UCS for all the tested concentrations.

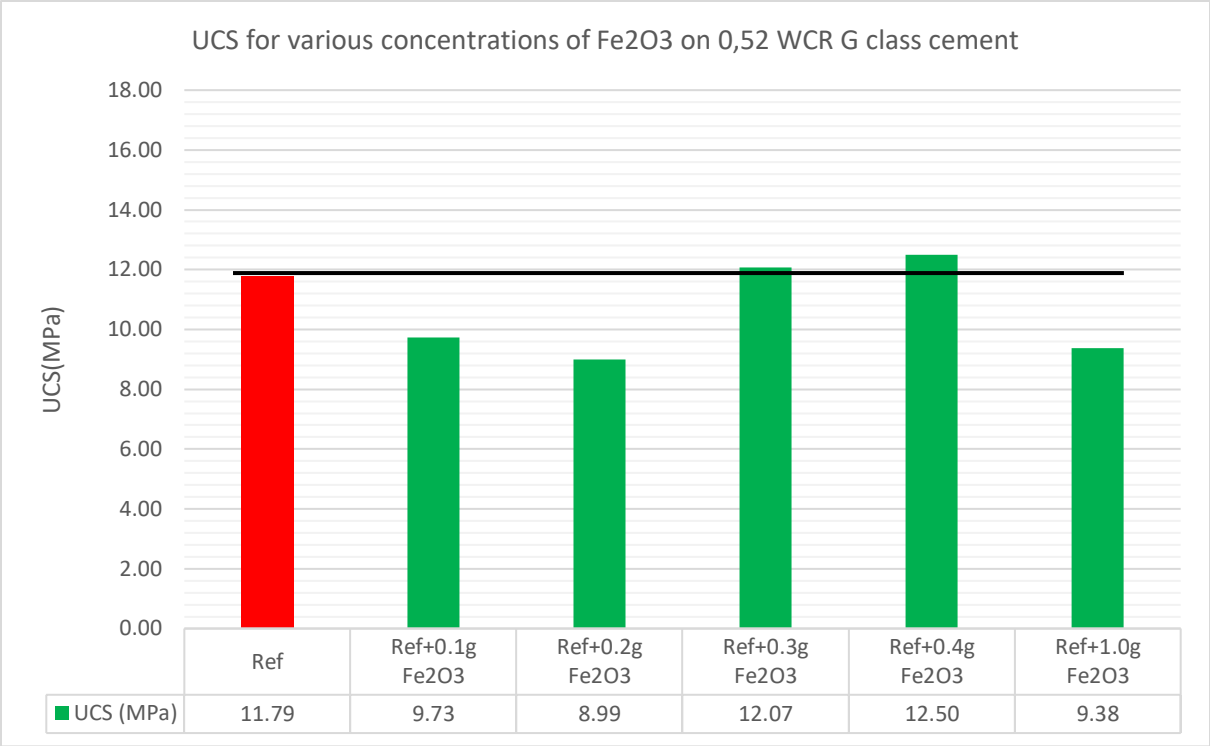

Figure 4.20 UCS for different concentrations of Fe2O3

From figure 4.20 one can observe large contrasts in the effect of added iron oxide nanoparticles. Ref is the zero-additive average value, and the line is inserted to easier compare the results to the control value. From the graph it shows that both 0,1 and 0,2 grams of added Fe_2O_3 contributes to a decrease in compressive strength. One can observe that if the dosage is increased further, to 0,3 grams added, the strength is slightly increased and that the largest increase is observed at a dosage of 0,4 grams. This increase is relatively small compared to the increase observed from other nanoparticle additions. Increasing the dosage too much leads to a decrease in compressive strength as observed from ref+1.0grams of Fe_2O_3.

The results obtained were slightly unexpected as previous studies proved substantially larger strength gains. This discrepancy can be attributed to the differences in materials used for testing and execution of said tests. It is however possible that the addition of nano-Fe_2O_3 provided several other benefits, which were not tested for in the experiments for this thesis.

Based on the stress-strain curve generated for the UCS measurements, the Young´s modulus of the plugs were calculated, and the results are shown below:

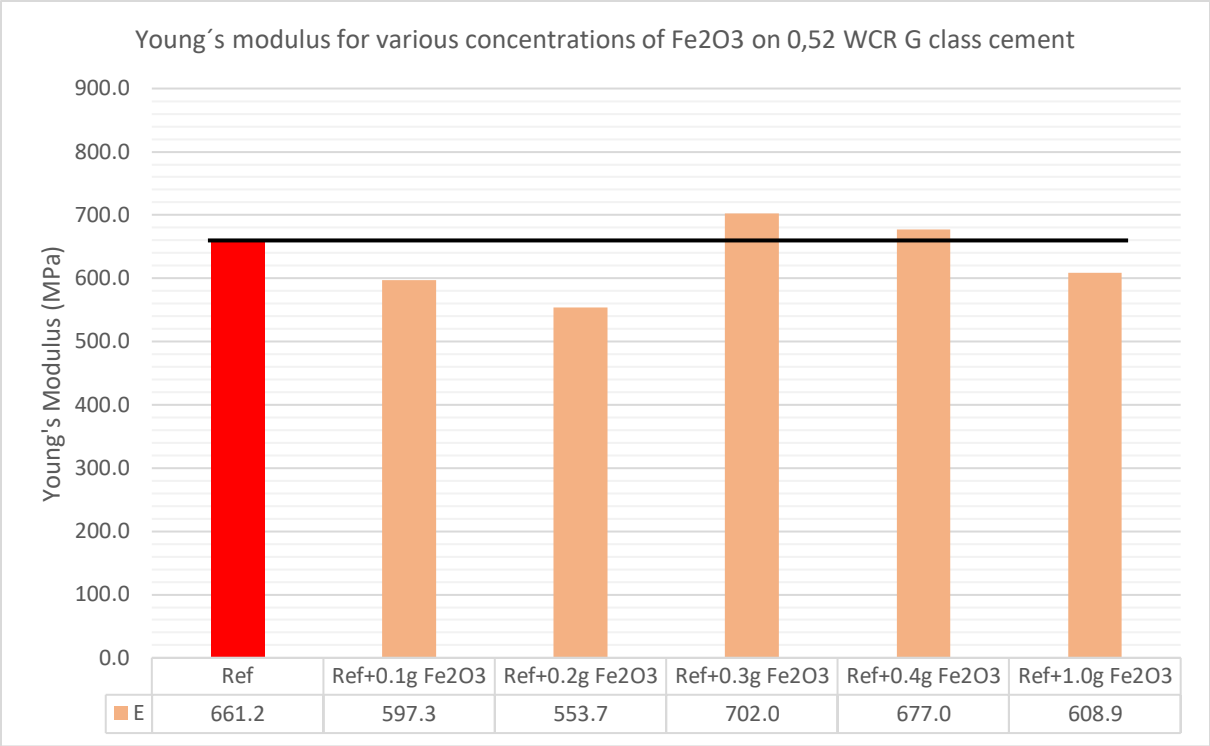

Figure 4.21 Young´s modulus for various concentrations of Fe2O3 on 0,52 WCR G class cement

From figure 4.21 one can observe that the results displayed are almost identical to the results shown from the UCS measurements. The only difference being that the peak UCS occurs at 0,4 grams added whilst the peak E occurs at 0,3 grams added. Furthermore, the Young´s modulus of both high (1,0 grams) and low (0,1 and 0,2 grams) concentrations are below that of the zero-additive plug. This could be beneficial in terms of energy absorption, however, the UCS for these concentrations is also lower compared to the control. The largest increase in Young´s modulus is as mention earlier observed at 0,3 grams of added nano-Fe_2O_3 and is at an increase of 6,2%.

From the stress-strain curve generated by UCS measurements, the resilience was calculated by finding the area under the curve, and the results are shown below;

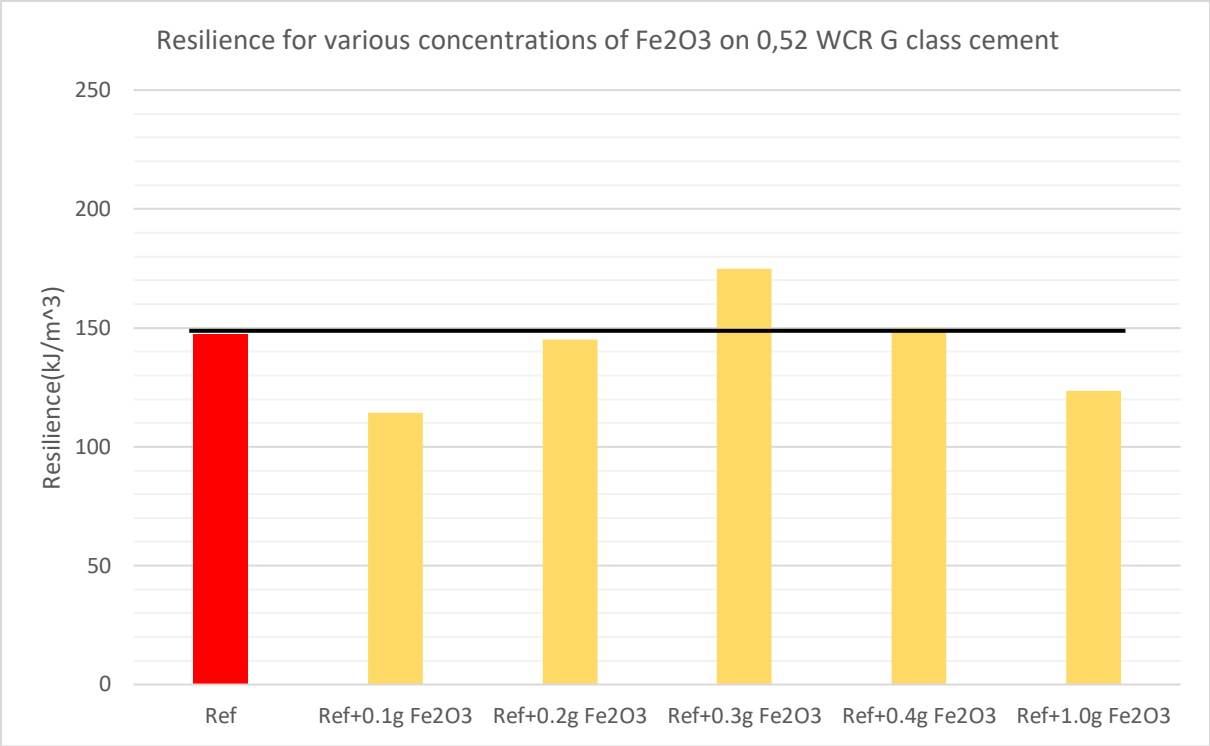

Figure 4.22 Resilience for various concentrations of Fe2O3 on 0,52 WCR G class cement

From figure 4.22 one can observe that the highest increase in resilience is a result of adding 0,3 grams of nano-Fe_2O_3 which leads to an increase of 18,4%. This shows that the ratio between UCS change and E change favors the concentration of 0,3 rather than 0,4 grams added, which appeared to be the better performing plug. Furthermore, the resemblance from the Young´s modulus and UCS results adhere, where both low and high concentrations lead to a decrease in the resilience compared to the control. These results show that for the correct dosage of nano-Fe_2O_3 the resultant cement will be able to absorb a larger amount of energy compared to the zero-additive samples.

4.1.7 Effect of TiO_2

From previous conducted studies it has been shown that the addition of nano-TiO_2 improves tensile, flexural and compressive strength when it is added to different cement based materials. [51], [52] Even though these studies vary in materials and methods used, they should give an indication of the general trend of the results obtained in this thesis. Therefore, a wide range of concentrations were tested to screen out the optimal concentration which would yield the greatest strength increase. Depicted below are the results from the destructive tests with added nano-TiO_2

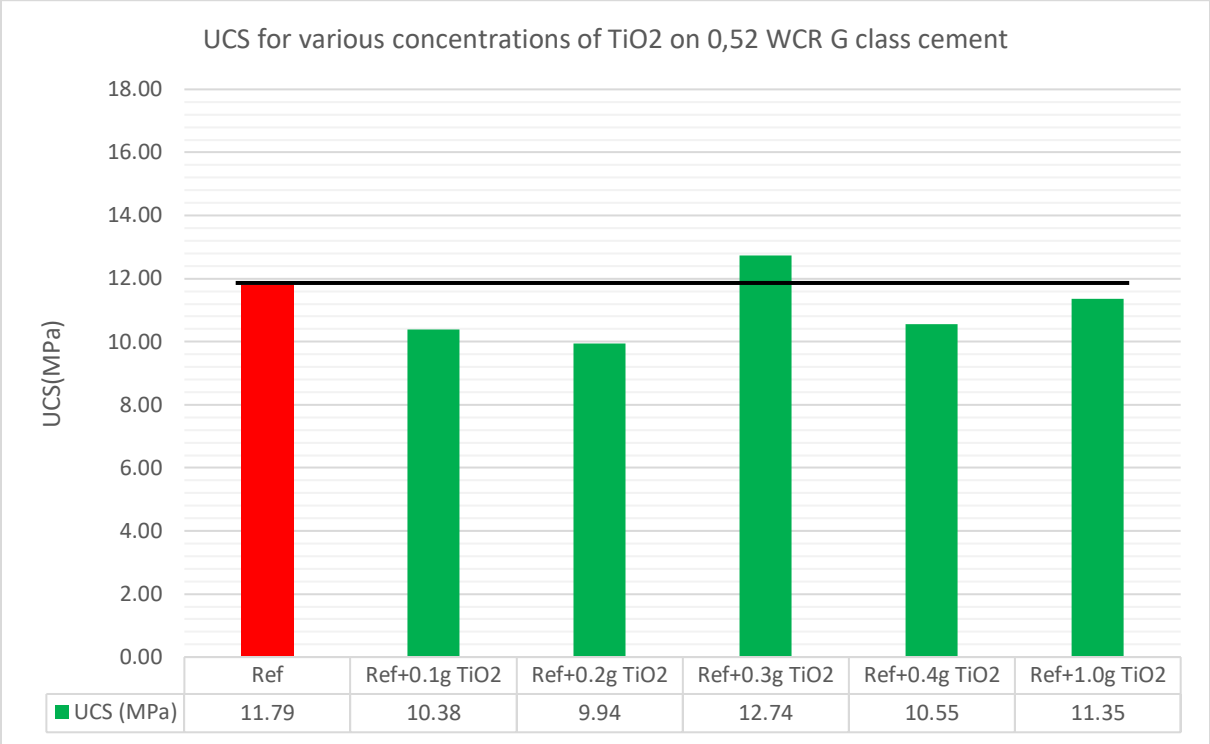

Figure 4.23 UCS for different concentrations of TiO2

From figure 4.23 one can observe the various effects the added titanium dioxide nanoparticles had on the cement strength. The red bar is the average value of the zero-additive plugs, and a straight line is drawn from it to easier compare the obtained results to the reference point. From the graph it shows that both 0,1 and 0,2 grams of added TiO_2 leads to a decrease in compressive strength, where the latter has the lowest UCS of the two. The highest UCS observed is obtained through the addition of 0,3 grams of titanium dioxide, which leads to an increase of approximately 8% compared to the control. For both 0,4 and 1,0 grams added, the strength decreases. There appears to be no definite trend displayed from the graph in terms of strength increase versus dosage, but it is possible that the peak dosage lies in the proximity of 0,3 grams added and that through testing concentrations in smaller increments closer to this, it would produce a graph with a clear trend.

Based on the stress-strain curve generated for the UCS measurements, the Young´s modulus of the plugs were calculated, and the results are shown below:

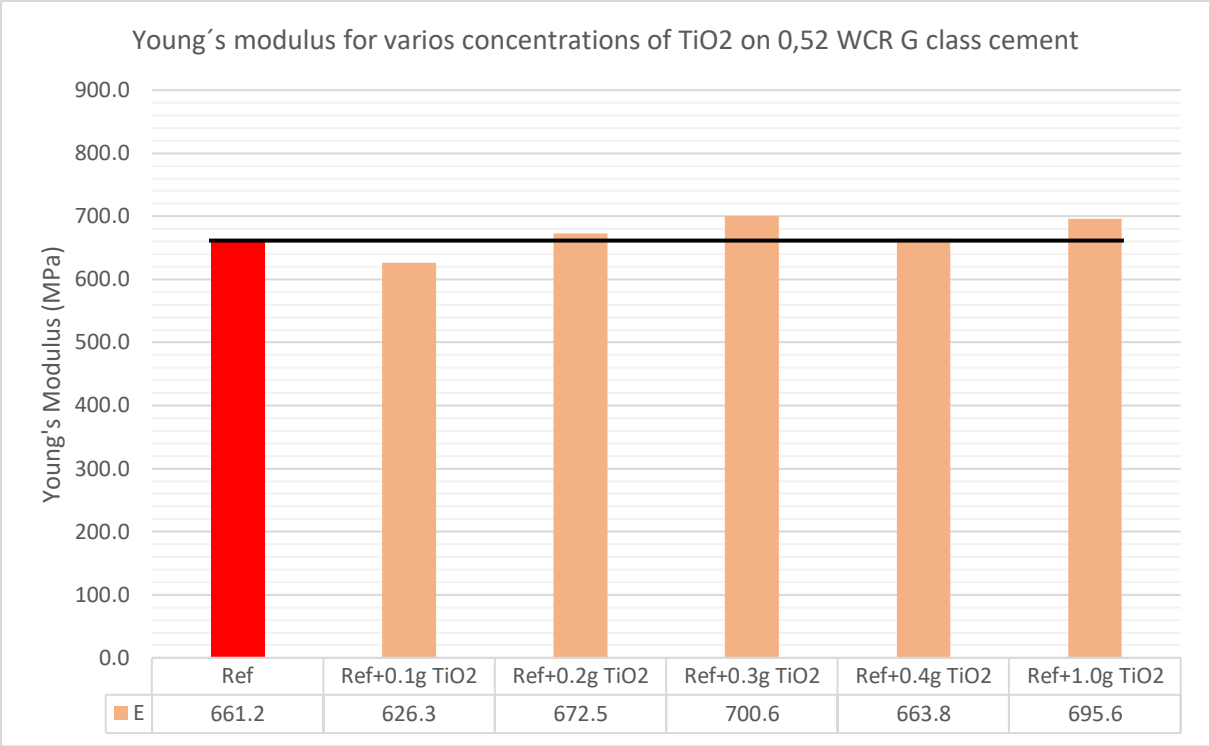

Figure 4.24 Young´s modulus for various concentrations of TiO2 on 0,52 WCR G class cement

From figure 4.24 it shows that the results display similar values relative to each other compared to the UCS measurement. The highest E is observed from the addition of 0,3 grams of nano-TiO_2 which causes an increase of 5,9% compared to the control. All of the tested samples display a Young´s modulus which is in the close proximity of the control plug, which indicates that the UCS will be the major factor in deciding the resilience of the plugs. The trend appears to be a growing increase in E until the peak at 0,3 grams added, with a downwards trend afterward with an additional spike at the highest tested concentration.

From the stress-strain curve generated by UCS measurements, the resilience was calculated by finding the area under the curve, and the results are shown below;

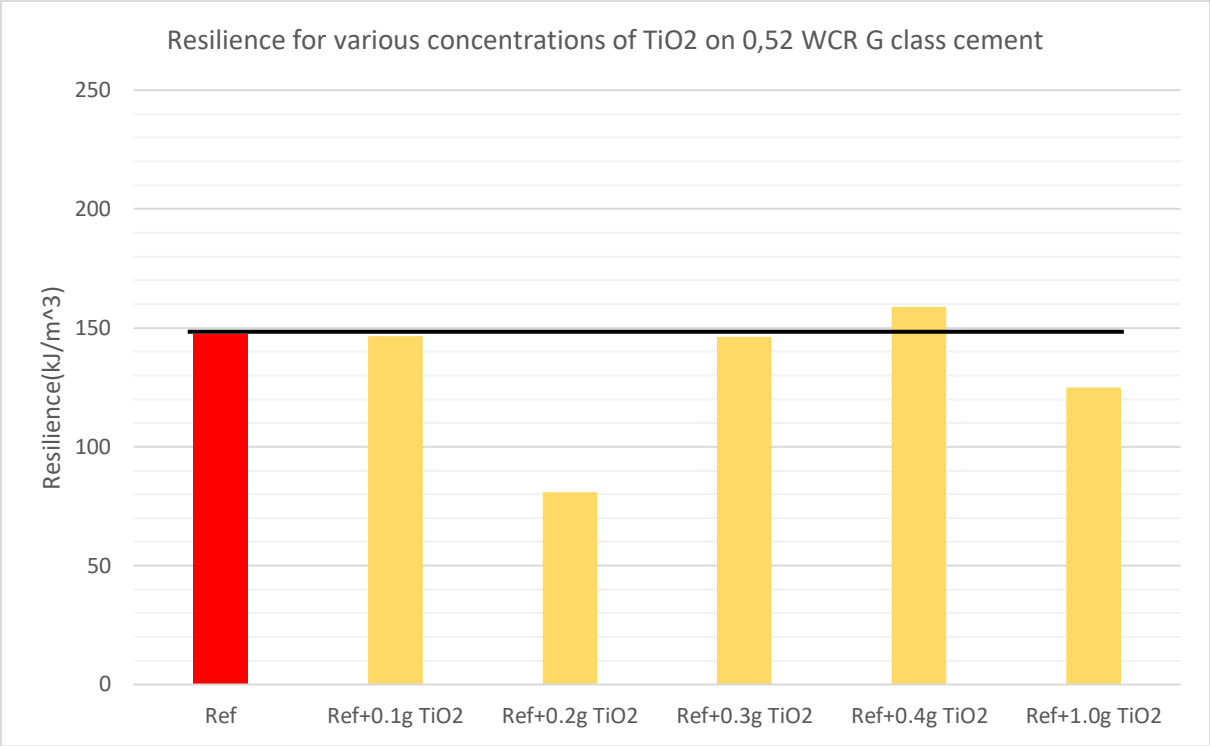

Figure 4.25 Resilience for various concentrations of TiO2 on 0,52 WCR G class cement

From figure 4.25 one can observe that for all except one of the tested concentrations the resilience decreases. The only increase is observed from the addition of 0,4 grams and results in an increase of 7,7%. The lowest resilience is observed from the addition of 0,2 grams of nano-TiO_2 and results in a decrease of 45,2% compared to control. This massive reduction in resilience indicates that this dosage of the nanoparticle will be able to absorb approximately half the energy of the control before it breaks, which is highly undesirable. Furthermore, both 0,1 and 0,3 grams added lie right below the control with decreases of 0,7 and 0,9% respectively. From this graph, it appears that the performance of the cement plugs with added nano-TiO_2 is extremely sensitive to the dosage added, but resilience can be improved by adding the correct amount of nanoparticles.

4.1.8 Effect of hybrid mixture

The testing of SiO_2 as well as MWCNT-COOH on 0,52 WCR G class cement unveiled positive results. Knowing from other studies that the addition of nano-silica does not interfere with additional additives and that it is synergetic with their functions [11], combining this with the benefits received from small concentrations of MWCNT-COOH could prove to increase compressive strength vastly. The selected concentrations are based on the best systems from

the 0,52 WCR destructive test of the respective nanoparticles, and the goal was to find the combination of concentrations which generated the best results in terms of strength increase. The results are depicted below;

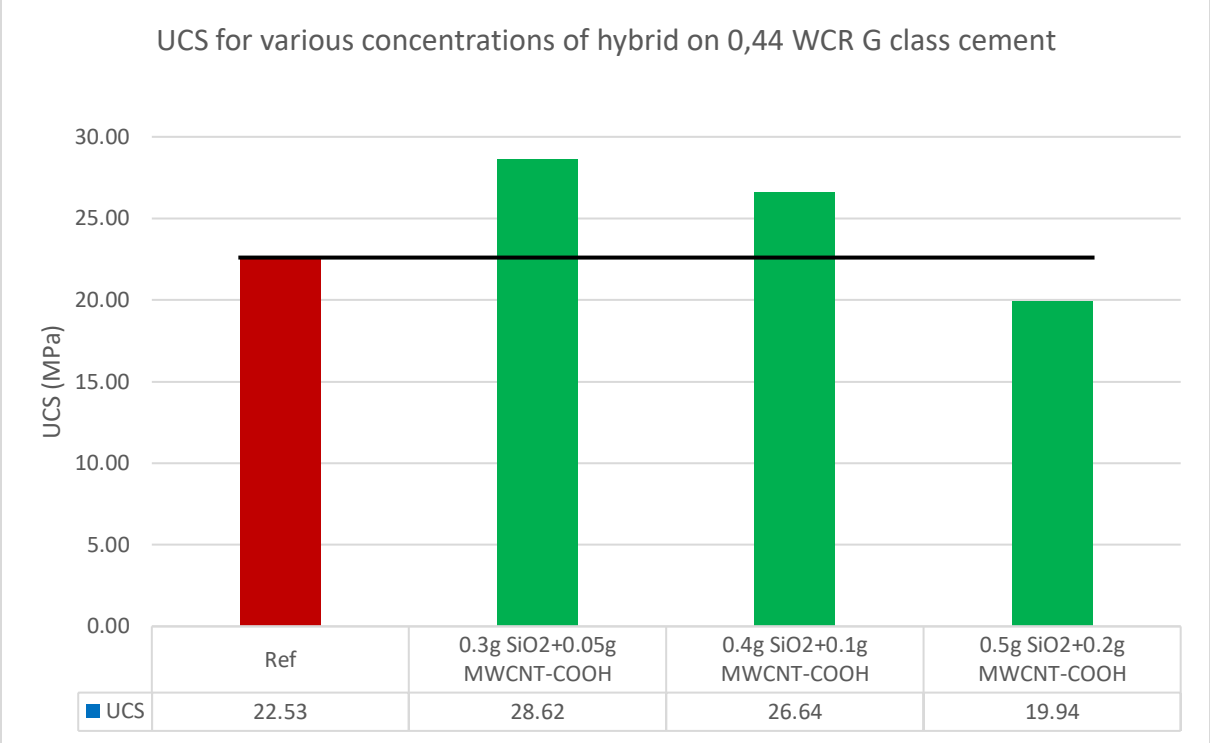

Figure 4.26 UCS for different combinations of hybrid mixture

From figure 4.26 one can observe that the average value of zero-additive 0,44 WCR G class cement plugs are marked in dark red. A straight line is drawn from the control to easier visualize the strength change in the obtained results. The largest increase is observed with the smallest tested concentrations, and has a strength increase of 27,1% compared to control. One can observe from the graph a downwards trend with increasing concentrations, with the highest concentration tested leading to a decrease in overall strength.

From the graph it is highly possible that by tweaking the combination of concentrations, it would be possible to further increase the strength gain which was achieved. It also shows that by adding too much nano, the overall strength is impaired. The graph shows that by combining the binding effects of nano-silica with the benefits provided by the MWCNTs the result is a cement matrix which demonstrates a larger compressive strength compared to control.
Based on the stress-strain curve generated for the UCS measurements, the Young´s modulus of the plugs were calculated, and the results are shown below:

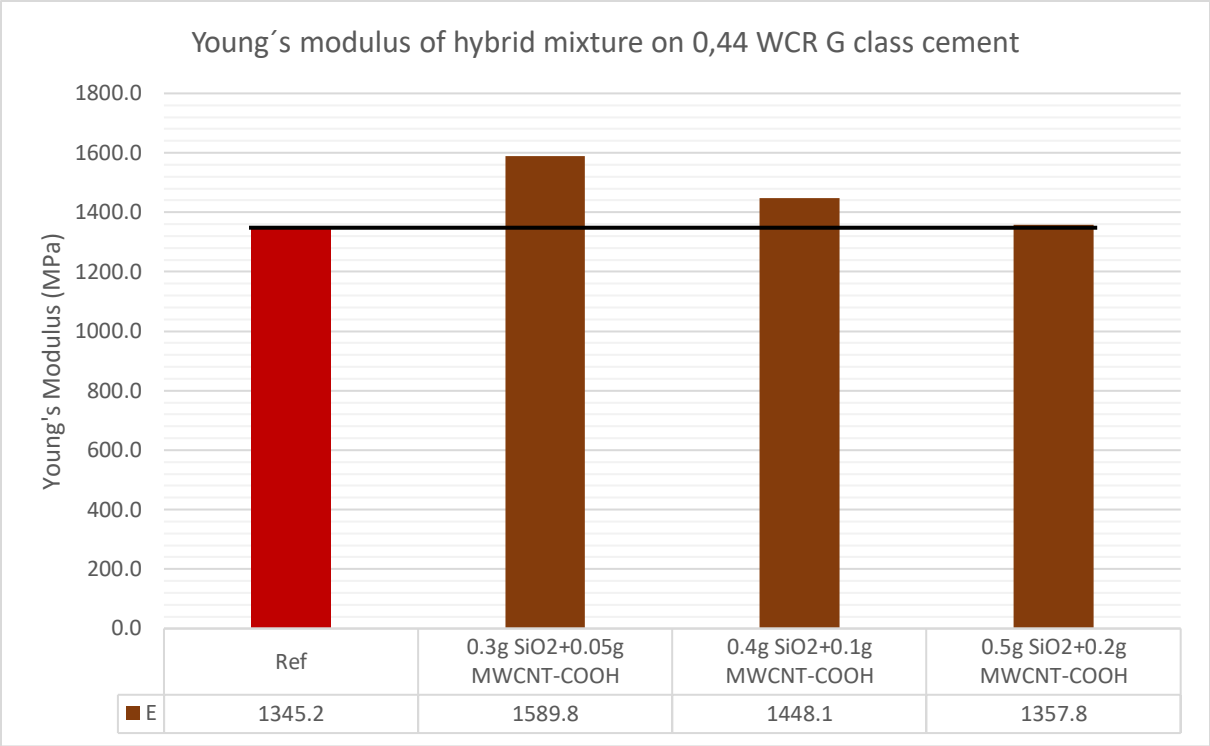

Figure 4.27 Young´s modulus of hybrid mixture on 0,44 WCR G class cement

From figure 4.27 it shows that for all tested concentrations and variations of this hybrid mixture, the Young´s modulus of the cement sample increases, which implies increased brittleness in all of the tested samples. The largest increase in E is observed from the addition of 0,3 grams of SiO_2 and 0,05 grams of MWCNT-COOH which leads to an increase of 18,2%. The trend which appears in figure 4.27 matches the trend from the UCS measurements, where an increase in concentration leads to a decrease in value compared to the peak dosage.

From the stress-strain curve generated by UCS measurements, the resilience was calculated by finding the area under the curve, and the results are shown below;

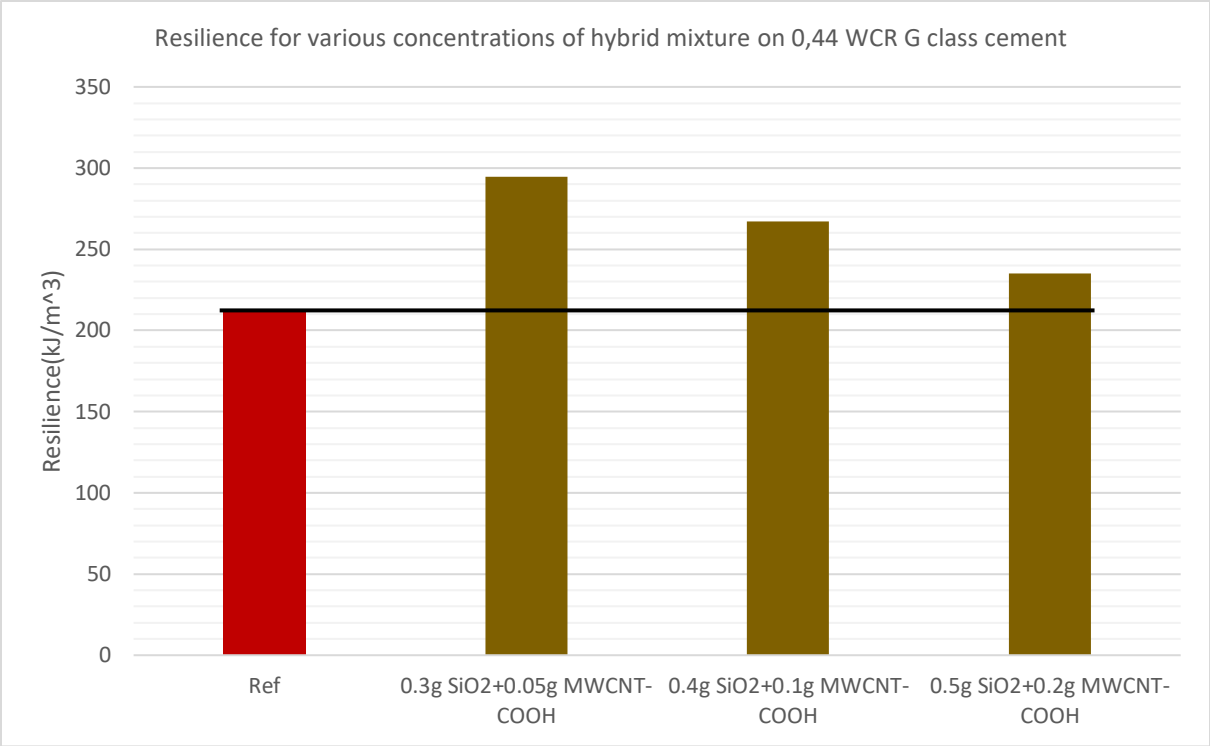

Figure 4.28 Resilience for various concentrations of hybrid mixture on 0,44 WCR G class cement

The results displayed in figure 4.28 show a matching trend to the trends observed in both the measurement for UCS and the calculation of E. The highest resilience is obtained from the lowest concentration tested and yields an increase of 38,4%. Additionally, all of the tested concentrations result in a resilience which is higher than the control.

4.1.9 Results from test matrices 10-12

The results from these test batches are not directly comparable to the previous batches or each other as the conditions and procedures when these were made was altered. Test matrix 10, 11 and 12 used a 48, 47- and 46-day timeframe respectively, as this was the only available option due to unforeseen circumstances. However, the results from these batches are not worthless, as the relevant zero-additive plugs endured the exact same conditions as the rest of the batch for each matrix, the results can be directly compared to their own zero-additive plugs.

4.1.9.1 Effect of nano-silica on 0,44 WCR G class cement

After mixing and pouring into molds, the cement was left to set in the molds for 48 hours. The cement was then polished, and non-destructive measurements were performed on the samples

before they were put in a water bath to cure for 24 hours. After 24 hours the samples were removed from the water and left in air for the remaining time before being crushed.

From previous results, the addition on nano-silica proved to be highly beneficial on the hardened cement paste from a 0,52 WCR cement slurry. The results indicated that the nanoparticles were helpful in several different concentrations, but it proved especially favorable in a certain range of concentrations. Therefore, a small selection of concentrations was chosen for this test. When testing this batch, it was reasonable to expect a cement which improved relative to the control. Depicted below are the destructive results from the selected concentrations of nano-SiO_2;

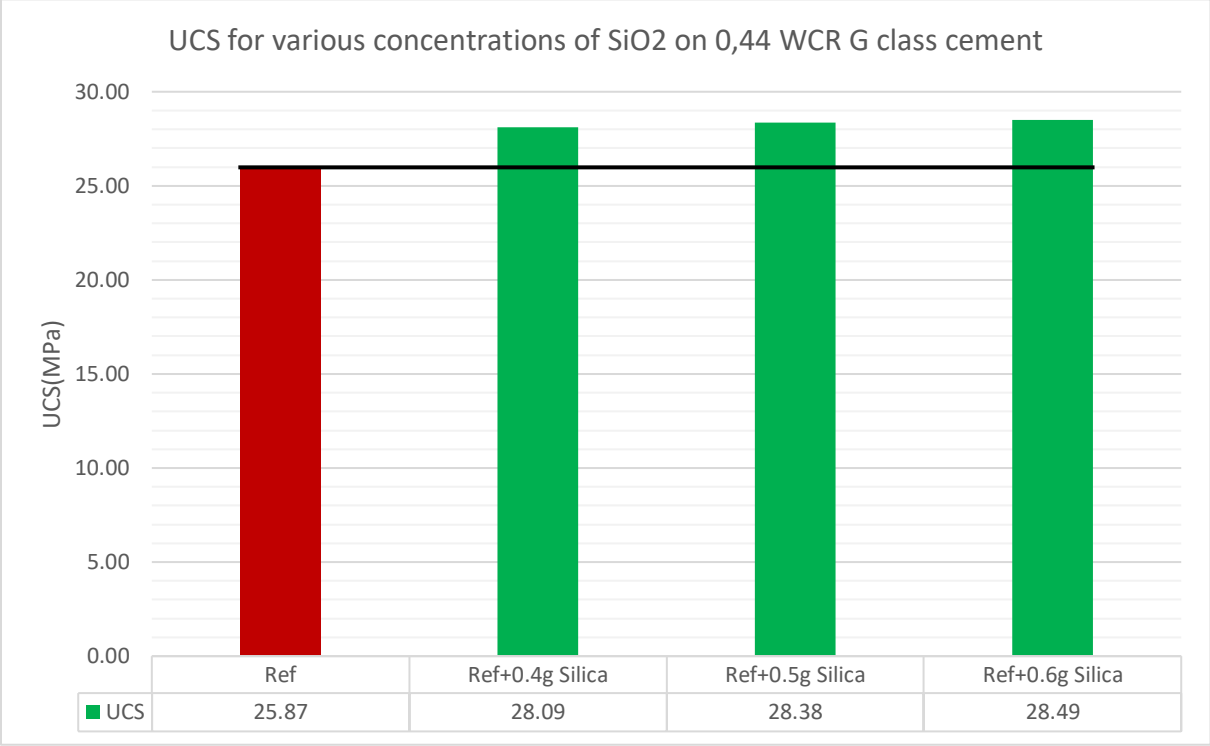

Figure 4.29 UCS for various concentrations of SiO2 on 0,44 WCR G class cement

From figure 4.29 the average of the two zero-additive cement samples is named “Ref” and a straight line is drawn from it to easier visualize its value relative to the other samples. One can observe that for all the tested concentrations of added nano-silica, the UCS value increases. The largest increase is observed from the addition of 0,6 grams of nano-SiO_2 which lead to an increase of 10,1%. From the addition of 0,5 and 0,4 grams the UCS increased by 9,7% and 8,6% respectively.

These results match the prediction for the samples even though there were large uncertainties in the magnitude of the effects the silica would display due to the extended period of time they were left to cure. When compared to the 0,52 WCR silica results, it is uncertain whether the reduced effect is due to the change in WCR or the change in curing procedure. These results further support the fact that addition of silica accelerates the formation of C-S-H gels, and thus significantly improves early strength which explains the discrepancy in the increased UCS. [11] This also validates the fact that the silica fills the gaps between the larger cement particles, resulting in a denser matrix which in turn results in a stronger cement matrix compared to the control, which explains why the UCS is higher even after the control sample is allowed to fully form C-S-H gel and reach peak strength.

4.1.9.2 Effect of MWCNT

After mixing and pouring into molds, the cement was left to set in the molds for 48 hours. The cement was then briefly removed from the molds and a thin layer of paper towels were placed at the bottom of the mold before the cement was placed inside. It was left in this state up until the day of crushing, where it was polished and tested both non-destructively and destructively.

From previous results it is known that the effect of MWCNT-COOH is highly beneficial to the cement properties, however, from the results in this thesis the effect of pure MWCNT is unknown. Based on previous results, a reasonable range of concentrations were chosen for testing this additive, and the results are shown below;

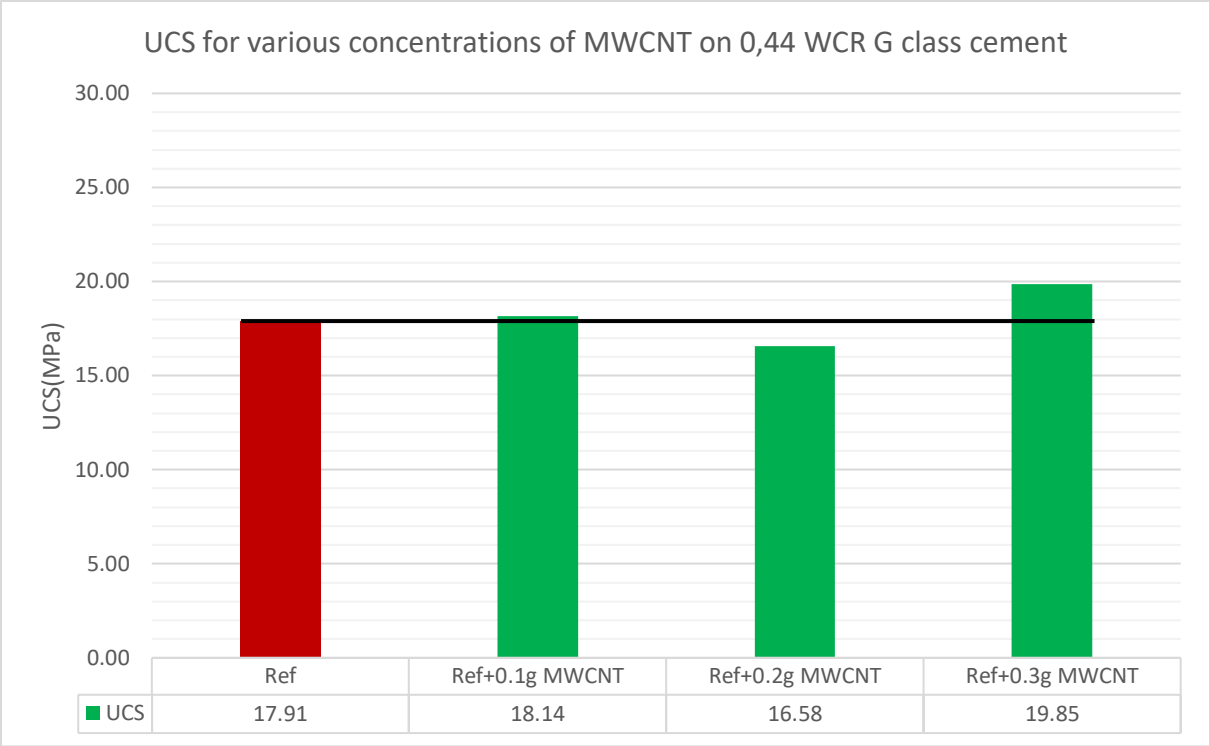

Figure 4.30 UCS for various concentrations of MWCNT on 0,44 WCR G class cement

The "Ref" value in red is the average value of the two zero-additive plugs from this batch. One can observe from figure 4.30 that the overall strength of these plugs is below expected value of 0,44 WCR cement plugs. This is possibly due to the fact that they were not placed in water for curing after 48 hours of setting, but also likely due to the fact that they were placed on paper towels which drained the remaining available water from the samples and hindered proper hydration.

One can also observe that for two of the three tested concentrations, the UCS increases. The largest strength increase is observed when adding 0,3 grams of MWCNT which lead to an increase of 10,9%. The addition of 0,1- and 0,2-grams lead to an increase of 1,3% and a decrease of 7,4% respectively. From these results it appears that the addition of MWCNT is beneficial in terms of UCS when added in the right concentration.

From previous studies, the benefits of MWCNT on UCS is known. [19], [23] As these samples underwent a rather unusual procedure and non-standardized testing, it is not expected to achieve identical results. However, the results from all these tests showed the same end result; an increase in UCS. From this thesis the increases in UCS are smaller than that of the other conducted studied, and this could be a result of several factors.

4.1.9.3 *Effect of Al_2O_3*

After mixing and pouring into molds, the cement was left to set in the molds for 48 hours. After this time period, instead of removing the samples and polishing them before placing them in a water bath, they were left in the molds for an additional 44 days before removal. They were subsequently removed from the molds, polished and measured. Non-destructive testing was performed and afterwards they were subjected to destructive testing for UCS measurement.

As this nanoparticle had not been tested previously in this thesis, a small range of concentrations were chosen which were believed to result in the desired effect. The results are shown in the figure below;

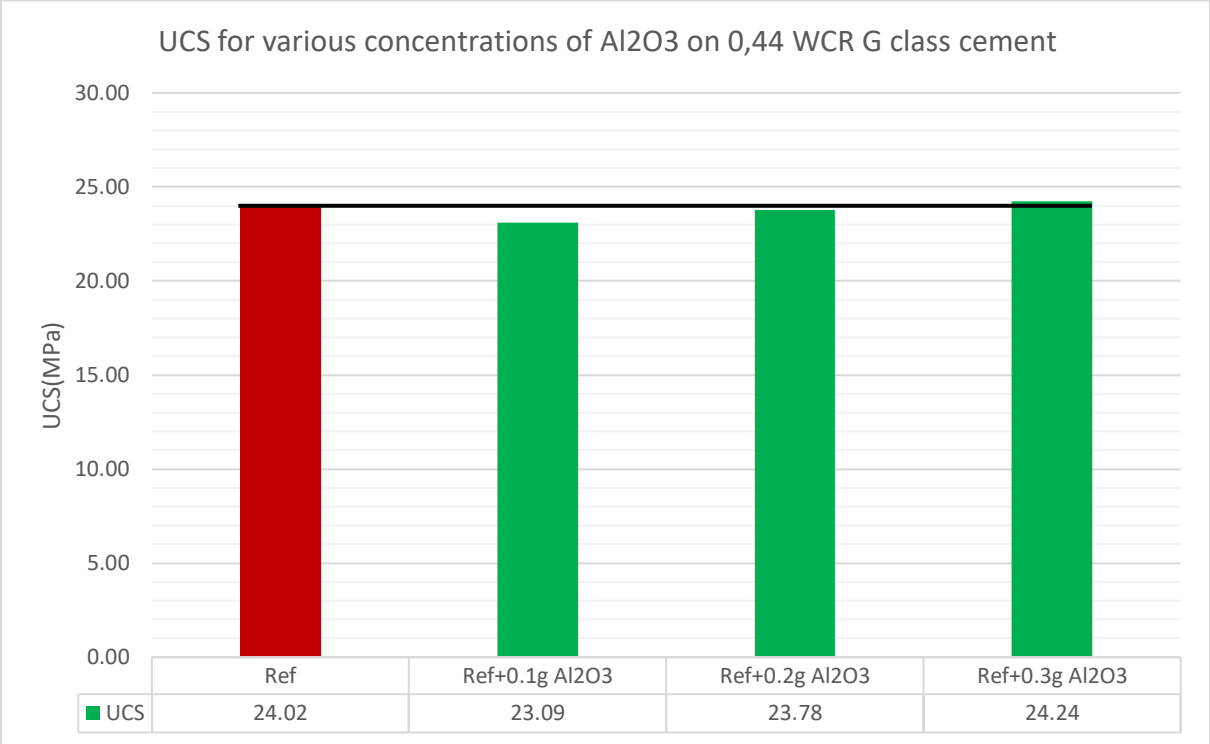

Figure 4.31 UCS for various concentrations of Al2O3 on 0,44 WCR G class cement

The "Ref" value in red is the average value of the two zero-additive plugs from this particular batch. From figure 4.31 one can observe a very clear trend. The UCS increases almost linearly with an increase of added nano-Al_2O_3, where the largest and only increase in UCS is observed from the highest concentration of tested nano which is 0,3 grams. This leads to an increase of a mere 0,9%, whereas the addition of 0,1 and 0,2 grams causes decreases of 3,9% and 1% respectively.

From these results it appears that an even higher increase in UCS could be achieved if the amount of added nano increased. Furthermore, the aluminum oxide did increase the strength of the sample if added in a certain dosage, which matches results from other studies. [23]

4.1.10 Results from test batch 13-16

Even though the procedure for making the batches are the same as for test batch 5-8, the destructive testing was performed on a separate and different machine. It is therefore better to look at these samples relative to their own zero-additive reference plugs and not extend or use the average from earlier batches, even if the results themselves are comparable.

4.1.10.1 Effect of ZnO

This additive had not previously been tested in this thesis on any type of cement, but the work of Nochaiya et al [24] indicates that the addition of nano-ZnO would prove beneficial to the cement strength. The procedure of this batch varies slightly from others, as after 48 hours of cement setting, the sample containing the highest amount of nanoparticle had not set enough for the plug to be polished and/or removed from the mold. The decision was therefore made that all the samples in this batch would simply air-dry until the time of crushing, such that the samples in the batch are all comparable to one another. From the previous results in this thesis, a general trend regarding the addition of nanoparticles is observed: The strength of the cement sample tends to decrease as the dosage in nanoparticle added increases. The concentrations chosen were therefore relatively low, and the best performing dosage from Nochaiya et al's work was also tested, and the results are displayed below;

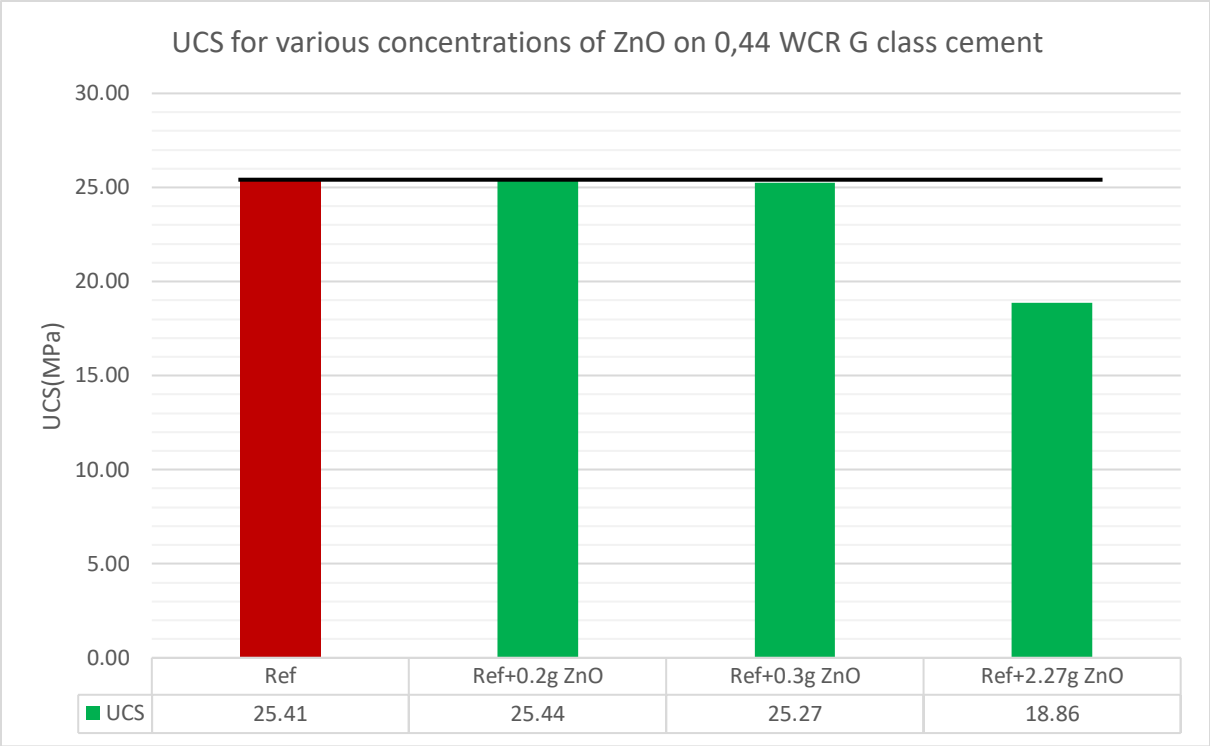

Figure 4.32 UCS for various concentrations of ZnO on 0,44 WCR G class cement

From figure 4.32 the value of "Ref" is the average of the two zero-additive cement samples which were made in this batch. Furthermore, one observes that for both the addition of 0,2 and 0,3 grams of added nano zinc oxide, the strength barely changes. There are, however, miniscule changes where the addition of 0,2 grams leads to an increase of 0,12% and the addition of 0,3 grams leads to a decrease of 0,56%. The addition of 2,27 grams of nano-ZnO leads to a massive decrease in strength, which decreases 25,8% compared to control. The apparent trend from this graph is that an increasing amount of added nano-zinc oxide leads to a larger decrease in cement strength.

From the work of Nochaiya et al [24] some similarities can be seen. From test batch 13, the addition of 2,27 grams (1%bwoc) did not set after 2 days, whereas from the previous conducted study the addition of 2% and 5% ZnO would not set after 3 days of curing, which indicates that the addition of the nanoparticle in certain concentrations elongates the setting time of the cement. Interestingly, there is a large discrepancy in the measured values of 1% ZnO between the experiments, where Nochaiya et al found this to increase the strength of the sample by 15%, this thesis found that in this scenario, the strength would drastically decrease. This could be attributed to several factors regarding uncertainty, procedure, testing apparatus, geometry of the samples etc.

4.1.10.2 Effect of MWCNT and Al_2O_3 hybrid

A sample containing both MWCNT and aluminum oxide was tested due to the fact that both MWCNT and nano- Al_2O_3 have shown positive results previously, and due to the fact that according to the work of Gurumurthy et al [23], a substantial increase in cement strength was observed by addition of the two nanoparticles together. A select few concentrations were tested in addition to the concentrations tested in the previous study. The results are presented below:

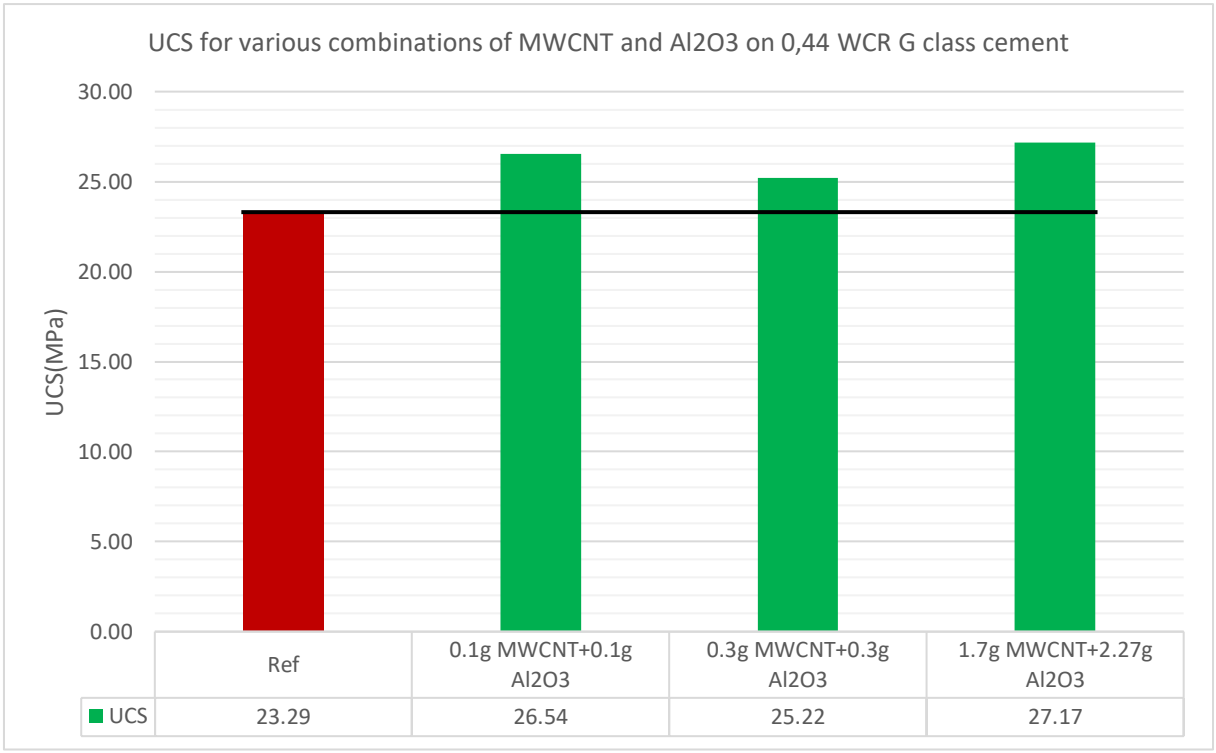

Figure 4.33 UCS for various combinations of MWCNT and Al2O3 on 0,44 WCR G class cement

From figure 4.33, the value "ref" is the average UCS for the two zero-additive cement samples which were made in this batch. The results show that for all tested concentrations and combinations, the resultant UCS is higher than the control sample. The addition of 0,1 grams of each nanoparticle lead to an increase of 13,9% relative to the control sample. When increasing the concentrations to 0,3 grams of each, the UCS increased by 8,3%. The best performing concentration tested was the addition of 1,7 grams of MWCNT and 2,27 grams of Al_2O_3 (0,75%bwoc MWCNT & 1%bwoc Al_2O_3) which increased the UCS by 16,7%.

Based on the work of Gurumurthy et al [23], the addition of the same concentration of each nanoparticle lead to an increase of UCS by 58,31%. The discrepancy between these results may be due to a number of factors, however, the observed increase from this particular nanoparticle combination in these concentrations is one of the largest increases in UCS observed on 0,44 WCR G class cement from all performed experiments in this thesis.

4.1.10.3 Effect of SiO_2 and Fe_2O_3 hybrid

Previous results from testing on both 0,52 and 0,44 WCR G class cement indicates that the addition of nano-silica is highly beneficial to the cement strength. Even though the addition of iron oxide was only beneficial in certain concentrations, it was interesting to examine whether one could produce a synergetic effect by combining the two nanoparticles together in the same cement slurry. The results are shown in the graph below:

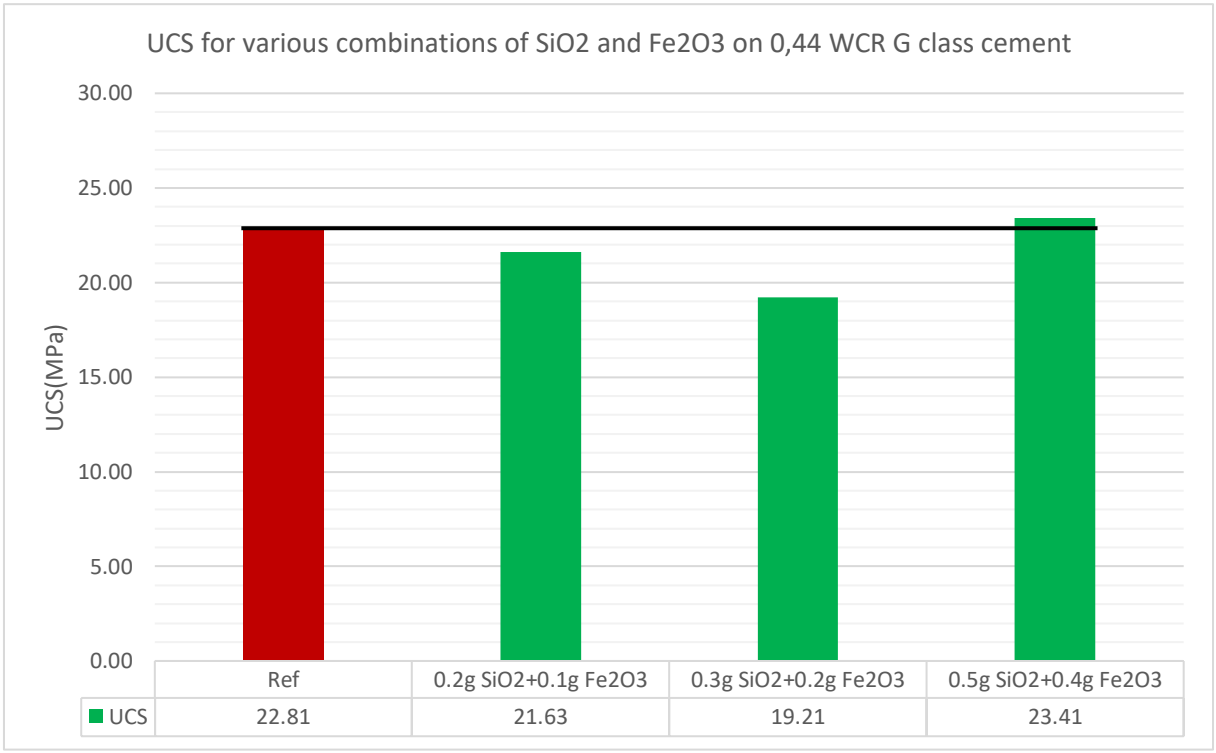

Figure 4.34 UCS for various combinations of SiO2 and Fe2O3 on 0,44 WCR G class cement

From figure 4.34 the value of "ref" is the average value of the two zero-additive samples belonging to this batch. From this graph one can see that only one of the tested combinations leads to an increase in UCS. The first combination consisting of 0,2 grams of silica with 0,1 grams of iron oxide lead to a decrease of 5,2%, whereas the addition of 0,3 grams SiO_2 and 0,2

grams of Fe_2O_3 lead to an even larger decrease of 15,8%. The combination which increased the UCS was the combination of 0,5 grams of nano-silica and 0,4 grams of iron oxide, which lead to an increase of 2,6% relative to the control sample.

It is difficult to distinguish whether this increase stems from the increased amount of nano-silica added, which has proven to work, or if the added nanoparticles work together in a symbiotic relationship to improve the cement specimen. It is also worth noting that the largest observed increase from this test is smaller than the increase observed for either one of the nanoparticles in isolation. This comparison is inherently flawed, as iron oxide was never tested on 0,44 WCR G class cement, but the increase on the tested sample was larger compared to its own control in the 0,52 WCR G class cement test. Regardless, the results show that this combination of nanoparticles can improve the cement strength by a small amount if the concentrations are correct.

4.1.10.4 Effect of MWCNT-COOH and TiO_2 hybrid

Previous results from testing on both 0,52 and 0,44 WCR G class cement indicates that the addition of MWCNT-COOH can improve cement strength. Even though the addition of titanium oxide was only beneficial in one concentration, it was interesting to examine whether one could produce a synergetic effect by combining the two nanoparticles together in the same cement slurry. The results are shown in the graph below:

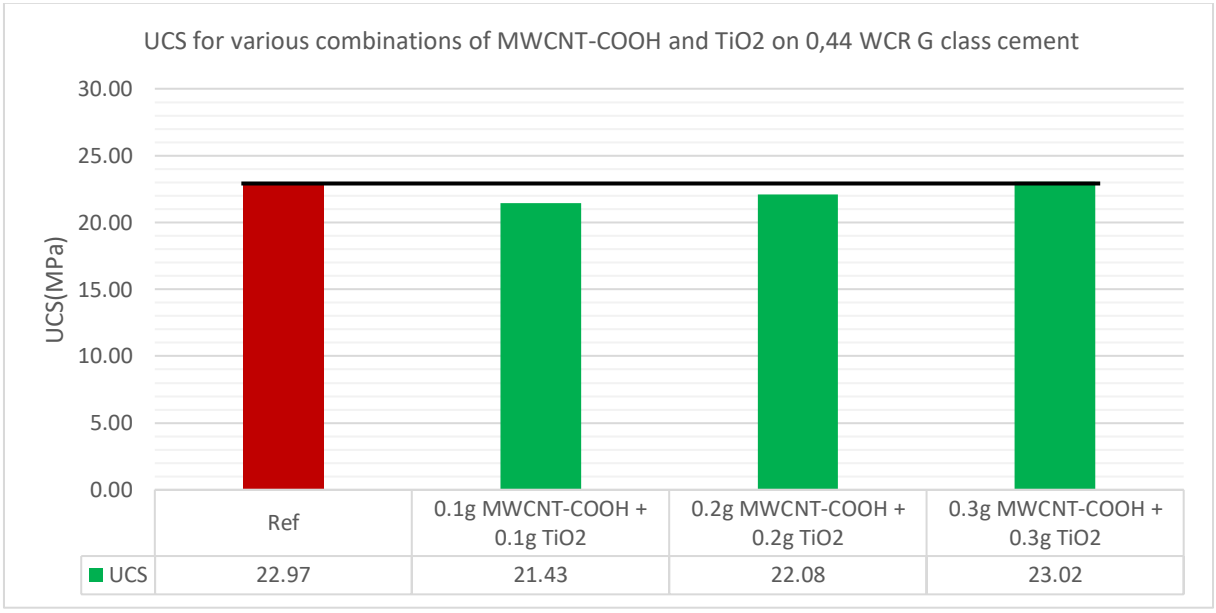

Figure 4.35 UCS for various combinations of MWCNT-COOH and TiO2 on 0,44 WCR G class cement

From figure 4.35 the value of "Ref" is the average value of the two zero-additive cement specimens made in this batch. Immediately, an apparent trend is visible. These results indicate that the cement strength increases with an increase in amount of added nano. From the results one can see that for the lower concentrations of nano, the cement strength actually decreases compared to the control. For the highest tested concentrations which consist of 0,3 grams of both MWCNT-COOH and TiO_2 the cement strength increases by 0,22%.

Taking into account the trend visible from figure 4.35, it is possible that the optimal concentration of added nanoparticles lies above the tested values, even though this is counterintuitive based on previous results. When testing both MWCNT-COOH and TiO_2 previously in this thesis, it was noted that for too high concentrations of added nanoparticle, the resultant cement specimen would exhibit a substantial decrease in compressive strength. The UCS increase facilitated by this particular nanoparticle hybrid is almost insignificant but could potentially be larger if the correct combination of nanoparticles were to be found.

4.2 Effect of silicone rubber on 0,44 WCR G class cement

Test batch no 7 studied the effects of added silicone rubber in the cement slurry, which used a water to cement ratio of 0,44 with a 7-day timeframe. When comparing the results from the various tests, the reference point is an average value from several different measurements, as described in chapter 4.1.

The principle behind addition of rubber is simple, reducing brittleness and allowing for a more flexible matrix deformation where the rubber allows for additional deformation in areas where the load is highest which would, in theory, lead to additional ductility.

In the chapters below the results from both untreated rubber (marked as UT) and treated rubber (marked as T) will be reviewed. The rubber used is described in chapter 3.1.4, and was acid-treated according to the procedure described in chapter 3.1.4. The theory behind this treatment is to break the surface of the rubber, allowing it to more easily interact with the cement slurry to improve performance.

4.2.1 Change of mass with plastic additives on 0,44 WCR G class cement

The samples which contained added silicone rubber were made and tested in accordance with chapter 3.2.1. It was found that for batches containing 0,44 WCR cement the change in mass between 48 hr and 72 hr was negligible, which is why the graphs uses change in mass after 24 and 48 hrs. To calculate the change in mass equation 3-1 is used, and the change is based off of the plugs own dry weight. Shown below is the change of mass observed from the samples containing rubber.

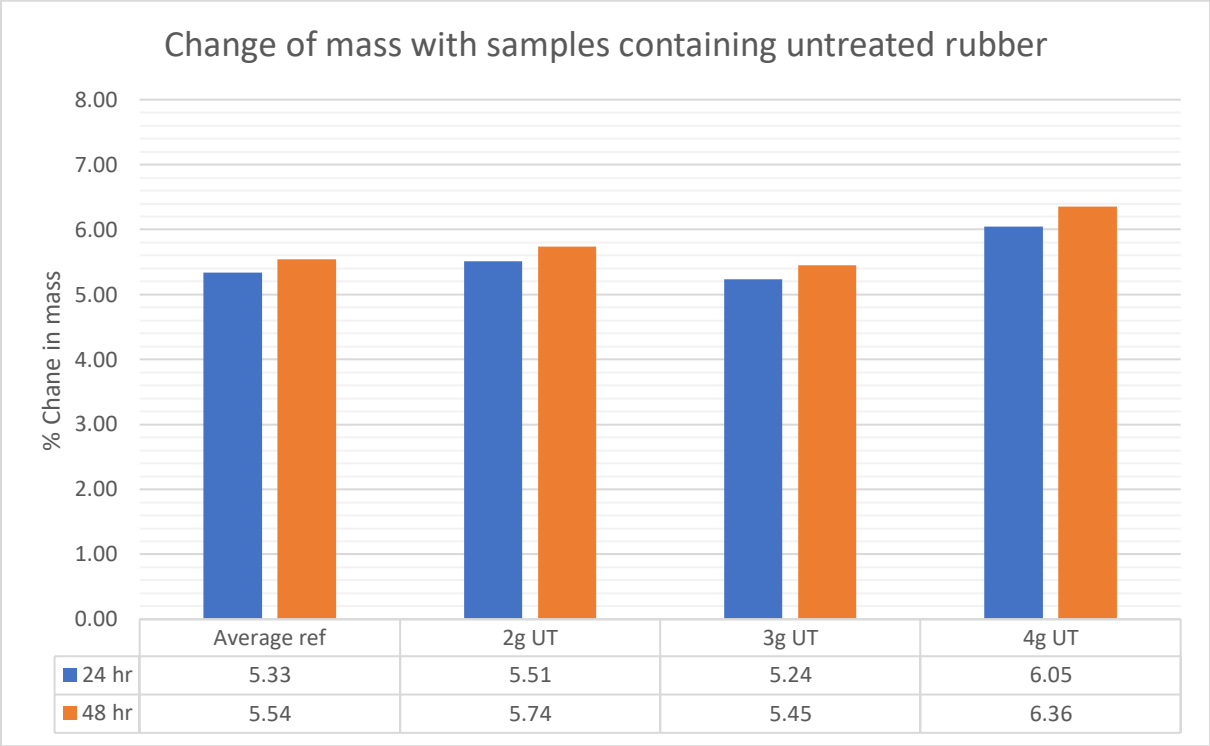

Figure 4.36 Change of mass with samples containing untreated rubber

In figure 4.36, "average ref" refers to the average value of the zero-additive 0,44 WCR cement samples, and the increase in mass is 5,33% and 5,54% after 24 and 48 hours respectively. It shows that the lowest mass increase is observed for the addition of 3 grams untreated rubber, which lies right below the control. Both 2 and 3 grams of added untreated rubber lies in the close proximity of the control, where the dosage of 2 grams has a slightly larger mass increase compared to control. The largest mass increase is observed from the addition of 4 grams of untreated rubber, with an increase of 6,36% after 48 hours, which by comparison is significantly larger than the control.

These results show that there is likely little to no drastic changes to the inner structure of the samples with added untreated rubber. There appears to be no cement bindings caused by the rubber that partly or fully blocks of some of the pore space, as was the case for some nanoparticles. There is, however, possibilities that the untreated rubber intrudes the cement matrix in such a way that it blocks the migration fluid paths through the cement, leading to reduced leakage rates, but this information would not be detected through this type of measurement.

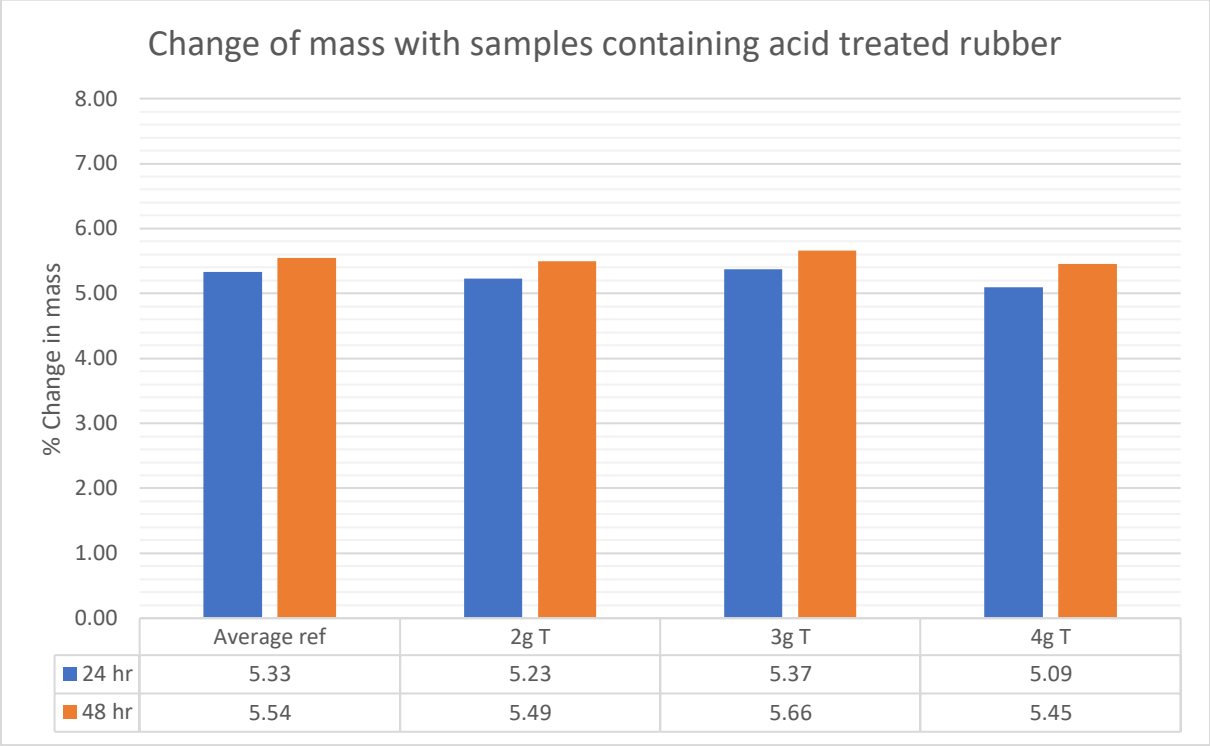

Figure 4.37 Change of mass with samples containing acid treated rubber

In figure 4.37 the change of mass for the samples containing acid treated rubber is displayed. The average reference point is the aforementioned value of zero-additive 0,44 WCR cement. From this graph one can observe a very close spread in the mass change for the various dosages of acid treated rubber added. The only dosage which displays an increase in changed mass compared to control, is the addition of 3 grams of acid treated rubber, which leads to a change in mass of 5,37% and 5,66% after 24 and 48 hours respectively. This additional increase is small relative to the control sample. Both 2 grams and 4 grams of added acid treated rubber leads to a slight decrease in change of mass compared to control. The greatest decrease is observed from the addition of 4 grams of treated rubber.

These results, similar to the untreated rubber results, show that no major changes with regards to change of mass occurred with the addition treated rubber. The changes which are observed, are of small magnitudes, which indicates little changes in the inner binding structure of the cement sample. The samples which contained treated rubber show a better trend than the ones using untreated rubber, with two 2/3 improving compared to the control. This could be an indication that the purpose of the acid treatment was successful and that the rubber better bonded with the cement to have a higher impact on the hardened cement paste.

4.2.2 Destructive results of rubber additives on 0,44 WCR G class cement

4.2.2.1 Uniaxial compressive strength of rubber on 0,44 WCR G class cement

The procedure for obtaining the destructive test results are explained in chapter 3.3.7.3 and is calculated using equation 3-7. In figure 4.38 the straight line is the UCS value of the reference point, and it is included to easier visualize where the different additives place in terms of strength increase. The destructive results from addition of untreated rubber is depicted below;

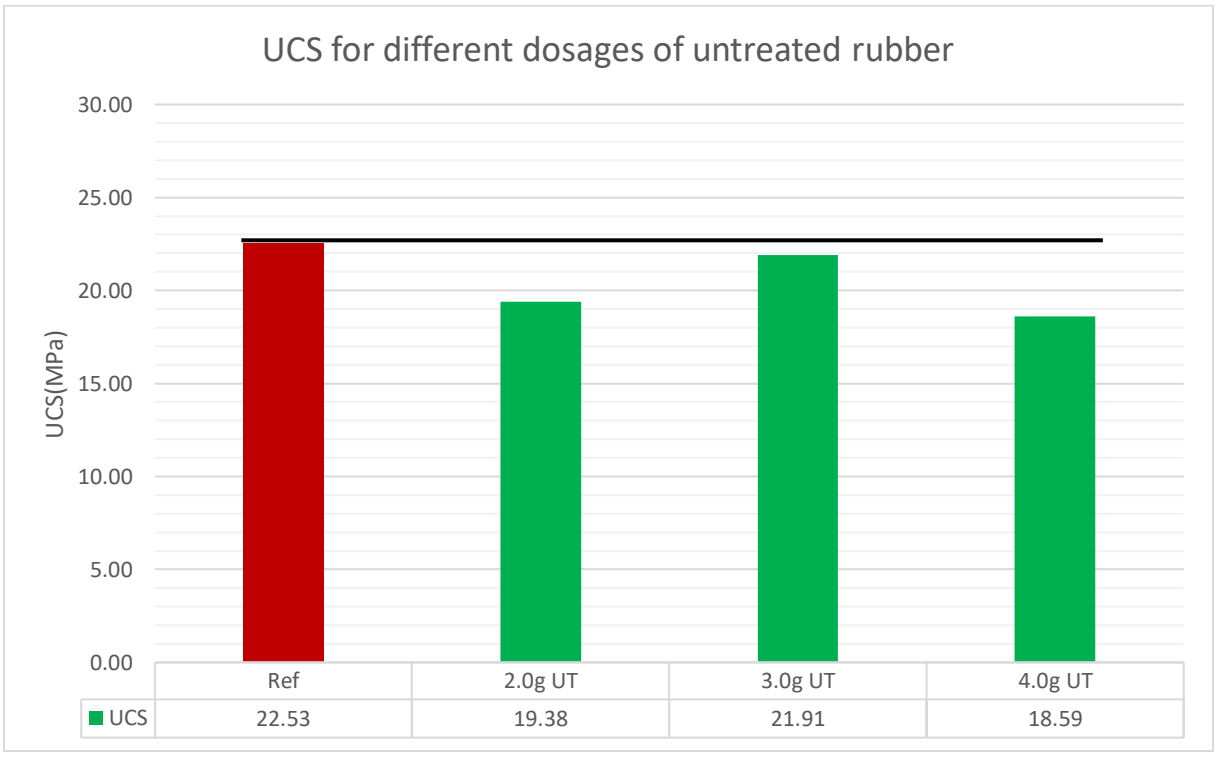

Figure 4.38 UCS for different concentrations of untreated rubber

From the figure above, it is observed that for all tested concentrations of untreated rubber, the UCS is lower compared to control. The highest UCS is achieved through the addition of 3,0

grams of untreated rubber, with a UCS of 21,91 MPa it translates to a 2,7% decrease in strength compared to the control. The lowest UCS obtained was by addition of 4,0 grams of untreated rubber, which caused a decrease of 17,5% compared to the control. The lowest concentration added caused a decrease in strength of 13,9% compared to the control.

The trend which can be observed from the graph indicates that the peak concentration is achieved in the proximity of 3,0 grams of untreated rubber added, and that concentrations below or above this will cause a lower UCS. It is also observed that no tested amount of untreated rubber will cause an increase in UCS compared to the zero-additive cement. It appears that even though the positive effect of UT rubber has been shown from other conducted studies these results were not able to be replicated in this thesis. There is a large uncertainty in the measurements regarding the samples with added rubber, as explained in chapter 4.4, which could help explain these results.

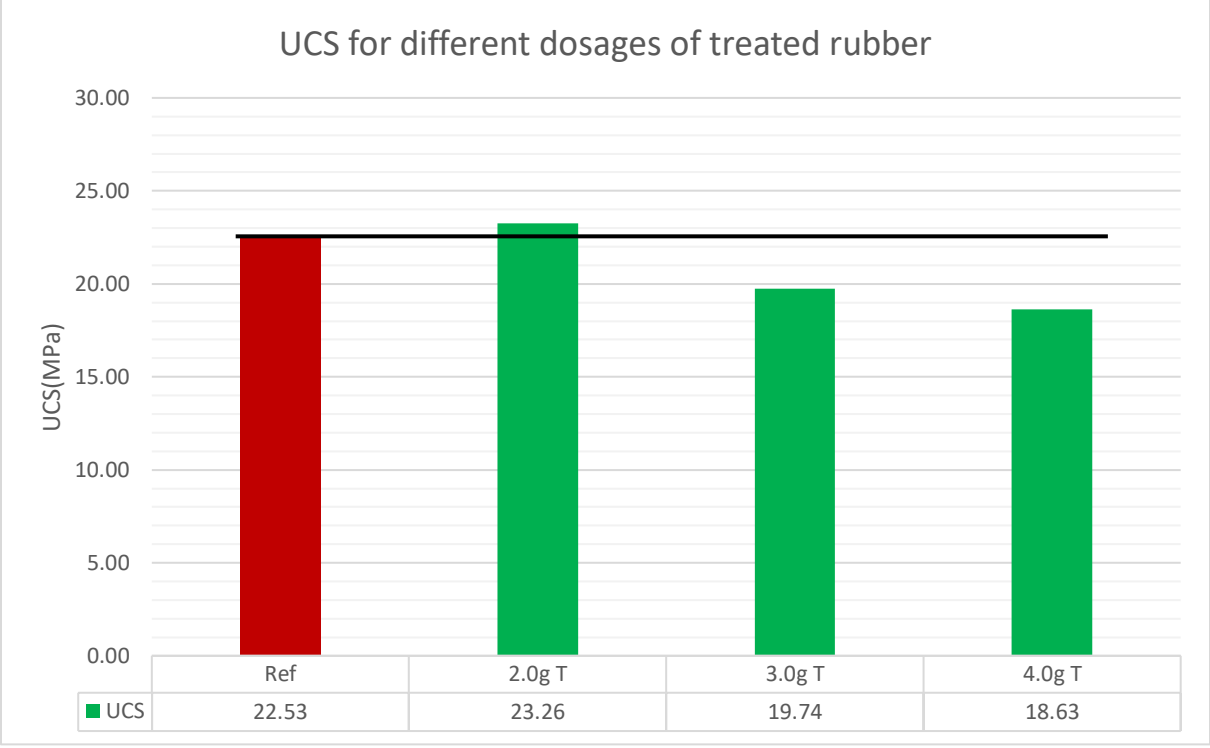

Figure 4.39 UCS for different dosages of treated rubber

From figure 4.39 one can observe that the highest UCS is achieved through the addition of 2,0 grams of acid treated rubber. It gives a sample with a UCS of 23,26 MPa, which is a 3,28% increase compared to control. Furthermore, the other tested dosages of 3,0 and 4,0 grams added, results in a sample with a UCS lower than the control.

The trend that appears in the figure above is that performance with regards to UCS peaks at the addition of 2,0 grams, and increasing the dosage will lead to a decrease in UCS with the higher dosages leading to a bigger decrease. In similarity to the untreated rubber results, it appears that the highest tested dosage leads to the worst result. Assuming the trend observed from figure 4.39 is accurate, it is possible that the addition of less than minimum tested amount could yield a greater UCS.

While the principle behind the addition of rubber is simple, it appears to have negative effects if added in the wrong dosages, as allowing for a more flexible matrix deformation does not necessarily lead to a better sample in terms of strength. It seems like instead of the rubber mitigating the highest loads and creating a more ductile sample, the matrix surrounding the rubber received additional load, which caused an uneven load distribution in the sample which in turn caused the sample to fail earlier than the control.

4.2.2.2 Effect of rubber ash on 0,44 WCR G class cement

After mixing and pouring into molds, the cement was left to set in the molds for 48 hours. The samples were then removed, polished and placed in a water bath for an additional 48 hours before being removed and left in air for the remaining time before destructive testing. The results from the destructive testing are displayed in the figure below;

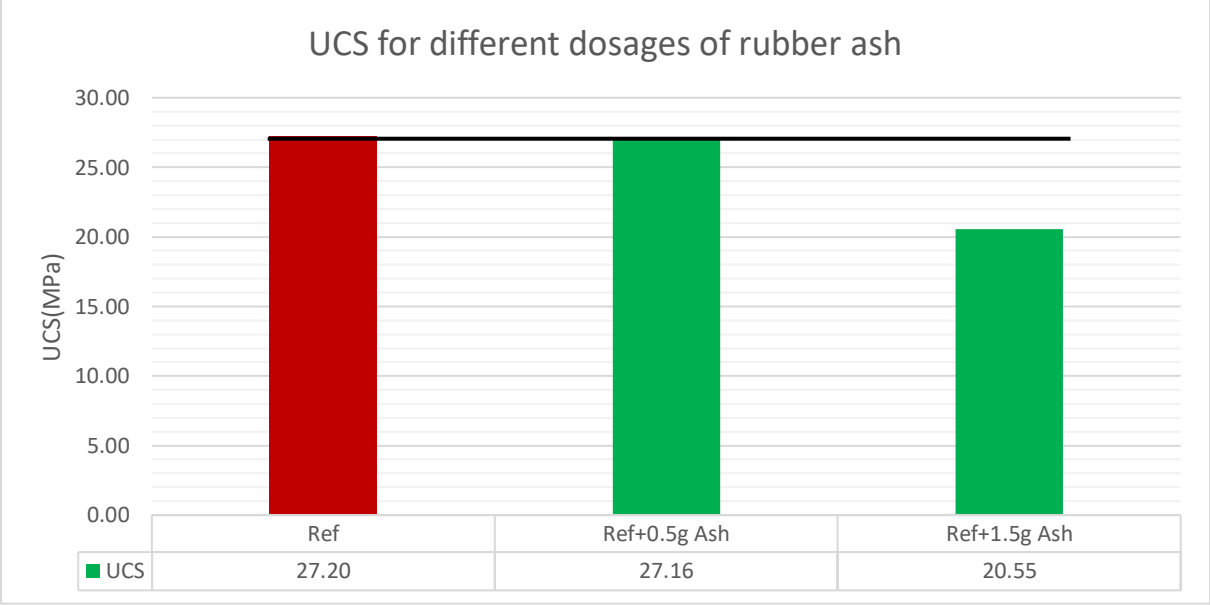

Figure 4.40 UCS for different dosages of rubber ash

From figure 4.40 the value of "Ref" is the average value of the two zero-additive samples from this batch. The results show that none of the tested dosages of added rubber ash leads to an increase in compressive strength. The results also indicate a downwards trend, where additional added rubber ash leads to a further decrease of compressive strength. The largest decrease causes the UCS to reduce by 24,5%.

These results further support the theory from before. It appears as if the addition of any rubber additive is generally harmful to the cement samples compressive strength. This is conflicting with results from other studies [35] but is very apparent from the results obtained in this thesis.

4.2.2.3 Young´s modulus of rubber additives on 0,44 WCR G class cement

To further investigate the effects of adding rubber to the cement slurry, Young's modulus can be analyzed. To give a better description of the changes in material hardness, which was discussed briefly above, an overview of the Young´s modulus of the various samples will prove beneficial. Shown below is the Young's modulus for all of the cement samples containing treated and untreated rubber.

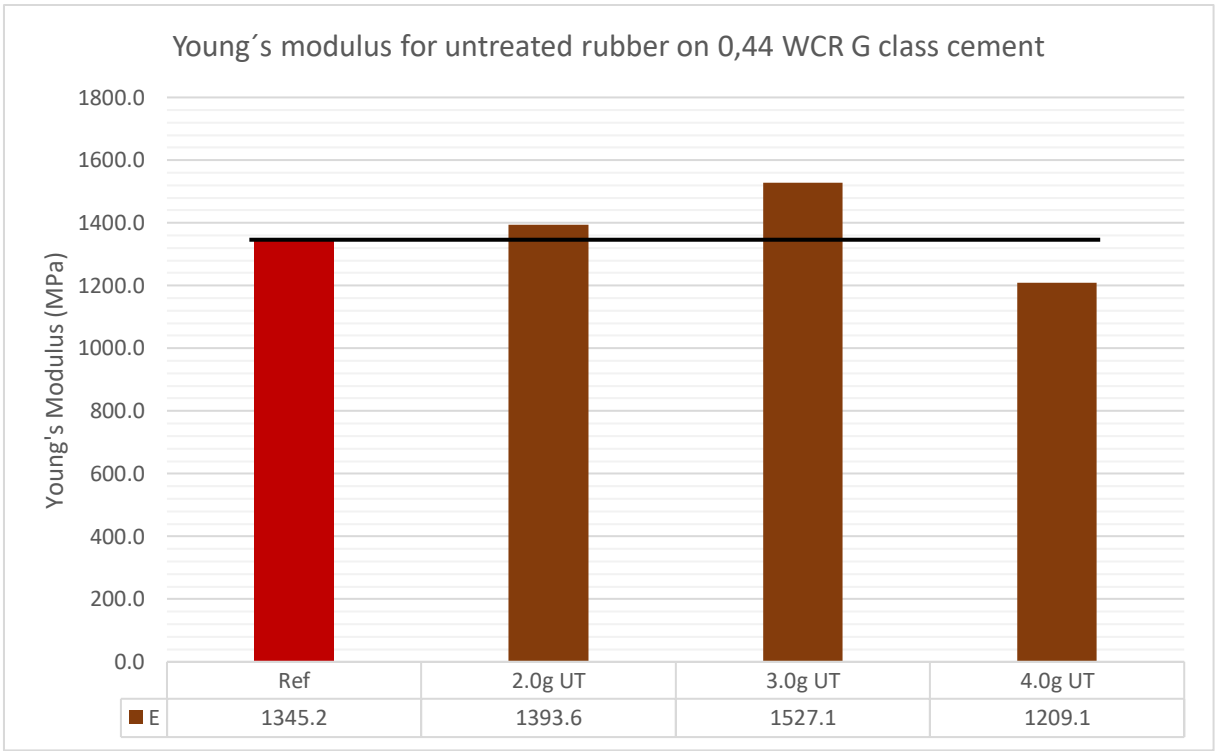

Figure 4.41 Young´s modulus for untreated rubber on 0,44 WCR G class cement

From figure 4.41 it shows that only the addition of 4,0 grams of untreated rubber leads to a decrease in E. The highest increase in Young´s modulus is observed from the addition of 3,0 grams which leads to an increase of 13,5%. These results indicate that by addition of untreated rubber in lower dosages, the resultant cement sample is able to deform less before reaching the ultimate stress and hence is a more brittle material compared to the control. This further supports the theories from chapter 4.2.2.1.

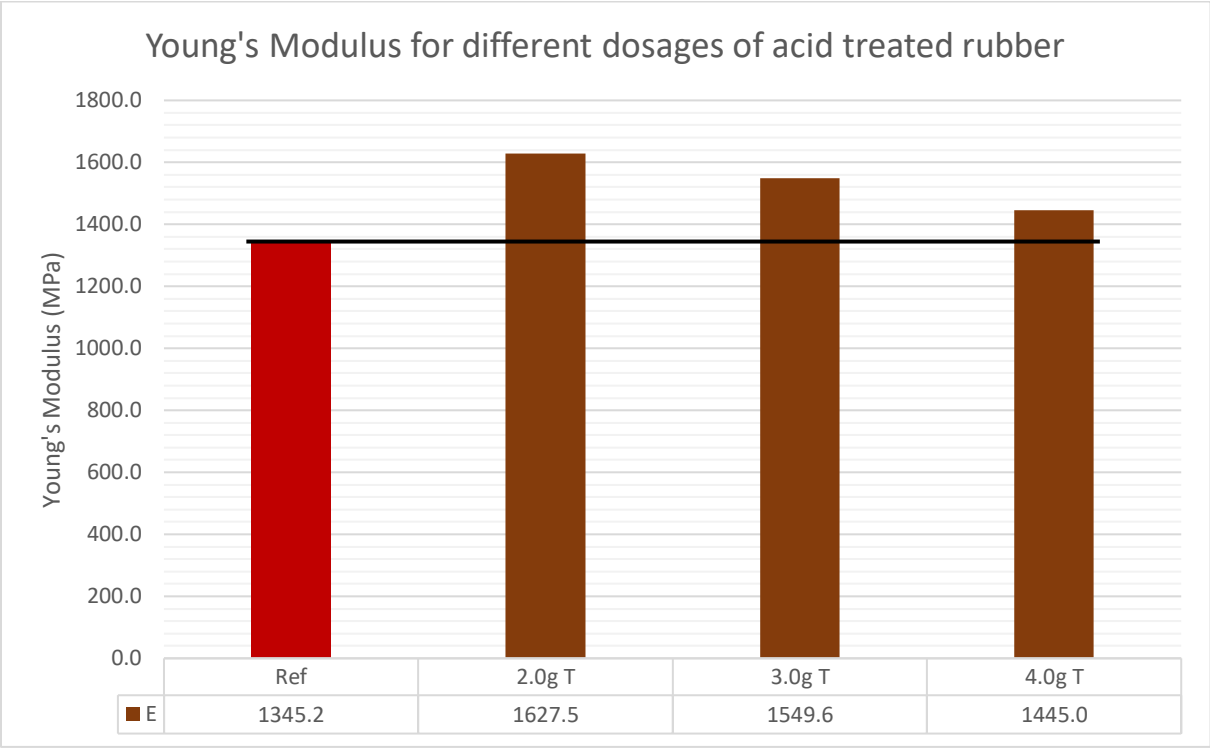

Figure 4.42 Youngs Modulus for different dosages of acid treated rubber

In figure 4.42 the Young's modulus for the cement samples containing acid treated rubber is displayed. From this graph one can observe that for all tested dosages, the Young's modulus increases. The largest increase, which is 21,0%, is observed through the addition of 2,0 grams of treated rubber. The trend displayed in the figure above matches that of the UCS values, where it is a downward trend with increasing dosages. These results also suggest that the added rubber made the cement samples more brittle, and not more ductile which was the desired outcome.

4.2.2.4 Resilience of rubber additives on 0,44 WCR G class cement

As mentioned in chapter 3.3.8, resilience measures the total amount of energy the sample can absorb until reaching maximum stress, known as UCS. This parameter takes both the UCS and

the Young´s modulus into account and can be used to better describe the property of the cement sample. One of the primary objectives of the additives is to increase the UCS, as it is highly desirable to obtain a high UCS, but combining this with a low value of E will cause the plug to be able to deform without sustaining permanent damage whilst still being able to withstand high pressures. Shown in the figures below is the resilience for all the samples containing rubber;

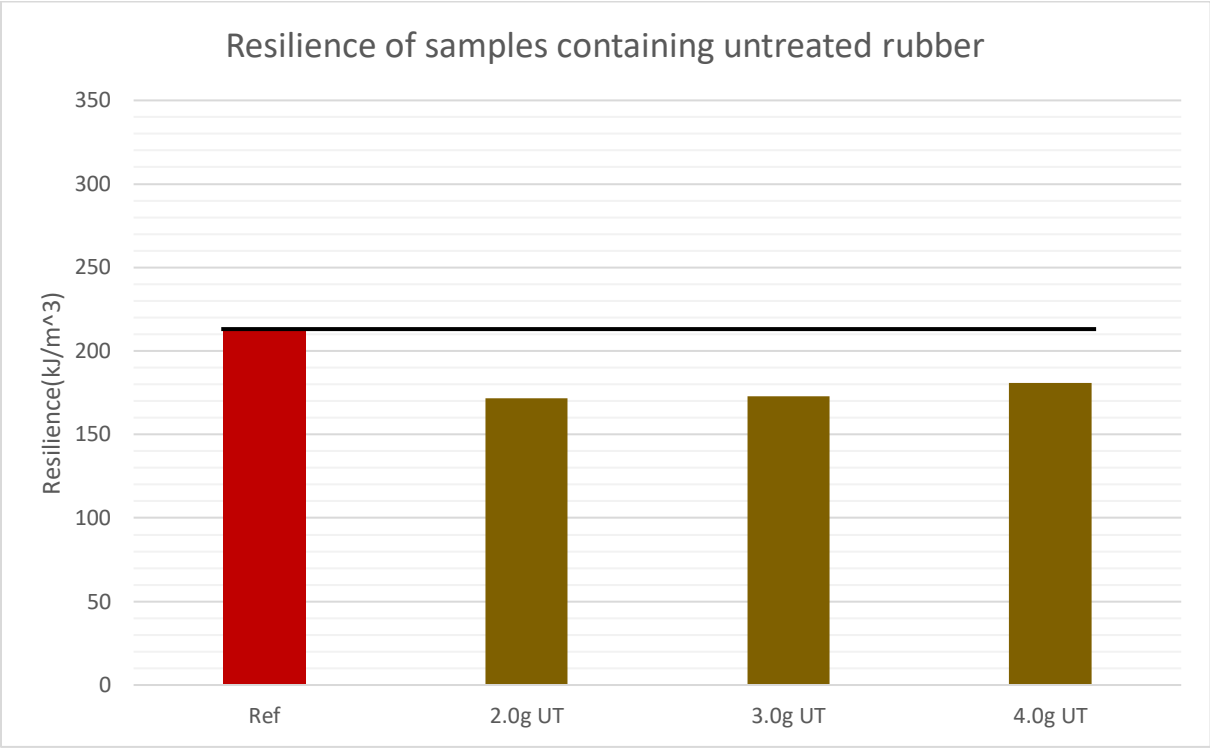

Figure 4.43 Resilience of samples containing untreated rubber

From figure 4.43 one can observe that for all samples containing untreated rubber, the resultant resilience was lower than the control. This means that all the tested samples are able to absorb less energy before sustaining permanent damage, i.e they are weaker than the regular cement sample. The largest decrease is observed from the sample containing 2,0 grams of untreated rubber, which lead to a decrease of 19,4% compared to control. Based on these results combined with the UCS results, it appears to be undesirable to add untreated rubber to the cement slurry, regardless of the dosage added.

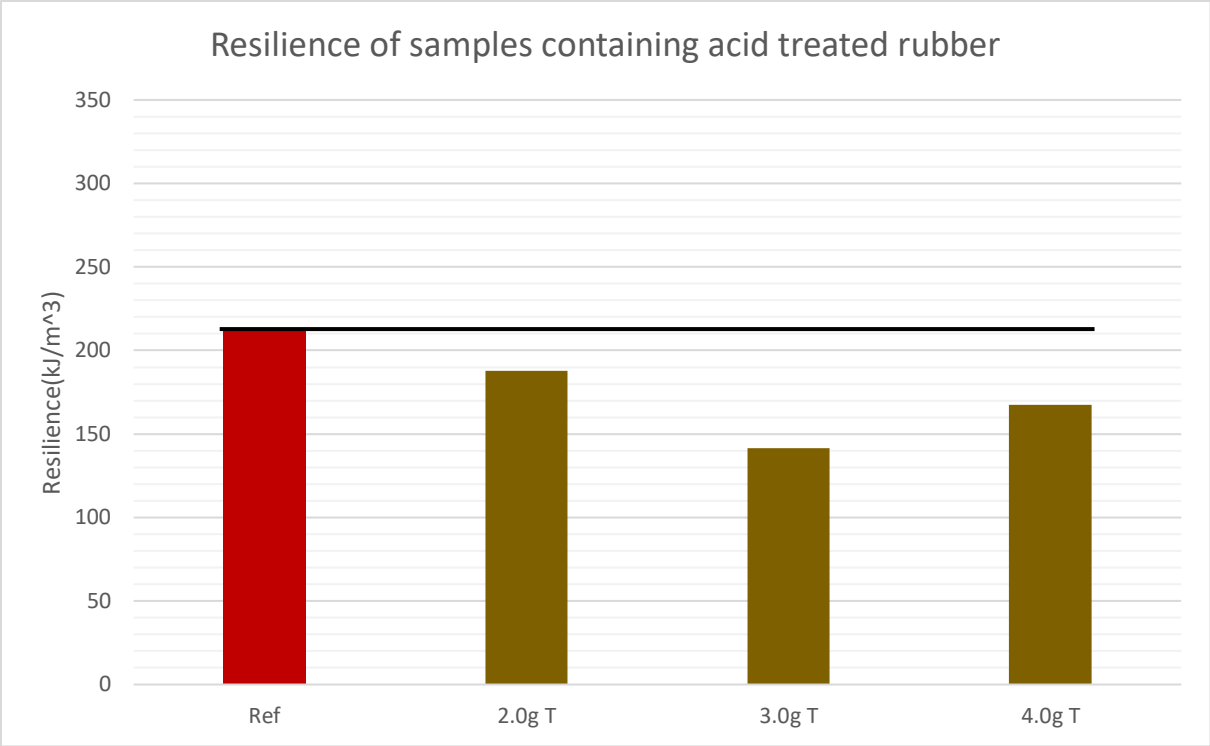

Figure 4.44 Resilience of samples containing acid treated rubber

The figure above displays the resilience of all the samples which contained acid treated rubber. In likeness to figure 4.43, it can be observed that for all dosages of treated rubber, the resilience is lower than the control. The largest decrease is observed when adding 3,0 grams of treated rubber which causes a decrease of 33,5% compared to the control. Based off these results in combination with the previously obtained results, it is not possible to definitively conclude whether adding acid treated rubber is desirable as it has both positive and negative effects.

4.2.3 M-modulus of rubber on 0,44 WCR G class cement

The procedure for obtaining the non-destructive test results are explained in chapter 3.3.2.3 and is calculated using equation 3-6 with data measured at 7 days, right before the samples were subjected to destructive testing. In figure 4.45 the straight line is the value of the reference point, and it is included to easier visualize where the different additives place in terms of change of M-modulus relative to the reference point. The non-destructive results for untreated rubber are depicted below;

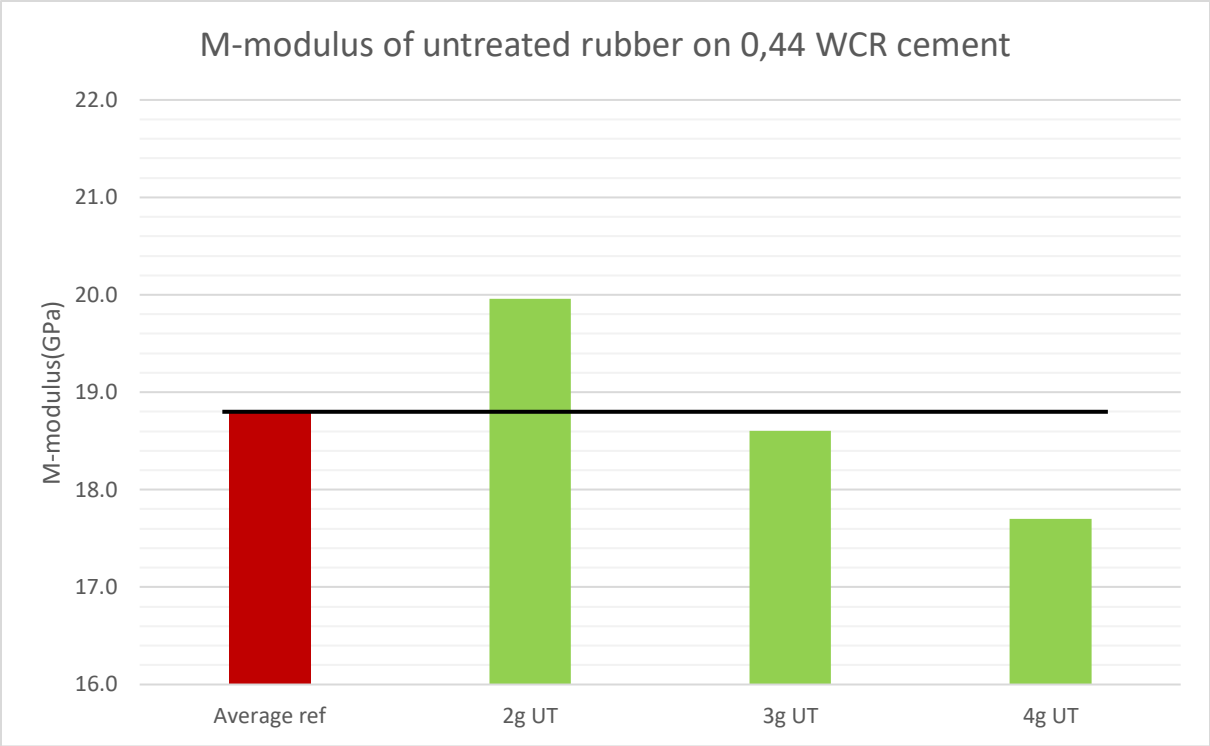

Figure 4.45 M-modulus of untreated rubber on 0,44 WCR cement

From figure 4.45 it shows that the observed trend deviates from the trend observed in figure 4.38 to a large extent, which is unexpected. It does, however, display a clear trend for the M-modulus of the various samples, where it appears to decrease with an increase of added rubber. The highest modulus of elasticity is achieved with the addition of 2 grams of untreated rubber, which causes an increase of 6,18% compared to the control. The M-modulus is reduced for the other tested concentrations of 3 and 4 grams, which leads to a reduction of 1,04% and 5,85% respectively.

One similarity between the graph above and the UCS results of the same samples, is that the addition of the highest amount of rubber leads to the worst result, which further supports the evidence that the addition of too much rubber leads to an overall worse cement matrix. The addition of 2 grams of untreated rubber lead to a substantial decrease in uniaxial compressive strength, yet displays the greatest increase in m-modulus. The sample which displayed the greatest UCS shows a minor decrease in m-modulus, which is consistent with the measured UCS result as they both decrease by a small amount.

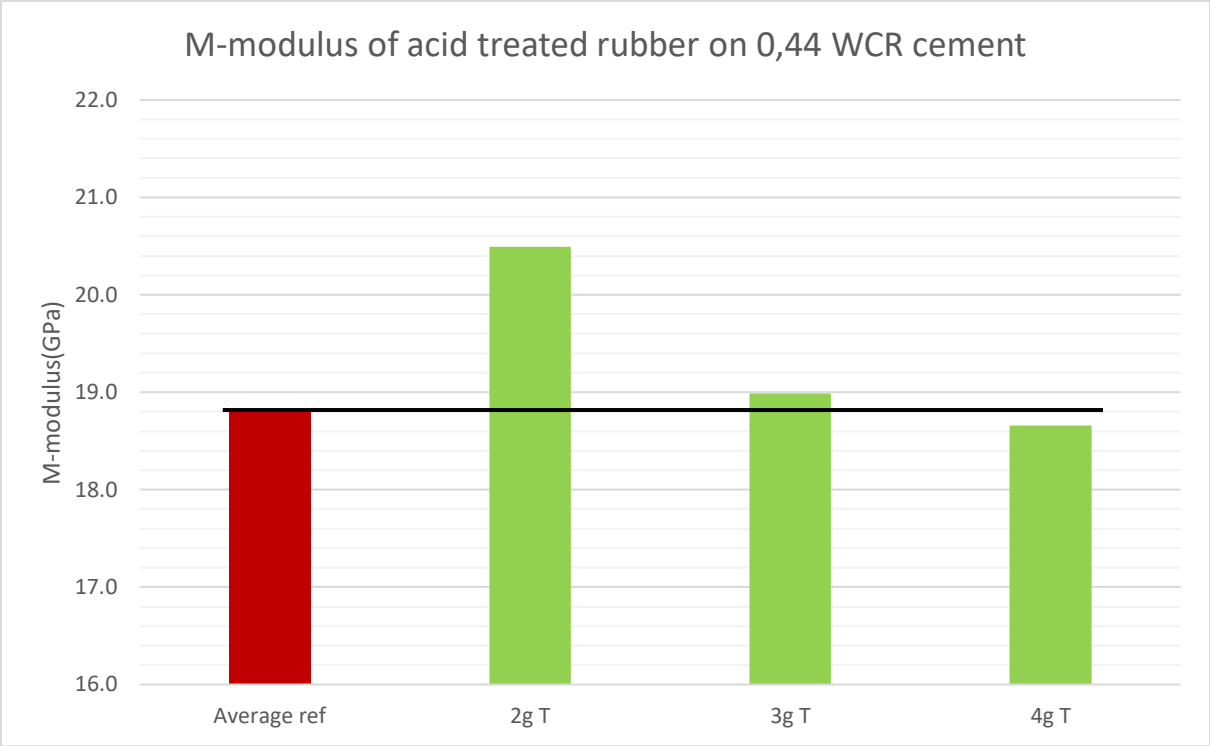

Figure 4.46 M-modulus of acid treated rubber on 0,44 WCR cement

From figure 4.46 one can observe the average value of the neat cement plug marked in dark red, with a straight line drawn from it to easier compare the results to the control. Firstly, one observes a trend which is similar to that of M-modulus of untreated rubber, with the highest M-modulus being achieved through the lowest dosage of rubber added, and that the effects decrease with an increase in concentration. The addition of 2 grams of treated rubber, caused the sample to increase its M-modulus by 8,99%, giving it a modulus of elasticity of 20,5 GPa. The second highest M-modulus is achieved by adding 3 grams of treated rubber, which causes an increase of 0,98% compared to control. Again, one observes that the highest dosage of rubber, 4 grams, causes the worst result where the M-modulus decreases by 0,74%.

One observes that the trend from figure 4.46 is matching the trend from figure 4.39. The highest value is achieved from the addition of 2 grams of treated rubber in both cases, where additional rubber will cause the value to decrease relative to the peak. It appears as the rubber can be beneficial towards the strength of the samples, if the concentration of rubber is low enough. Additionally, the addition of acid treated rubber proved to be more beneficial towards the strength of the samples compared to the untreated rubber. Furthermore, addition of too much rubber of either treated or untreated appears to weaken the sample.

4.3 Further investigation of best system

After performing numerous tests with different additives, the best performing additive in terms of strength increase on 0,44 WCR G class cement was selected for further testing. That system is a combination of nano-SiO_2 and MWCNT-COOH with the concentrations being 0,3 grams of nano-silica and 0,05 grams of MWCNT-COOH. This chapter will go through how this system affects the hardened cement and cement slurry and will focus on; final compressive strength after heat treatment, leakage rates after heat cycling, heat development of cement and rheology of cement slurry. Other results for this system, such as UCS, M-modulus, resilience and water absorption can be found in chapter 4.1.8

4.3.1 Compressive strength of heat-treated cement

A regular batch of samples were made containing only two zero-additive plugs and two plugs of the top performing system. The cement was left to set in air for 24 hours before being placed in an oven with a temperature of 105°C for 6 days. The cement was then removed, polished and non-destructively tested before being subjected to destructive testing. The experiment was performed to gain a better understanding of how the system performs in an environment which more closely mimics that of a deep cementing job in a well. Depicted below are the destructive results:

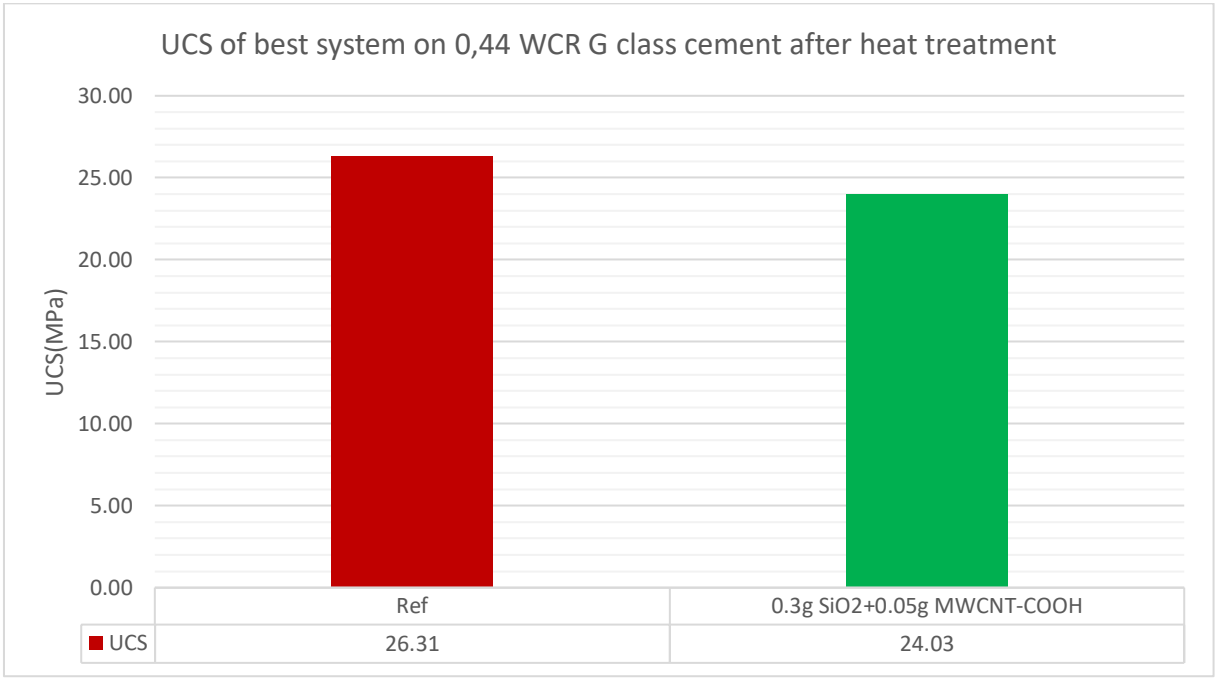

Figure 4.47 UCS of best system on 0,44 WCR G class cement after heat treatment

From figure 4.47 the value of "Ref" is the average value of the two zero-additive cement specimens. In this instance, the values of the two samples varied greatly, where one had a UCS of 21,4 MPa and the other had a UCS of 31,2 MPa, which averaged out to 26,3 MPa overall. When observing the graph above, one can see that the addition of the nanoparticles appears to have decreased the UCS by 8,7%.

The unusually large discrepancy of the control samples indicates that these measurements are unreliable. Usually, the solution to this problem would have been to re-do the experiment, however, due to time restrictions this was not an option. The results from this experiment are therefore inconclusive, and nothing concrete can be determined from looking at these results.

4.3.2 Leakage testing of best system

The making and procedure for this system is covered in chapter 3.3.10, and the theory behind fluid leakage through/around cement is covered in chapter 1.1 and can be seen in figure 1.2. The results for each 24-hour test interval are presented in the tables below;

For the zero-additive sample, the data looks as follows:

Table 4.1 Leakage of zero-additive cement sample

Duration in the oven (hr)	Added water (g)	Water leaked (%)	Matrix water absorption (%)
24	59,756	3,98	18,28
24 + 48	40,020	11,22	28,82
24 + 48 + 72	40,016	24,30	30,66

When measuring after a test, several measurements were taken, but the most interesting ones to examine is the amount of water that managed to get through or around the cement plug, and how much of the added water the cement matrix itself absorbed. An interesting trend is observed from the data; the amount of water which leaked through the cement sample more than doubles after each heat cycle it endured. Similarly, the amount of water the cement matrix is able to absorb also increases with each heat cycle. These results could be an indication that the sample has formed cracks or other deformations due to the conditions it was subjected to.

Table 4.2 Leakage of nano-additive cement sample

Duration in the oven (hr)	Added water (g)	Water leaked (%)	Matrix water absorption (%)
24	49,724	0,00	15,90
24 + 48	39,999	0,00	23,76
24 + 48 + 72	40,190	0,00	37,47

The first observation one can make from examining the data, is that for all measurements, the amount of water which leaked through or around the cement is zero. Corresponding to the observations made for the zero-additive sample, the amount if absorbed water increases witch each heat cycle. An interesting note is the large jump in water absorption at the last performed test, which could indicate internal changes in the sample before this test. It is, however, also possible that this large change is due to the fact that the sample was allowed to completely dehydrate in the extended period for which it was left in the oven and the increase in absorption is simply a rehydration of the sample.

When comparing the results from the separate samples, the first thing to take note of is obviously the difference in amount of leaked water. As the nano-sample had zero leakage for all tests, and the zero-additive sample showed strictly opposite results with increasing leakage for each test, it appears as if adding this nano-combination to the cement slurry helps with reducing and preventing leakage. Initial questions arose pondering whether the absence of leak in the nano-sample was due to the smaller amount of water added in the first measurement, and it was decided to add approximately the same amount of water to each of the samples for the following tests. This would ensure that the added water induced the same amount of hydrostatic pressure on each sample. This change did not affect the leakage rate of the nano-sample, and even though the added amount of water decreased for the control, the amount of water leakage rose.

The amount of water evaporation was measured for both of the samples and it was an inconsequential amount. The water evaporation for the control sample was higher than the evaporation for the nano-sample for every measurement taken. This is likely due to the isolation of the collection chamber for the leaked water, and the fact that evaporation happened at two

separate locations in the control sample. As the nano-sample did not leak, no water was present in the collection chamber and thus significantly less water evaporation occurred.

It is also worth noting that the amount of cement added to the pipe is not exactly the same for the control sample and the nano-sample. When pouring cement slurry into a steel pipe, it is hard to accurately measure the amount of cement which has been added, and as a result of this the sample which contained nanoparticles had a slightly larger volume than the control sample. It is known that an increased length of cement reduces the risk of leakage, and thus this could have had an impact on the tests. Furthermore, it is possible that given extra time, the cement sample containing nanoparticles could have leaked.

4.3.3 Rheology of cement slurry

The rheology of fluids is an extremely important factor in the petroleum industry due to the amount of fluid transport happening (mud/cement pumping, crude oil producing, wet gas producing etc). When circulating e.g cement it is of utmost importance to know its rheological properties to be able to accurately calculate needed pump pressure, rate and other parameters. Performing measurements of the cement slurries are therefore of great importance, and the SiO_2+MWCNT-COOH system was tested simultaneously with a zero-additive control slurry to characterize its properties.

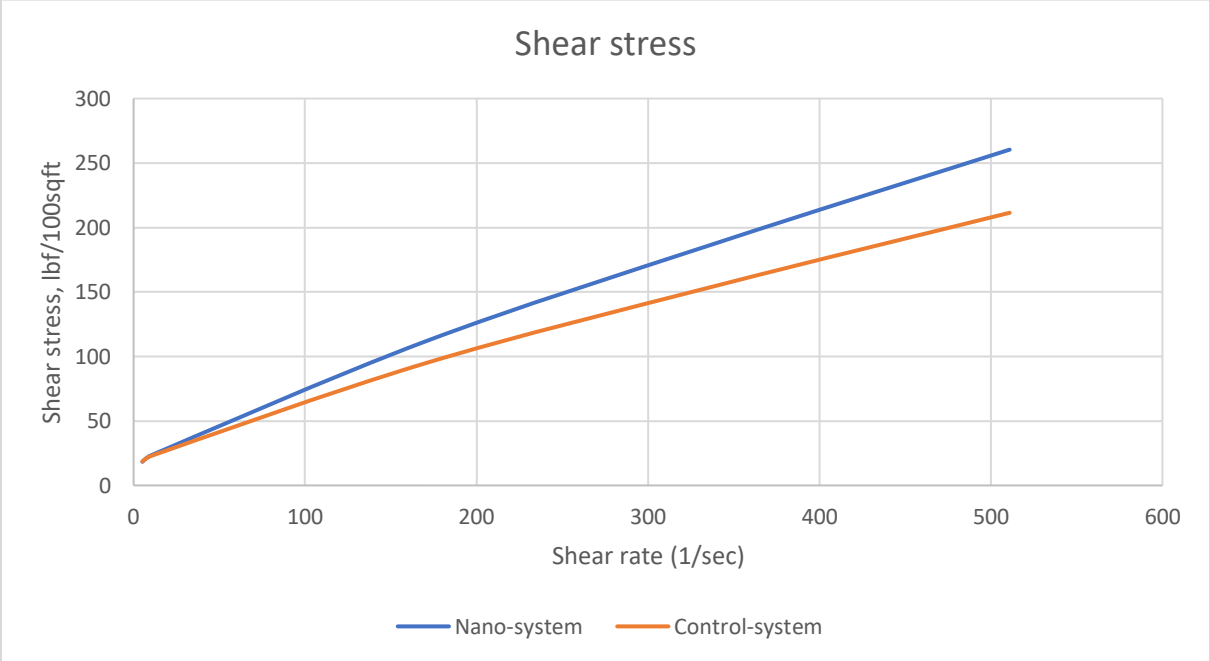

Figure 4.48 Shear stress of cement slurries

In figure 4.48 the shear stress of the two systems are plotted together, and it shows that the system containing nanoparticles exhibits higher shear rheology compared to the control system for almost all measured points. At very low shear rate (5,1 sec^{-1}) the shear stress of the nano-system is lower than the control, but for all other points it is higher. From the figure one can also observe that the difference in shear stress increases at higher shear rates, and the largest difference is observed at the shear rate of 510,9 sec^{-1}.

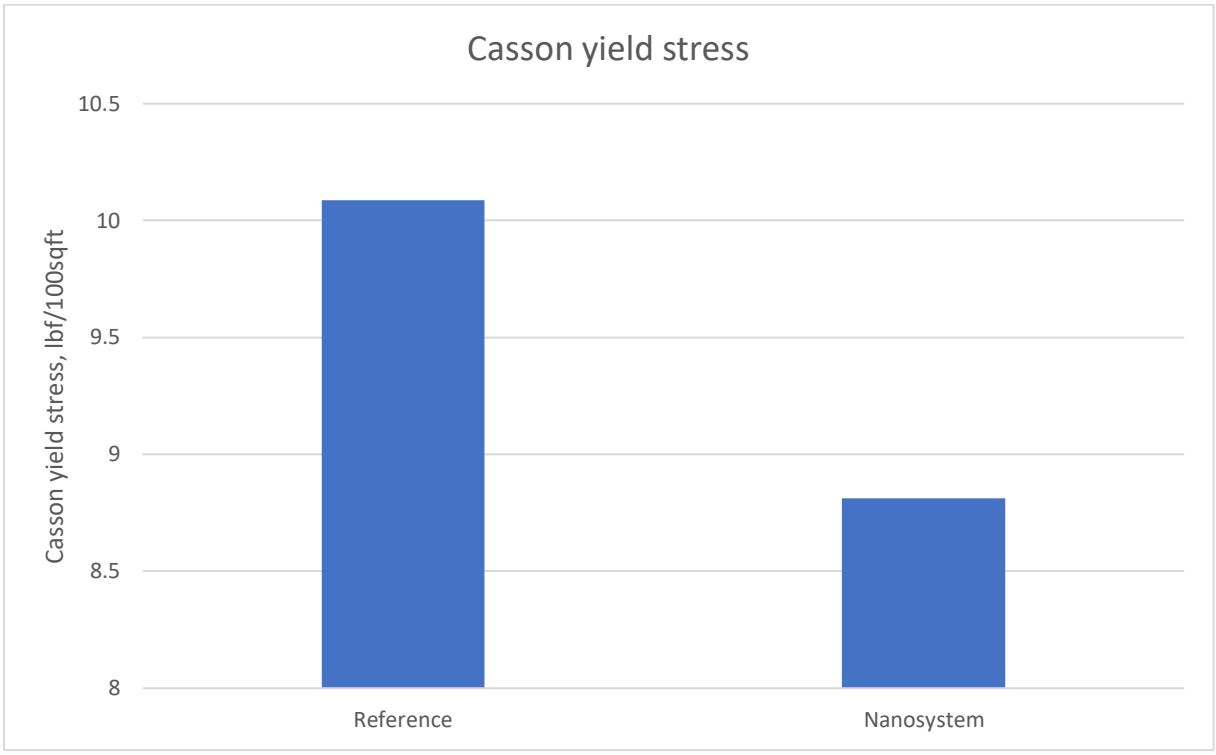

Figure 4.49 Casson yield stress of the two tested systems

The figure above depicts the Casson yield stress of the two tested systems. One can see that the system containing nanoparticles is exhibiting a lower yield stress than the control system. In essence, this means that the cement slurry containing nanoparticles would require less force to set in motion which could be beneficial when e.g setting cement plug via wiper darts. Having a lower yield stress could mean allowing more of the available pump power to be used for other actions and is generally a positive property.

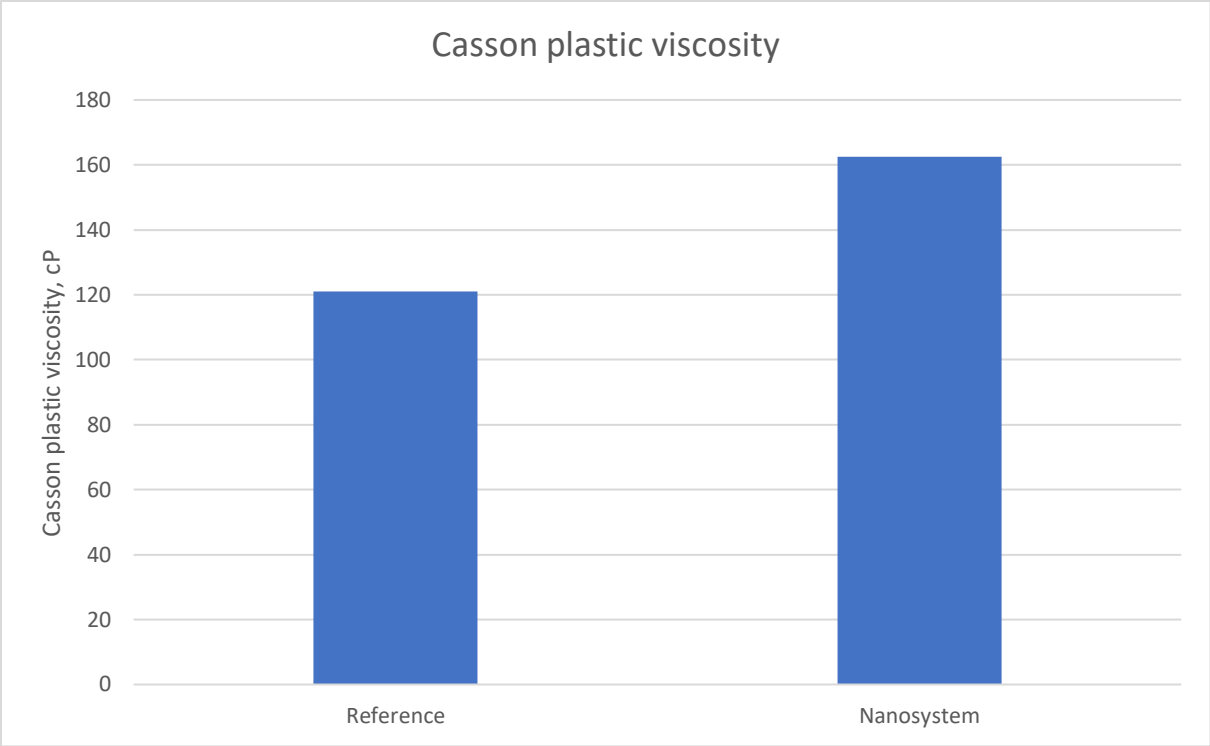

Figure 4.50 Casson plastic viscosity of the two tested systems

The figure above showcases the Casson plastic viscosity of the measured systems. One can observe that the PV of the system containing nanoparticles is higher than the control, which means it has a higher resistance to flow. This equates to larger friction in the pipe and thus it requires more pumping power. In addition, it means that the cement is thicker and ensures better solids transport and hole cleaning, which could be beneficial in a cementing job. Usually, washers and spacers clean out the area which is meant to be cemented, but this will not always be completely clean. A high viscosity cement could help further clean the area and properly displace the aforementioned washers to ensure a high-quality tail cement.

Naturally, different wells require different rheological properties of cement, and this can be found through simulation software. To determine whether these rheological properties are good or not for a certain scenario, one would have to run simulations, but due to time constraints this work was not completed in this thesis.

4.3.4 Heat development

When cement is mixed with water, an exothermic reaction occurs which liberates heat. The heat development of Portland cement has several stages and has been studied through this experiment. Two temperature loggers were placed inside the cement and measured the temperature of the cement every 5 minutes for approximately 72 hours during the hydration process. The slurries which were studied were a control slurry containing zero additives, and a slurry which contained the SiO_2 and MWCNT-COOH nano-additives. Both systems used a WCR of 200/454=0,44 and were subjected to rheological testing prior to being placed in the insulated box for measurement of heat development. The various stages of heat development for Portland cement is covered in chapter 2.2

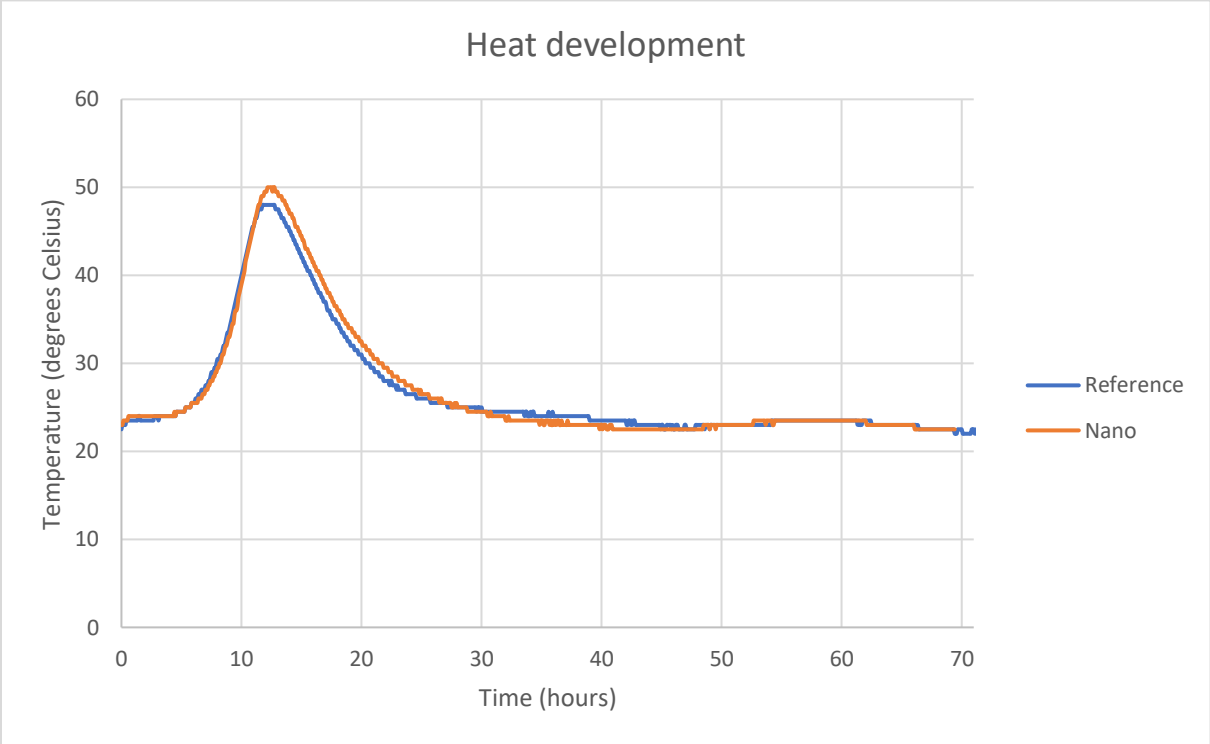

Figure 4.51 Heat development as a result of cement hydration

From figure 4.51 one can observe that the whole of the preinduction period is not plotted, as that stage only lasts for a few minutes and the cement slurry was being tested before the temperature logging commenced. As a result of this the logging starts in stage 2 with no heat evolution. The heat buildup starts after approximately 4 hours, and peaks at the end of stage 3/beginning of stage 4. The peak temperature for the zero-additive cement is measured at 48ºC

and the highest temp for the nano-system is recorded as 50ºC. During the diffusion period (stage 5), very little differences between the systems are observed.

The temperature loggers used could only measure temperatures in 0,5ºC increments, and as a result of this the measured temperatures includes some inaccuracies. Furthermore, the same amount of cement was used for both tests, and the amount of cement should therefore not cause any differences in temperatures as explained by PCA [45].

Previously conducted studies [53] suggest that the addition of SiO_2 nanoparticles may shorten the dormant period (stage 2), but this is not evident from the study conducted in this thesis. The results does indicate that the added nanoparticles may act as a nucleation site due to their large reactive surfaces, and thus accelerating the hydration process which results in a more complete hydration after a certain amount of time which can be seen in figure 4.51 as an increased temperature relative to the control.

4.4 Uncertainty

This section will cover some of the uncertainties which were involved and were likely to affect the experiments

Plug preparation: When polishing plugs such that the surface was flat, sandpaper was used. Initially, for 0,52 WCR samples this was no issue, however, when switching over to much denser 0,44 WCR samples, it was found that the sandpaper used was of too little coarseness. Additionally, the plugs were polished such that they reached the brim of the plastic mold, and the brim was also found to not be level in all cases. This caused some of the samples from the first batch of 0,44 WCR cement plugs to be **crooked**, or **pointy**. To address this issue, additional sandpaper of higher coarseness was acquired, and the plugs were removed from the mold and measured using a level measuring tool to ensure that they were completely flat. Even after this, some plugs were still a slightly uneven when measuring the UCS. The problem with crooked or pointy plugs is that when measuring UCS, the load distribution will be uneven, leading to a drastically lower result than what could have been achieved.

Slurry preparation: When making the cement slurry, the containers which contained cement was not allowed to be cleaned or rinsed with water as there were no proper depositing containers

for this, and using the sink was not allowed as it might plug the pipes or similar. As a result, paper towels were used to clean out the container between making each plug. A thorough cleaning of the containers were done, but there is still a possibility of cement residue being left inside the container between each slurry formulation which means there is a possibility that this could have affected some batches. This could have been avoided if a new container was used for each plug, but this solution is costly and unrealistic.

Equipment: All types of machinery used has added uncertainty. The scales used are accurate to a certain decimal point, where the uncertainty is defined as the smallest increment divided by two. This causes any weight measurement to contain some uncertainty. When measuring sonic, the machine would have to be calibrated between each batch as it would deviate from the calibrated value after some time, which means there are some uncertainties in the sonic measurements as well. When measuring the UCS for test batch 9-17, a machine with a hand-operated hydraulic pump had to be used. The machine used a state-of-the-art load cell, so the measured data is good, however the loading speed deviation might have caused some inaccuracies. Generally, a lot of the lab-equipment utilized were in heavily used condition, which could affect the experiments.

Quantity of experiments: To ensure the highest possible accuracy of results for an experiment, it should be performed multiple times. This practice is well known, but rarely followed in these types of experiments due to the costs associated with it. Even in most of the cited experimental literature in this thesis, the experiments were only performed once. In this thesis, an attempt was made to increase certainty of results by making two identical plugs for each concentration, effectively doing the experiment twice. However, some of samples contained imperfections, and thus some uncertainty in the results may be present due to the slurry molding process and surface irregularities that induces higher stress concentration during testing. In order to obtain the best possible representative of the measurement, the average value of the plugs was presented.

Human error: Human error is always a factor which can cause uncertainty in results. Errors could have been made during procedure or inaccurate readings could have been taken.

5. Empirical UCS vs Vp modeling

There are several empirical models available from literature which describes the UCS-V_p relationship, including the Horsrud model which was covered in chapter 3.3.4. The Horsrud model was derived based on shale data from the North Sea and can therefore be inaccurate in cases regarding cement strength. This chapter will analyze the predictive power of the Horsrud model and derive a new UCS-V_p based model using experimental data obtained in this thesis.

5.1 Analysis of Horsrud model

To analyze the predictive power of the Horsrud model, actual destructive UCS of several samples from this thesis was plotted against the theoretical UCS obtained from using the Horsrud model. Test batch no. 3 and test batch no. 2 was used, to include both a collection of weak (TiO_2) and strong (MWCNT-COOH) cement samples.

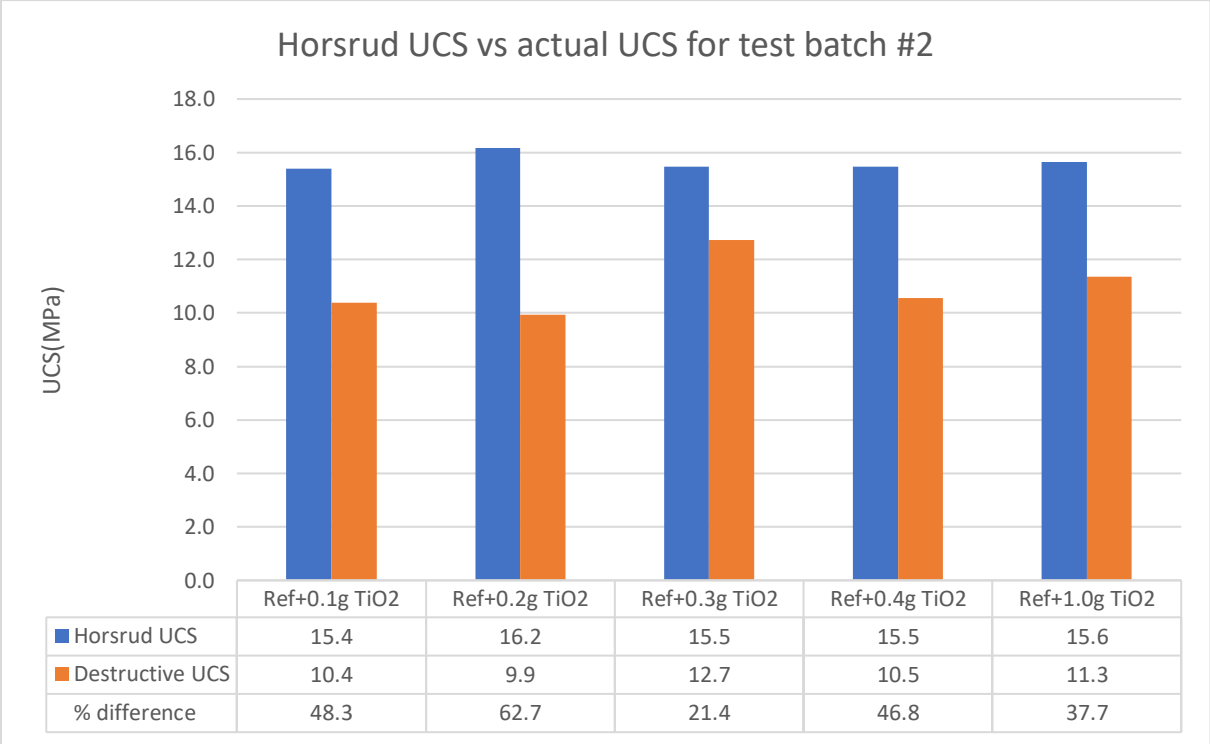

	Ref+0.1g TiO2	Ref+0.2g TiO2	Ref+0.3g TiO2	Ref+0.4g TiO2	Ref+1.0g TiO2
Horsrud UCS	15.4	16.2	15.5	15.5	15.6
Destructive UCS	10.4	9.9	12.7	10.5	11.3
% difference	48.3	62.7	21.4	46.8	37.7

Figure 5.1 Horsrud vs actual UCS for test batch no. 3

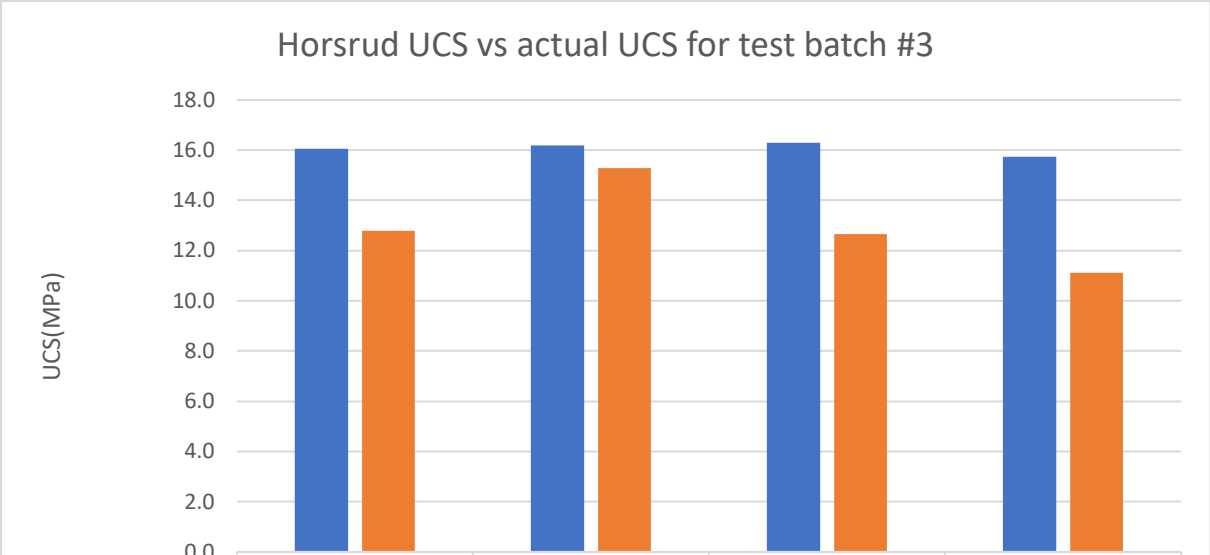

	Ref+0.1g MWCNT-COOH	Ref+0.2g MWCNT-COOH	Ref+0.3g MWCNT-COOH	Ref+0.4g MWCNT-COOH
Horsrud UCS	16.1	16.2	16.3	15.7
Destructive UCS	12.8	15.3	12.7	11.1
% difference	25.7	5.8	28.8	41.5

Figure 5.2 Horsrud vs actual UCS for test batch no. 2

From figure 5.1 and 5.2 one can observe a large difference in the theoretical UCS calculated from the Horsrud model and the results obtained through testing. The model overestimates the UCS of the plug, which is especially evident in figure 5.1. With large deviations up to 62,7% it is clear that a new model was required to more accurately predict the UCS based on the P-wave velocity of the cement samples.

5.2 New model development and testing

When developing a new model, data obtained through experimental tests performed in this thesis was used for modeling. Other experimental data from Senoor and Zakaria (2018) was used for testing and evaluating the model. The model is based off sonic measurements at the day of crushing, and the destructive UCS result. Figure 5.3 below displays the UCS vs V_p of the datapoints used to make the model. The UCS-V_p relation can be well described by a function of power law, and a trendline of format power law is added to provide the formula.

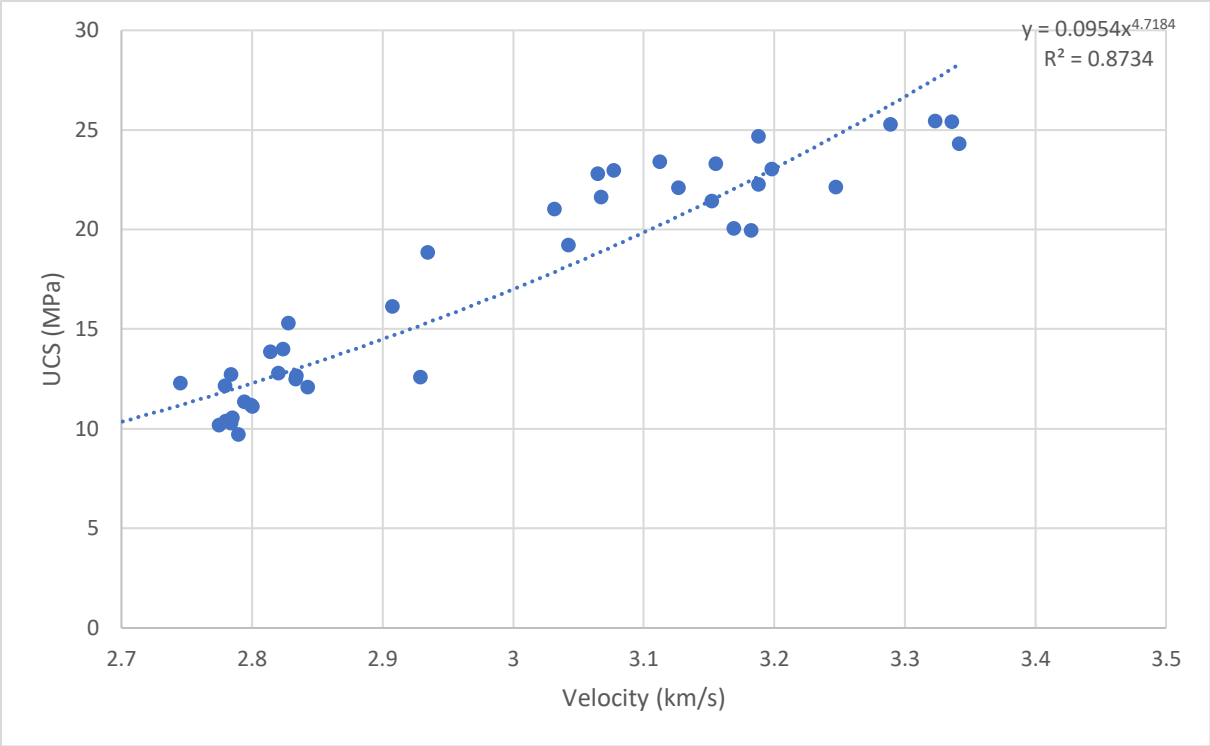

Figure 5.3 UCS vs Vp plot using measured data

Equation 5-1

$$UCS = 0{,}0954 * V_p^{4{,}7184}$$

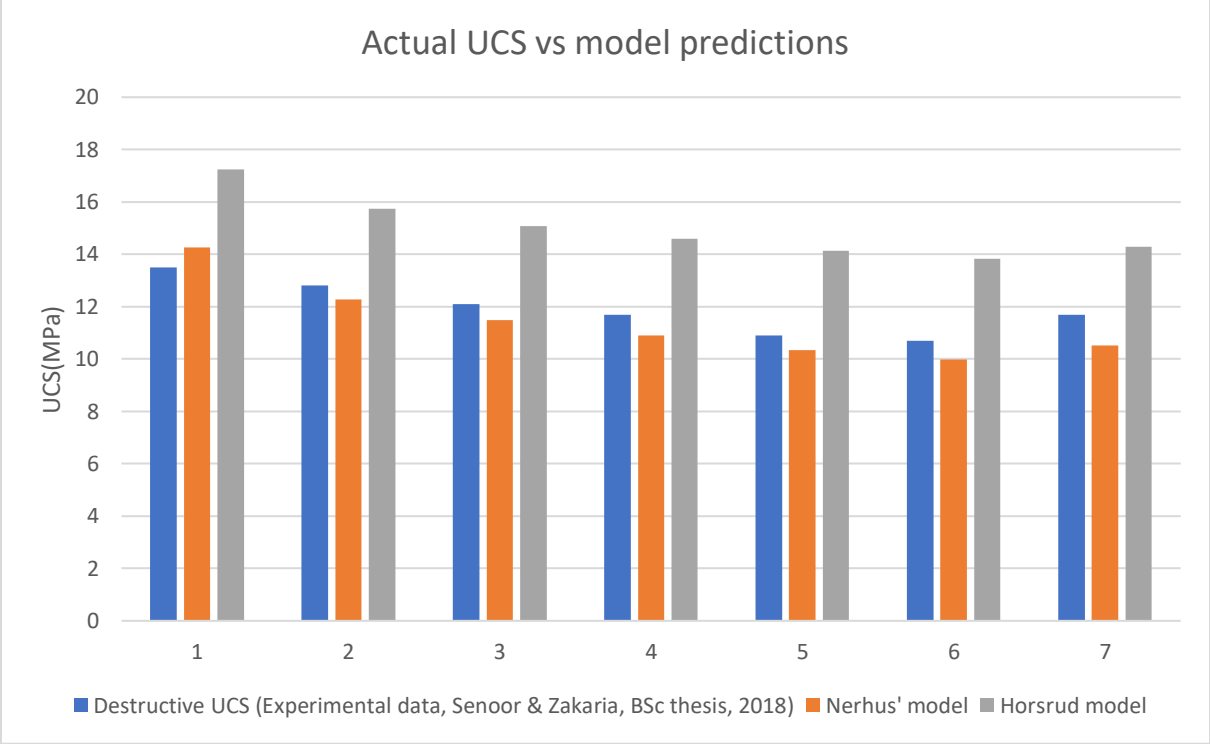

Figure 5.4 Actual UCS vs model predictions

From figure 5.4 one can observe that the model developed in this thesis matches the experimental data rather well. It tends to slightly underestimate the UCS of the plugs, but the difference is small. For reference, the Horsrud model prediction is also included, which overestimates the UCS by a rather large amount. This can be rationalized based on the description in chapter 3.3.4, and it is possible that the Horsrud model is better suited to describe sedimentary rock.

6. Summary and conclusion

A table summarizing the most relevant results from the experimental work performed in this thesis is found below. The general conclusions will be covering the questions posed in chapter 1.2 and will be presented in accordance with how the questions are listed.

From the experimental work, the following observations were made:

- For all tested nanoparticles, the UCS increased with varying degrees compared to the control plug given the right concentration of nanoparticle added. The M-modulus increased for nearly all of the tested nanoparticles at a certain concentration, with the exception of a few anomalies. The resilience of the cement increased for all of the analyzed nanoparticles, with the exception of TiO_2. The water absorption showed varying results, where SiO_2 and MWCNT displayed a decrease in water absorption and TiO_2 and Fe_2O_3 displayed an increase in water absorption.
- The effect of added nanoparticle varies greatly with the water to cement ratio. It was found that the nanoparticles generally had a much larger impact on 0,52 WCR than 0,44 WCR in terms of cement strength.
- It was found for all nanoparticles, except the combination of MWCNT and Al_2O_3, that with an increase in concentration, a decrease in desired cement properties is observed with varying degrees.
- For the addition of untreated silicone rubber, acid treated silicone rubber and rubber-ash it was found that this has a negative impact on cement strength with the exception of one instance. The resilience is decreased for all analyzed instances, and the M-modulus has varying results.
- When combining nanoparticles in a hybrid mixture, the results varied greatly in terms of strength increase. Some mixtures (MWCNT-COOH+SiO_2 and Al_2O_3+MWCNT) improved drastically compared to the effect of each nanoparticle separately whilst other mixtures (SiO_2+Fe_2O_3 and MWCNT-COOH+TiO_2) showed significantly worse results compared to each nanoparticle separately.
- The effect of MWCNT with and without a COOH group showed no significant differences in terms of strength increase when tested on the same WCR.

- The developed model manages to relatively accurately predict a samples UCS based off its sonic measurements.
- The addition of MWCNT-COOH+SiO_2 nano-system;
    - Greatly improved the cement in terms of leakage. No leakage was observed after several heat cycles, whereas for the control plug, increasing leakage was observed for each cycle.
    - showed an inconclusive decrease in cement strength after being exposed to a high temperature environment.
    - Increased shear stress and Casson plastic viscosity, while reducing Casson yield stress of the cement slurry relative to the control slurry.
    - Accelerated the hydration process, which resulted in a higher peak temperature compared to control

Table 6.1 Best results from destructive tests

TB	Additive	Concentration (%bwoc)	WCR	Curing time (days)	UCS (MPa)	M (GPa)	UCS increase (%)
TB#1-5	none	-	≈ 0,524	7	11,8	14,3	-
TB#1	SiO_2	0,26			16,1	15,7	36,9
TB#2	MWCNT-COOH	0,11			15,3	14,9	29,8
TB#3	TiO_2	0,16			12,7	14,0	8
TB#4	Fe_2O_3	0,21			12,5	14,8	6,1
TB#5-8	none	-	≈ 0,441		22,5	18,8	-
TB#6	MWCNT-COOH	0,13			24,3	21,3	7,9
TB#8	MWCNT-COOH + SiO_2	0,02 + 0,13			28,6	19	27,1
TB#7	Acid treated rubber	0,89			23,3	20,5	3,3
TB#9	none	-		49	27,2	16	-0,1
	Rubber-ash	0,22			27,2	17	
TB#10	none	-		48	25,9	17,3	10,1
	SiO_2	0,26			28,5	18,0	
TB#11	none	-		47	17,9	19,6	10,9
	MWCNT	0,13			19,9	17,3	
TB#12	none	-		46	24,0	19,6	0,9
	Al_2O_3	0,13			24,2	19,7	
TB#13	none	-	≈ 0,441	7	25,4	18,9	0,1
	ZnO	0,9			25,4	18,3	
TB#14	none	-			23,3	17,9	16,7
	MWCNT + Al_2O_3	0,75 + 1			27,2	18,7	
TB#15	none	-			23,0	17,2	0,2
	MWCNT-COOH + TiO_2	0,13 + 0,13			23,0	19,1	
TB#16	none	-			22,8	16,9	2,6
	SiO_2 + Fe_2O_3	0,22 + 0,18			23,4	17,7	

7. Future work

Over the course of this thesis, several ideas developed for how to improve certain experiments and what could be focused on in future work relating to this;

Larger cement samples: The current size of the cement samples offered several challenges during the experimental work. The specimen size is so small that they are highly influenced by the smallest imperfection, and more prone to uncertainties. Enlarging the cement specimens could improve consistency in the measurements and make several aspects of the experiments easier. Furthermore, this should lead to less deviation in measurements and make the destructive results even more reliable.

Variation in curing time: As this thesis predominantly used a 7-day timeframe, it would be interesting to study the strength development of the various slurries over 1, 3, 7, and 28 days to further study the strength development effects of the various additives. It could also bring a better understanding of the 7-day vs 28-day strength of cement relationship. This would mean making 4 sets of the same plug, and crushing them at 1, 3, 7 and 28 days to study the effect of the additives at different times and how they compare to the control sample.

HPHT: All plugs were conditioned and cured at atmospheric pressure and room temperature, with the exception of TB#17, which had increased temperature with normal pressure. Examining the effect of additives when plugs are exposed to more realistic downhole conditions such as high pressure and high temperature would be an interesting direction to take this research further.

Improve leakage testing: The leakage test performed in this thesis was not optimal, and there can be made several improvements. One of the things that would be interesting to analyze is to impose a pressure on the part containing fluid and examine the leakage. Additionally, measuring pressure of both sides of the cement to analyze communication through the sample should also be investigated.

SEM and element analysis: Analyzing the internal structure of some of the cement samples was originally planned to be performed in this thesis, but it was not able to be arranged. Gaining information and characterizing the internal structure of the cement samples can improve understanding of the effects the additives may have, and can contribute to configuring even better cement slurries.

References

[1] S. Norge, *NORSOK Standard D-010: Well integrity in drilling and well operations, Rev. 4*. Standards Norway: Lysaker, 2013.

[2] E. B. Nelson and D. Guillot, Eds., *Well cementing*, 2nd ed. Sugar Land, Tex: Schlumberger, 2006.

[3] B. Vignes and B. S. Aadnoy, "Well-Integrity Issues Offshore Norway," presented at the IADC/SPE Drilling Conference, Jan. 2008, doi: 10.2118/112535-MS.

[4] S. Bachu and T. L. Watson, "Possible indicators for CO2 leakage along wells," p. 6.

[5] R. J. Davies *et al.*, "Oil and gas wells and their integrity: Implications for shale and unconventional resource exploitation," *Mar. Pet. Geol.*, vol. 56, pp. 239–254, Sep. 2014, doi: 10.1016/j.marpetgeo.2014.03.001.

[6] "Cementing operations - PetroWiki." https://petrowiki.org/Cementing_operations (accessed Apr. 05, 2020).

[7] A. Vinod, A. Kundan, M. Kumar, V. Kalpande, and R. Pandey, "Prediction of Pre-Drill Well Cost & Scope of NPT Management in Shallow Water, Western Offshore Basin, ONGC, Mumbai," Dec. 2013.

[8] "Sealing Materials for Well Integrity - Oil&Gas Portal." http://www.oil-gasportal.com/sealing-materials-for-well-integrity/?print=print (accessed Jun. 01, 2020).

[9] T. Vrålstad, A. Saasen, E. Fjær, T. Øia, J. D. Ytrehus, and M. Khalifeh, "Plug & abandonment of offshore wells: Ensuring long-term well integrity and cost-efficiency," *J. Pet. Sci. Eng.*, vol. 173, pp. 478–491, Feb. 2019, doi: 10.1016/j.petrol.2018.10.049.

[10] T. Rocha-Valadez, A. R. Hasan, S. Mannan, and C. S. Kabir, "Assessing Wellbore Integrity in Sustained-Casing-Pressure Annulus," *SPE Drill. Complet.*, vol. 29, no. 01, pp. 131–138, Jan. 2014, doi: 10.2118/169814-PA.

[11] R. C. Patil and A. Deshpande, "Use of Nanomaterials in Cementing Applications," presented at the SPE International Oilfield Nanotechnology Conference and Exhibition, Jan. 2012, doi: 10.2118/155607-MS.

[12] A. I. El-Diasty and A. M. S. Ragab, "Applications of Nanotechnology in the Oil & Gas Industry: Latest Trends Worldwide & Future Challenges in Egypt," presented at the North Africa Technical Conference and Exhibition, Apr. 2013, doi: 10.2118/164716-MS.

[13] A. K. Santra, P. Boul, and X. Pang, "Influence of Nanomaterials in Oilwell Cement Hydration and Mechanical Properties," presented at the SPE International Oilfield Nanotechnology Conference and Exhibition, Jan. 2012, doi: 10.2118/156937-MS.

[14] "Nanoparticles - what they are, how they are made," *Nanowerk*. https://www.nanowerk.com/how_nanoparticles_are_made.php (accessed Feb. 10, 2020).

[15] M. Amanullah, M. K. AlArfaj, and Z. A. Al-abdullatif, "Preliminary Test Results of Nano-based Drilling Fluids for Oil and Gas Field Application," presented at the SPE/IADC Drilling Conference and Exhibition, Jan. 2011, doi: 10.2118/139534-MS.

[16] G. Maserati *et al.*, "Nano-emulsions as Cement Spacer Improve the Cleaning of Casing Bore During Cementing Operations," presented at the SPE Annual Technical Conference and Exhibition, Jan. 2010, doi: 10.2118/133033-MS.

[17] M. F. Fakoya and S. N. Shah, "Emergence of nanotechnology in the oil and gas industry: Emphasis on the application of silica nanoparticles," *Petroleum*, vol. 3, no. 4, pp.

391–405, Dec. 2017, doi: 10.1016/j.petlm.2017.03.001.
[18] M. Khalil, B. M. Jan, C. W. Tong, and M. A. Berawi, “Advanced nanomaterials in oil and gas industry: Design, application and challenges,” *Appl. Energy*, vol. 191, pp. 287–310, Apr. 2017, doi: 10.1016/j.apenergy.2017.01.074.
[19] S. S.-H. Gillani *et al.*, “Improving the mechanical performance of cement composites by carbon nanotubes addition,” *Procedia Struct. Integr.*, vol. 3, pp. 11–17, Jan. 2017, doi: 10.1016/j.prostr.2017.04.003.
[20] M. Carmichael and P. Arulraj, “Influence of nano materials on consistency, setting time and compressive strength of cement mortar,” *IRACST-Eng Sci Technol Int J ESTIJ*, vol. 2, pp. 158–162, Jan. 2012.
[21] C. Vipulanandan and A. Mohammed, “Smart cement modified with iron oxide nanoparticles to enhance the piezoresistive behavior and compressive strength for oil well applications,” *Smart Mater. Struct.*, vol. 24, no. 12, p. 125020, Nov. 2015, doi: 10.1088/0964-1726/24/12/125020.
[22] S. Lv, J. Liu, T. Sun, Y. Ma, and Q. Zhou, “Effect of GO nanosheets on shapes of cement hydration crystals and their formation process,” *Constr. Build. Mater.*, vol. 64, pp. 231–239, Aug. 2014, doi: 10.1016/j.conbuildmat.2014.04.061.
[23] G. Gurumurthy *et al.*, “Effect of Multiwalled Carbon Nanotubes and Nano Aluminum Oxide On Flexural and Compressive Strength of Cement Composites,” *Int. J. Adv. Res. Sci. Eng.*, vol. 3, no. 8, pp. 215–223, 2014.
[24] T. Nochaiya, Y. Sekine, S. Choopun, and A. Chaipanich, “Microstructure, characterizations, functionality and compressive strength of cement-based materials using zinc oxide nanoparticles as an additive,” *J. Alloys Compd.*, vol. 630, pp. 1–10, May 2015, doi: 10.1016/j.jallcom.2014.11.043.
[25] N. A. Ogolo, O. A. Olafuyi, and M. O. Onyekonwu, “Enhanced Oil Recovery Using Nanoparticles,” presented at the SPE Saudi Arabia Section Technical Symposium and Exhibition, Jan. 2012, doi: 10.2118/160847-MS.
[26] B. Moradi, P. Pourafshary, F. J. Farahani, M. Mohammadi, and M. A. Emadi, “Application of SiO_2 Nano Particles to Improve the Performance of Water Alternating Gas EOR Process,” presented at the SPE Oil & Gas India Conference and Exhibition, Nov. 2015, doi: 10.2118/178040-MS.
[27] D. Kumar, S. S. Chishti, A. Rai, and S. D. Patwardhan, “Scale Inhibition Using nano-silica Particles,” presented at the SPE Middle East Health, Safety, Security, and Environment Conference and Exhibition, Jan. 2012, doi: 10.2118/149321-MS.
[28] N. M. Taha and S. Lee, “Nano Graphene Application Improving Drilling Fluids Performance,” presented at the International Petroleum Technology Conference, Dec. 2015, doi: 10.2523/IPTC-18539-MS.
[29] K. Parekh, S. Jauhari, and R. V. Upadhyay, “Mechanism of acid corrosion inhibition using magnetic nanofluid,” *Adv. Nat. Sci. Nanosci. Nanotechnol.*, vol. 7, no. 4, p. 045007, Oct. 2016, doi: 10.1088/2043-6262/7/4/045007.
[30] “LUDOX® TM-50 colloidal silica 420778,” *Silica preparation*. https://www.sigmaaldrich.com/catalog/product/aldrich/420778 (accessed Mar. 17, 2020).
[31] “MWCNTs (>95%, OD: 20-30 nm).” https://www.us-nano.com/inc/sdetail/228 (accessed Mar. 17, 2020).

[32] “Titanium Oxide (TiO2) Nanopowder / Nanoparticles Dispersion (TiO2 Nanoparticles Aqueous Dispersion, Anatase, 15 wt%, 5-15 nm).” https://www.us-nano.com/inc/sdetail/630 (accessed Mar. 17, 2020).
[33] “Aluminum Oxide Al2O3 Nanopowder / Nanoparticles (Al2O3, 100% alpha, 99+%, 80nm).” https://www.us-nano.com/inc/sdetail/208 (accessed Mar. 17, 2020).
[34] “Zinc Oxide ZnO Nanoparticles / ZnO Nanopowder (ZnO, High Purity 99.95%, 18nm).” https://www.us-nano.com/inc/sdetail/7712 (accessed Mar. 17, 2020).
[35] F. H. Z. Fridriksson, “An improved cement slurry formulation for oil and geothermal wells,” Jun. 2017, Accessed: Mar. 17, 2020. [Online]. Available: https://uis.brage.unit.no/uis-xmlui/handle/11250/2462337.
[36] X. Colom, F. Carrillo, and J. Cañavate, “Composites reinforced with reused tyres: Surface oxidant treatment to improve the interfacial compatibility,” *Compos. Part Appl. Sci. Manuf.*, vol. 38, no. 1, pp. 44–50, Jan. 2007, doi: 10.1016/j.compositesa.2006.01.022.
[37] W. C. Lyons and G. J. P. BS, *Standard Handbook of Petroleum and Natural Gas Engineering*. Elsevier, 2011.
[38] P. Horsrud, “Estimating Mechanical Properties of Shale From Empirical Correlations,” *SPE Drill. Complet.*, vol. 16, no. 02, pp. 68–73, Jun. 2001, doi: 10.2118/56017-PA.
[39] G. Mavko, T. Mukerji, and J. Dvorkin, *The Rock Physics Handbook*. Cambridge University Press, 2020.
[40] D. R. Askeland, “Mechanical Testing and Properties,” in *The Science and Engineering of Materials: Solutions Manual*, D. R. Askeland, Ed. Dordrecht: Springer Netherlands, 1991, pp. 63–80.
[41] “kompressibilitet,” *Store norske leksikon*. Mar. 09, 2020, Accessed: Mar. 17, 2020. [Online]. Available: http://snl.no/kompressibilitet.
[42] H. Ormestad, “elastisitet – fysikk,” *Store norske leksikon*. Mar. 02, 2018, Accessed: Mar. 17, 2020. [Online]. Available: http://snl.no/elastisitet_-_fysikk.
[43] “IUPAC - modulus of elasticity (M03966).” https://goldbook.iupac.org/terms/view/M03966 (accessed Apr. 20, 2020).
[44] F. C. Campbell, *Elements of Metallurgy and Engineering Alloys*. ASM International, 2008.
[45] R. T. Index, “Portland Cement, Concrete, and Heat of Hydration,” 1997.
[46] H. A. Barnes, J. F. Hutton, and K. Walters, *An Introduction to Rheology*. Elsevier, 1989.
[47] M. Viloria Ochoa, *Analysis of drilling fluid rheology and tool joint effect to reduce errors in hydraulics calculations*. Texas A&M University, 2006.
[48] N. Cunningham, “What is Yield Stress and Why does it Matter?,” p. 3.
[49] S. Aarnes, “A comprehensive experimental investigation of MWCNTs in oil-well cementing and the development of a new empirical model for UCS estimation,” Jun. 2018, Accessed: Mar. 24, 2020. [Online]. Available: https://uis.brage.unit.no/uis-xmlui/handle/11250/2568579.
[50] Y. Hu, D. Luo, P. Li, Q. Li, and G. Sun, “Fracture toughness enhancement of cement paste with multi-walled carbon nanotubes,” *Constr. Build. Mater.*, vol. 70, pp. 332–338, Nov. 2014, doi: 10.1016/j.conbuildmat.2014.07.077.

[51] J. Sorathiya, S. Shah, and S. M. Kacha, “Effect on Addition of Nano ‘Titanium Dioxide’(TiO2) on Compressive Strength of Cementitious Concrete,” *Kalpa Publ. Civ. Eng.*, vol. 1, pp. 219–225, 2017.
[52] B. Ma, H. Li, J. Mei, X. Li, and F. Chen, “Effects of Nano-TiO2 on the Toughness and Durability of Cement-Based Material,” *Advances in Materials Science and Engineering*, 2015. https://www.hindawi.com/journals/amse/2015/583106/ (accessed Mar. 26, 2020).
[53] G. Land and D. Stephan, “Controlling cement hydration with nanoparticles,” *Cem. Concr. Compos.*, vol. 57, pp. 64–67, Mar. 2015, doi: 10.1016/j.cemconcomp.2014.12.003.

Appendix A – Force vs deformation for all cement samples

The peak point in the force vs deformation plots is what was used to calculate UCS for each sample. Each plug will have its own plot, categorized by which test batch it was in. **NOTE:** For test batch 9-17, Y-axis is load (kN) while X-axis is deformation (%)

Test batch no.1:

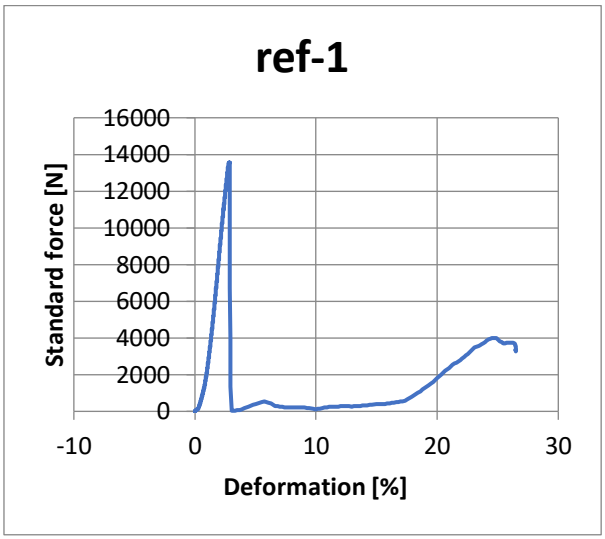

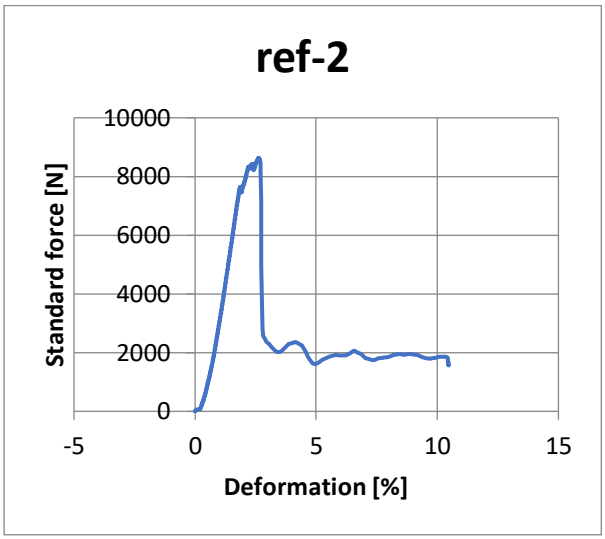

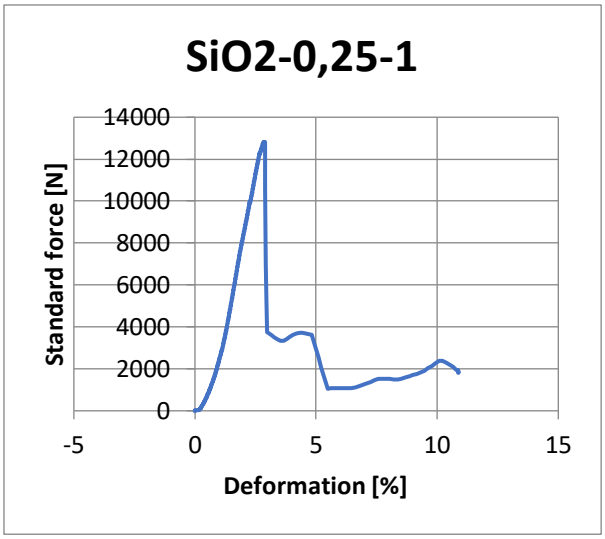
SiO2-0,25-1
Standard force [N]
14000
12000
10000
8000
6000
4000
2000
0
-5
0
5
10
15
Deformation [%]

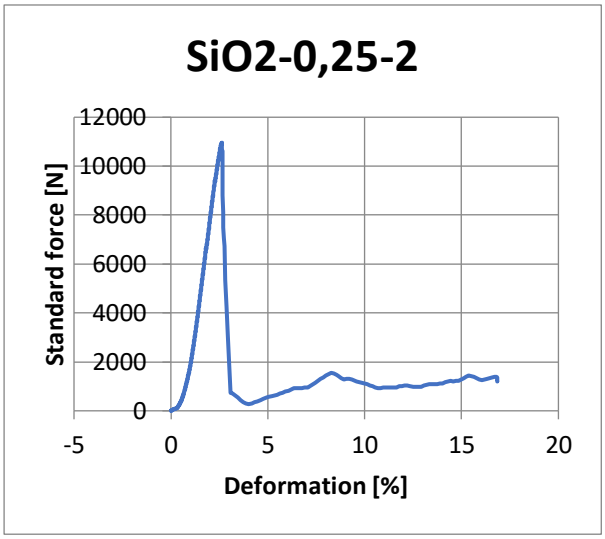
SiO2-0,25-2
Standard force [N]
12000
10000
8000
6000
4000
2000
0
-5
0
5
10
15
20
Deformation [%]

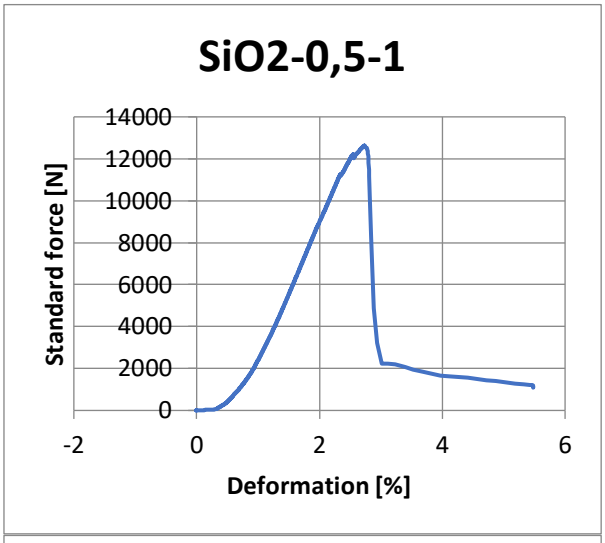
SiO2-0,5-1
Standard force [N]
14000
12000
10000
8000
6000
4000
2000
0
-2
0
2
4
6
Deformation [%]

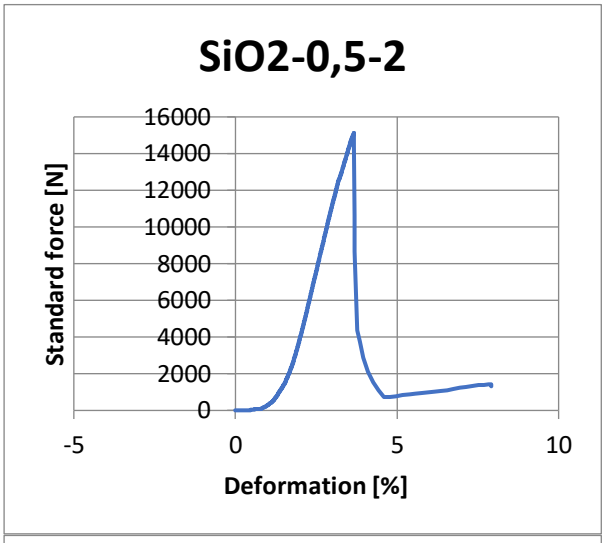
SiO2-0,5-2
Standard force [N]
16000
14000
12000
10000
8000
6000
4000
2000
0
-5
0
5
10
Deformation [%]

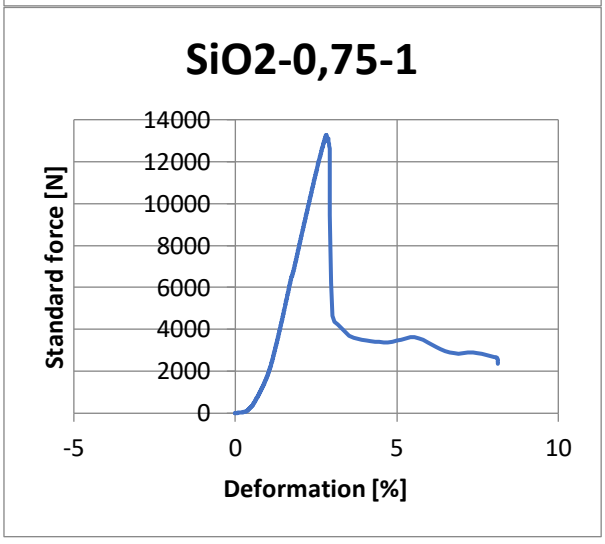
SiO2-0,75-1
Standard force [N]
14000
12000
10000
8000
6000
4000
2000
0
-5
0
5
10
Deformation [%]

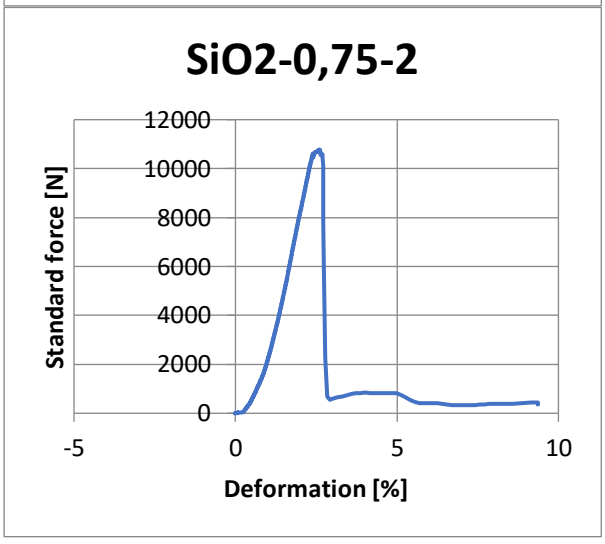
SiO2-0,75-2
Standard force [N]
12000
10000
8000
6000
4000
2000
0
-5
0
5
10
Deformation [%]

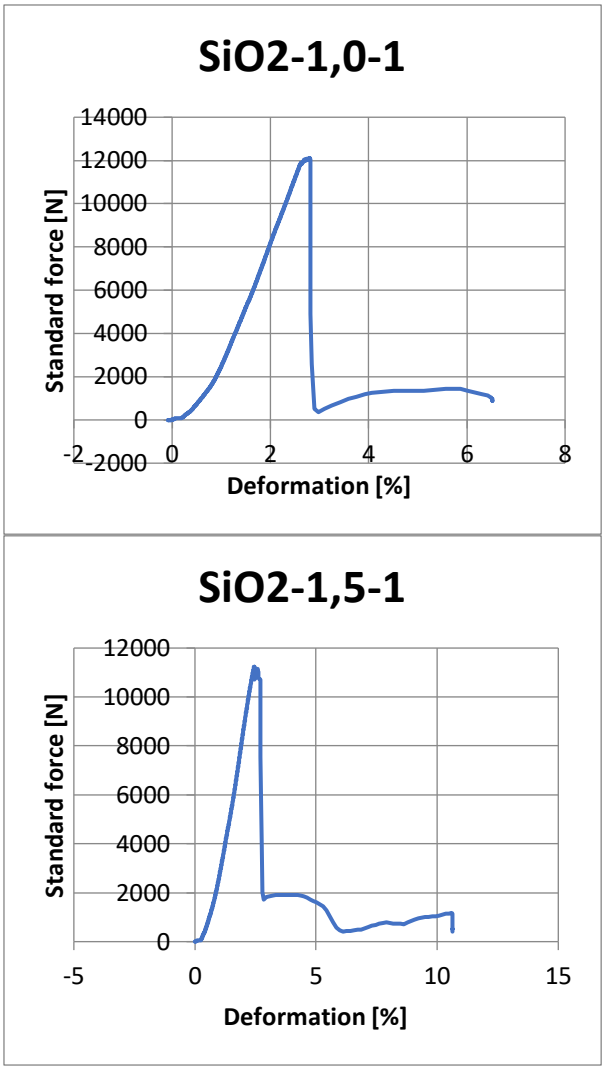

Test batch no. 2:

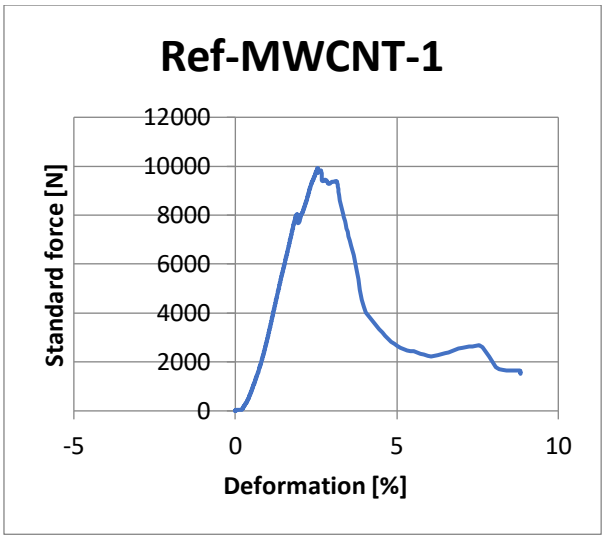

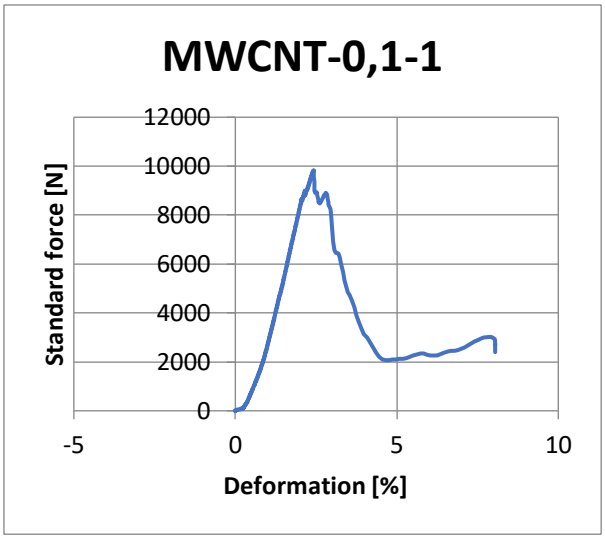

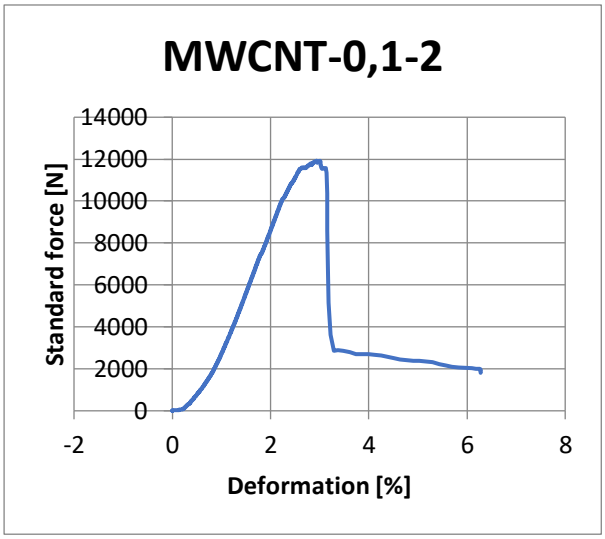

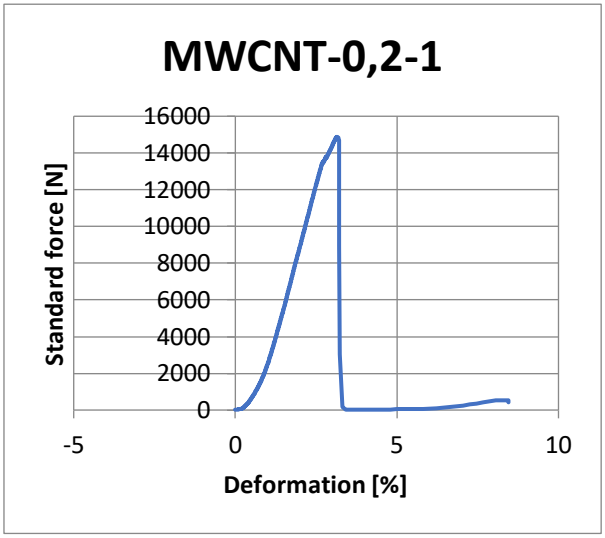

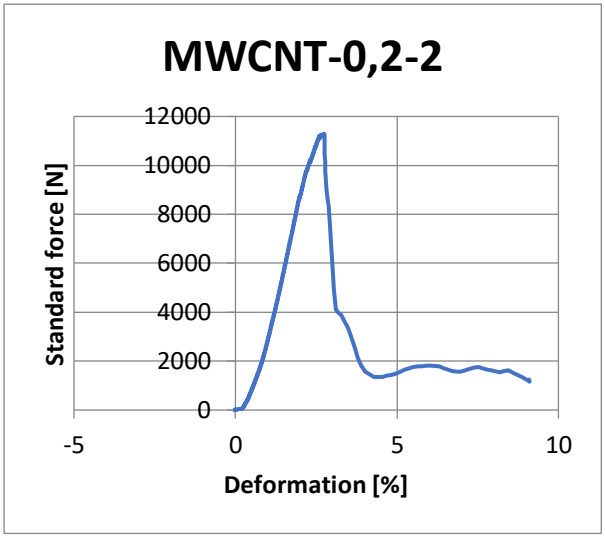

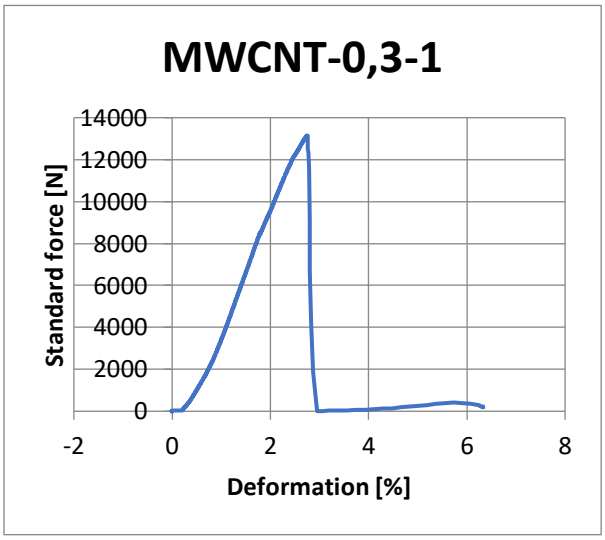

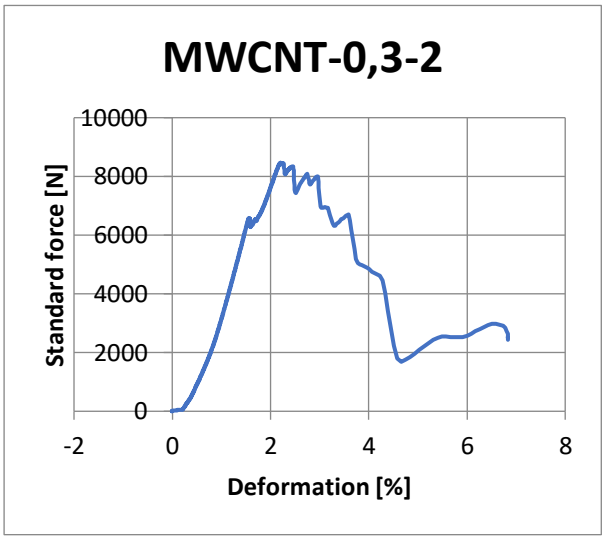

Test batch no. 3:

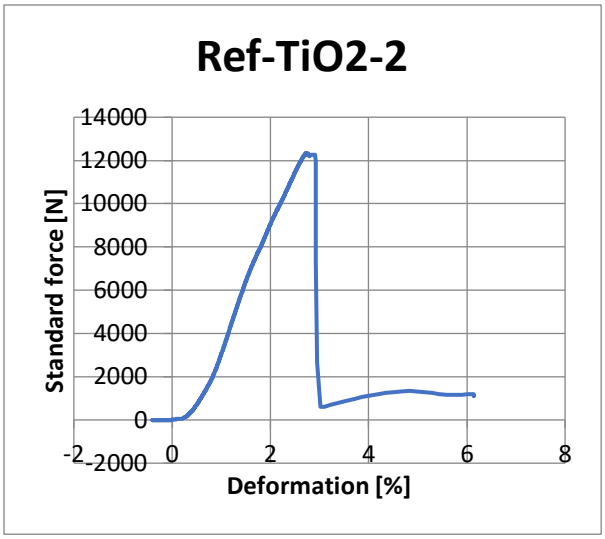
Ref-TiO2-2
Standard force [N]
14000
12000
10000
8000
6000
4000
2000
0
-2000
-2
0
2
4
6
8
Deformation [%]

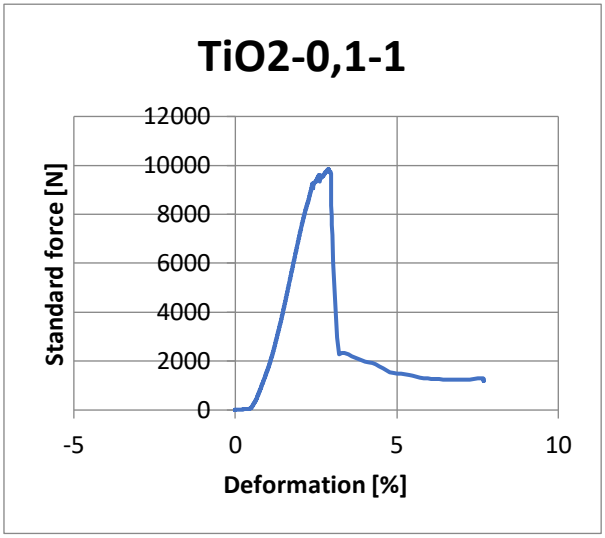
TiO2-0,1-1
Standard force [N]
12000
10000
8000
6000
4000
2000
0
-5
0
5
10
Deformation [%]

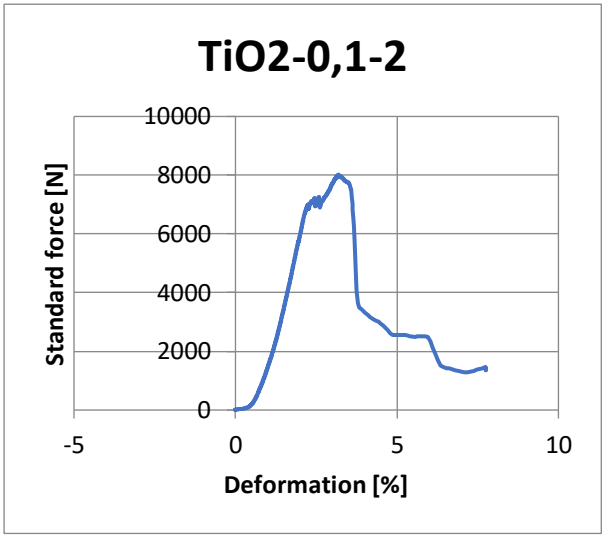
TiO2-0,1-2
Standard force [N]
10000
8000
6000
4000
2000
0
-5
0
5
10
Deformation [%]

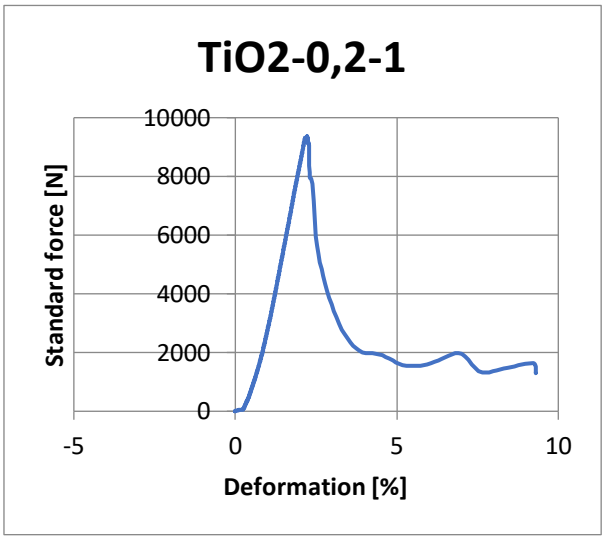
TiO2-0,2-1
Standard force [N]
10000
8000
6000
4000
2000
0
-5
0
5
10
Deformation [%]

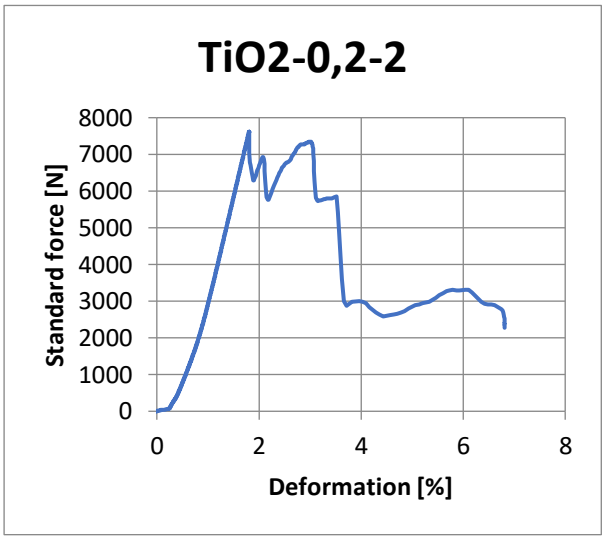
TiO2-0,2-2
Standard force [N]
8000
7000
6000
5000
4000
3000
2000
1000
0
0
2
4
6
8
Deformation [%]

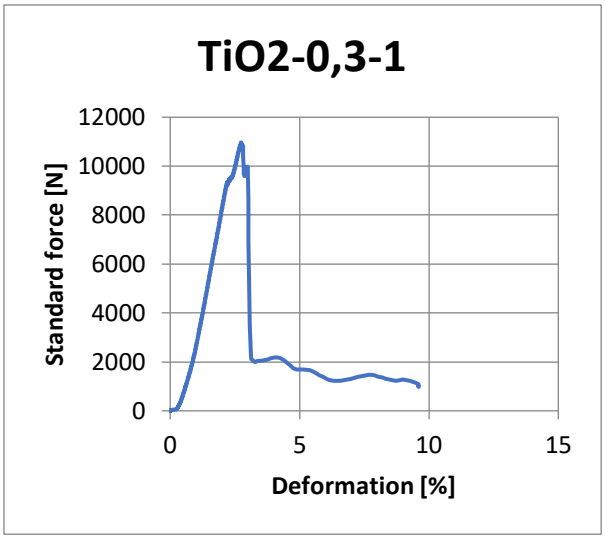

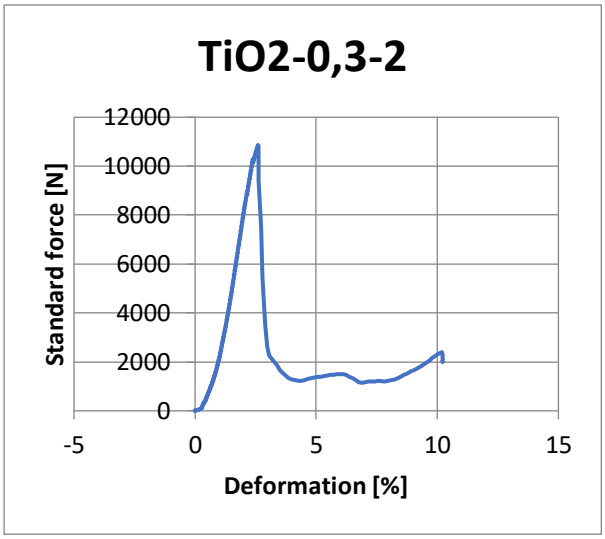

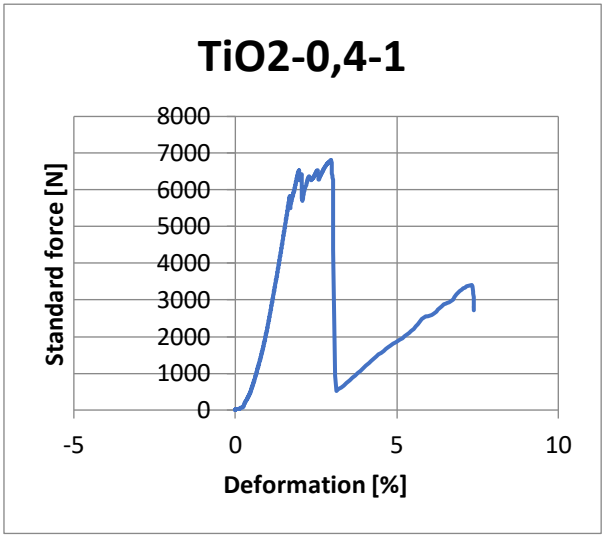

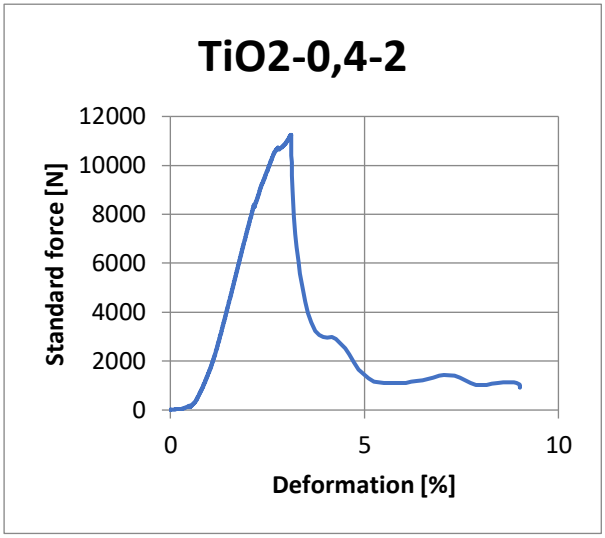

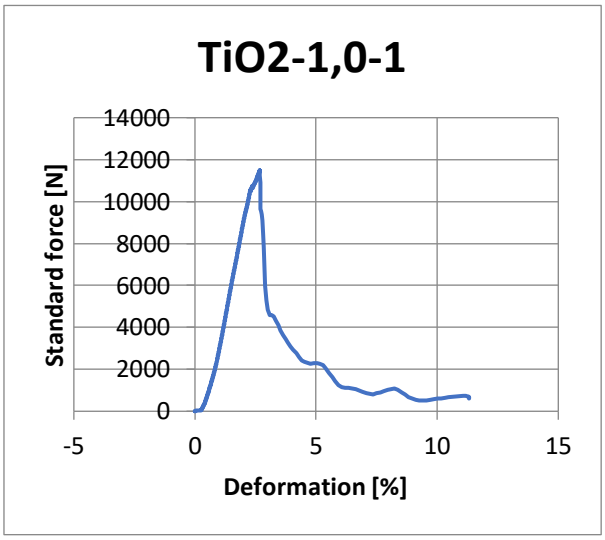

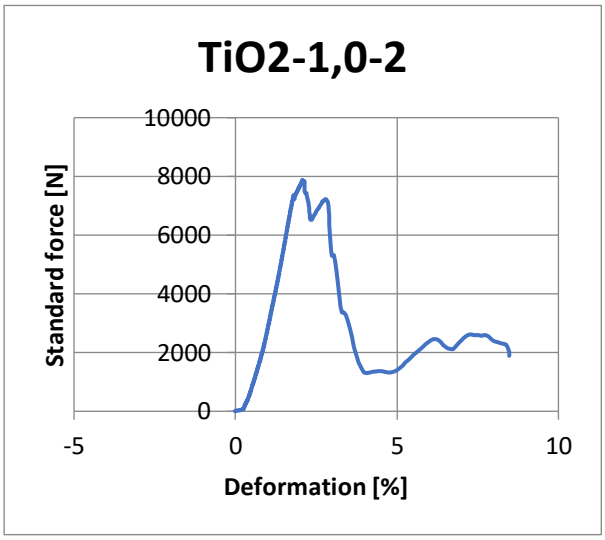

Test batch no.4:

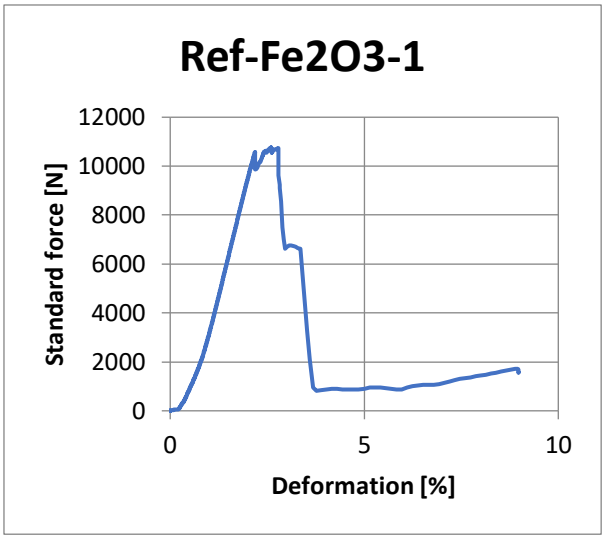
Ref-Fe2O3-1
Standard force [N]
12000
10000
8000
6000
4000
2000
0
0
5
10
Deformation [%]

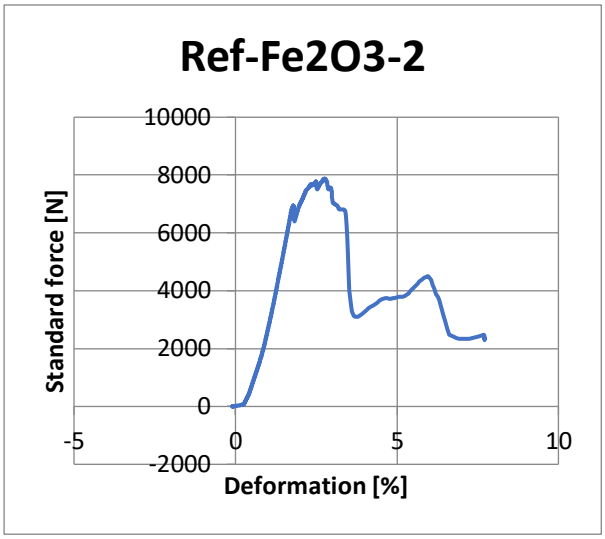
Ref-Fe2O3-2
Standard force [N]
10000
8000
6000
4000
2000
0
-2000
-5
0
5
10
Deformation [%]

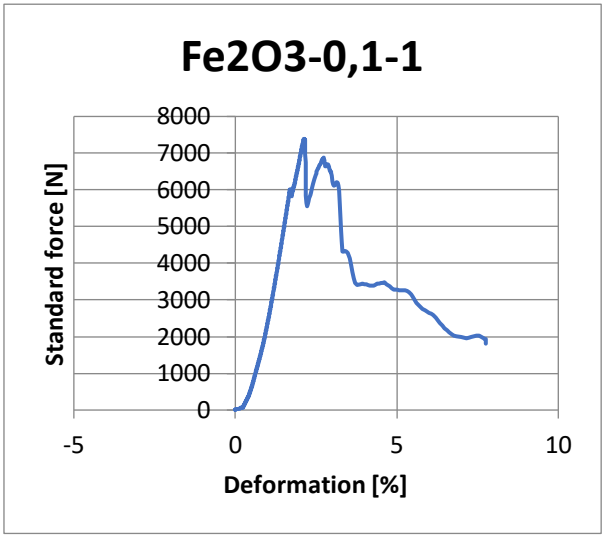
Fe2O3-0,1-1
Standard force [N]
8000
7000
6000
5000
4000
3000
2000
1000
0
-5
0
5
10
Deformation [%]

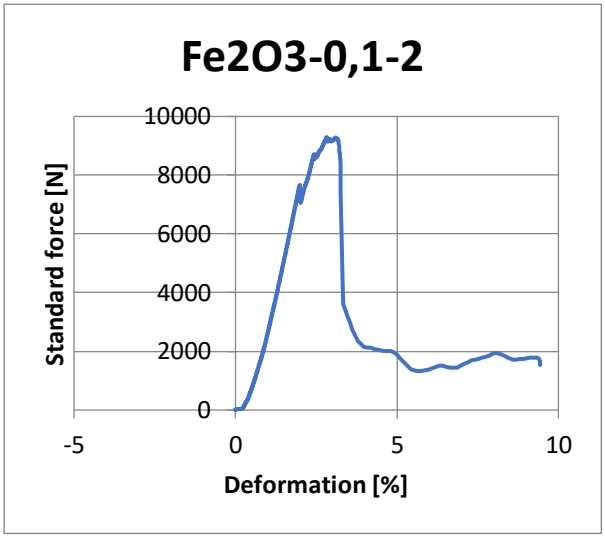
Fe2O3-0,1-2
Standard force [N]
10000
8000
6000
4000
2000
0
-5
0
5
10
Deformation [%]

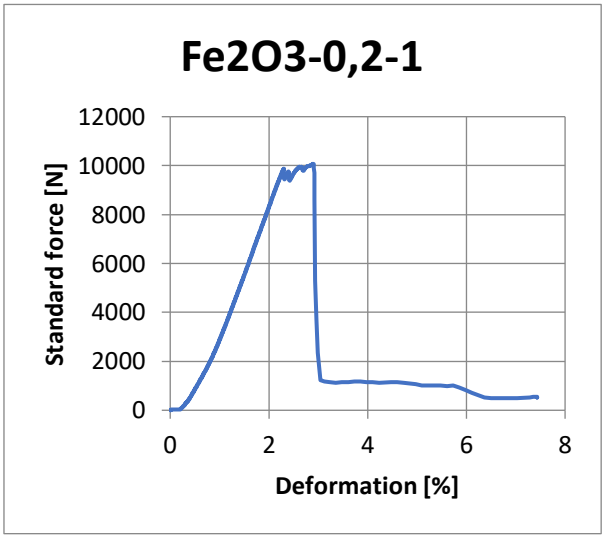
Fe2O3-0,2-1
Standard force [N]
12000
10000
8000
6000
4000
2000
0
0
2
4
6
8
Deformation [%]

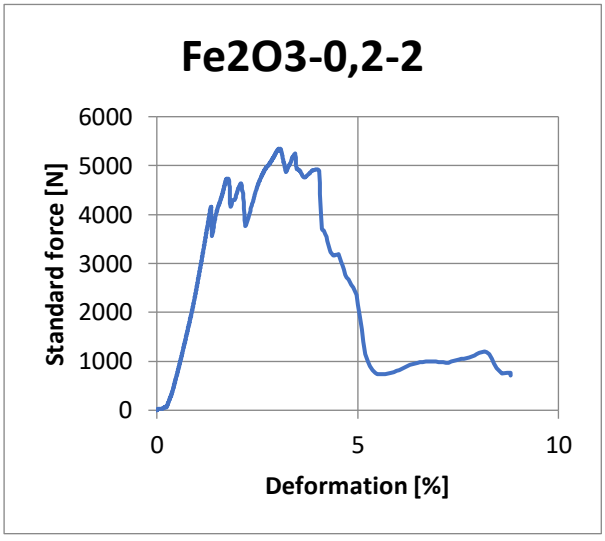
Fe2O3-0,2-2
Standard force [N]
6000
5000
4000
3000
2000
1000
0
0
5
10
Deformation [%]

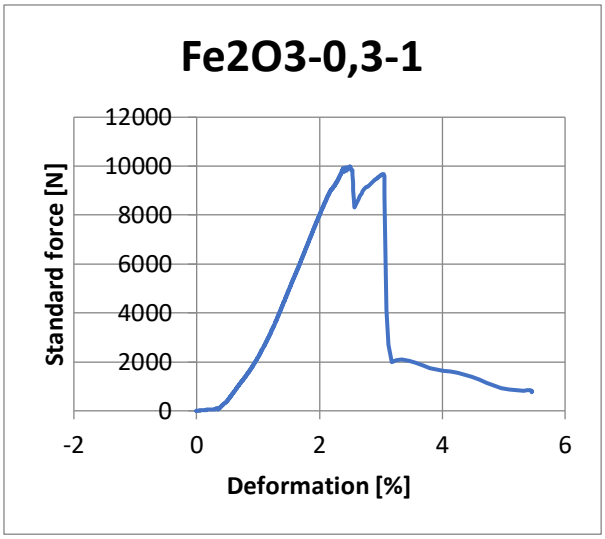

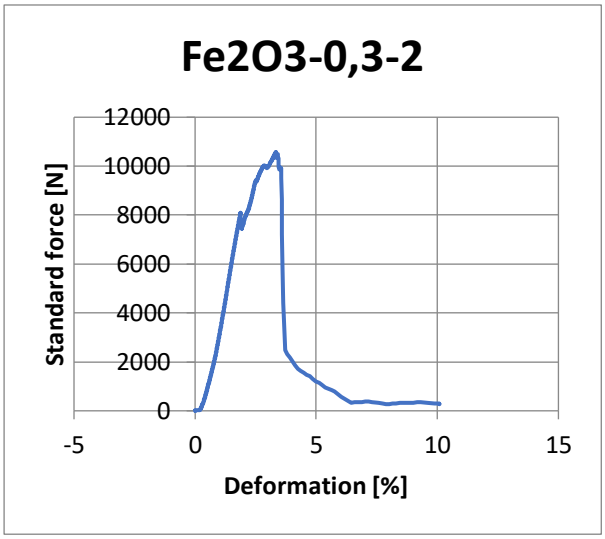

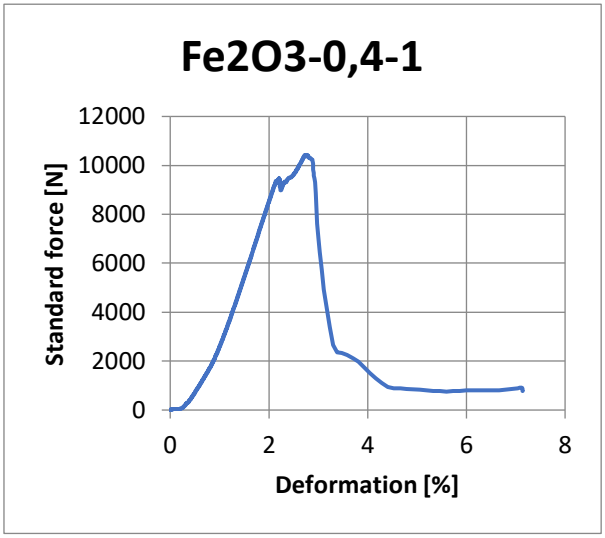

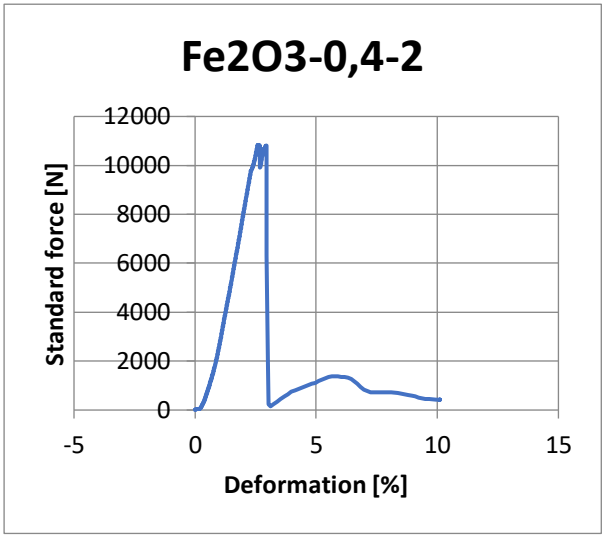

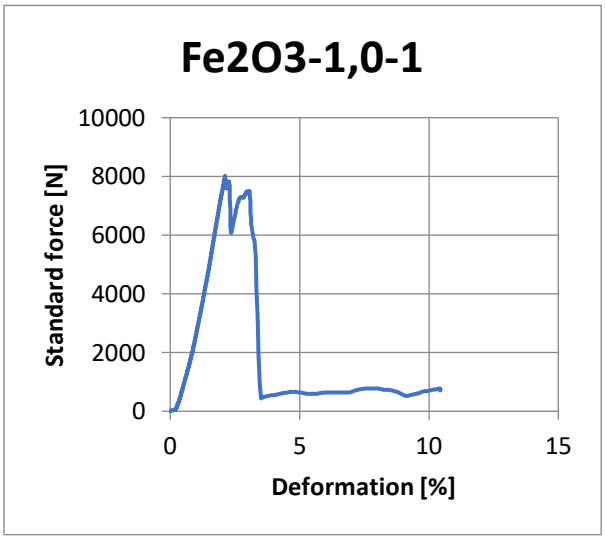

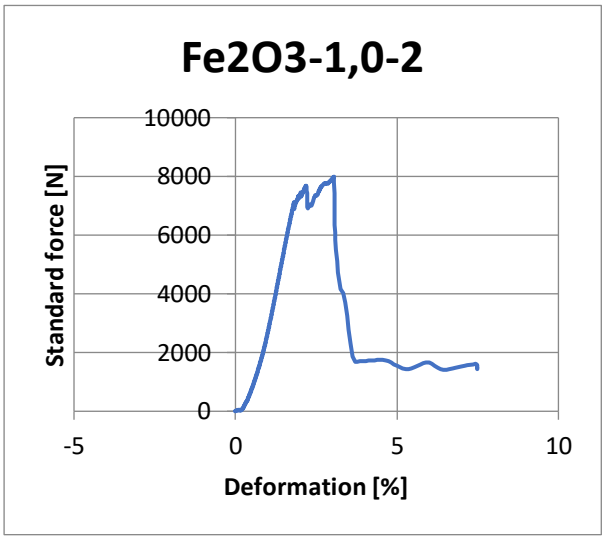

Test batch no. 5:

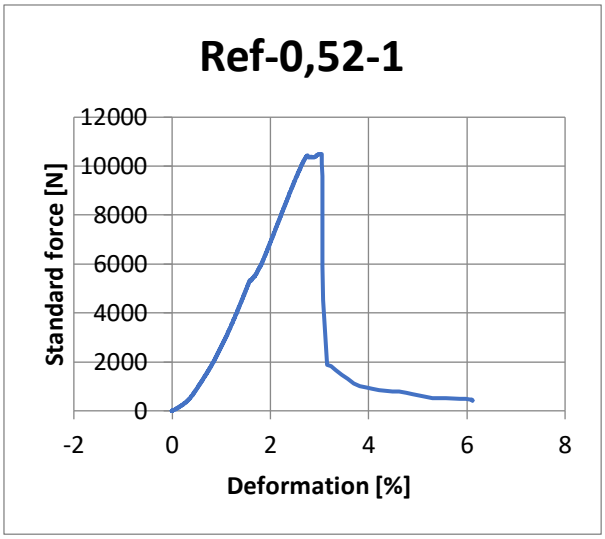
Ref-0,52-1
Standard force [N]
12000
10000
8000
6000
4000
2000
0
-2
0
2
4
6
8
Deformation [%]

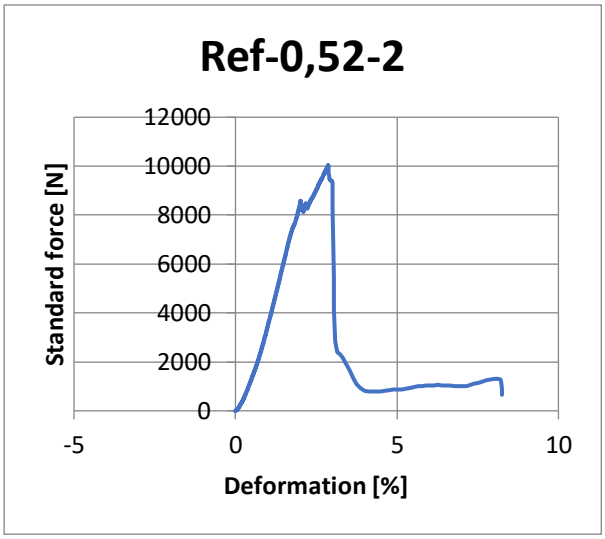
Ref-0,52-2
Standard force [N]
12000
10000
8000
6000
4000
2000
0
-5
0
5
10
Deformation [%]

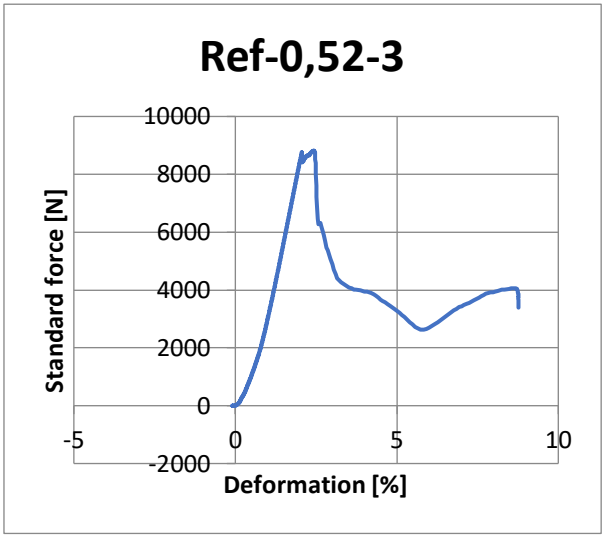
Ref-0,52-3
Standard force [N]
10000
8000
6000
4000
2000
0
-2000
-5
0
5
10
Deformation [%]

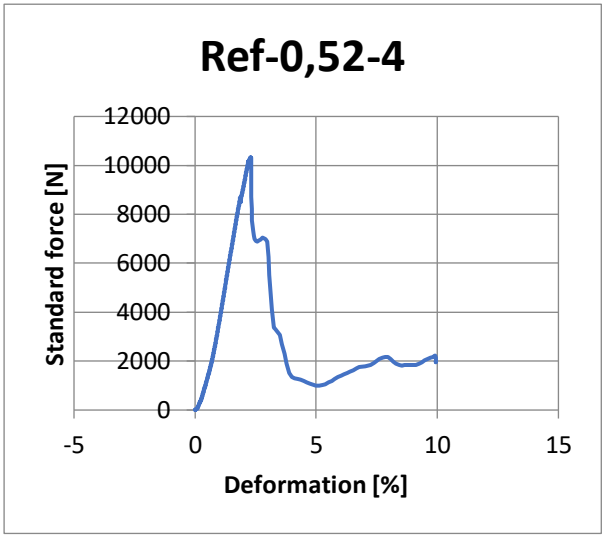
Ref-0,52-4
Standard force [N]
12000
10000
8000
6000
4000
2000
0
-5
0
5
10
15
Deformation [%]

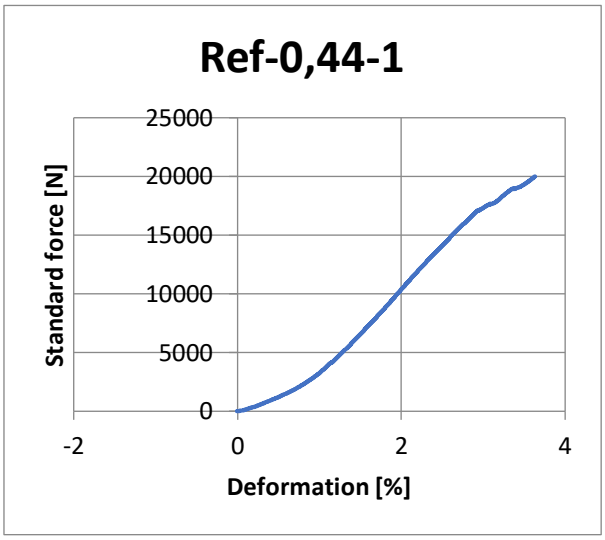
Ref-0,44-1
Standard force [N]
25000
20000
15000
10000
5000
0
-2
0
2
4
Deformation [%]

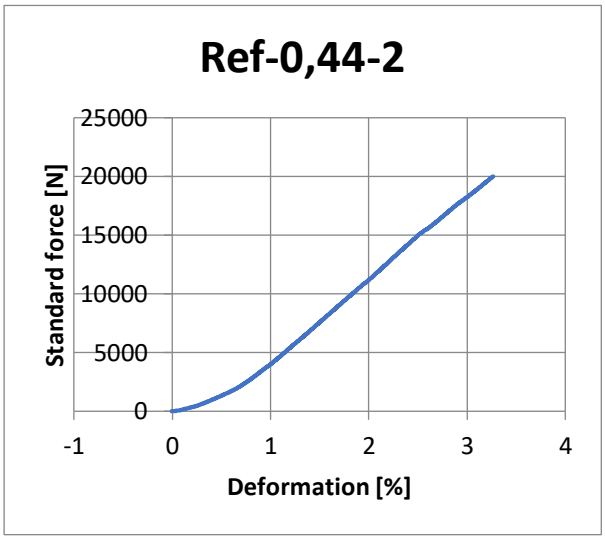
Ref-0,44-2
Standard force [N]
25000
20000
15000
10000
5000
0
-1
0
1
2
3
4
Deformation [%]

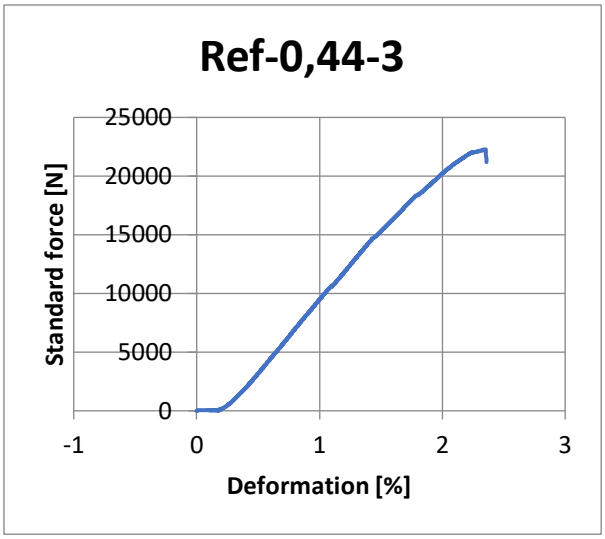

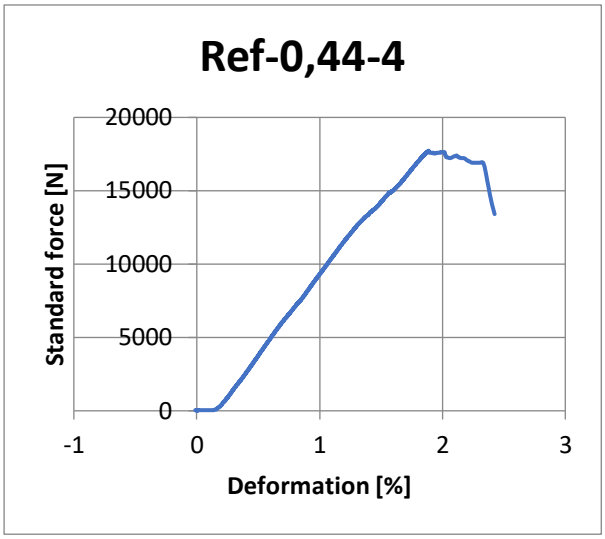

Test batch no. 6:

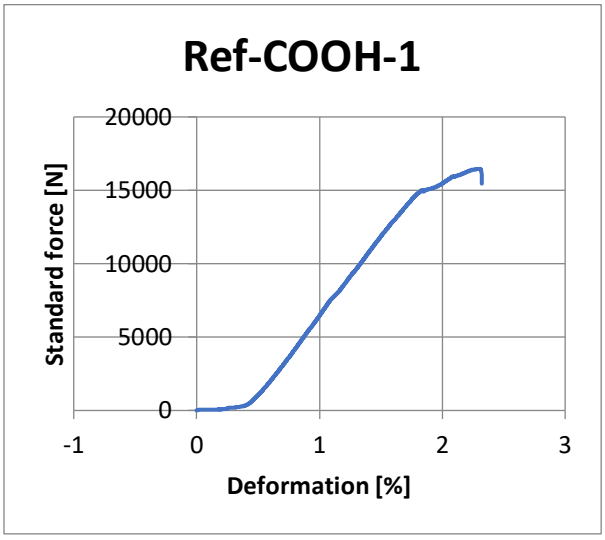

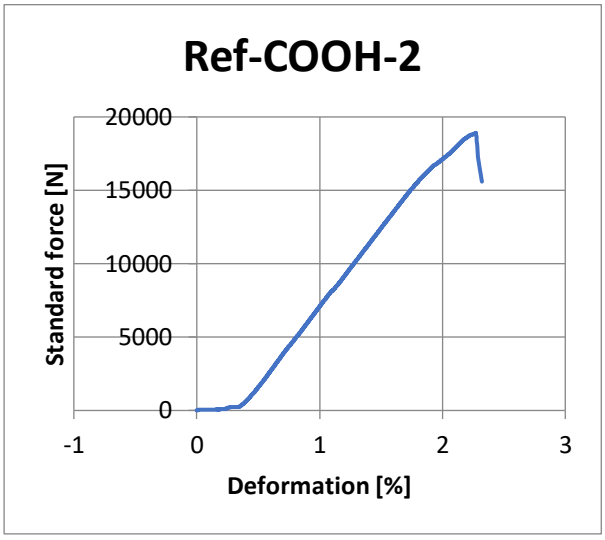

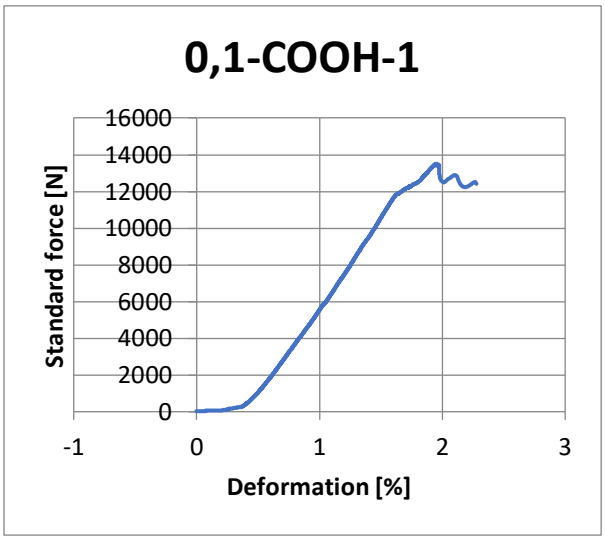

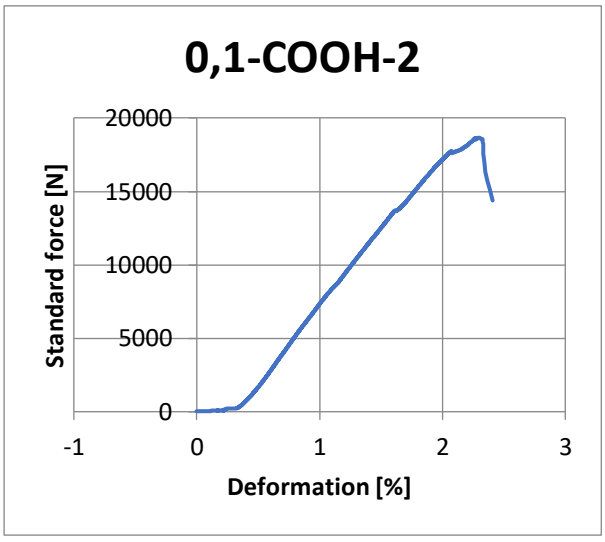

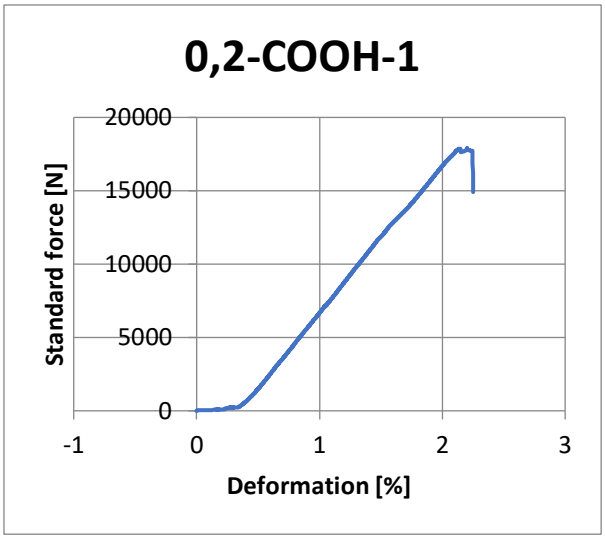
0,2-COOH-1
Standard force [N]
20000
15000
10000
5000
0
-1
0
1
2
3
Deformation [%]

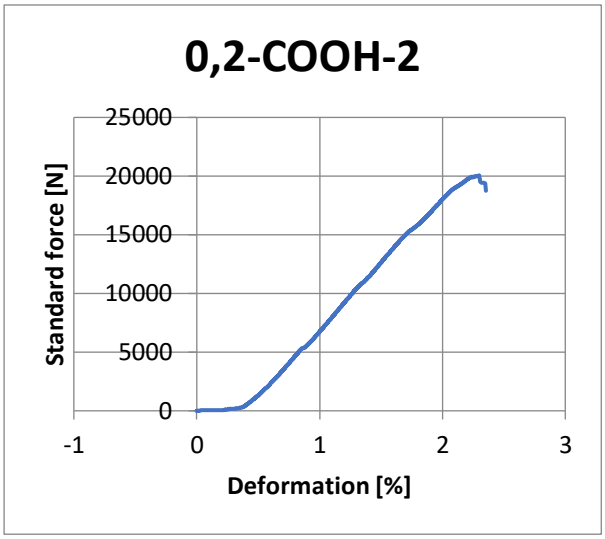
0,2-COOH-2
Standard force [N]
25000
20000
15000
10000
5000
0
-1
0
1
2
3
Deformation [%]

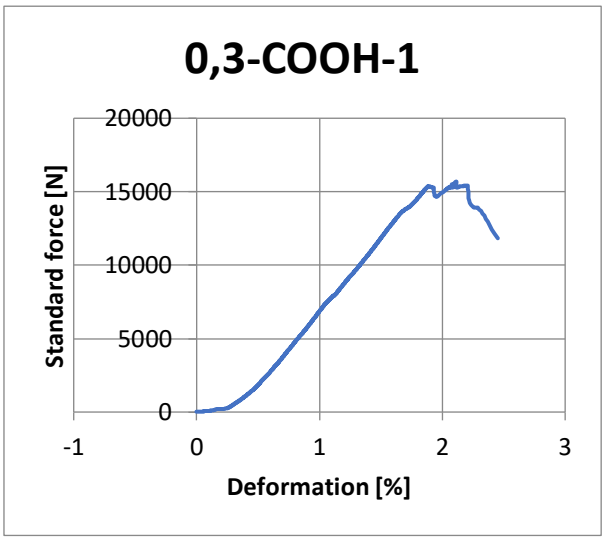
0,3-COOH-1
Standard force [N]
20000
15000
10000
5000
0
-1
0
1
2
3
Deformation [%]

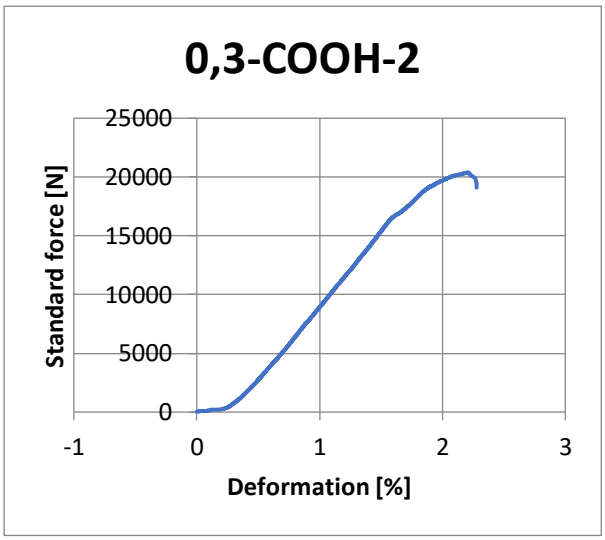
0,3-COOH-2
Standard force [N]
25000
20000
15000
10000
5000
0
-1
0
1
2
3
Deformation [%]

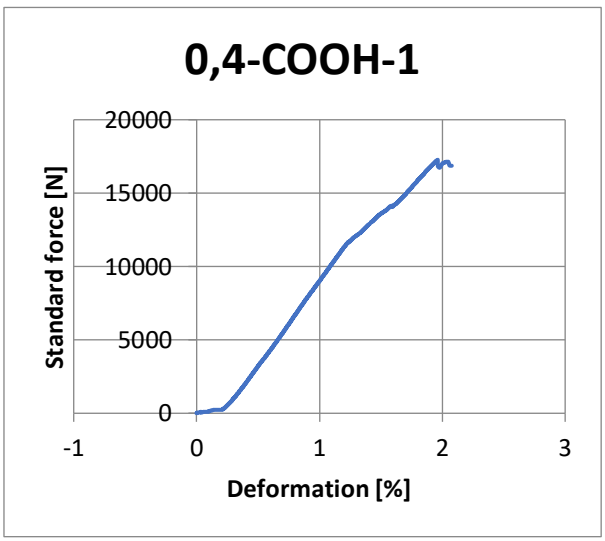
0,4-COOH-1
Standard force [N]
20000
15000
10000
5000
0
-1
0
1
2
3
Deformation [%]

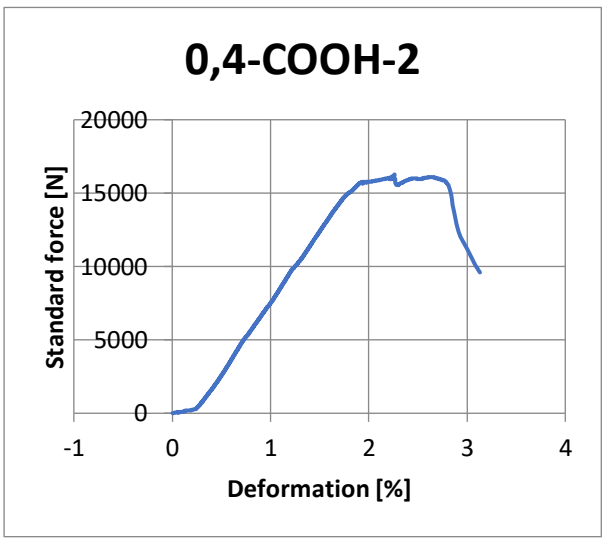
0,4-COOH-2
Standard force [N]
20000
15000
10000
5000
0
-1
0
1
2
3
4
Deformation [%]

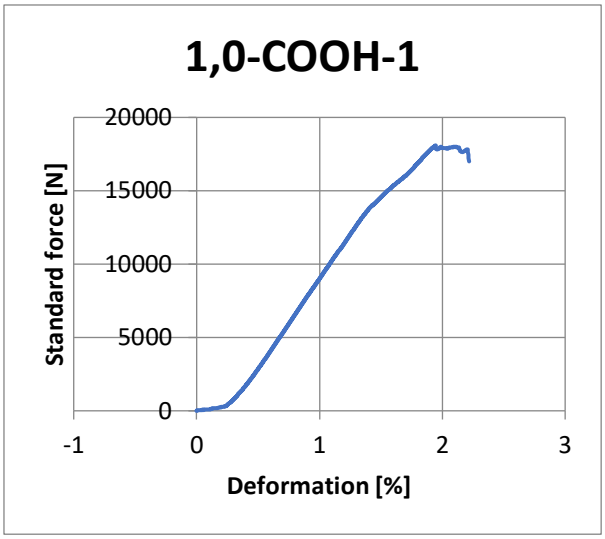

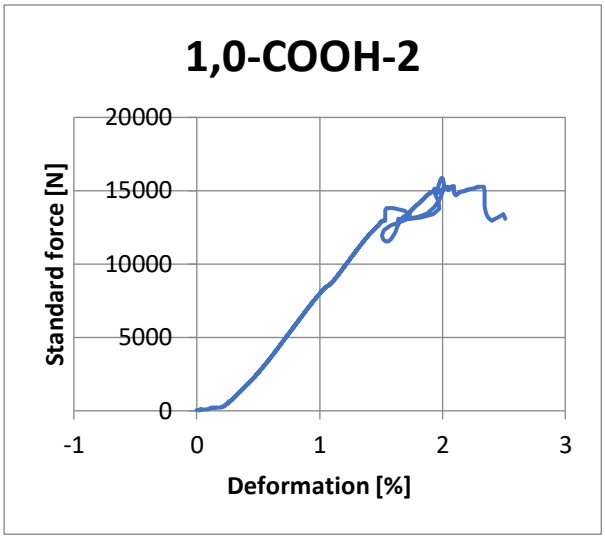

Test batch no. 7:

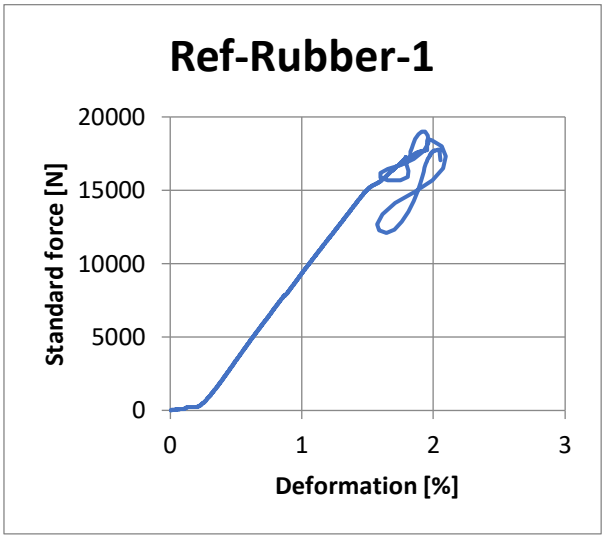

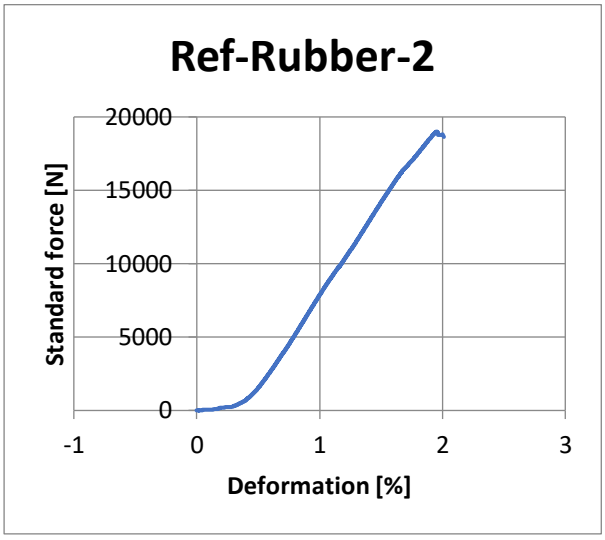

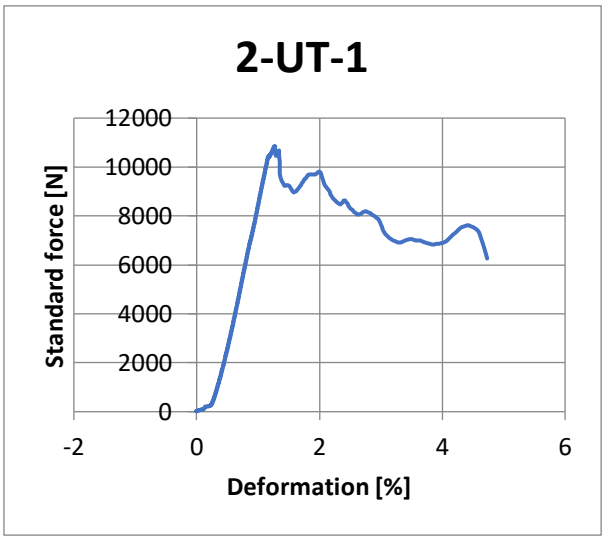

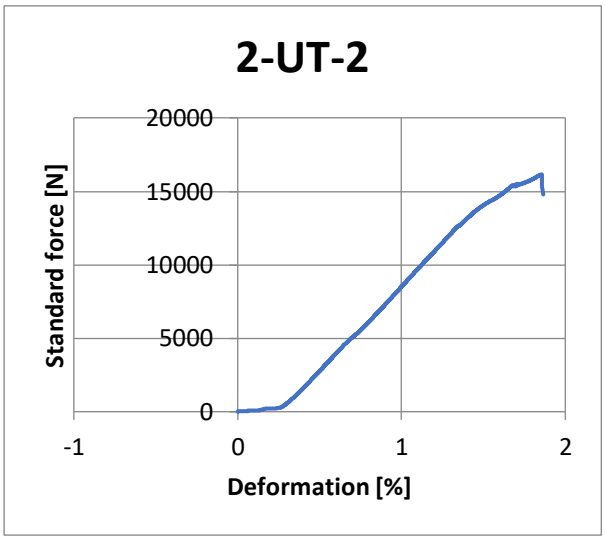

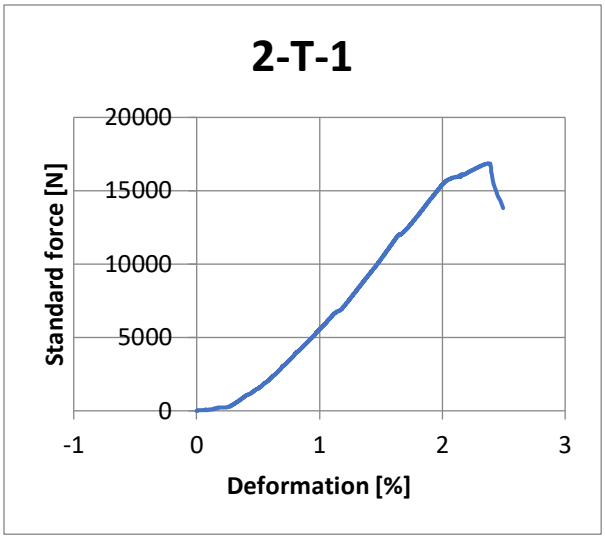
2-T-1
Standard force [N]
20000
15000
10000
5000
0
-1
0
1
2
3
Deformation [%]

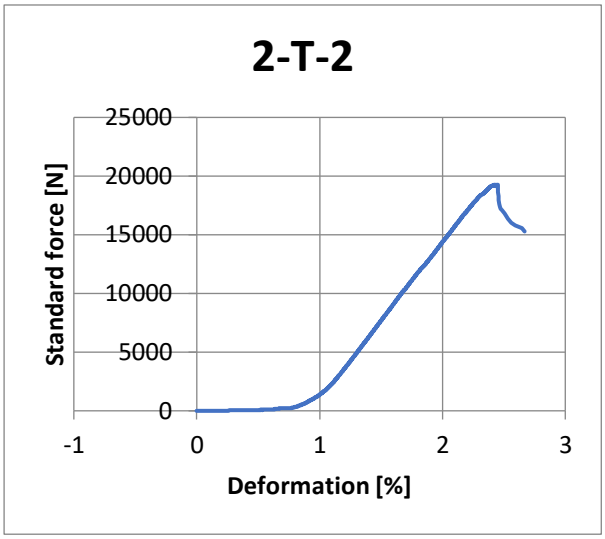
2-T-2
Standard force [N]
25000
20000
15000
10000
5000
0
-1
0
1
2
3
Deformation [%]

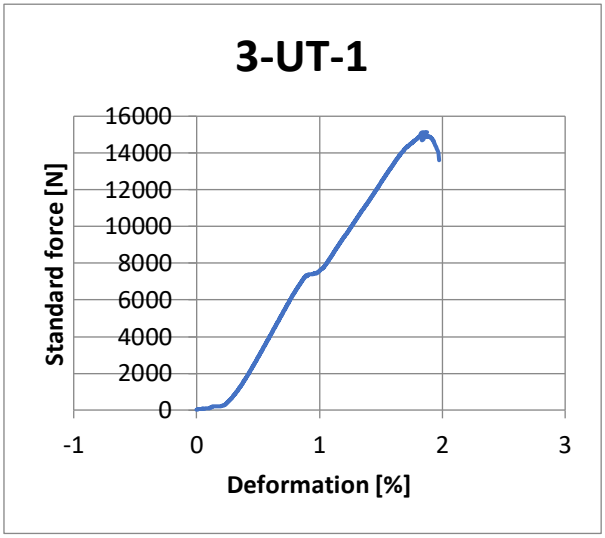
3-UT-1
Standard force [N]
16000
14000
12000
10000
8000
6000
4000
2000
0
-1
0
1
2
3
Deformation [%]

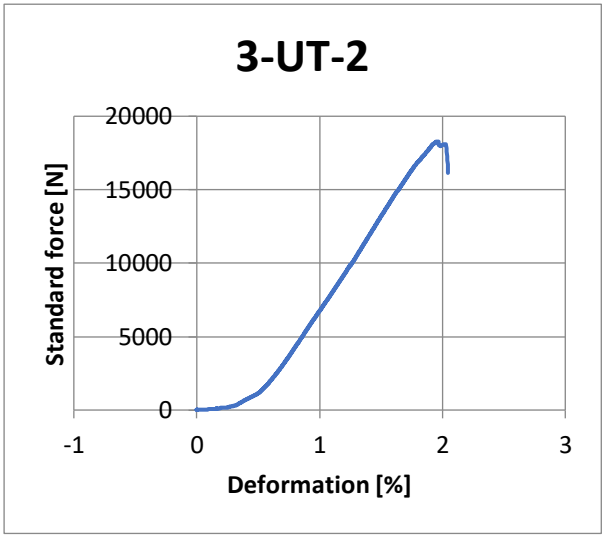
3-UT-2
Standard force [N]
20000
15000
10000
5000
0
-1
0
1
2
3
Deformation [%]

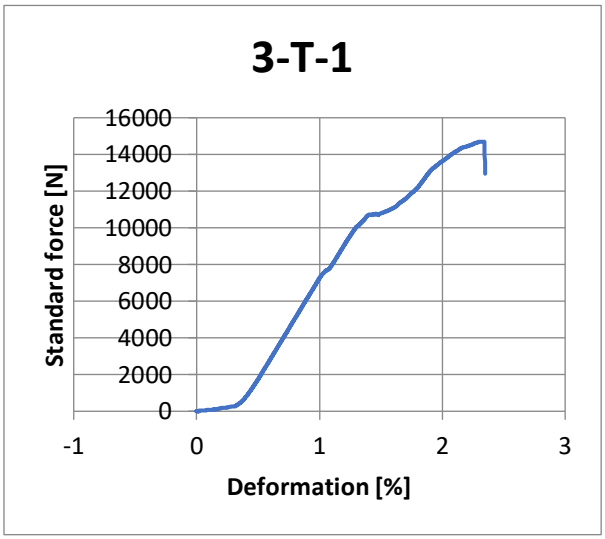
3-T-1
Standard force [N]
16000
14000
12000
10000
8000
6000
4000
2000
0
-1
0
1
2
3
Deformation [%]

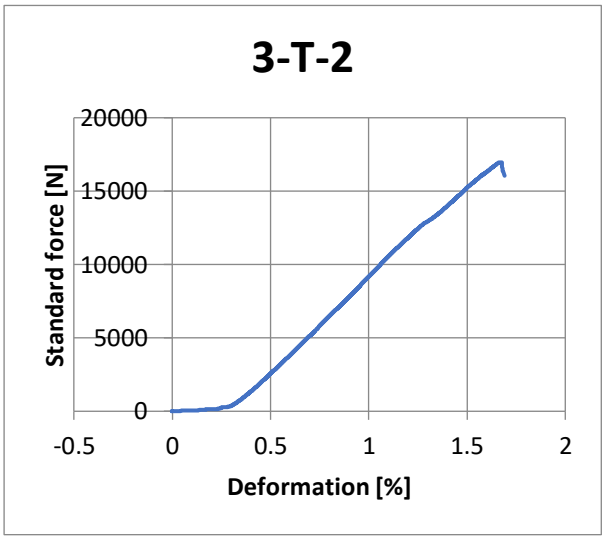
3-T-2
Standard force [N]
20000
15000
10000
5000
0
-0.5
0
0.5
1
1.5
2
Deformation [%]

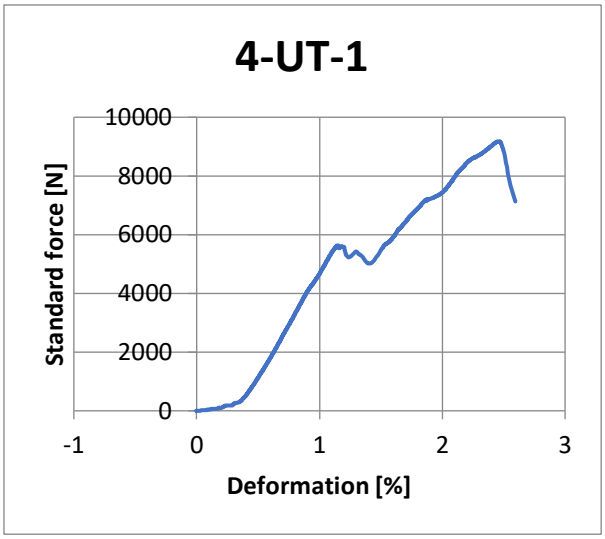

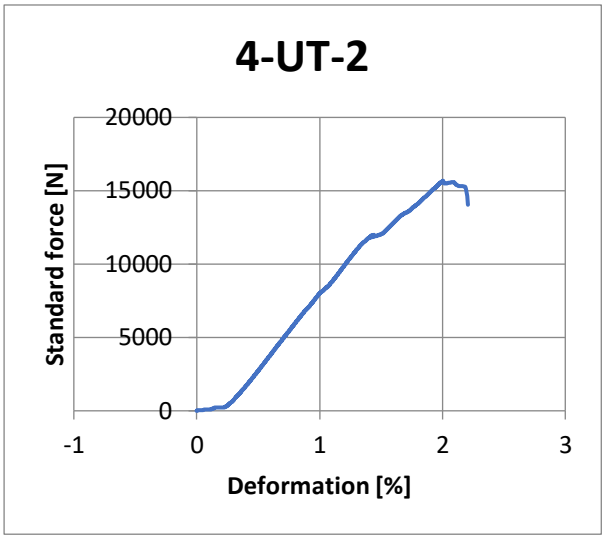

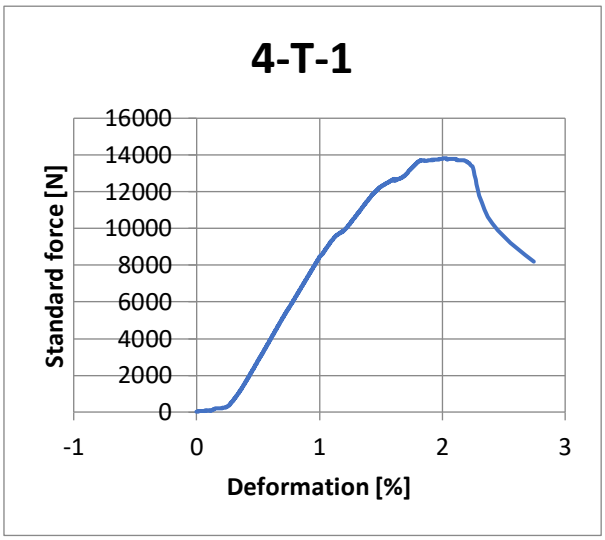

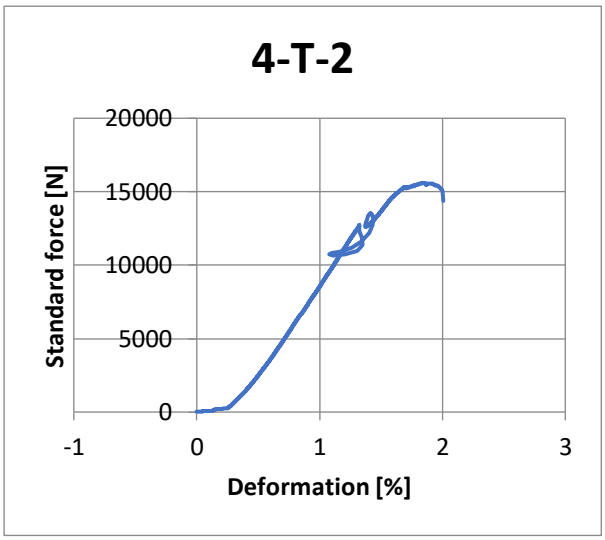

Test batch no. 8:

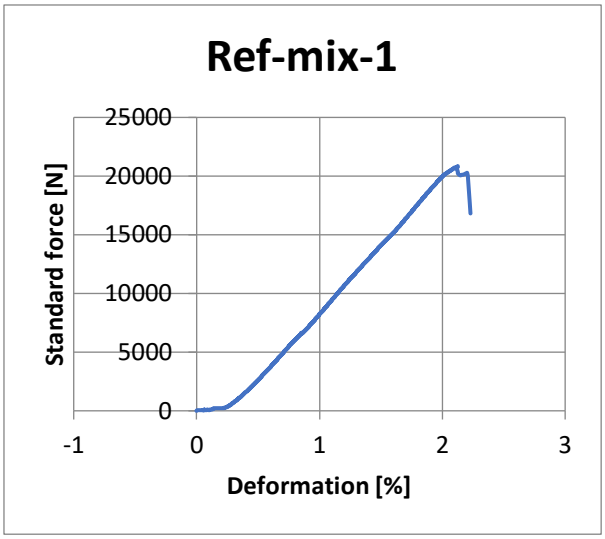
Ref-mix-1
Standard force [N]
25000
20000
15000
10000
5000
0
-1
0
1
2
3
Deformation [%]

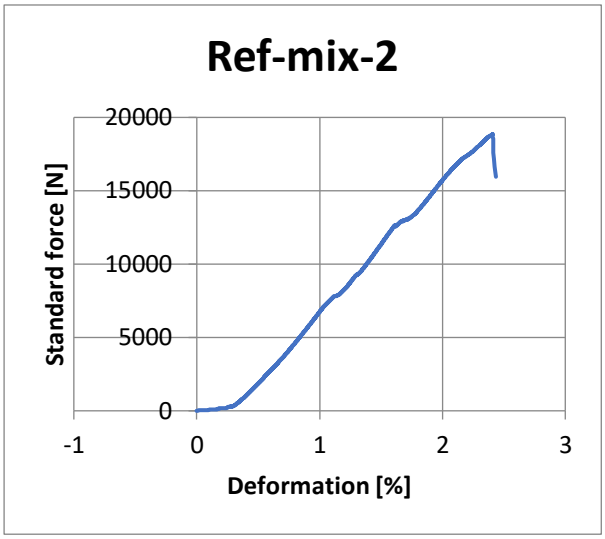
Ref-mix-2
Standard force [N]
20000
15000
10000
5000
0
-1
0
1
2
3
Deformation [%]

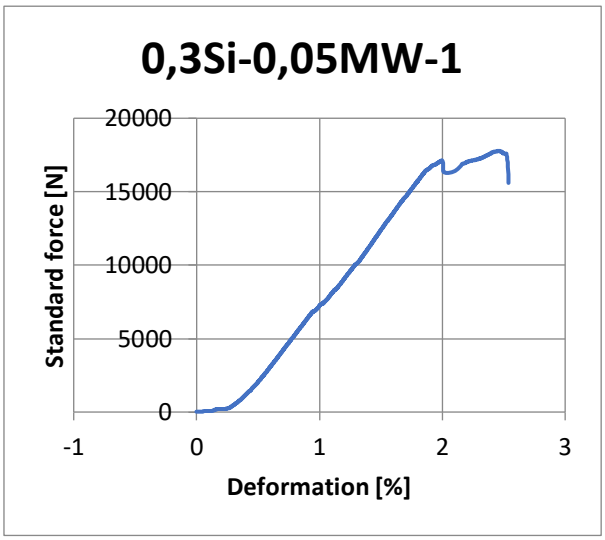
0,3Si-0,05MW-1
Standard force [N]
20000
15000
10000
5000
0
-1
0
1
2
3
Deformation [%]

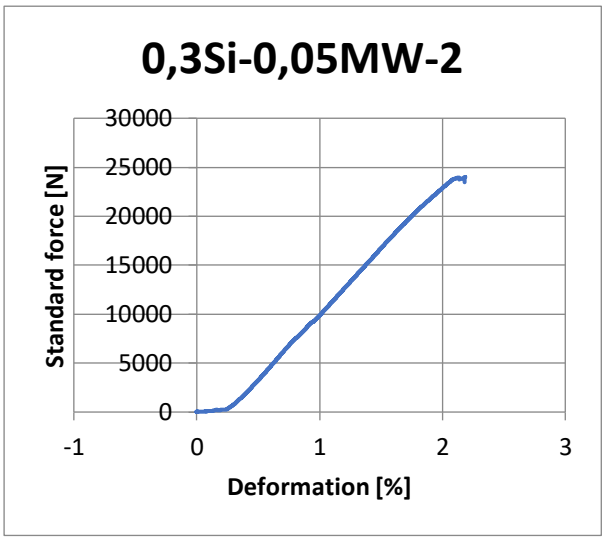
0,3Si-0,05MW-2
Standard force [N]
30000
25000
20000
15000
10000
5000
0
-1
0
1
2
3
Deformation [%]

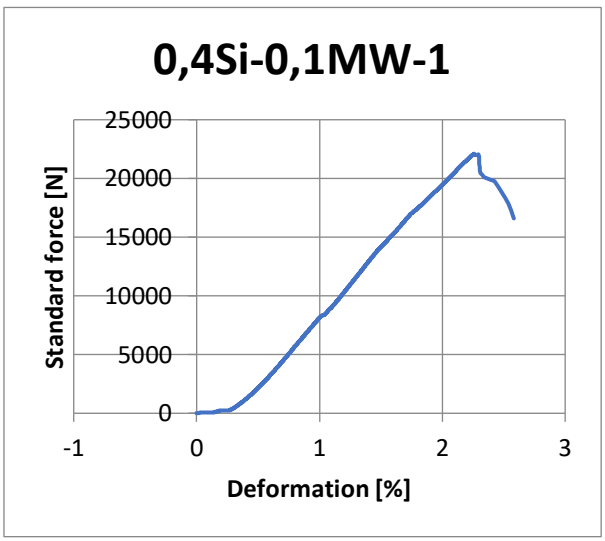
0,4Si-0,1MW-1
Standard force [N]
25000
20000
15000
10000
5000
0
-1
0
1
2
3
Deformation [%]

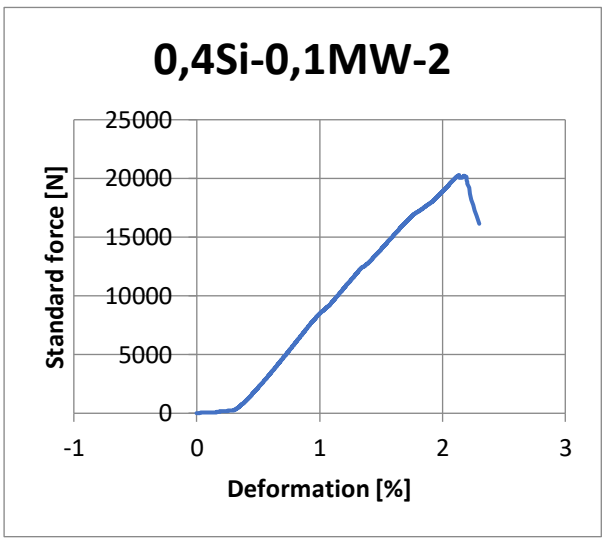
0,4Si-0,1MW-2
Standard force [N]
25000
20000
15000
10000
5000
0
-1
0
1
2
3
Deformation [%]

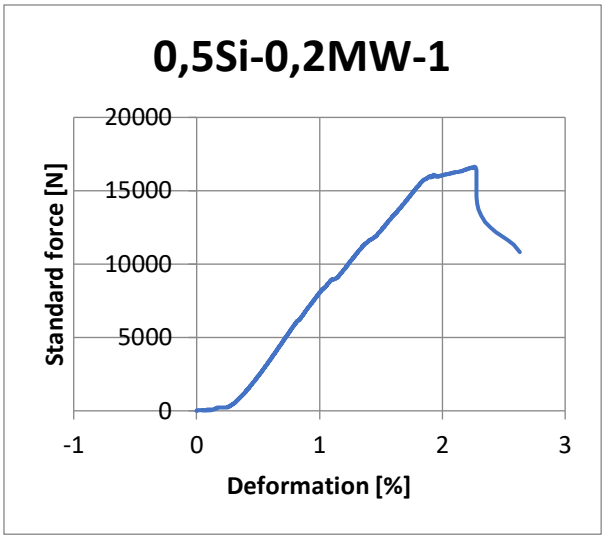

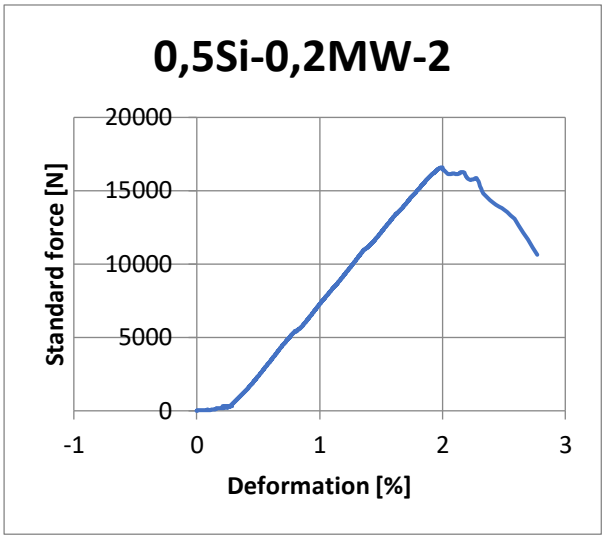

Test batch no. 9:

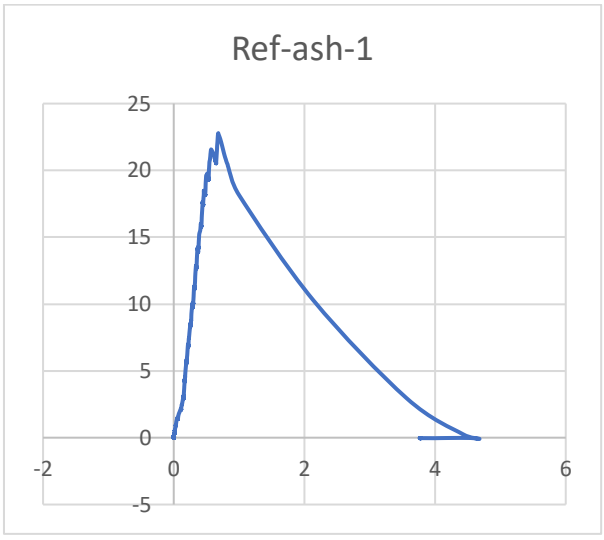

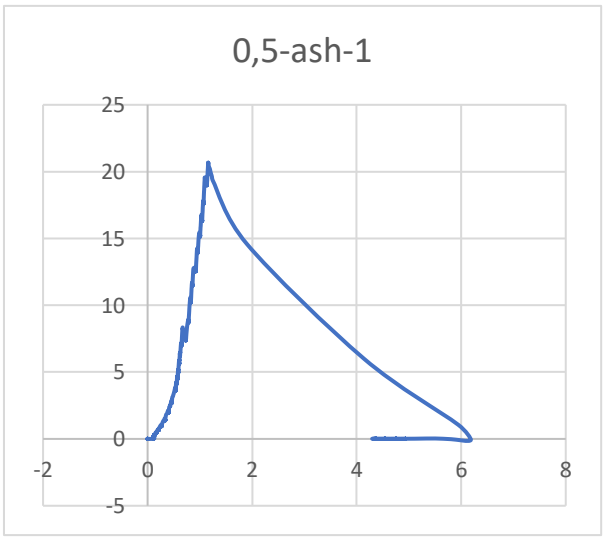

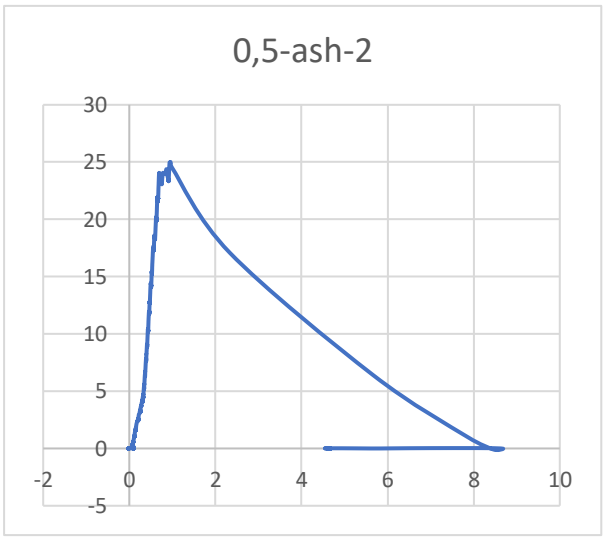

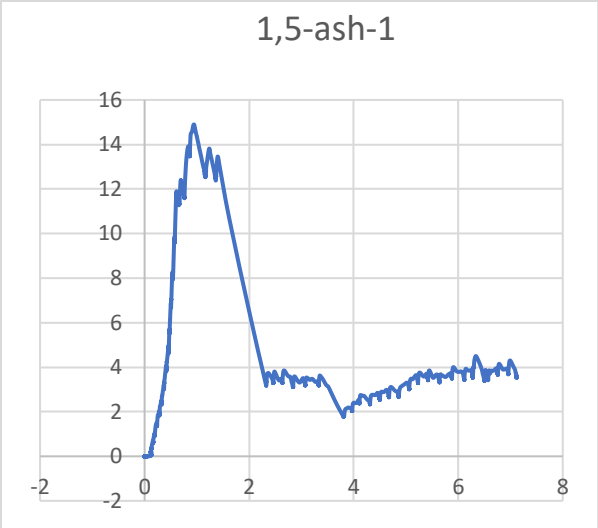

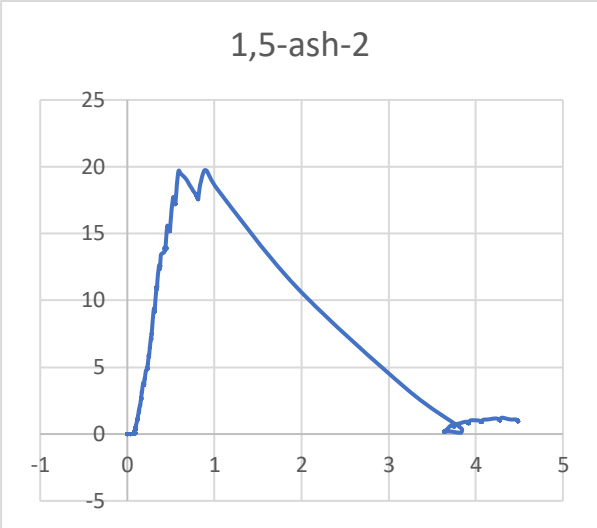

Test batch no. 10:

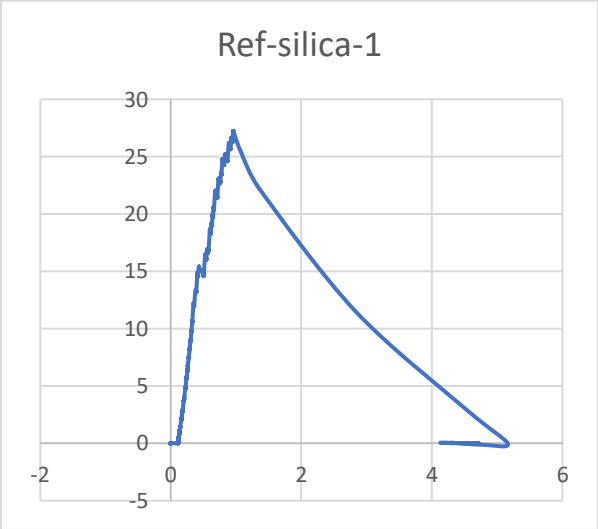

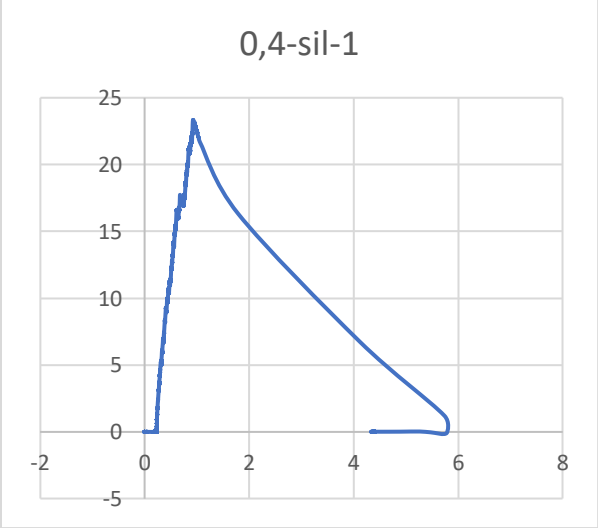

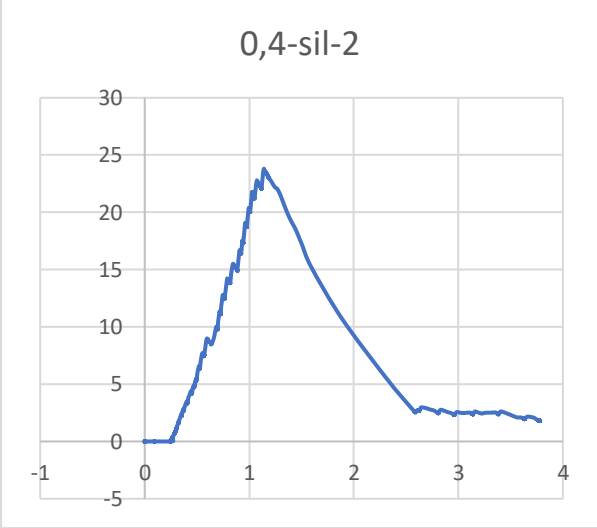

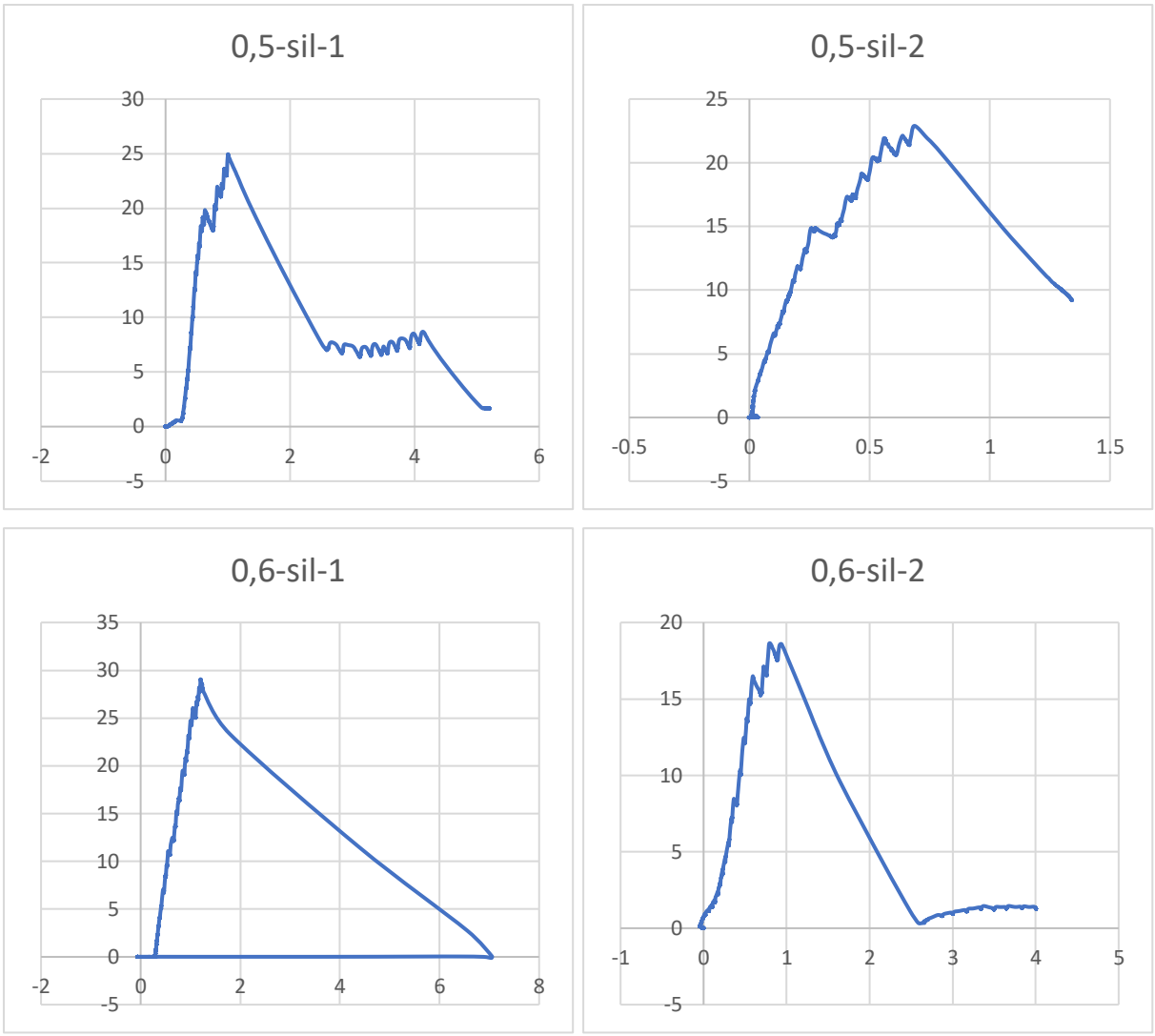

Test batch no. 11:

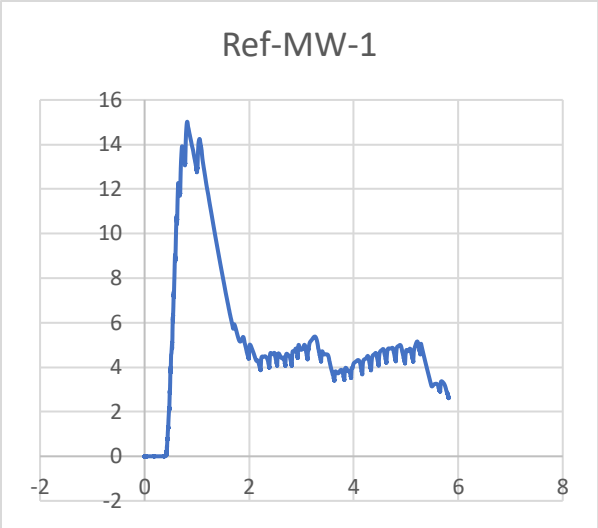
Ref-MW-1
16
14
12
10
8
6
4
2
0
-2
-2
0
2
4
6
8

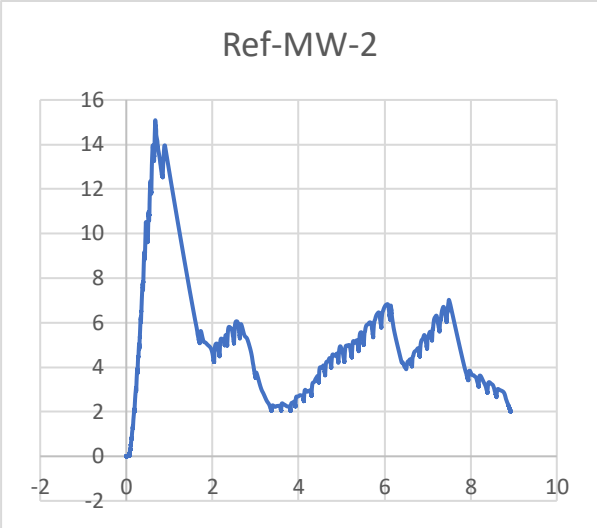
Ref-MW-2
16
14
12
10
8
6
4
2
0
-2
-2
0
2
4
6
8
10

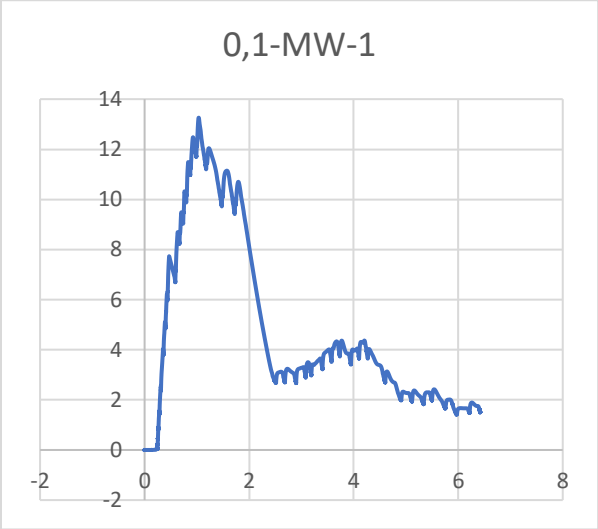
0,1-MW-1
14
12
10
8
6
4
2
0
-2
-2
0
2
4
6
8

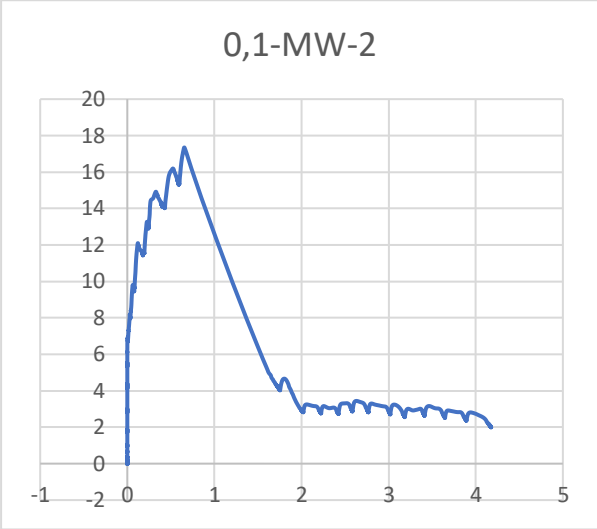
0,1-MW-2
20
18
16
14
12
10
8
6
4
2
0
-2
-1
0
1
2
3
4
5

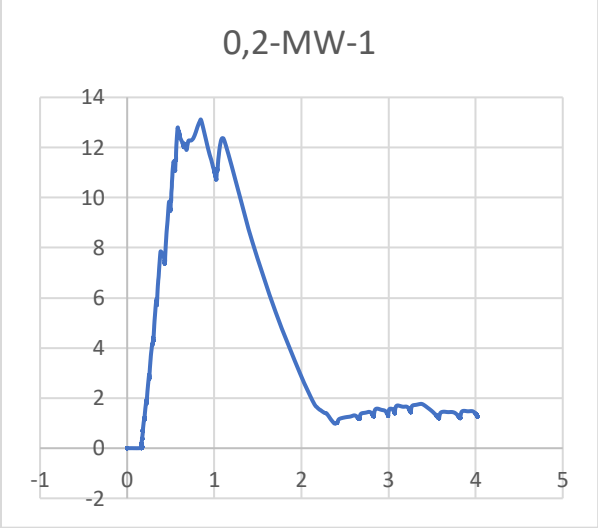
0,2-MW-1
14
12
10
8
6
4
2
0
-2
-1
0
1
2
3
4
5

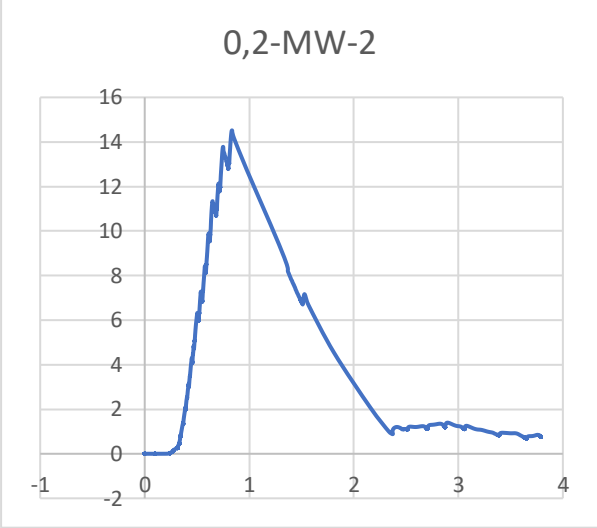
0,2-MW-2
16
14
12
10
8
6
4
2
0
-2
-1
0
1
2
3
4

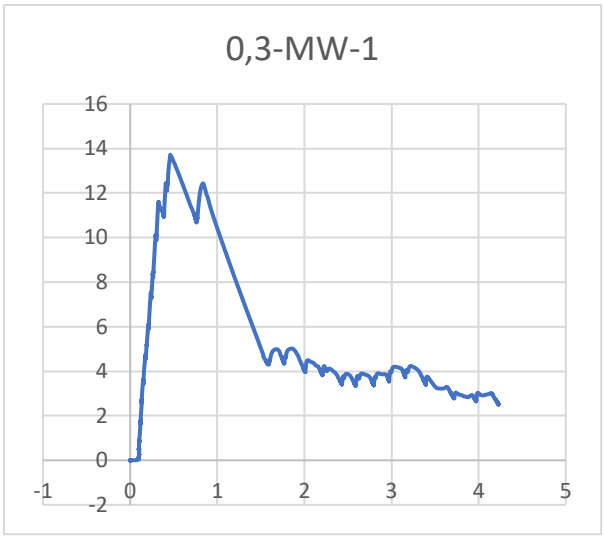

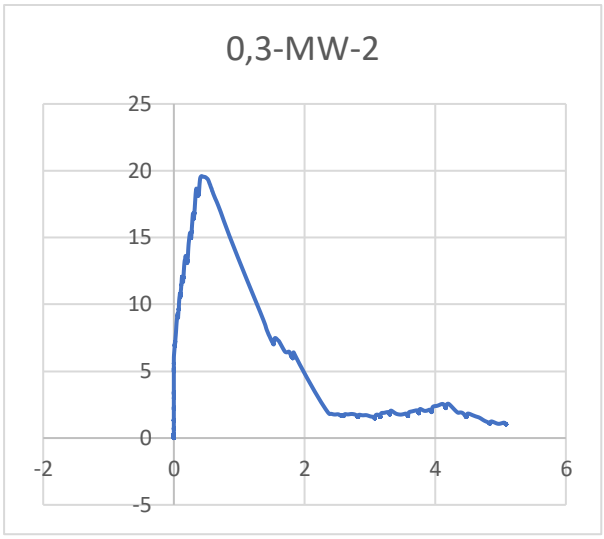

Test batch no. 12:

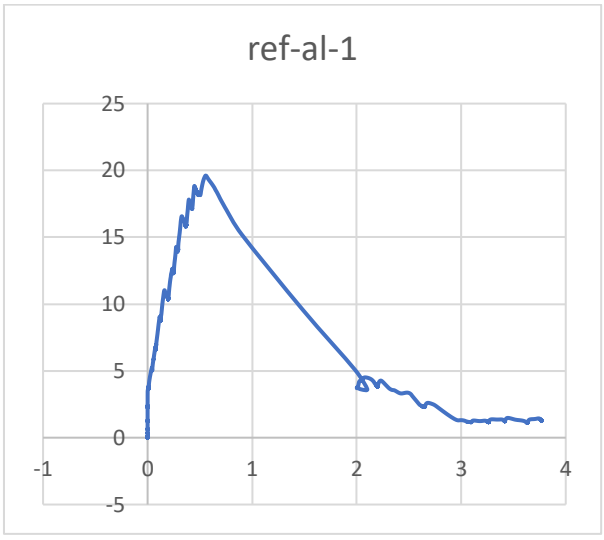

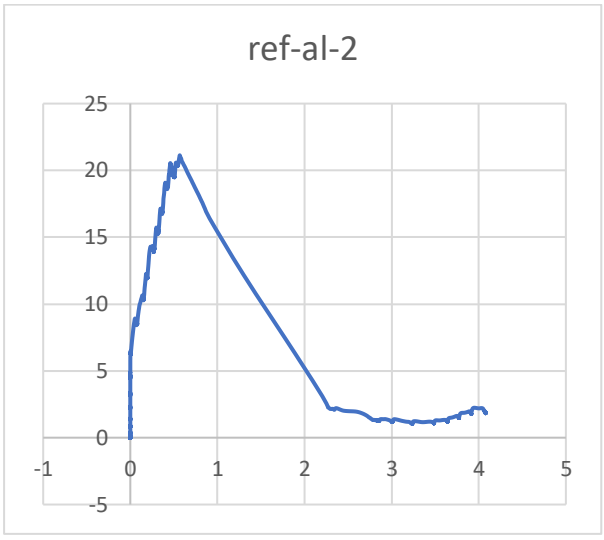

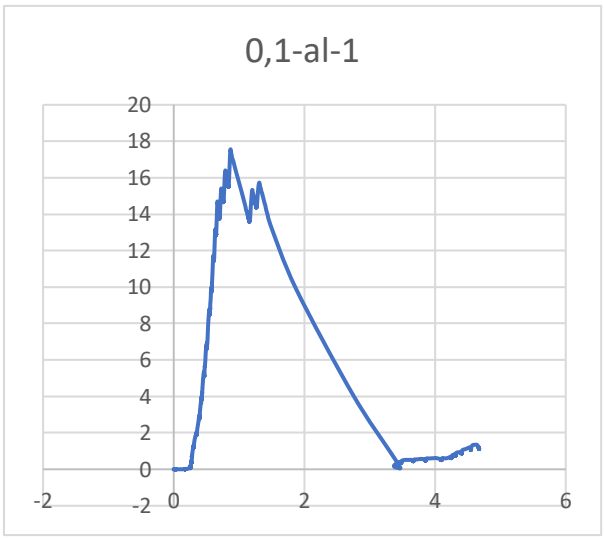

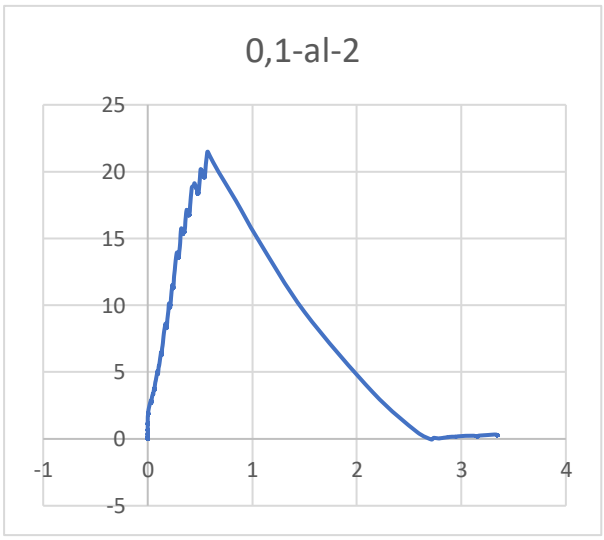

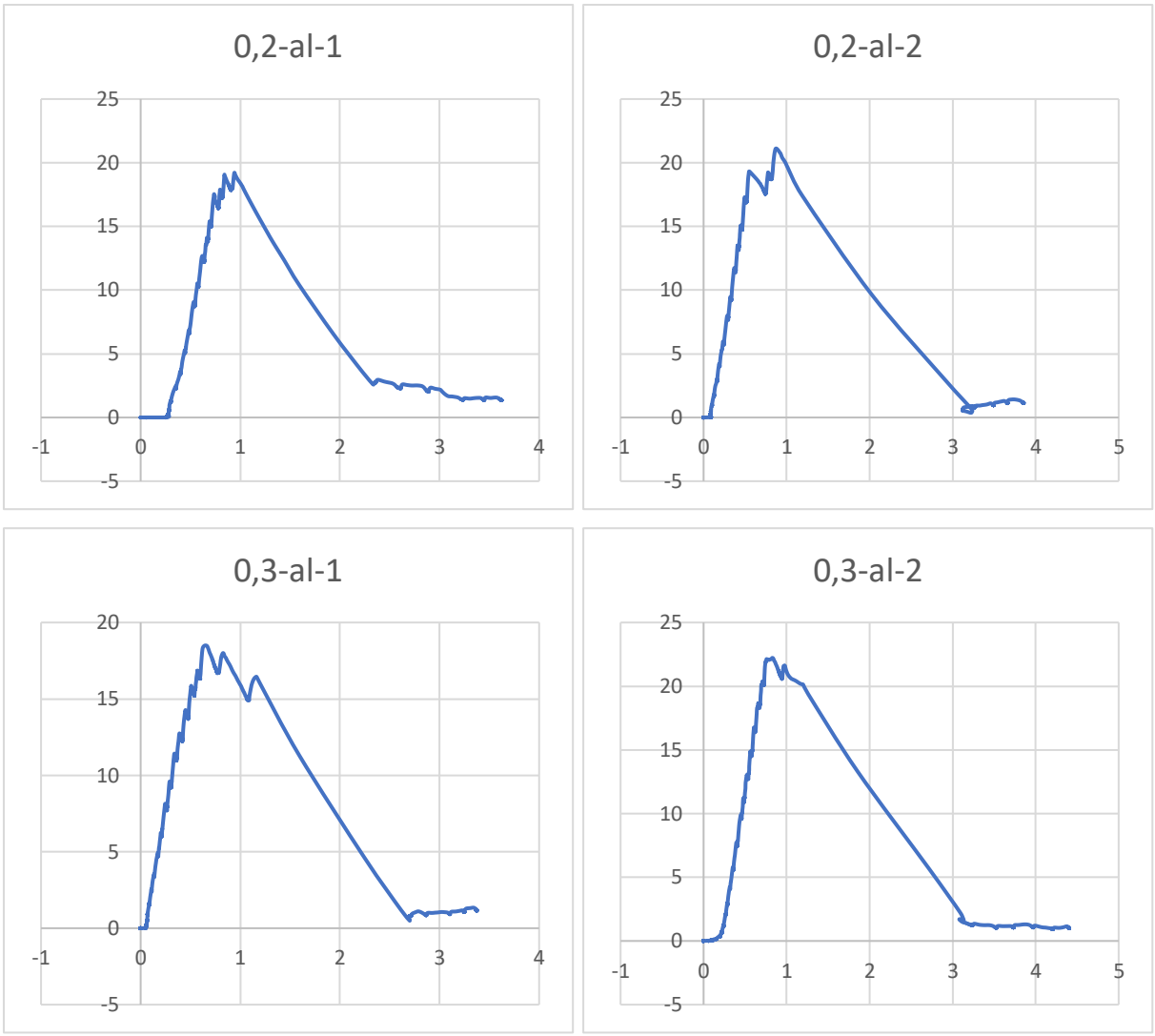

Test batch no. 13:

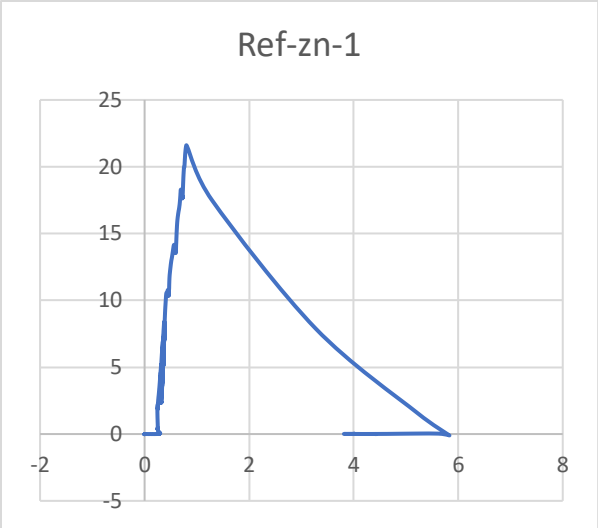
Ref-zn-1
25
20
15
10
5
0
-5
-2
0
2
4
6
8

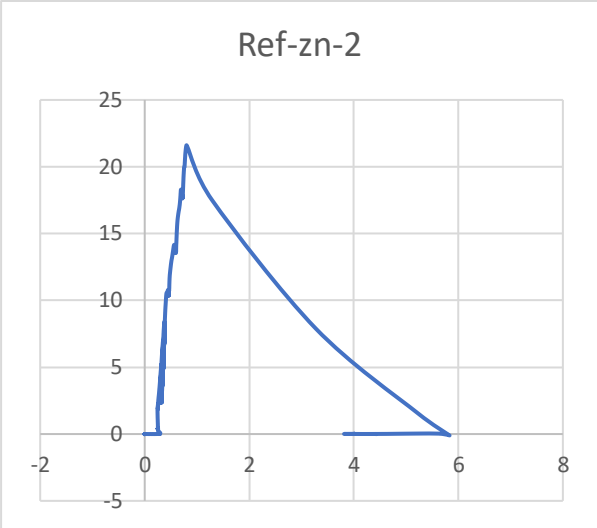
Ref-zn-2
25
20
15
10
5
0
-5
-2
0
2
4
6
8

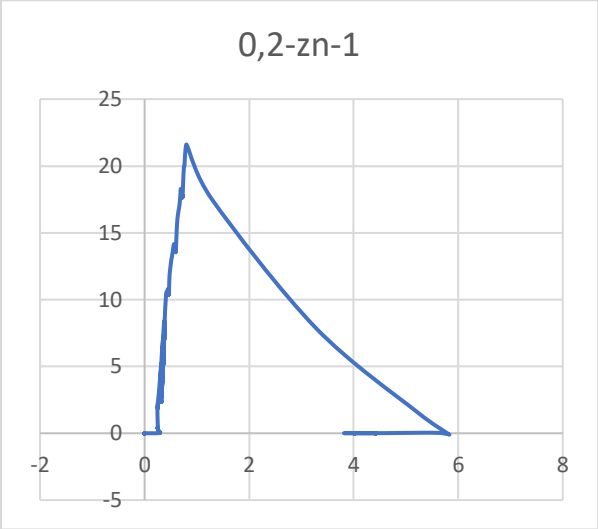
0,2-zn-1
25
20
15
10
5
0
-5
-2
0
2
4
6
8

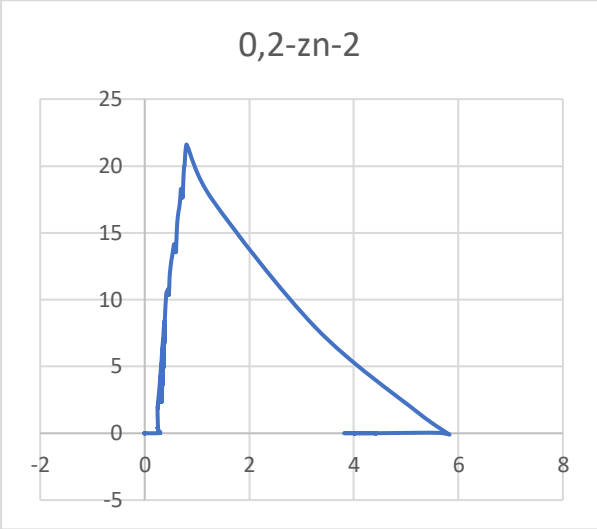
0,2-zn-2
25
20
15
10
5
0
-5
-2
0
2
4
6
8

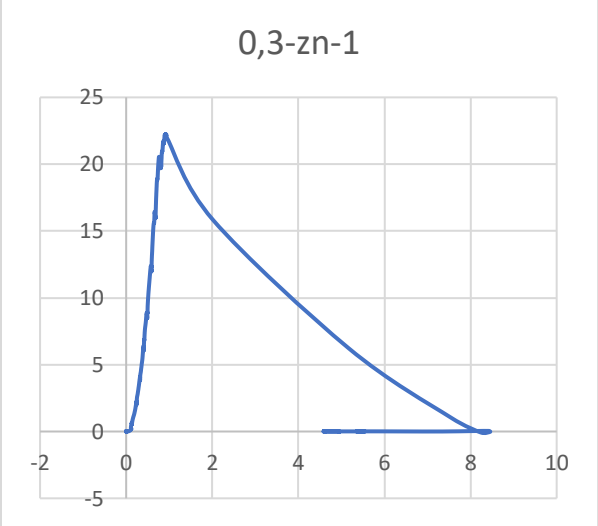
0,3-zn-1
25
20
15
10
5
0
-5
-2
0
2
4
6
8
10

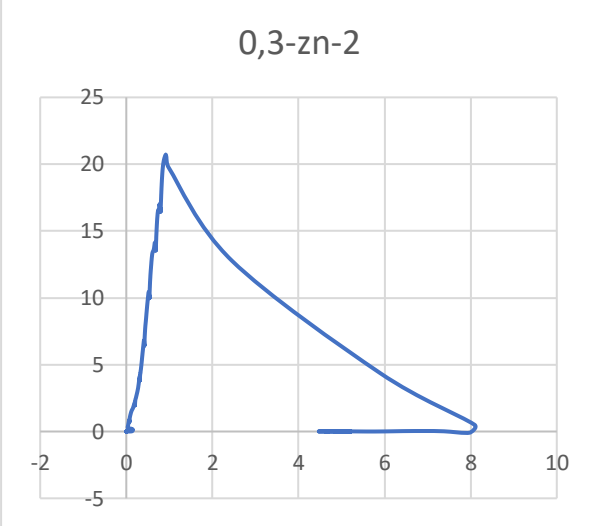
0,3-zn-2
25
20
15
10
5
0
-5
-2
0
2
4
6
8
10

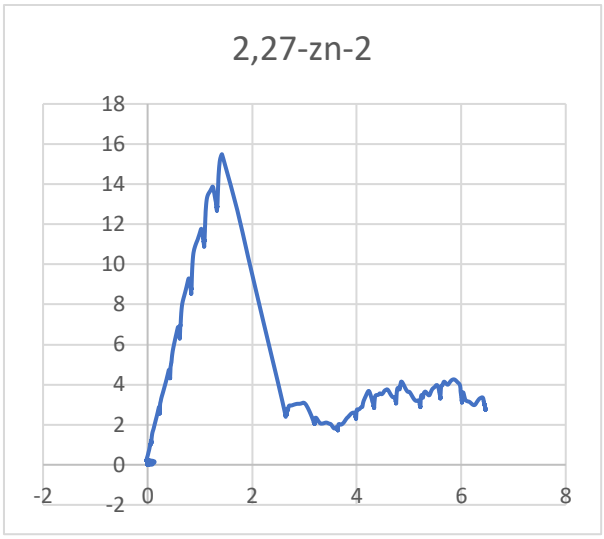

Test batch no. 14:

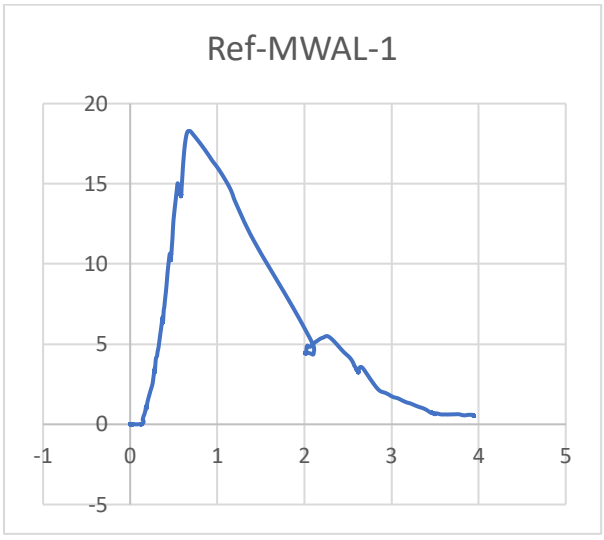

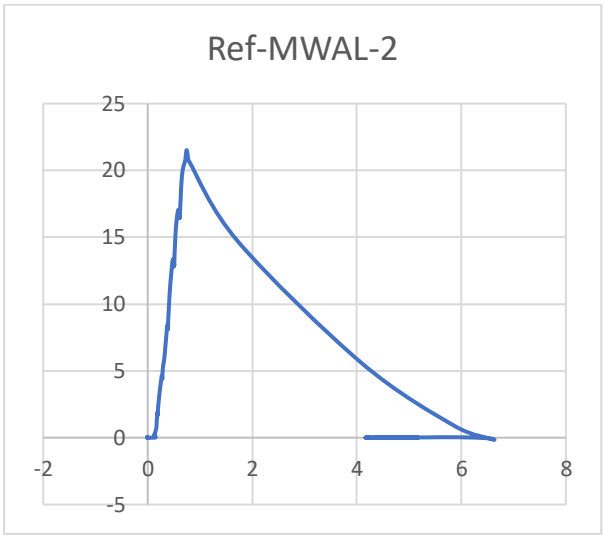

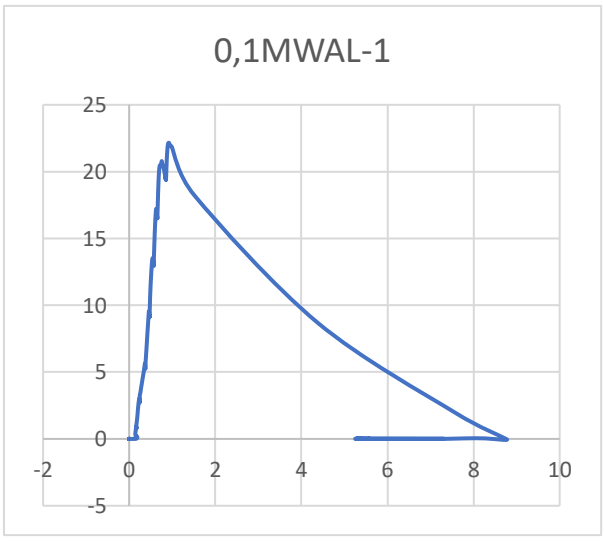

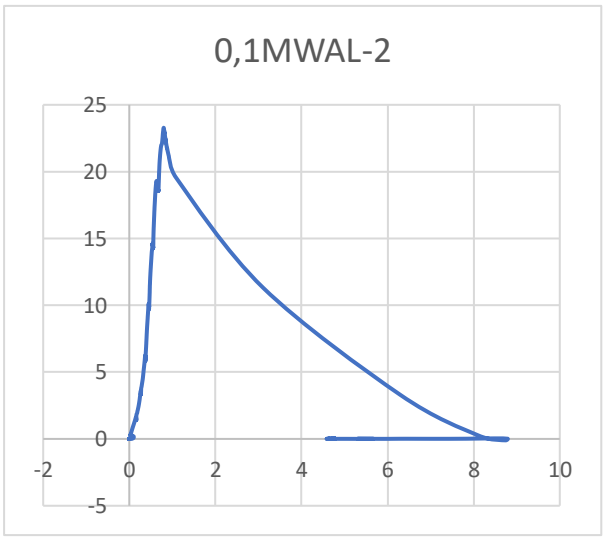

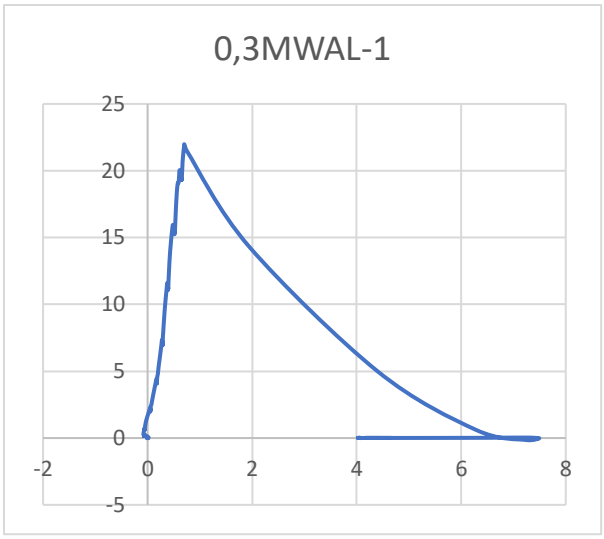

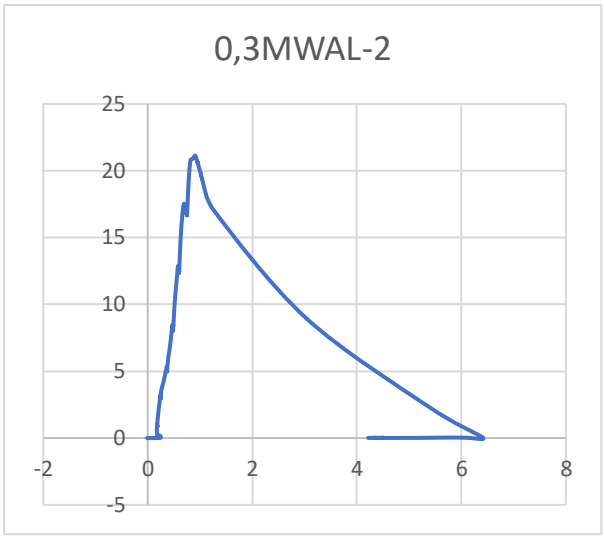

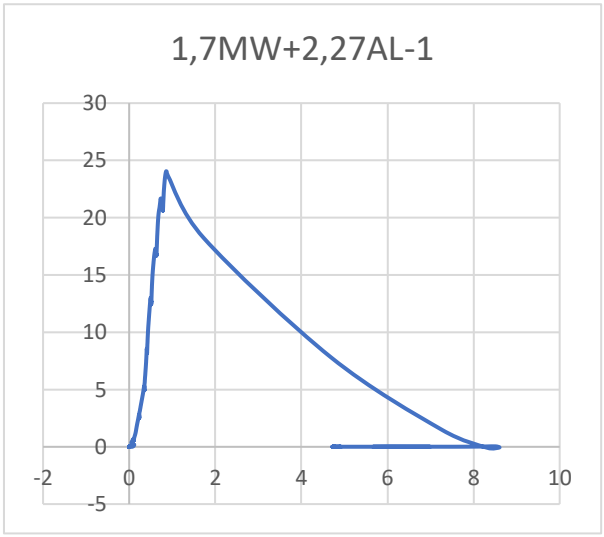

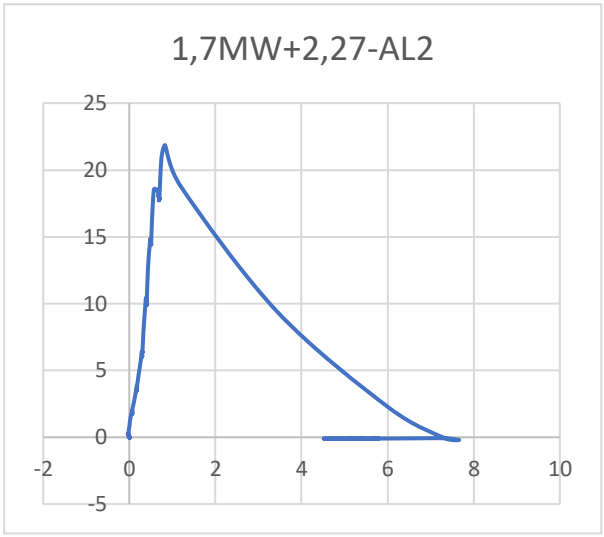

Test batch no. 15:

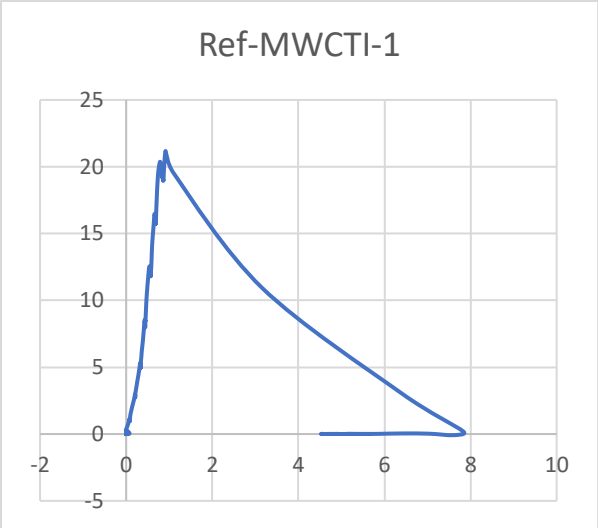
Ref-MWCTI-1
25
20
15
10
5
0
-5
-2
0
2
4
6
8
10

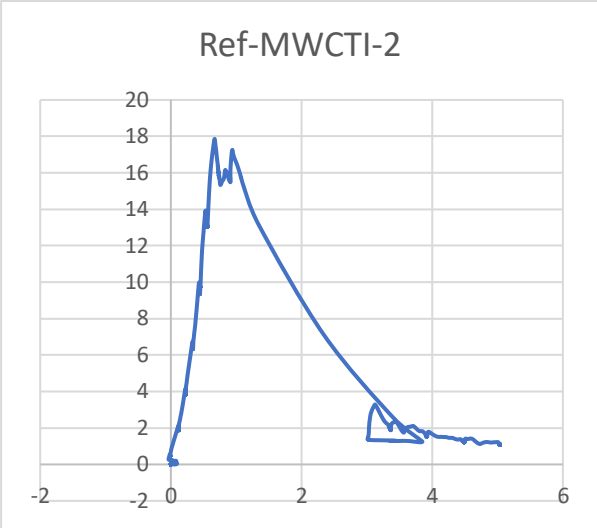
Ref-MWCTI-2
20
18
16
14
12
10
8
6
4
2
0
-2
-2
0
2
4
6

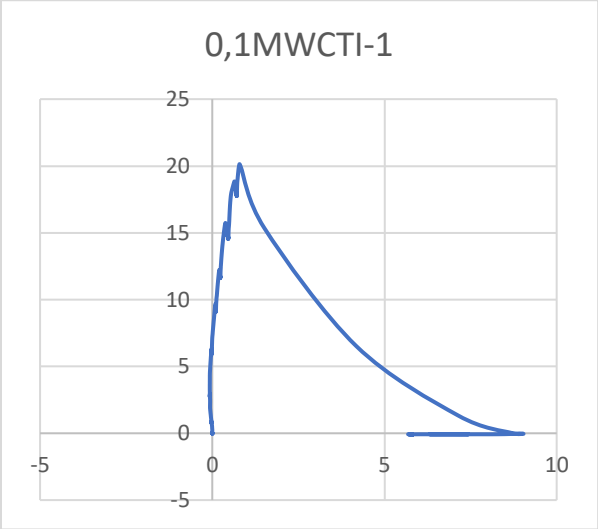
0,1MWCTI-1
25
20
15
10
5
0
-5
-5
0
5
10

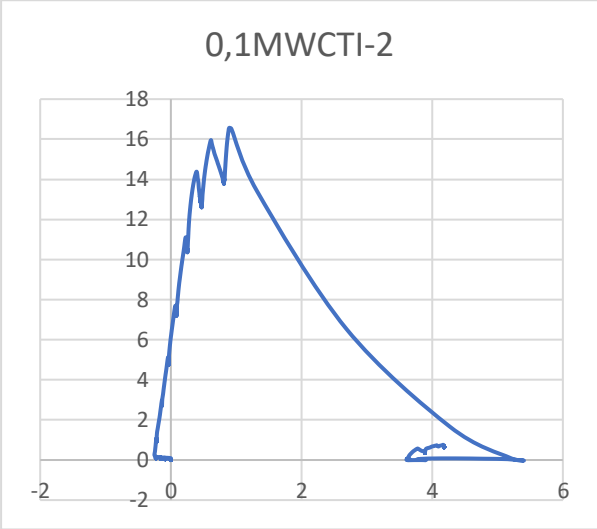
0,1MWCTI-2
18
16
14
12
10
8
6
4
2
0
-2
-2
0
2
4
6

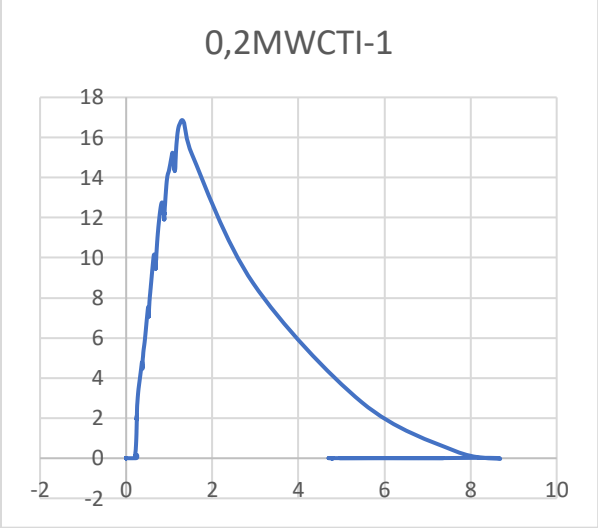
0,2MWCTI-1
18
16
14
12
10
8
6
4
2
0
-2
-2
0
2
4
6
8
10

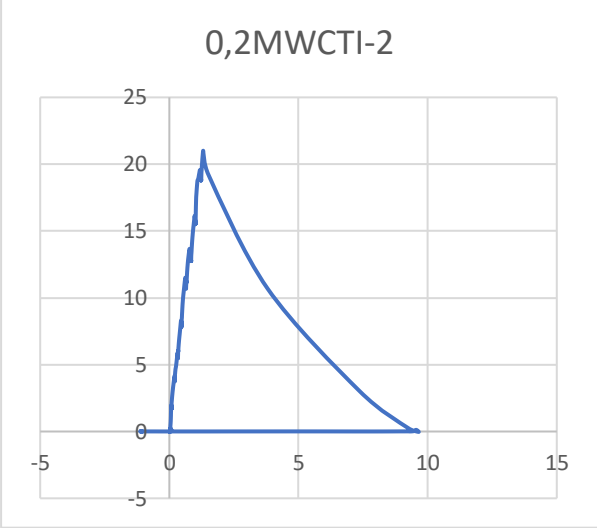
0,2MWCTI-2
25
20
15
10
5
0
-5
-5
0
5
10
15

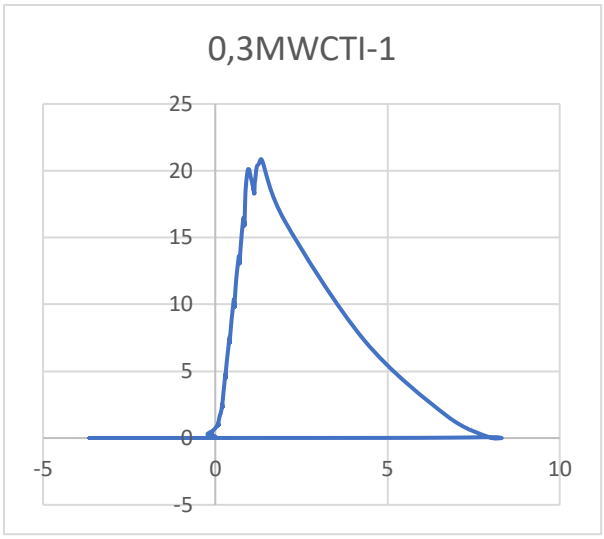

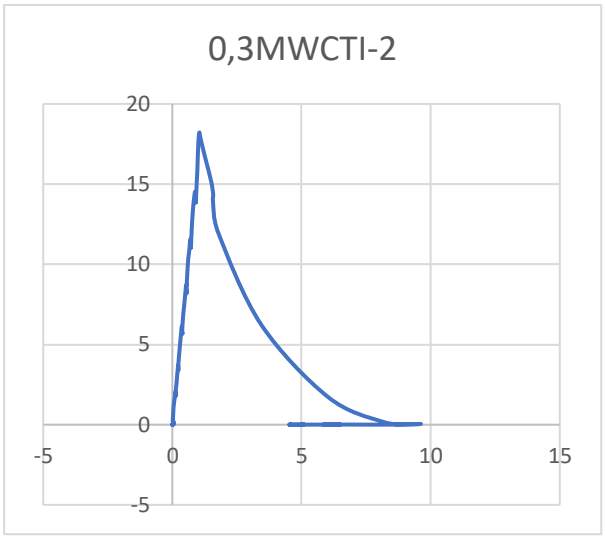

Test batch no. 16:

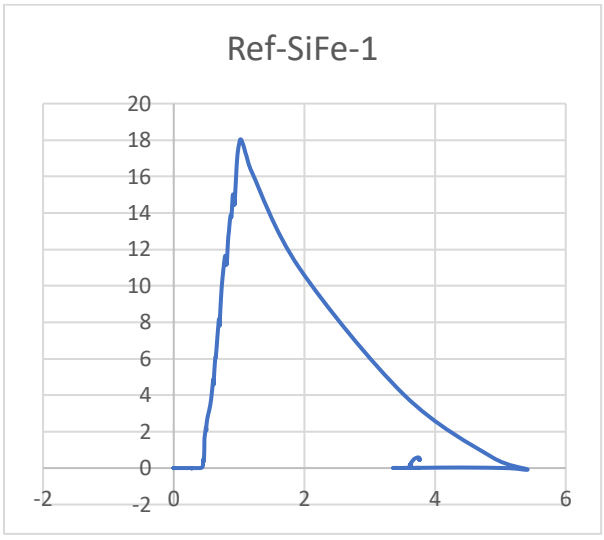

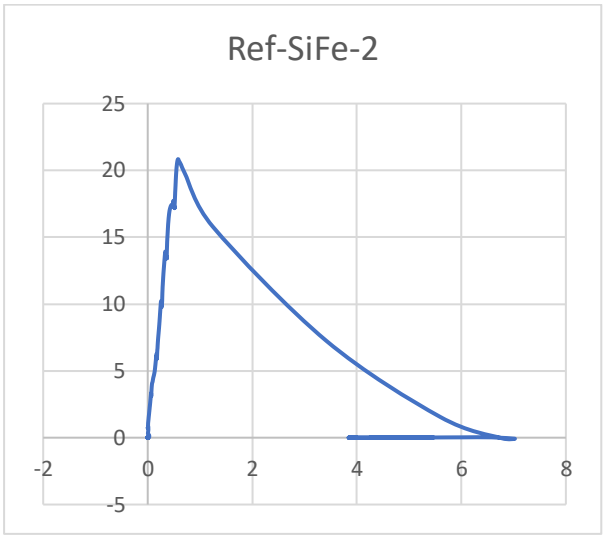

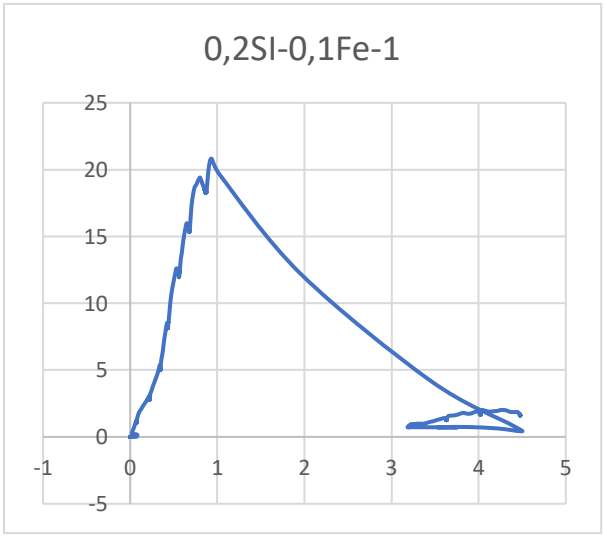

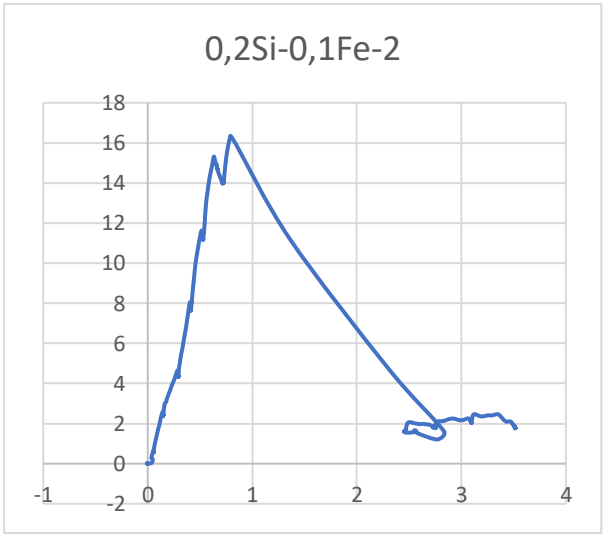

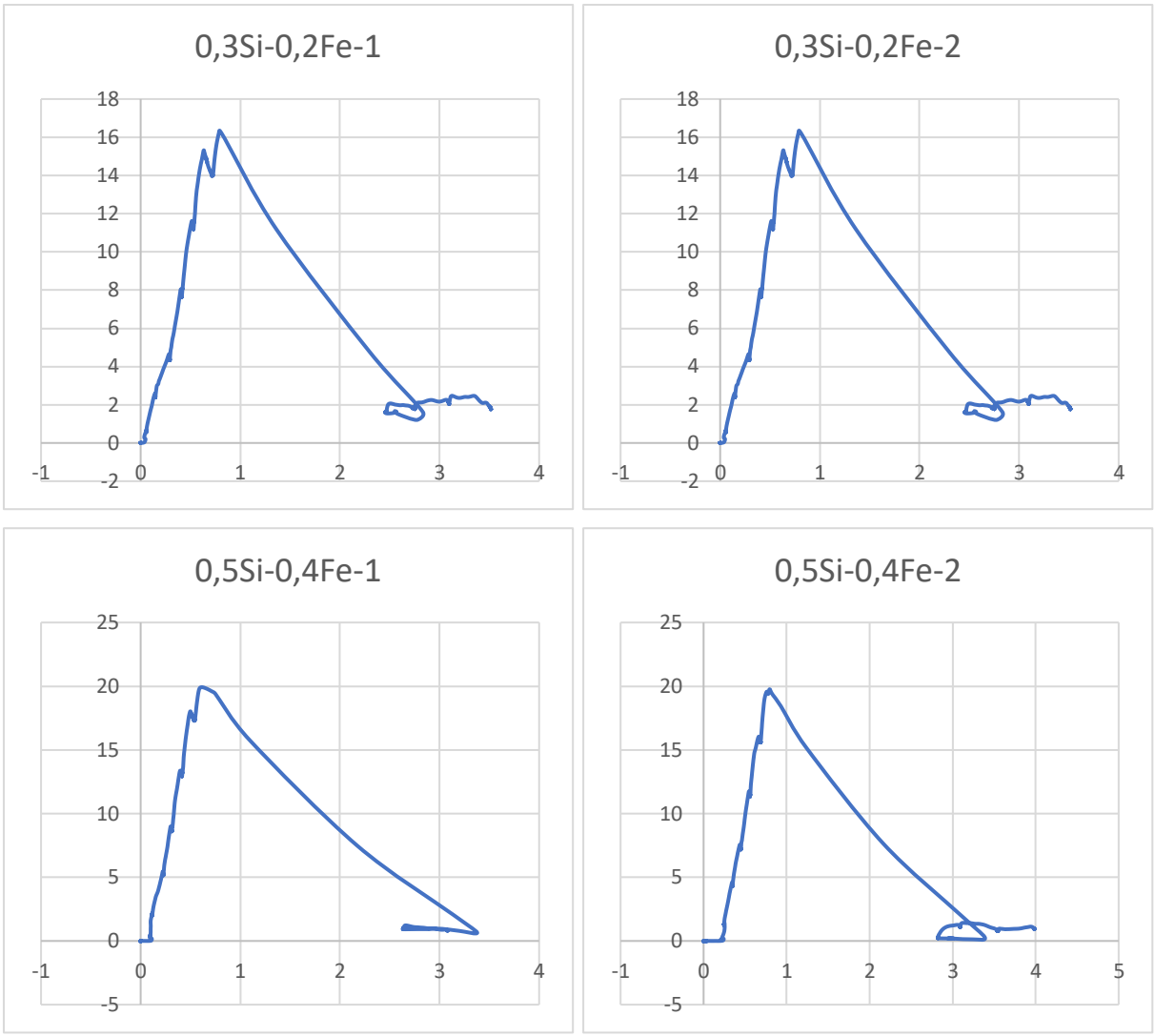

Test batch no. 17:

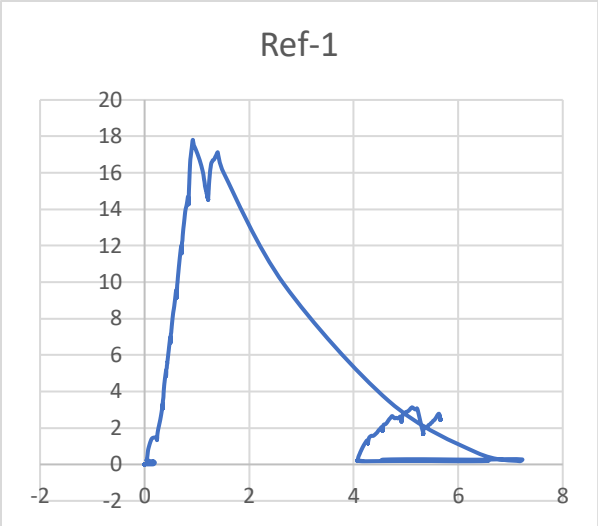
Ref-1
20
18
16
14
12
10
8
6
4
2
0
-2
-2
0
2
4
6
8

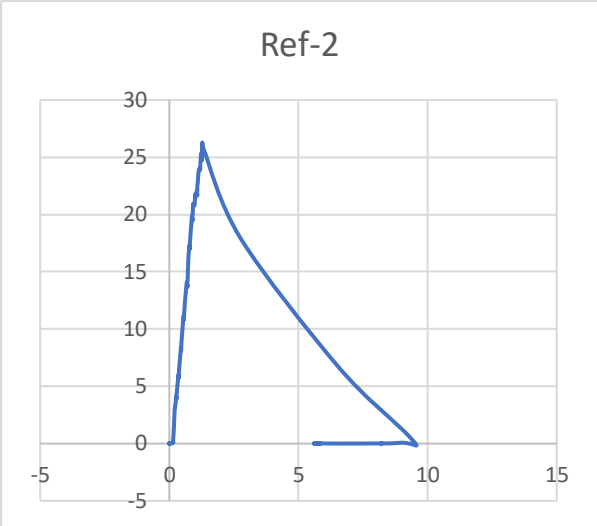
Ref-2
30
25
20
15
10
5
0
-5
-5
0
5
10
15

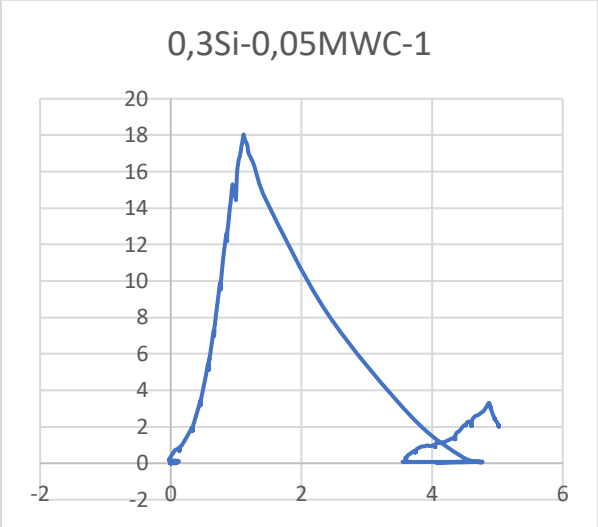
0,3Si-0,05MWC-1
20
18
16
14
12
10
8
6
4
2
0
-2
-2
0
2
4
6

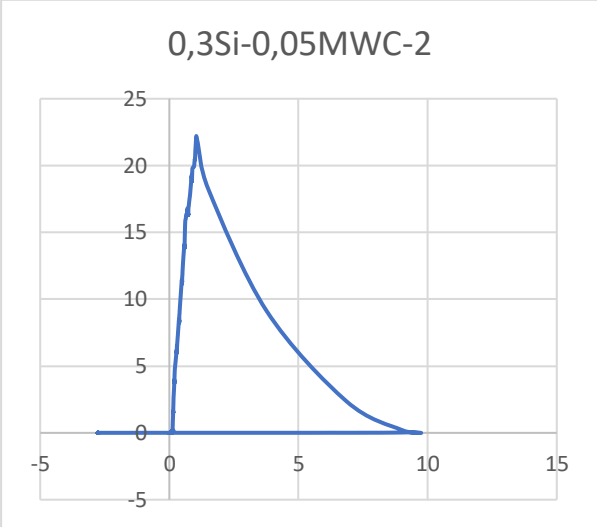
0,3Si-0,05MWC-2
25
20
15
10
5
0
-5
-5
0
5
10
15

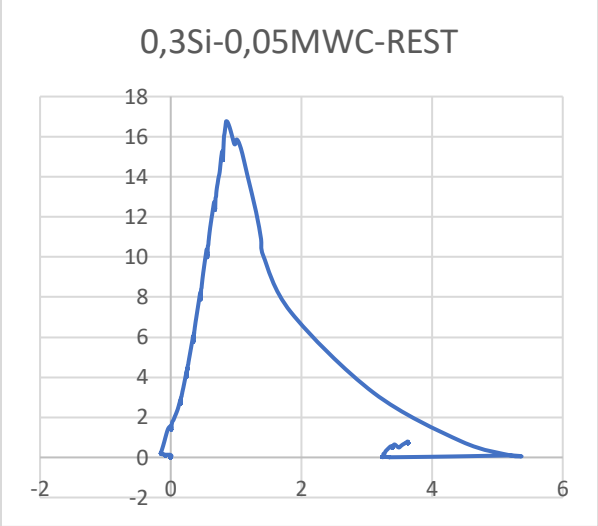
0,3Si-0,05MWC-REST
18
16
14
12
10
8
6
4
2
0
-2
-2
0
2
4
6

Appendix B – Non-destructive measurements for all batches

Appendix C contains the raw measured data like weight, OD, length and sonic from all test batches at the day of crushing, and some calculated values like volume, modulus of elasticity(M) and P-wave velocity.

Test batch no. 1:

Plug #	OD, mm	Length, mm	Mass, g	Volume, m3	Sonic, µs	Density, kg/m3	Velocity, m/s	M, Gpa
Ref-1	33,01	68,52	107,834	5,86406E-05	25,1	1839	2730	13,7
Ref-2	33,05	67,71	106,856	5,80879E-05	24,4	1840	2775	14,2
Ref + 0.25 SiO2-1	33,07	67,84	107,274	5,82699E-05	23,8	1841	2850	15,0
Ref + 0.25 SiO2-2	33,03	67,78	107,317	5,80776E-05	24,4	1848	2778	14,3
Ref + 0.5 SiO2-1	33,08	67,72	107,634	5,8202E-05	23,7	1849	2857	15,1
Ref + 0.5 SiO2-2	32,99	66,84	106,808	5,71335E-05	22,6	1869	2958	16,4
Ref + 0.75 SiO2-1	33,01	67,58	106,908	5,78361E-05	23,6	1848	2864	15,2
Ref + 0.75 SiO2-2	33,08	67,1	105,542	5,76691E-05	24,1	1830	2784	14,2
Ref + 1.0 SiO2-1	33,06	67,14	106,353	5,76338E-05	24,2	1845	2774	14,2
Ref + 1.0 SiO2-2	33,07	68,26	107,879	5,86306E-05	24,5	1840	2786	14,3
Ref + 1.5 SiO2-1	33,09	67,69	107,092	5,82114E-05	24,8	1840	2729	13,7
Ref + 1.5 SiO2-2	33,07	67,63	107,38	5,80895E-05	24,5	1849	2760	14,1

Test batch no. 2:

Plug #	OD, mm	Length, mm	Mass, g	Volume, m3	Sonic, µs	Density, kg/m3	Velocity, m/s	M, Gpa
Ref-1	33,1	67,86	107,422	5,83929E-05	24,5	1840	2770	14,1
Ref-2	33,03	66,2	106,091	5,67238E-05	23,4	1870	2829	15,0
Ref + 0.1 MWCNT-1	33,02	67,77	106,952	5,80339E-05	24,1	1843	2812	14,6
Ref + 0.1 MWCNT-2	32,79	67,6	107,167	5,70847E-05	23,9	1877	2828	15,0
Ref + 0.2 MWCNT-1	33,02	68,15	108,548	5,83593E-05	24,1	1860	2828	14,9
Ref + 0.2 MWCNT-2	32,97	67,87	107,6	5,79436E-05	24	1857	2828	14,9

Ref + 0.3 MWCNT-1	32,92	67,31	106,323	5,72914E-05	24,1	1856	2793	14,5
Ref + 0.3 MWCNT-2	33,04	66,12	106,656	5,66895E-05	23	1881	2875	15,5
Ref + 0.4 MWCNT-1	32,86	67,35	107,606	5,71166E-05	23,4	1884	2878	15,6
Ref + 0.4 MWCNT-2	32,97	67,78	107,476	5,78668E-05	24,9	1857	2722	13,8

Test batch no. 3:

Plug #	OD, mm	Length, mm	Mass, g	Volume, m3	Sonic, µs	Density, kg/m3	Velocity, m/s	M, Gpa
Ref-1								
Ref-2			104,122		22,5			
Ref + 0.1 TiO2-1	33,1	68,3	105,887	5,87715E-05	24,4	1802	2799	14,1
Ref + 0.1 TiO2-2	33,1	68,18	105,302	5,86682E-05	24,7	1795	2760	13,7
Ref + 0.2 TiO2-1	33,02	68,06	105,849	5,82822E-05	24	1816	2836	14,6
Ref + 0.2 TiO2-2	32,93	67,91	105,836	5,78372E-05	24,1	1830	2818	14,5
Ref + 0.3 TiO2-1	33,02	68,1	105,101	5,83165E-05	24,5	1802	2780	13,9
Ref + 0.3 TiO2-2	33,02	67,76	105,18	5,80253E-05	24,3	1813	2788	14,1
Ref + 0.4 TiO2-1	33,03	68,03	105,336	5,82918E-05	24,5	1807	2777	13,9
Ref + 0.4 TiO2-2	32,99	67,88	105,283	5,80225E-05	24,3	1815	2793	14,2
Ref + 1 TiO2-1	32,97	67,76	105,207	5,78497E-05	24,4	1819	2777	14,0
Ref +1 TiO2-2	32,89	68,32	105,713	5,80451E-05	24,3	1821	2812	14,4

Test batch no. 4:

Plug #	OD, mm	Length, mm	Mass, g	Volume, m3	Sonic, µs	Density, kg/m3	Velocity, m/s	M, Gpa
Ref-1	33,02	67,95	106,857	5,8188E-05	23,2	1836	2929	15,8
Ref-2	33,06	68,07	106,559	5,84321E-05	23,5	1824	2897	15,3
Ref + 0.1 Fe2O3-1	33,07	68,07	105,635	5,84674E-05	24,4	1807	2790	14,1
Ref + 0.1 Fe2O3-2	33	68,34	106,018	5,84511E-05	24,5	1814	2789	14,1
Ref + 0.2 Fe2O3-1	33,03	68,03	105,446	5,82918E-05	24,1	1809	2823	14,4
Ref + 0.2 Fe2O3-2	33,06	68,29	105,432	5,86209E-05	24,5	1799	2787	14,0

Ref + 0.3 Fe2O3-1	32,96	67,81	105,943	5,78573E-05	24,5	1831	2768	14,0
Ref + 0.3 Fe2O3-2	32,88	68,28	106,549	5,79758E-05	23,4	1838	2918	15,6
Ref + 0.4 Fe2O3-1	32,85	68	106,142	5,76328E-05	24,1	1842	2822	14,7
Ref + 0.4 Fe2O3-2	32,94	68,01	106,141	5,79575E-05	23,9	1831	2846	14,8
Ref + 1,0 Fe2O3-1	32,98	68,26	105,922	5,83119E-05	24,7	1816	2764	13,9
Ref + 1,0 Fe2O3-2	32,91	68,07	105,403	5,7903E-05	23,8	1820	2860	14,9

Test batch no. 5:

Plug #	OD, mm	Length, mm	Mass, g	Volume, m3	Sonic, μs	Density, kg/m3	Velocity, m/s	M, Gpa
Ref-0,52-1	33,18	68,36	105,891	5,91078E-05	24,9	1791	2745	13,5
Ref-0,52-2	32,9	68,18	106,183	5,79614E-05	25,3	1832	2695	13,3
Ref-0,52-3	33,04	67,65	105,684	5,80013E-05	24,3	1822	2784	14,1
Ref-0,52-4	32,89	67,82	106,267	5,76203E-05	24,4	1844	2780	14,2
Ref-0,44-1	32,6	67,83	105,272	5,6617E-05	21,8	1859	3111	18,0
Ref-0,44-2	32,51	67,37	103,179	5,5923E-05	21,1	1845	3193	18,8
Ref-0,44-3	32,85	67,44	102,546	5,71582E-05	21,7	1794	3108	17,3
Ref-0,44-4	32,76	67,3	103,236	5,67274E-05	22,2	1820	3032	16,7

Test batch no. 6:

Plug #	OD, mm	Length, mm	Mass, g	Volume, m3	Sonic, μs	Density, kg/m3	Velocity, m/s	M, Gpa
Ref-1	32,75	67,42	105,077	5,67938E-05	20,7	1850	3257	19,6
Ref-2	32,71	67,93	105,693	5,70838E-05	21,2	1852	3204	19,0
Ref + 0.1 COOH-1	32,8	67,82	105,605	5,73054E-05	21,2	1843	3199	18,9
Ref + 0.1 COOH-2	32,77	67,87	106,46	5,72428E-05	20,9	1860	3247	19,6
Ref + 0.2 COOH-1	32,78	67,9	106,682	5,7303E-05	21,2	1862	3203	19,1
Ref + 0.2 COOH-2	32,72	67,89	107,07	5,7085E-05	20,4	1876	3328	20,8
Ref + 0.3 COOH-1	32,67	67,79	107,034	5,68269E-05	20,5	1884	3307	20,6

Ref + 0.3 COOH-2	32,7	67,5	108,006	5,66877E-05	20,2	1905	3342	21,3
Ref + 0.4 COOH-1	33,1	67,5	110,133	5,80831E-05	21,3	1896	3169	19,0
Ref + 0.4 COOH-2	32,85	68,12	109,842	5,77345E-05	20,7	1903	3291	20,6
Ref + 1.0 COOH-1	32,81	68,03	108,031	5,75179E-05	20,7	1878	3286	20,3
Ref + 1.0 COOH-1	33,02	67,86	109,072	5,81109E-05	20,5	1877	3310	20,6

Test batch no. 7:

Plug #	OD, mm	Length, mm	Mass, g	Volume, m3	Sonic, μs	Density, kg/m3	Velocity, m/s	M, Gpa
Ref-1	32,98	67,42	105,855	5,75944E-05	20,6	1838	3273	19,7
Ref-2	32,8	67,28	105,036	5,68491E-05	20,1	1848	3347	20,7
Ref + 2 UTR-1	32,46	67,22	104,21	5,5627E-05	19,9	1873	3378	21,4
Ref + 2 UTR-2	32,59	67,5	104,685	5,6307E-05	20,6	1859	3277	20,0
Ref + 2 TR-1	32,22	67,36	105,063	5,49216E-05	20,6	1913	3270	20,5
Ref + 2 TR-2	32,48	67,44	104,764	5,58778E-05	20,4	1875	3306	20,5
Ref + 3 UTR-1	32,6	67,76	104,649	5,65586E-05	21,6	1850	3137	18,2
Ref + 3 UTR-2	32,6	67,35	104,607	5,62164E-05	21,3	1861	3162	18,6
Ref + 3 TR-1	32,95	67,65	104,039	5,76857E-05	21,6	1804	3132	17,7
Ref + 3 TR-2	33,08	67,23	104,995	5,77809E-05	20,8	1817	3232	19,0
Ref + 4 UTR-1	32,7	67,91	102,015	5,70321E-05	22,4	1789	3032	16,4
Ref + 4 UTR-2	32,75	67,59	102,924	5,6937E-05	21,6	1808	3129	17,7
Ref + 4 TR-1	32,55	67,39	100,59	5,60773E-05	22	1794	3063	16,8
Ref + 4 TR-2	32,67	67,59	103,037	5,66592E-05	21,1	1819	3203	18,7

Test batch no. 8:

Plug #	OD, mm	Length, mm	Mass, g	Volume, m3	Sonic, μs	Density, kg/m3	Velocity, m/s	M, Gpa
Ref-1	32,8	67,27	102,412	5,68406E-05	21,1	1802	3188	18,3
Ref-2	32,81	68,22	104,227	5,76785E-05	21,4	1807	3188	18,4
0.05 COOH & 0,3 SiO2-1	32,55	67,64	105,068	5,62854E-05	20,5	1867	3300	20,3
0.05 COOH & 0,3 SiO2-2	32,71	67,52	105,325	5,67392E-05	21,1	1856	3200	19,0
0.1 COOH & 0,4 SiO2-1	32,48	67,47	105,209	5,59027E-05	21,2	1882	3183	19,1

0.1 COOH & 0,4 SiO2-2	32,85	67,81	105,594	5,74717E-05	21,1	1837	3214	19,0
0.2 COOH & 0,5 SiO2-1	32,56	67,78	104,829	5,64365E-05	21,3	1857	3182	18,8
0.2 COOH & 0,5 SiO2-2	32,84	67,71	104,683	5,73521E-05	21,9	1825	3092	17,4

Test batch no. 9:

Plug #	OD, mm	Length, mm	Mass, g	Volume, m3	Sonic, µs	Density, kg/m3	Velocity, m/s	M, Gpa
Ref-1	32,73	67,55	95,157	5,68339E-05	21,7	1674	3113	16,2
Ref-2	32,72	67,53	95,498	5,67823E-05	22	1682	3070	15,8
0,5 ash-1	32,58	66,66	92,887	5,55722E-05	21	1671	3174	16,8
0,5 ash-2	32,88	67,25	95,792	5,71013E-05	21	1678	3202	17,2
1,5 ash-1	32,82	67,39	93,53	5,70115E-05	21,8	1641	3091	15,7
1,5 ash-2	32,73	67,48	94,25	5,6775E-05	21,1	1660	3198	17,0

Test batch no. 10:

Plug #	OD, mm	Length, mm	Mass, g	Volume, m3	Sonic, µs	Density, kg/m3	Velocity, m/s	M, Gpa
Ref-1	32,61	67,44	95,935	5,6326E-05	21,2	1703	3181	17,2
Ref-2	32,58	67,28	97,135	5,6089E-05	21,3	1732	3159	17,3
0,4 silica-1	32,72	67,51	96,058	5,67655E-05	21,1	1692	3200	17,3
0,4 silica-2	32,67	67,26	97,124	5,63826E-05	20,5	1723	3281	18,5
0,5 silica -1	32,61	67,15	95,693	5,60838E-05	21	1706	3198	17,4
0,5 silica-2	32,93	67,08	96,911	5,71303E-05	20,8	1696	3225	17,6
0,6 silica-1	32,48	67,35	95,905	5,58033E-05	20,6	1719	3269	18,4
0,6 silica-2	32,82	67,21	96,51	5,68592E-05	20,9	1697	3216	17,6

Test batch no. 11:

Plug #	OD, mm	Length, mm	Mass, g	Volume, m3	Sonic, µs	Density, kg/m3	Velocity, m/s	M, Gpa
Ref-1	32,55	66,5	101,516	5,53367E-05	20,1	1835	3308	20,1
Ref-2	32,9	65,13	99,73	5,53685E-05	20	1801	3257	19,1
0,1 MWCNT-1	32,76	67,53	102,886	5,69212E-05	21,2	1808	3185	18,3

0,1 MWCNT-2	32,8	67,46	102,391	5,70012E-05	21,7	1796	3109	17,4
0,2 MWCNT -1	32,53	67,51	102,316	5,61082E-05	21,2	1824	3184	18,5
0,2 MWCNT-2	32,65	67,55	102,023	5,65564E-05	20,6	1804	3279	19,4
0,3 MWCNT-1	32,58	67,3	100,361	5,61057E-05	21,9	1789	3073	16,9
0,3 MWCNT-2	32,8	67,65	101,722	5,71617E-05	21,4	1780	3161	17,8

Test batch no. 12:

Plug #	OD, mm	Length, mm	Mass, g	Volume, m3	Sonic, μs	Density, kg/m3	Velocity, m/s	M, Gpa
Ref-1	32,88	67,54	103,264	5,73475E-05	20,2	1801	3344	20,1
Ref-2	32,85	67,71	103,11	5,7387E-05	20,8	1797	3255	19,0
0,1 Al2O3-1	32,78	67,81	102,982	5,72271E-05	20,3	1800	3340	20,1
0,1 Al2O3-2	32,86	67,54	103,498	5,72778E-05	20,6	1807	3279	19,4
0,2 Al2O3 -1	32,83	67,72	103,527	5,73256E-05	20,7	1806	3271	19,3
0,2 Al2O3-2	32,91	67,86	103,713	5,77244E-05	20,9	1797	3247	18,9
0,3 Al2O3-1	32,8	67,67	103,642	5,71786E-05	21	1813	3222	18,8
0,3 Al2O3-2	32,62	67,41	103,568	5,63355E-05	20,2	1838	3337	20,5

Test batch no. 13:

Plug #	OD, mm	Length, mm	Mass, g	Volume, m3	Sonic, μs	Density, kg/m3	Velocity, m/s	M, Gpa
Ref-1	32,91	67,36	96,948	5,72991E-05	20,3	1692	3318	18,6
Ref-2	32,92	67,42	97,728	5,7385E-05	20,1	1703	3354	19,2
0,2 ZnO -1	32,94	67,53	96,188	5,75485E-05	20,4	1671	3310	18,3
0,2 ZnO-2	32,85	67,39	96,439	5,71158E-05	20,2	1688	3336	18,8
0,3 ZnO-1	32,81	67,44	96,753	5,7019E-05	20,3	1697	3322	18,7
0,3 ZnO-2	33	67,4	97,639	5,76471E-05	20,7	1694	3256	18,0
2,27 ZnO-1								
2,27 ZnO-2	32,35	67,5	103,577	5,54807E-05	23	1867	2935	16,1

Test batch no. 14:

Plug #	OD, mm	Length, mm	Mass, g	Volume, m3	Sonic, μs	Density, kg/m3	Velocity, m/s	M, Gpa
Ref-1	33	67,4	103,898	5,76471E-05	21,3	1802	3164	18,0
Ref-2	32,99	67,33	103,325	5,75524E-05	21,4	1795	3146	17,8
0,1MW+0,1Al-1	33,1	67,42	104,7	5,80142E-05	21,4	1805	3150	17,9
0,1MW+0,1Al-2	32,95	67,31	104,57	5,73958E-05	21,2	1822	3175	18,4
0,3MW+0,3Al-1	33,08	67,34	104,306	5,78754E-05	21,5	1802	3132	17,7
0,3MW+0,3Al-2	32,9	67,35	104,398	5,72558E-05	21,6	1823	3118	17,7
1,7025MW+2,27 Al-1	32,93	67,36	104,345	5,73688E-05	21,1	1819	3192	18,5
1,7025MW+2,27 Al-2	32,69	67,41	104,989	5,65775E-05	21,1	1856	3195	18,9

Test batch no. 15:

Plug #	OD, mm	Length, mm	Mass, g	Volume, m3	Sonic , μs	Density, kg/m3	Velocity, m/s	M, Gpa
Ref-1	32,9	67,42	104,034	5,7315E-05	22,2	1815	3037	16,7
Ref-2	32,9	67,64	104,517	5,7502E-05	21,7	1818	3117	17,7
0,1MWc+0,1 Ti-1	33,06	67,63	105,599	5,8054E-05	21,6	1819	3131	17,8
0,1MWc+0,1 Ti-2	33	66	103,844	5,645E-05	20,8	1840	3173	18,5
0,2MWc+0,2 Ti-1	33	67,14	105,004	5,7425E-05	21,4	1829	3137	18,0
0,3MWc+0,ti -2	33,1	67,62	105,875	5,8186E-05	21,7	1820	3116	17,7
0,3MWc+0,3 Ti-1	32,9	67,3	106,496	5,7213E-05	21	1861	3205	19,1
0,3MWc+0,3 Ti-2	32,86	67,66	107,251	5,738E-05	21,2	1869	3192	19,0

Test batch no. 16:

Plug #	OD, mm	Length, mm	Mass, g	Volume, m3	Sonic, μs	Density , kg/m3	Velocity, m/s	M, Gpa
Ref-1	32,86	67,45	102,936	5,7201E-05	22,1	1800	3052	16,8
Ref-2	33,04	67,41	103,991	5,7796E-05	21,9	1799	3078	17,0
0,2Si+0,1Fe-1	33,14	67,61	104,637	5,8318E-05	22,1	1794	3059	16,8
0,2Si+0,1Fe-2	33,02	67,36	104,629	5,7683E-05	21,9	1814	3076	17,2
0,3Si+0,2Fe-1	33	67,5	104,522	5,7733E-05	22,1	1810	3054	16,9

0,3Si+0,2Fe-1	32,83	67,57	104,781	5,7199E-05	22,3	1832	3030	16,8
0,5Si+0,4Fe-1	32,78	67,41	104,78	5,6889E-05	21,5	1842	3135	18,1
0,5Si+0,4Fe-2	32,94	67,35	104,525	5,7395E-05	21,8	1821	3089	17,4

Test batch no. 17:

Plug #	OD, mm	Length, mm	Mass, g	Volume, m3	Sonic, μs	Density, kg/m3	Velocity, m/s	M, Gpa
Ref-1	32,58	67,24	88,186	5,6056E-05	22,7	1573	2962	13,8
Ref-2	32,76	67,31	89,013	5,6736E-05	22,8	1569	2952	13,7
0,3Si+0,05MWC-1	32,69	63,69	84,271	5,3455E-05	22	1576	2895	13,2
0,3Si+0,05MWC-2	32,64	67,31	88,626	5,6321E-05	22,6	1574	2978	14,0
0,3Si+0,05MWC-rest	32,81	66,56	87,106	5,6275E-05	23	1548	2894	13,0

Appendix C – Miscellaneous pictures

Picture above shows one of the specimens containing 2,27 grams of Zinc oxide, which did not set properly after the initial curing time which led to the sample being destroyed when polishing was attempted. This particular sample was not subjected to destructive testing due to its structural flaws.

Picture above shows the inner structure of a sample containing rubber silicone after it was subjected to destructive testing. One can clearly see the difference in the finely and coarsely cut rubber.

The picture above shows the water from the leakage test. The water depicted was the water which did not leak through the sample, but stayed on top. On the left side, the water from the zero-additive sample is shown, and on the right side the water from the cement with added nanoparticle is shown.